DD3R zeolite membranes in separation and catalytic processes

Modelling and application

Cover illustration: 8-ring window of zeolite DD3R

DD3R zeolite membranes in separation and catalytic processes

Modelling and application

Proefschrift

ter verkrijging van de graad van doctor
aan de Technische Universiteit Delft,
op gezag van de Rector Magnificus prof. ir. K. C. A. M. Luyben,
voorzitter van het College voor Promoties,
in het openbaar te verdedigen
op dinsdag 21 september 2010 om 15.00 uur

door

Johan VAN DEN BERGH

scheikundig ingenieur
geboren te Dordrecht, Nederland

Dit proefschrift is goedgekeurd door de promotor:
Prof. dr. F. Kapteijn

Samenstelling promotiecommissie:

Rector Magnificus	Voorzitter
Prof. dr. F. Kapteijn	Technische Universiteit Delft, Promotor
Dr. ir. T. J. H. Vlugt	Technische Universiteit Delft
Prof. dr. J. A. Moulijn	Technische Universiteit Delft
Prof. dr. ir. A. Nijmeijer	Technische Universiteit Twente
Prof. dr. J. Kärger	Universität Leipzig
Prof. dr. ir. W. Zhu	Zhejiang Normal University
Prof. dr. ir. G. V. Baron	Vrije Universiteit Brussel
Prof. dr. ir. H. van Bekkum	Technische Universiteit Delft, reservelid

The research reported in this thesis was conducted in the Catalysis Engineering section of the Chemical Engineering department of the Faculty of Applied Sciences (TNW) of the Delft University of Technology, and within the scope of the NOW-DFG International Research and Training Group ‘Diffusion in Porous Materials’.

Proefschrift, Technische Universiteit Delft
Met samenvatting in het Nederlands / With summary in Dutch
ISBN 978-90-5335-298-4

Cover design: Johan van den Bergh
Printed by Ridderprint B.V., Ridderkerk, The Netherlands

Dank God in alles

Contents

Preface

Around 2004 the annual energy consumption of the Dutch (petro-)chemical industry was estimated to be 460 PJ of which 200 PJ could be allocated to separation processes [1]. In 2009, 15% of the global energy consumption was required for separation and purification processes to produce commodities. Moreover, it is expected that in 2040 the global commodity demand is three times higher than in 2009 leading to an enormous energy demand increase in the coming decades related to separation processes [2]. These two examples clearly illustrate that development of new innovative energy-efficient separation technologies can lead to significant process improvements in terms of energy usage and operating costs. In particular thermally driven separation processes, like distillation, are very energy consumptive [3]. Membrane technology is considered a serious candidate to replace traditionally used thermally-driven separation processes, because of the large energy reduction that can be achieved [2-4]. An application, particularly relevant for this thesis is natural gas purification, which is by far the largest industrial gas separation application [5]. The proven, well-accepted and mostly used amine based absorption process has several downsides such as: relative complex multi-column operation that requires careful monitoring and operation, high energy consumption required for solvent regeneration and high corrosion rate of equipment due to the solvent [5,6]. A membrane process could offer an energy efficient, simple and continuous alternative. However, in order to compete with the relatively cheap absorption technology stable membranes with improved fluxes and selectivities are required [5,7].

Membrane technology

The operation principle of a membrane is straightforward. If we consider a binary mixture of components A and B, both components will have a different permeability across the membrane leading to a certain selectivity. In a crude approach the different permeability can be solely due to size effects, which can lead to complete exclusion of one component in the

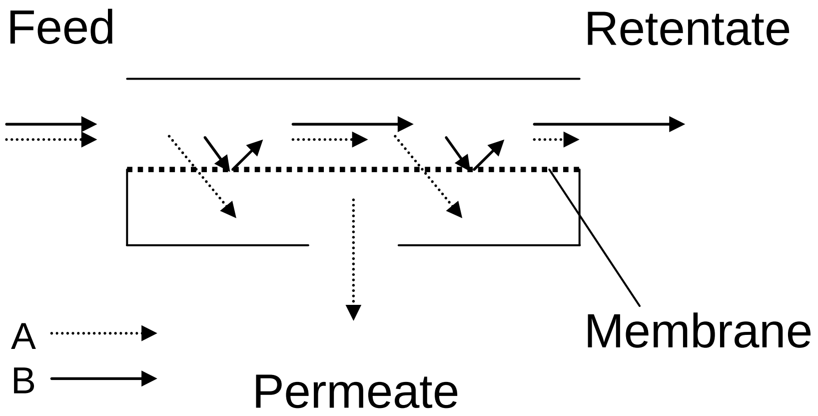

Figure 1. Schematic representation of a membrane process.

ideal case. As illustrated in Figure 1, a feed mixture of components A and B is fed to the membrane, component A permeates through the membrane, component B is completely rejected in this case. This leads to a permeate flow of purely component A and a retentate flow enriched in component B.

DD3R zeolite membrane

The membrane properties, like pore size, are decisive for which components can be separated and under which conditions (*e.g.* temperature or acidity) the membrane can be used. The main subject of this thesis is a *DD3R zeolite membrane*, a relative new type of ceramic membrane recently developed by NGK insulators [8]. Zeolites are crystalline, micro-porous alumino-sillicates with uniform pores of molecular dimensions. In 1987 [9] the concept mostly applied nowadays to make zeolite membranes [10-12] has been defined: an intergrown layer of zeolite crystals. Such a zeolite membrane consists of a macro-porous support layer with a thin zeolite layer in the order of a micrometer on top. The support layer gives the membrane the required mechanical strength. Figure 2 shows a typical cross-section of a thin zeolite film on top of a support layer and a top view of the same membrane.

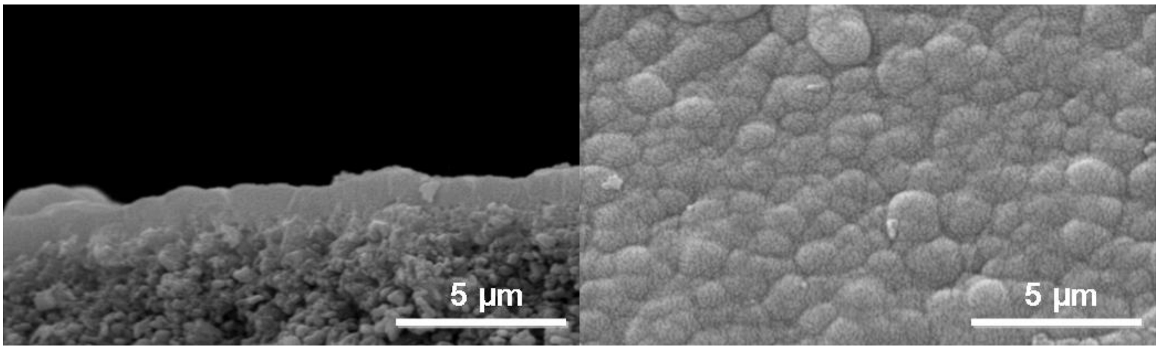

Figure 2. NaA zeolite membrane cross section (left) and top view (right) [13].

Zeolite DD3R consists of three different building blocks (cages) of which only the one with an 8-ring window opening is accessible (Figure 3) [14]. The accessible cavities have three of these windows each, which connect to form a 2-dimensional pore network. Two key aspects differentiates DD3R from other zeolites that make this zeolite particularly interesting to study: its small pore size and the possibility to synthesize it in an all-silica form. The 8-ring window has approximate dimensions of 0.36 × 0.44 nm which makes this material very interesting for separation of light gases which is not possible with larger-pore zeolites, like zeolite MFI, as illustrated in Figure 4. Other 8-ring zeolites are available, however very few have been synthesized successfully in all-silica form. Since it appears to be extremely challenging to make high quality membranes for gas separation from aluminium containing zeolites [15], the all-silica nature of DD3R is a clear advantage. Interesting applications for DD3R can be, for instance, separation of CO_2 or N_2 from CH_4 (natural gas purification) or H_2 purification. In addition to this molecular sieving ability zeolites offer a high thermal and chemical stability which makes them very suitable for use under conditions where chemical reactions are carried out. Instead of replacing a separation unit now also a membrane reactor, an example of process intensification, can be thought of with its specific advantages. A potential application could be in situ hydrogen removal in an alkane dehydrogenation reaction to improve the single pass conversion. More detailed information on zeolites, zeolite membranes and membrane reactors are given in Chapter 1, where the state of development of zeolite membranes in catalysis is reviewed.

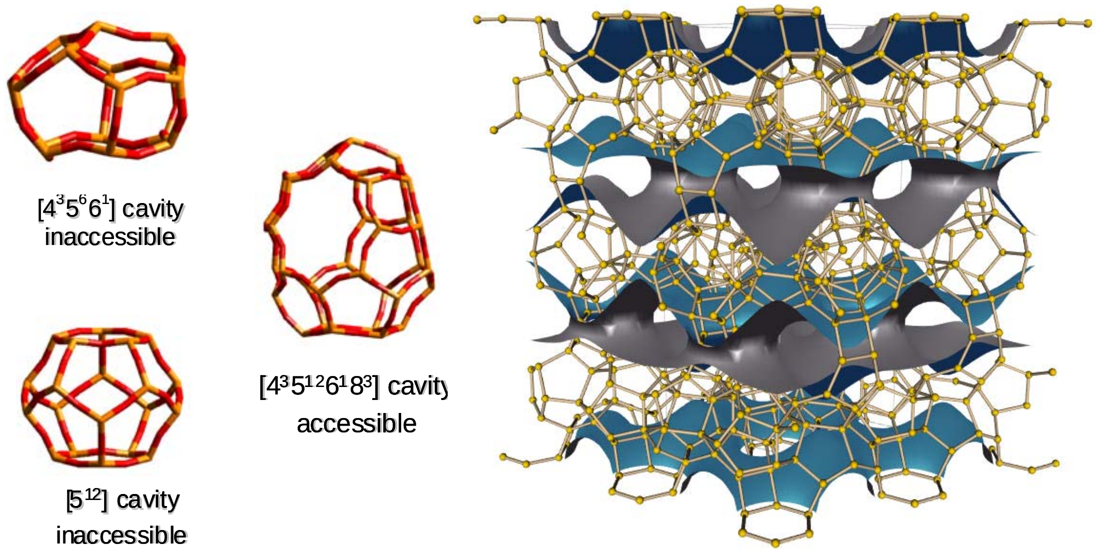

Figure 3. Building blocks and framework of zeolite DD3R.

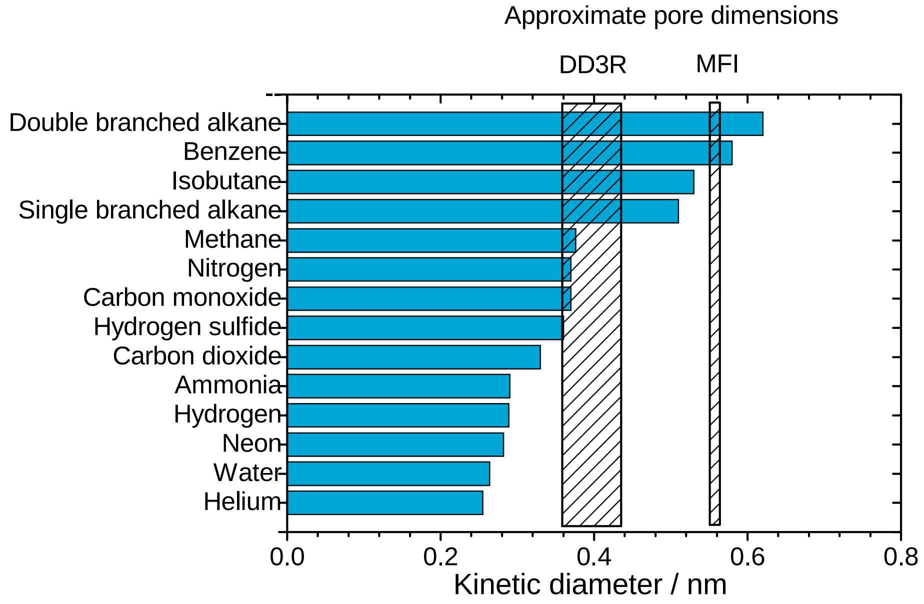

Figure 4. Kinetic diameters of several gases compared to the approximate pore dimensions of DD3R and MFI. After McLeary *et al.* [16].

Mass transport modelling

An important part of this thesis is devoted to modelling of mass transport in zeolites. It is important for process design to be able to describe mixture mass transport accurately. A lot of work has been done in this field and the Maxwell-Stefan approach to mass transport led to very promising results [10,17-22]. This continuum approach treats the adsorbed molecules inside the zeolite as a homogeneous phase. However, each zeolite has its specific topology in which, windows, cages, channels and intersections can be identified, depending on the zeolite type. These different parts of the zeolite can lead to segregated adsorption [23,24]. Moreover, it has been shown that strong concentration dependencies of the diffusivity exist that appear to be strongly related to the zeolite topology [25-29]. It is noteworthy that these problems become manifest particularly in case of small-pore cage-type zeolites like DD3R [24]. Segregated adsorption and loading dependency of the diffusivity severely complicate modelling of mass transport. The challenge is to gain understanding of how these microscopic phenomena influence the macroscopic mass transport properties and translate this understanding in tractable engineering model equations.

Study of the intrinsic diffusion mechanism experimentally can be highly challenging and time consuming, while the diffusivity data can be disguised by phenomena like intracrystalline and surface barriers [30]. Therefore, computer simulations are a powerful tool for development of mass transport models to complement and aid the interpretation of experimental diffusion data.

Aim of the thesis

Anticipating the special properties of the DD3R typology in gas separation, the goal of the project has been to study the *application of DD3R zeolite membranes in separation and catalysis*. Special attention is paid to the understanding and modelling of mass transport across such a membrane. This research should contribute to demonstrated examples of successful use of this type of membrane, which is an important step in the process leading to widespread application of zeolite membranes in the chemical industry.

The thesis objective has been approached by performance testing of a disc- and tubular-shaped DD3R membrane supplied by NGK-insulators. Several gas separations and one reactive separation has been studied: the dehydrogenation of isobutane in a DD3R zeolite membrane reactor. The permeation properties of a series of light gases and mixtures thereof have been analyzed as a function of temperature and pressure and compared to mass transport mechanisms available in literature. It became apparent that loading dependency of the diffusivity was a recurring problem that severely complicates mass transport modelling. Because currently available models did not lead to satisfactory results a new approach to describe diffusion in zeolites has been proposed and applied to single component and binary mixture diffusivity data obtained from computer simulations (molecular dynamics, MD).

Furthermore, this new model has been applied to model experimental zeolite membrane permeation data relevant for natural gas purification applications.

Thesis outline

A review of the current state of zeolite membranes in catalysis is provided in **Chapter 1**. Although this chapter aims specifically at catalytic applications, many conclusions are representative for the state of development of zeolite membranes in general. In **Chapter 2** the single component and binary separation and permeation characteristics of a disc-shaped DD3R membrane are discussed. The focus is on the separation mechanisms of this type of membrane. Considered applications are, for instance: natural gas purification (N_2/CH_4 and CO_2/CH_4 separation), CO_2/air and N_2/O_2 separation. The temperatures studied in this chapter are relatively low (220 - 373 K). In **Chapter 3** the performance of a tubular-shaped DD3R membrane is considered up to 773 K. The gases studied are relevant for catalytic applications like the water gas shift (CO_2, CO and H_2) and the isobutane dehydrogenation reaction. An in-depth discussion on the mass transport mechanism of zeolite membranes at high temperatures is presented. The dehydrogenation of isobutane in a DD3R zeolite membrane reactor is discussed in **Chapter 4**. Application of the DD3R membrane under long-term high temperature operation is investigated and its performance is compared to a conventional packed bed reactor. **Chapter 5** is devoted to the introduction of a new approach to model diffusion in zeolites: the Relevant Site Model (RSM). In **Chapter 5A** the RSM equations are derived for single component and mixture systems. Additionally, the concept of free space relevant for diffusion is introduced. The RSM is validated for single component and binary (CO_2/N_2 and Ar/Ne) diffusivity data in zeolite DDR in **Chapter 5B** and **Chapter 5C**, respectively. All diffusivity data have been obtained from MD simulations. In **Chapter 5D** application of the RSM to other zeolites is studied by analysis of single component and mixture diffusivity data in zeolites DDR, CHA, FAU and MFI. In this chapter all diffusivity data are calculated from MD simulations and taken from literature. In **Chapter 5E**, the RSM is applied to experimental single component (N_2, CO_2 and CH_4) and mixture (CO_2/CH_4, N_2/CH_4 and CO_2/Air) membrane permeation data. Furthermore, a comparison of the RSM and its state-of-the-art rival model (the so-called Reed Ehrlich approach) is made. Finally, because of their similarity, reconciliation of the RSM and dynamically corrected transition state theory is looked for in **Chapter 5F**. In the last chapter, **Chapter 6**, the outcome of the thesis is summarized and evaluated. Note that all chapters have been written in a paper format and can be read independently. Because of this some overlap may occur.

Enjoy!

Johan, Delft, 20-07-2010

References

[1] H. van Suijdam; C. A. M. van der Klein; P. W. Kwant; Tj. R. Gorter; J. Maat; J. H. W. de Wit; B. Ph. ter Meulen; J. de Wit; D. den Ouden; L. A. M. van der Wielen; H. E. A. van der Akker; P. Scholten; van Damme; E. E. Wolff, and H. M. Wijngaard, Innovation Roadmap Scheidingstechnologie, **2004**.

[2] W. J. Koros, Closing Technology Gaps to Enable Energy-Efficient Membrane-Based Separations, Presentation at EuroMembrane 2009, Montpellier, **2009**.

[3] W. J. Koros, *AIChE Journal*, 50, **2004**, 2326.

[4] R. D. Noble and R. Agrawal, *Industrial & Engineering Chemistry Research*, 44, **2005**, 2887.

[5] R. W. Baker and K. Lokhandwala, *Industrial & Engineering Chemistry Research*, 47, **2008**, 2109.

[6] D. Aaron and C. Tsouris, *Separation Science and Technology*, 40, **2005**, 321.

[7] R. W. Baker, *Industrial & Engineering Chemistry Research*, 41, **2002**, 1393.

[8] T. Tomita, K. Nakayama, and H. Sakai, *Microporous and Mesoporous Materials*, 68, **2004**, 71.

[9] H. Suzuki, Composite membrane having a surface layer of an ultrathin film of cage-shaped zeolite and processes for production thereof, **1987**, US Patent 4,699,892.

[10] F. Kapteijn, W. Zhu, J. A. Moulijn, and T. Q. Gardner, Zeolite Membranes: Modeling and Application, in: Structured Catalysts and Reactors, Cybulski, A. and Moulijn, J. A. (Eds), Ch. 20, **2005**, Taylor & Francis Group, Boca Raton, FL, 701.

[11] J. Caro and M. Noack, *Microporous and Mesoporous Materials*, 115, **2008**, 215.

[12] M. A. Snyder and M. Tsapatsis, *Angewandte Chemie-International Edition*, 46, **2007**, 7560.

[13] S. Aguado, J. Gascon, J. C. Jansen, and F. Kapteijn, *Microporous and Mesoporous Materials*, 120, **2009**, 170.

[14] H. Gies, *Zeitschrift fur Kristallographie*, 175, **1986**, 93.

[15] J. Caro, D. Albrecht, and M. Noack, *Separation and Purification Technology*, 66, **2009**, 143.

[16] E. E. McLeary, J. C. Jansen, and F. Kapteijn, *Microporous and Mesoporous Materials*, 90, **2006**, 198.

[17] J. M. van de Graaf, F. Kapteijn, and J. A. Moulijn, *AIChE Journal*, 45, **1999**, 497.

[18] F. Kapteijn, W. J. W. Bakker, G. H. Zheng, J. Poppe, and J. A. Moulijn, *Chemical Engineering Journal and the Biochemical Engineering Journal*, 57, **1995**, 145.

[19] R. Krishna and J. M. van Baten, *Chemical Engineering Science*, 64, **2009**, 3159.

[20] F. Kapteijn, J. A. Moulijn, and R. Krishna, *Chemical Engineering Science*, 55, **2000**, 2923.

[21] R. Krishna and J. A. Wesselingh, *Chemical Engineering Science*, 52, **1997**, 861.

[22] G. R. Gavalas, *Industrial & Engineering Chemistry Research*, 47, **2008**, 5797.

[23] R. Krishna and J. M. van Baten, *Separation and Purification Technology*, 61, **2008**, 414.

[24] R. Krishna and J. M. van Baten, *Chemical Physics Letters*, 446, **2007**, 344.

[25] R. Krishna and J. M. van Baten, *Microporous and Mesoporous Materials*, 109, **2008**, 91.

[26] R. Krishna and J. M. van Baten, *Chemical Engineering & Technology*, 30, **2007**, 1235.

[27] J. R. Xiao and J. Wei, *Chemical Engineering Science*, 47, **1992**, 1123.

[28] J. R. Xiao and J. Wei, *Chemical Engineering Science*, 47, **1992**, 1143.

[29] A. I. Skoulidas and D. S. Sholl, *Journal of Physical Chemistry A*, 107, **2003**, 10132.

[30] L. Heinke, P. Kortunov, D. Tzoulaki, and J. Karger, *Adsorption-Journal of the International Adsorption Society*, 13, **2007**, 215.

1

Zeolite membranes in catalysis; What is new and how bright is the future?

In the early 90s, when the first zeolite membranes were developed, the expected time to successful application in separation and catalytic processes was underestimated. Major reasons for this were the great complexity, like for instance the challenging synthesis of thin defect free membranes and a good understanding of multi-component transport in zeolite membranes; and the high installation costs. But, reasons to use zeolite membranes – their thermal and chemical stability, catalytic and separation properties – are without doubt well founded and industrial application appears to be technically feasible. However, the currently estimated installed membrane cost (€ 1000 – 3000 m^{-2}) appears to be too high and can be considered the predominant hurdle with respect to successful widespread industrial application. For current supported zeolite membrane technology the support price is a dominant cost factor which should be reduced.

Zeolite membranes are developing into a more mature technology, which is emphasized by the industrial application of zeolite membranes in alcohol dehydration. Yet it remains a technology with high *potential*, since further applications are still lacking. But, taking into account the solid progress made in the last decade and the demonstrated technological benefits, application of zeolite membranes in the field of catalysis has a serious prospect.

This chapter is based on the following publication:

J. van den Bergh, N. Nishiyama and F. Kapteijn, Zeolite membranes in catalysis; what is new and how bright is the future?, In: Novel concepts in catalysis and chemical Reactors, A. Cybulski, J. A. Moulijn and A. Stankiewicz (eds), Wiley, New York, **2010**, 211.

1 Introduction

Membranes in catalysis can be used to improve selectivity and conversion of a chemical reaction, improve stability and lifetime of the catalyst and improve the safety of operation. The best-known example is in situ removal of products of an equilibrium-limited reaction. But, many more ways of application of a membrane can be thought of [1-3], such as using the membrane as a reactant distributor to control the reactant concentration levels in the reactor, or performing catalysis inside the membrane and have control on reactant feed and product removal. Although we limit ourselves in this chapter to the topic of zeolite membranes in catalysis, much detail is relevant for separation processes as well.

Many types of membranes exist and each membrane has its specific field where it can be applied best. Comparing polymeric and inorganic membranes reveals that for harsher conditions and high temperature applications inorganic membranes outperform polymeric membranes. In the field of heterogeneous catalysis elevated temperatures are quite common and therefore this is a field where inorganic membranes could find their application par excellence.

Main advantage of zeolite membranes compared to other porous membranes is their uniform pore size due to the crystalline nature of the material. This may lead to molecular sieving effects. Currently known zeolites have pore sizes ranging from approximately 0.26 (6 ring window) to 0.74 nm (14 ring window) yielding an extensive library of materials to match a desired application. Dense membranes, like metallic or perovskitic, are often restricted to transport of only one component (*e.g.* H_2 or O_2). This is a limitation on the one hand, but implies an absolute separation for a limited number of very relevant (reactive) separations on the other.

In this chapter the focus will be on how zeolite membranes can be applied in the field of catalysis and to what extent this is successful. The latter will be illustrated by reviewing some commonly studied zeolite membrane applications. Finally, the current hurdles that impede industrial application are discussed and some remarks on the status of zeolite membranes in catalysis are made. But first, the properties of zeolite (membranes) will be explored in some more detail to acquaint the reader with this interesting class of materials.

1.2 Zeolites: a versatile, well-defined class of materials

Zeolite catalysts and adsorbents are widely accepted in industry. In 1948 commercial adsorbents based on synthetic aluminosilicates zeolite A and X were available [4]. Zeolite Y as FCC catalyst was commercially available in 1964 [5].

Zeolites are crystalline aluminosilicates with well-defined pores. These pores are of molecular dimensions and can be classified as small (8-ring) medium (10-ring) and large pore (12-ring) zeolites. Each zeolite has its specific pore connectivity forming a one, two or three-dimensional pore network. This interior network is well-defined and can consist of combinations of channels, cages, intersections or side-pockets that each have their influence on the adsorptive, catalytic, diffusive and molecular sieving properties of the zeolite. The aforementioned properties can be varied by selecting the type of zeolite, the chemical composition of the framework (*e.g.* Si-Al ratio) or the counter ion present in the structure to balance the charge of the framework aluminium atoms. The framework types of some well known zeo-types are presented in Figure 1. Zeolite structures can have anisotropic pore networks. A well-known example of this is the MFI pore network that consists of straight and sinusoidal channels with slightly different pore diameters of ~0.51-0.54 and 0.54 nm, respectively. Due to this anisotropy molecules enter a MFI crystal from either type of channels depending on the crystal facet.

Other materials, closely related to zeolites, with zeo-type structures are silico-aluminophosphates (SAPOs) and aluminophosphates (ALPOs) [6].

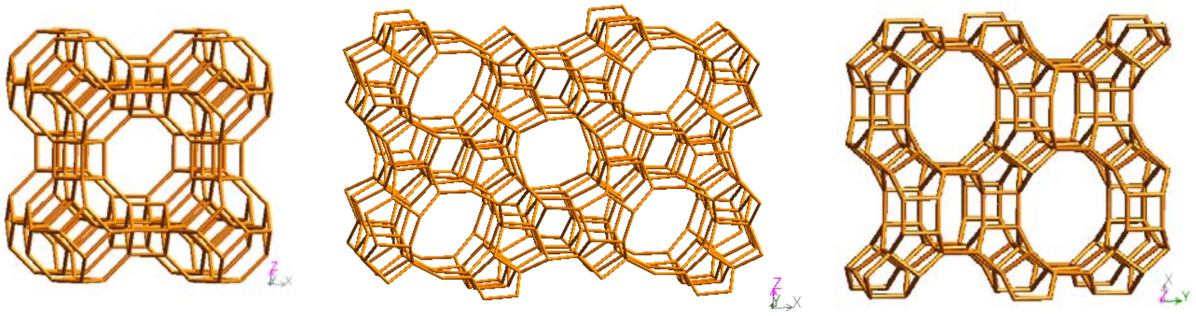

LTA 8-ring | MFI (ZSM-5) 10-ring | MOR 12-ring

3D ~0.3-0.4 nm | 3D ~0.55 nm | 1D ~0.68 nm

Figure 1. Framework types of some well-known zeolites with their specific pore size and pore network dimensions [6].

1.2.1 Zeolite catalysis

Aluminium containing zeolites are inherently catalytically active in several ways. The isomorphic substituted aluminium atom within the zeolite framework has a negative charge that is compensated by a counter ion. When the counter ion is a proton, a Brønsted acid site is created. Moreover, framework oxygen atoms can give rise to weak Lewis base activity. Noble metal ions can be introduced by ion exchanging the cat-ions after synthesis. Incorporation of metals like Ti, V, Fe and Cr in the framework can provide the zeolite with activity for redox reactions. A well-known example of the latter type is titanium silicalite-1 (TS-1): a redox molecular sieve catalyst [7].

It is not the catalytic activity itself that make zeolites particularly interesting, but the location of the active site within the well-defined geometry of a zeolite. Due to the geometrical constraints of the zeolite the selectivity of a chemical reaction can be increased by three mechanisms: reactant selectivity, product selectivity and transition-state selectivity. In the case of reactant selectivity bulky components in the feed do not enter the zeolite and will have no chance to react. When several products are formed within the zeolite, but only some are able to leave the zeolite, or some leave the zeolite more rapidly, we speak about product selectivity. When the geometrical constraints of the active site within the zeolite prohibit the formation of products or transition states leading to certain products, transition state selectivity applies.

1.2.2 Zeolite membranes

Because of their remarkable molecular sieving properties it is not surprising that many attempts have been made to make zeolite based membranes or films. The first zeolite membranes were reported about 20 years ago. The first systems were mixed matrix systems [8] and in 1987 the concept mostly applied nowadays to make zeolite membranes was defined: an intergrown layer of zeolite crystals [9]. Such a zeolite membrane consists of a macro-porous support layer with a thin zeolite layer in the order of a micrometer on top. The support layer gives the membrane the required mechanical strength. In time, the quality of zeolite membranes improved and in 2001 the first industrial-scale application of a zeolite membrane was accomplished by Mitsui [10]. They developed a large-scale pervaporation plant based on NaA zeolite membranes to dewater alcohol water mixtures (~90% alcohol), producing 530 L h^{-1} of solvents. Examples of zeolites that have been prepared as membrane are: MFI (ZSM-5 / Silicalite-1) [11], LTA (zeolite A) [12] , FAU (Faujasite) [13], MOR (Mordenite) [14], DDR (DD3R) [15,16], CHA (Chabasite, SAPO-34) [17], BEA (Beta) [18], FER (Ferrierite) [19] and SOD (Sodalite) [20].

The composition of the framework (Si-Al ratio) is a very important factor regarding the application of a zeolite membrane and influences the membrane properties in various ways. Zeolites with low Si-Al ratios are very hydrophilic and, therefore, often used for water separation. An advantage of this type of membranes in such applications is that possible membrane defects are sealed of by strongly adsorbing water. But, it is found that membranes synthesized with higher Si-Al ratios have less defects and higher quality membranes are obtained [21]. Therefore, for gas separation applications, high silica zeolite membranes are the preferred choice. As a final remark, the chemical and hydrothermal stability of a zeolite is high in general, but zeolites with low Si-Al ratios are the least stable. An example of this are the low silica zeolite A membranes that are very suitable for water removal from alcohols, but are unstable in the presence of acids [22]. All-silica zeolites are very stable and, therefore, much effort is put in synthesising zeolite membranes with this composition.

2 Application options

Membranes can be applied to catalysis in different ways. In the vast majority of literature reports the membrane is used on the reactor level (cm to m scale) enclosing the reaction mixture (Figure 2). In most cases the membrane is used as an inert permselective barrier in an equilibrium-limited reaction where at least one of the desired products is removed in situ to shift the extent of the reaction past the thermodynamic equilibrium. A second option is to apply the membrane on the particle level (mm scale) by coating catalyst particles with a selective layer. As a third option, application at the micro level (sub-μm scale) is distinguished. This option encompasses, for example, zeolite-coated crystals or active clusters (*e.g.* metal nano-particles). Advantages of the latter two ways of application are that there are no sealing issues, it is easy to scale up, the membrane area is large per unit volume and if there is a defect in the membrane this will have a very limited effect on the overall reactor performance. Because of these advantages it is believed that using a zeolite membrane on the particle or micro level will be much easier than application at the reactor level.

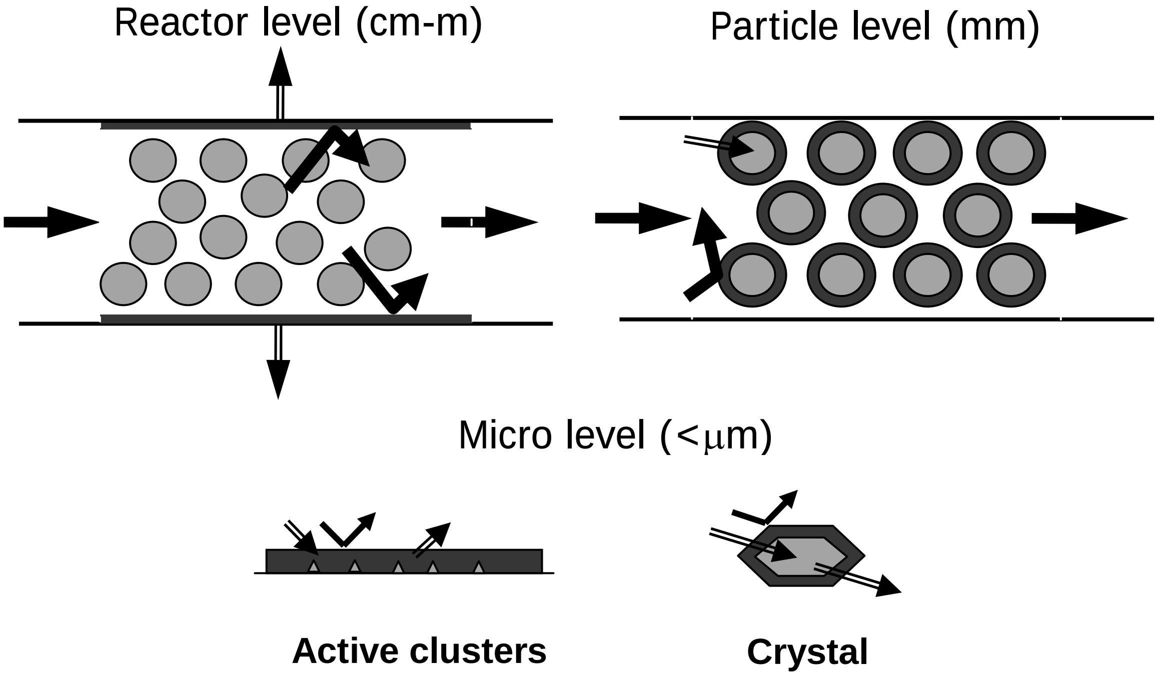

Figure 2. Membranes can be applied at the reactor, particle and micro level.

2.1 Reactor level

2.1.1 Membrane reactors: nomenclature

Membrane reactors are defined here based on their membrane function and catalytic activity in a structured way, predominantly following Sanchez and Tsotsis [2]. The acronym used to define the type of membrane reactor applied at the reactor level can be set-up as shown in Figure 3. The membrane reactor is abbreviated as MR and is placed at the back of the acronym. Because the word membrane suggests that it is permselective, an *N* is added to the acronym in the case that it is non-permselective. When the membrane is inherently catalytically active, or a thin catalytic film is deposited on top of the membrane, a *C* (catalytic) is added. When catalytic activity is present besides the membrane additional letters can be added to indicate the appearance of the catalyst, *e.g.* packed bed (*PB*) or fluidized bed (*FB*). In the case of an inert and non-permselective membrane the non-membrane catalytic activity is often not mentioned in the acronym.

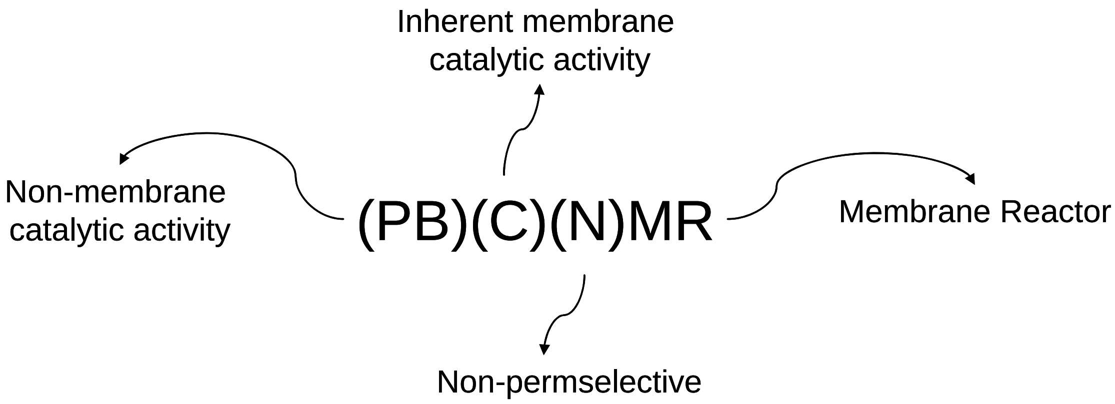

Figure 3. Meaning of acronyms used to define types of membrane reactors at the reactor level, after [2].

Before going into detail on the different membrane reactor configurations it is good to realize that the main function of the membrane can be different for each configuration:

- **Extractor**: Membrane is used to selectively remove components from a reaction mixture
- **Distributor**: Membrane is used to selectively feed components to a reaction mixture
- **Contactor**: Membrane is used to create a reaction front. When all reactants are fed from one side of the membrane it is called a **flow-through** contactor (or reactor), when reactants are fed from opposite sides of the membrane it is called an **interfacial** contactor.

2.1.2 Packed bed membrane reactor

Most research reports involve an inert, selective membrane that encloses a packed bed of catalyst particles: a packed bed membrane reactor (**PBMR**). It must be noted that the catalyst bed can also be fluidized for example, but other types than packed beds are rarely found in literature. Advantages of this type of reactor can be:

1) *Increase of single pass conversion* due to selective removal of products in an equilibrium limited reaction,
2) *Increase of selectivity* by selective removal of desired intermediate products or by selectively distributing one of the reactants and thereby suppressing undesired side reactions and
3) *Improving safety* by selective feeding of reactant and thereby preventing formation of, for example, explosive mixtures.

Typical examples of PBMRs were the membrane is used as extractor to shift the equilibrium conversion are dehydrogenation of alkanes [23] and esterification and etherification [22] reactions. An interesting point is that, for example in dehydrogenation, a low operating pressure is selected to obtain a higher conversion. In a membrane reactor, however, with increasing operating pressure both the reaction rate as membrane permeation rate can be increased without sacrificing a high conversion level, since this is ultimately not restricted to the equilibrium conversion of the feed composition. In this way a membrane reactor can lead to process intensification [24], but integration of the reaction and separation steps leads to a decrease in degrees of freedom to optimize the overall process performance.

Zeolite membranes can also be envisaged as distributors. Gora *et al.* used a silicalite-1 tubular membrane to selectively feed linear C6 alkanes from a mixed isomers feed to a platinum containing chlorinated alumina fixed-bed catalyst. By combining the separation and reaction step into one unit the ongoing isomerisation reaction of linear C6 alkanes provides a driving force for the separation of linear and branched isomers. Furthermore, combining these process steps might lead to higher energy efficiency, better process control and lower energy consumption [25]. An MFI membrane was used by Cruz-Lopez *et al.* [26] in the selective oxidation of butane to maleic anhydride, allowing the use of much higher butane feed concentrations while staying out of the flammability region.

2.1.3 Catalytic membrane reactor

In the case of a catalytic membrane reactor (**CMR**) the membrane is (made) intrinsically catalytically active. This can be done by using the intrinsic catalytic properties of the zeolite or by making the membrane catalytically active. When an active phase is deposited on top of a membrane layer this is also called a CMR because this becomes part of the composite membrane. In addition to the catalytic activity of the membrane a catalyst bed can be present (**PBCMR**). The advantages of a CMR can be:

1) *Improved selectivity* due to good control of contact time and thereby limiting the occurrence of unwanted consecutive reactions,
2) *Reduction of mass transfer limitations*,
3) *Shift in chemical equilibrium conversion* due to a reduced concentration level of faster diffusing components in the membrane and
4) *Safer operation* when the membrane is used as an interfacial contactor keeping certain reactants segregated and preventing the formation of flammable or explosive mixtures.

Hasegawa *et al.* [27] selectively oxidized CO in a hydrogen rich mixture using a Pt loaded Y-type zeolite membrane. The envisaged application is to protect fuel cell electrodes from CO poisoning by zeolite films. In the methanol to olefins (MTO) process methanol is converted by consecutive reactions into olefins and can further react into paraffins. Masuda *et al.* [28] applied a H-ZSM5 membrane in this reaction. The pressure drop over the membrane was used to control the contact time and a high selectivity (80-90%) at high conversions (60-98%) was obtained.

2.1.4 Non-selective membrane reactors

The last two configurations that involve a non-selective membrane are, to our best knowledge, not encountered in zeolite membrane reactors. Zeolite membranes are almost always selective and suffer from the trade off that high selectivities are typically combined with low fluxes. Therefore, when a non-selective membrane process is envisaged, a meso- or macro-porous membrane would be the preferred choice. In the case of a catalytic non-permselective membrane reactor (**CNMR**) the stoichiometric feeding of reactants can be controlled. A well-known example of such a membrane is presented by Sloot *et al.* [29] for the oxidation of H_2S to elemental sulphur and water. When the reaction is fast compared to mass transport in the membrane, a thin reaction zone is found in the membrane. The location of the reaction front is determined by the fluxes of the components to the reaction front. In this way the system self-regulates stoichiometric feeding of reactants.

A packed bed non-permselective membrane reactor (**PBNMR**) is presented by Diakov *et al.* [30] who increased the operational stability in the partial oxidation of methanol by feeding oxygen directly and methanol through a macro-porous stainless-steel membrane to the packed bed. Al-Juaied *et al.* [31] used an inert membrane to distribute either oxygen or ethylene in the selective ethylene oxidation. By accounting for the proper kinetics of the reaction the selectivity and yield of ethylene oxide could be enhanced over the fixed bed reactor operation.

2.2 Particle level

2.2.1 Basic concepts

Figure 4 shows the basic concept of the particle-level membrane reactor that gives (a) selective addition of reactants to the reaction zone and (b) selective removal of products from the reaction zone. In the first case, if the diffusivity of one reactant (A) is much larger than that of the other components (B), the reactant (A) selectively diffuses into a catalyst particle through a membrane. Undesired reactions or the adsorption of poisons on the catalysts can be prevented. In the second case, the reaction has a limited yield or selectivity controlled by thermodynamics. The selective removal of desired product from the catalyst particle gives enhancement of selectivity when the diffusivity of one product (R) is much higher than that of the other products (S).

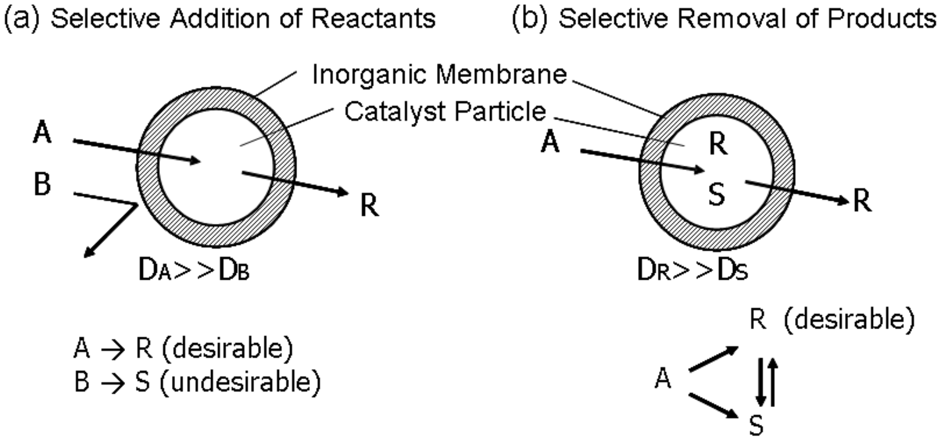

Figure 4. Principle of operation of a catalyst particle coated with a permselective membrane.

2.2.2 Reactant selective reactions

Van der Puil *et al.* have developed a coating method of silicalite-1 on spherical Pt/TiO_2 particles (silicalite/Pt/TiO_2) [32]. The silicalite/Pt/TiO_2 particles were used for hydrogenation of linear and branched alkenes. At 100 °C conversion ratios (selectivities) up to 70 were obtained. The high selectivity was caused by diffusion limitations. Nishiyama *et al.* [33,34] have developed the same type of catalyst: silicalite-1 on spherical Pt/TiO_2 particles (silicalite/Pt/TiO_2). Also in this case the silicalite/Pt/TiO_2 particles were used for hydrogenation of linear and branched alkenes. The composite silicalite-1/Pt/TiO_2 catalyst showed 1-hexene (1-Hex)/ 3,3-dimethylbut-1-ene (3,3-DMB) hydrogenation selectivities of 12 to 20 at 50˚C and 18 to 30 at 100˚C due to the selective permeation of the reactant 1-Hex into Pt/TiO_2 particles through the silicalite-1 layer. Deactivation of the catalyst was also reduced, probably by protection against poisoning impurities in the feed. Zhong *et al.* [35] reported defect-free zeolite-4A membranes coated on Pt/γ-Al_2O_3 particles. Oxidation of a mixture of CO and *n*-butane over this composite catalyst demonstrated the concept of reactant selectivity. The conversion of CO was over 90%, while *n*-butane hardly reacted. Since a trace amount of CO often co-exists in hydrocarbon feed streams and CO can poison the catalysts of desired reactions, the zeolite coated catalyst is attractive for the removal of CO from hydrocarbon streams.

2.2.3 Product selective reactions

As an example of the selective removal of products, Foley *et al.* [36] anticipated a selective formation of dimethylamine over a catalyst coated with a carbon molecular sieve layer. Nishiyama *et al.* [37] demonstrated the concept of the selective removal of products. A silica-alumina catalyst coated with a silicalite membrane was used for disproportionation and alkylation of toluene to produce *p*-xylene. The product fraction of *p*-xylene in xylene isomers (*para*-selectivity) for the silicalite-coated catalyst largely exceeded the equilibrium value of about 22%. The high *para*-selectivity in the toluene disproportionation is caused by the selective removal of *p*-xylene from the silica-alumina particles, which leads to an apparent equilibrium shift between xylene isomers.

The zeolite membrane has been also used as a catalytic membrane. Tsubaki *et al.* [38-40] reported a ‘capsule’ catalyst for isoparaffin synthesis based on the Fischer–Tropsch reaction. A H-ZSM-5 membrane was coated onto the surface of a pre-shaped Co/SiO_2 pellet. Syngas passed through the zeolite membrane to reach the Co/SiO_2 catalyst to be converted, and all straight-chain hydrocarbons formed left the particle through the zeolite channels undergoing hydrocracking as well as isomerization. A narrow, non-Anderson–Schultz–Flory product distribution was obtained. Contrary to a physical mixture of HZSM-5 and Co/SiO_2, C_{10+} hydrocarbons were suppressed completely on this catalyst, and the selectivity to middle isoparaffins was considerably improved.

2.3 Micro level

The principles of application of zeolite membranes at the micro level can be very similar as on the particle level, but now at the crystal (μm) scale, enclosing the active catalytic material. As described in the previous paragraph, the silica-alumina catalyst covered with the silicalite membrane showed excellent *p*-xylene selectivity in disproportionation of toluene [37] at the expense of activity, because the thickness of the silicalite-1 membrane was large (40 μm), limiting the diffusion of the products. In addition, the catalytic activity of silica-alumina was not so high. To solve these problems, Miyamoto *et al.* [41-43] have developed a novel composite zeolite catalyst consisting of a zeolite crystal with an inactive thin layer. In Miyamoto’s study [41], a silicalite-1 layer was grown on proton exchanged ZSM-5 crystals (silicalite/H-ZSM-5) [42]. The silicalite/H-ZSM-5 catalysts showed excellent *para*-selectivity of >99.9 %, compared to the 63.1% for the uncoated sample, and independent of the toluene conversion.

The excellent high *para*-selectivity can be explained by the selective escape of *p*-xylene from the H-ZSM-5 catalyst and inhibition of isomerization on the external surface of catalysts by the silicalite-1 coating. In addition to the high *para*-selectivity, the toluene conversion was still high even after the silicalite-1 coating because the silicalite-1 layers on H-ZSM-5 crystals were very thin.

High catalytic activity and selectivity of silicalite-1/H-ZSM-5 composites must be caused by the direct pore-to-pore connection between H-ZSM-5 and silicalite-1 as revealed by Fe-SEM and TEM [43]. The silicalite-1 crystals were epitaxially grown on the surface of the H-ZSM-5 crystals.

The zeolite overgrowth has been reported for FAU on EMT zeolite [44] and MCM-41 on FAU zeolite [45]. On the other hand, in this study, zeolite layers were grown on the zeolite with the same framework structure, resulting in high coverage of ZSM-5 crystals with silicalite layers and high *para*-selectivity. The zeolite crystals with oriented thin layer on their external surface are expected to form a new class of shape-selective catalysts.

3 Potential applications

In this paragraph an attempt is made to sketch the current status of zeolite membrane reactors with respect to specific applications. The application of zeolite membrane reactors is strongly related to the development status of zeolite membranes. Topics that are discussed are the most often studied reactions for zeolite membrane applications: dewatering, (de)hydrogenation and isomerisation (*e.g.* xylenes) and some special applications: zeolite membranes in micro-reactors and sensor applications.

3.1 Dehydration

In situ removal of water of can be beneficial by shifting the equilibrium conversion of, for example, esterification, etherification or condensation polymerization reactions. The state of development of zeolite membranes for this type of separation processes is high: the first commercial application of a zeolite-membrane process has been accomplished by Mitsui [10]. Water-selective zeolite membrane reactors are not commercially available, but several research groups have explored this type of application. In situ dehydration of esterification reactions have been recently investigated with Zeolite A [22,46], T-type [47] , MOR [22] and H-ZSM5 [48] membranes. The H-ZSM5 membrane was particularly interesting because there was no catalytic activity besides the membrane. In all cases a proof of principle has been demonstrated that the membrane reactor yields a higher conversion than the packed-bed reactor without membrane. Due to the very high membrane selectivity towards water, high conversions of 80 to 95 % are found.

Zeolite A is a very successful membrane for water separation from alcohols, but it suffers from stability issues under acid conditions [22]. Usually a liquid phase should be avoided and vapour permeation is preferred for this reason. Recent developments show that the hydrophilic MOR [22], PHI [49] and SOD [50] membranes are more stable under acid conditions in combination with a good membrane performance.

The preferred choice of a water selective membrane up to now has been hydrophilic membranes because of their high water affinity. However, recently Kuhn *et al.* reported an all-silica DDR membrane for dehydration of ethanol and methanol with high fluxes (up to 20 kg m^{-2} h^{-1}) and high selectivities (H_2O/ethanol ~ 1500 and H_2O/methanol ~ 70 at 373 K) in pervaporation operation. The separation is based on molecular sieving with high water fluxes comparable to well-performing hydrophilic membranes [51].

Recently, high-quality sodalite membranes for water separation have been developed by Khajavi *et al.* [20,52]. These zeolite membranes should allow an absolute separation of water from almost any mixture since only very small molecules such as water, hydrogen, helium and ammonia can theoretically enter through the six-membered window apertures. Water/alcohol separation factors >> 10,000 have been reported with reasonable water fluxes up to 2.25 kg m^{-2} h^{-1} at 473 K in pervaporation experiments. A demonstration of successful application of the SOD membrane has been given for esterification reactions [53].

Furthermore, the application of the SOD membrane in a Fischer-Tropsch reaction has been investigated. The advantages of water removal in a FT reaction are threefold: 1) reduction of H_2O promoted catalyst deactivation, 2) increased reactor productivity, and 3) displaced water gas shift (WGS) equilibrium to enhance the conversion of CO_2 to hydrocarbons [54]. Khajavi *et al.* report mixture H_2O/H_2 separation factors >> 10,000 and water fluxes of 2.3 kg m^{-2} h^{-1} under FT conditions for their HSOD membrane. A conceptual process design indicated that application of SOD membranes in the FT reaction could be economically viable [54].

3.2 Dehydrogenation

The proof of principle that hydrogen selective zeolite membranes can increase the conversion compared to a classical packed bed reactor in a dehydrogenation reaction has been demonstrated by various groups. Examples are the dehydrogenation of isobutane in combination with a ZSM5 membrane [23,55], dehydrogenation of cyclohexane with a FAU membrane [56] and dehydrogenation of ethylbenzene to styrene with a Fe-ZSM5 [57], Al-ZSM5 [57] and a silicalite membrane [58]. Note that in the cyclohexane dehydrogenation the FAU membrane removed both hydrogen and benzene selectively from the reaction mixture. The conversion increase in that case was attributed mostly to the removal of benzene, which had the highest permeance across the membrane. Table 1 summarises the results of the zeolite membrane reactors in terms of conversion increase, hydrogen permeance and hydrogen separation performance.

The separation factors are relatively low and consequently the MR is not able to approach full conversion. With a molecular sieve silica (MSS) or a supported palladium film membrane an (almost) absolute separation can be obtained. The MSS membranes however, suffer from a flux / selectivity trade-off meaning that a high separation factor is combined with a relative low flux. Pd membranes do not suffer from this trade-off and can combine an absolute separation factor with very high fluxes. A favourable aspect for zeolite membranes is their thermal and chemical stability. Pd membranes can become unstable due to impurities like CO, H_2S and carbonaceous deposits and for MSS membrane hydrothermal stability is a major concern [59]. But the performance of the currently used zeolite membranes is insufficient to compete with other inorganic membranes, which is also concluded by Caro *et al.* [60] for the use of zeolite membranes for hydrogen purification.

Table 1. A comparison of recent examples of zeolite membranes in dehydrogenation reactions.

Membrane type	*T* K	Dehydrogenated Hydrocarbon	H_2 permeance mol m^{-2} s^{-1} Pa^{-1}	H_2 / Hydrocarbon mixture selectivity	PBC[a] %	MRC[b] %	Ref.
ZSM5	783	i-Butane	$1.1 \cdot 10^{-7}$	70 (H_2 / i-Butane)	29.1	48.6	[24]
ZSM5	730	i-Butane	-	9 (H_2 / i-Butane)	10	55	[55]
FAU	473	Benzene	$8 \cdot 10^{-7}$	10 (Ben. / Cyclohex.) 4 (H_2 / Cyclohex.)	32.2	72.1	[56]
Fe-ZSM5	873	Ethylbenzene	$20 \cdot 10^{-7}$	25.8 (H_2 / Propane)	45.1	60.1	[57]
Silicalite	883	Ethylbenzene	$6 \cdot 10^{-7}$ (573 K)	15.4 (H_2 / n-Butane) (573 K)	67.5	74.8	[58]
MSS[c]	623	-	$9 \cdot 10^{-7}$	13 (H_2/CO_2)			[59]
MSS	623	-	$0.5 \cdot 10^{-7}$	> 1000 (H_2/CO_2)			[59]
Pd film	773	-	$40.9 \cdot 10^{-7}$	inf.			[60]
DDR	298	-	$0.2 \cdot 10^{-7}$	~100 (H_2/CH_4)[d]			[16]
DDR	298	-	$0.2 \cdot 10^{-7}$	>1000 (H_2/n-C_4)[d]			[16]
Nanoblock	298	-	$0.69 \cdot 10^{-7}$	>1200 (H_2/CH_4)			[61]

[a] PBC = Packed Bed Conversion; [b] MRC = Membrane Reactor Conversion; [c] MSS = Molecular Sieve Silica; [d] Permselectivity.

Interestingly, the currently used zeolite membranes are all 10-membered-ring zeolites or larger. It can be expected that smaller-pore zeolites, like 6- or 8-membered-ring zeolites, would yield significantly higher separation factors or even absolute separation. Examples of such zeolites are: 1) the small-pore zeolite DDR that yields ideal separation factors of H_2 with respect to CH_4 and *n*-C_4 of >100 and >1000, respectively at 298 K [15] and 2) the nanoblock zeolite membrane of Nishiyama *et al.*, which they claimed had a pore size smaller than 8-membered-ring zeolites and could separate H_2 from CH_4 with a selectivity of more than 1200

[61]. Although the fluxes of these membranes are still relatively low, they appear to be promising candidates with a significantly better performance than currently used zeolite membranes in hydrogen selective MRs.

3.3 Isomer separation

Separation of isomers is an application where zeolite membranes could be specifically interesting due to their well-defined pores that can lead to molecular sieving effects. An application that is often considered is the xylene isomerisation and related reactions.

Several research groups have attempted to improve the conversion and selectivity of the xylene isomerisation. Van Dyk *et al.* [62] carried out an isomerisation of *m*-xylene in a silicalite-1 PBMR and compared it with the performance of a classical packed bed reactor. The membrane had a very high *para* to *ortho* selectivity that led to 100 % selectivity in the permeate stream of the MR. The overall *para* selectivity (retentate + permeate) was enhanced from 58 to 65 % and the yield was increased from 21 to 23 %. Haag *et al.* [63] showed, however, how difficult it is to compare data in an experimental study. A comparison was made between a conventional packed bed reactor and a CMR (H-ZSM5). In the CMR the only catalytic activity was introduced by the intrinsic activity of the membrane. It was found by a kinetic study that the activity of the conventional H-ZSM5 catalyst was not comparable to the activity of the membrane. Furthermore, conversions well below the calculated equilibrium conversions were obtained making it difficult to draw conclusions based on the obtained data. No convincing improvements were achieved mainly due to the poor membrane performance. Tarditty *et al.* [64] used a CMR (Pt-ZSM5) and a PBMR (Ba-ZSM5) to perform a *m*-xylene isomerisation reaction. In both cases the MRs showed a reasonable improvement of the selectivity and yield as compared to a conventional packed bed reactor.

These three studies show that MFI membranes can enhance yield and selectivity in a xylene isomerisation process, but the improvements obtained are not yet convincing regarding commercial application. An approach that seems more promising is a membrane reactor applied at the particle level. Van Vu *et al.* [42] demonstrated that *para*-xylene can be synthesized from toluene and methanol with very high selectivities (>99.9), which sustained even at higher conversions. In their studies a H-ZSM5 catalyst particle was coated with a inert silicalite layer. The increase in selectivity may be attributed to the selective mass transport resistance introduced by the silicalite layer. Additionally, the coated catalyst particles deactivated slower compared to the uncoated particles, probably due to a reduction in coke formation by surface acid groups by the coating.

3.4 Micro-reactors

Reasons to use micro-reactors can be among other things: 1) reduced mass and heat transfer limitations, 2) high area to volume ratio, 3) safer operation and 4) ease to scale up by numbering out. Advantages of scaling down zeolite membranes are that it could be easier to create defect-free membranes and that by using single-crystal membranes the advantages of oriented crystals may be more efficiently exploited. Studies on zeolite membranes applied in micro reactors are scarce and most of them focus on demonstrating that zeolite films can very well be synthesized on the micro reactor scale.

The group of Yeung has shown that with a micro zeolite-membrane reactor the yield and selectivity of equilibrium-limited reactions can be improved similarly as on the macro scale. For the Knoevenagel condensation in situ water removal in a micro reactor using a NaA [65] and a ZSM5 [66] zeolite membrane increased the yield as compared to a conventional micro reactor. A typical yield increase from ~60 (equilibrium) to ~85% was demonstrated [66]. A slight yield increase and a reduction in catalyst deactivation could be achieved by application of a micro membrane-reactor in the oxidation of aniline. These advantages are attributed to the in situ removal of water by the ZSM5 zeolite membrane [67].

The application of zeolite membranes in micro reactors is still in an early stage of development, and suffers sometimes from unexpected problems arising from template removal [68]. However, several application examples of zeolite membranes in micro-structured devices have been demonstrated yielding similar advantages as was to be expected from experiences on the macro scale. Because of the high surface to volume ratio of micro reactors the application of zeolite membranes in these systems has great potential.

3.5 Chemical Sensors

Adequate techniques to accurately and selectively detect concentration levels are available, but are mostly expensive, slow and complex. Cheaper sensors are available but the working principle is usually not very selective. A wealth of different sensing techniques exists where typical sensor principles rely on changes in mass (micro balance), electrical properties (*e.g.* capacitance) or optical properties (*e.g.* IR). A good sensor has a fast response, high sensitivity and high selectivity. Additionally, for several applications sensors need to withstand harsh conditions (*e.g.* exhaust gases) for long times. Zeolites are potential candidates to improve the sensitivity and selectivity by exploiting their molecular sieving, selective adsorption and catalytic properties.

Three different ways how a zeolite membrane can contribute to a better sensor performance can be distinguished: 1) add-on selective adsorption or molecular sieving layer to the sensor thereby improving selectivity and sensitivity, 2) the zeolite layer acts as active sensing material and adds the selective adsorption and molecular sieving properties to this and 3) the zeolite membrane adds a catalytically active layer to the sensor improving the selectivity by specific reactions.

A very recent example of the first case is presented by Vilaseca *et al.* [69] where a LTA coating on a micro-machined sensor made the sensor much more selective to ethanol than methane. Moos *et al.* [70,71] report a H-ZSM5 NH_3 sensor based on impedance spectroscopy using the zeolite as active sensing material. At elevated temperatures (> 673 K) NH_3 still adsorbs significantly in contrast to CO_2, NO, O_2 and hydrocarbons leading to a NH_3 selective sensor. Arguments to use a zeolite based sensor in NH_3 detection for automotive applications are: low cost, high temperature stability, and it can be applied as thick film technology, of common use in the automotive industry [70]. The sensors were tested on an engine test bank and the authors claim that “the sensor itself meets all the technological and economical demands of the automotive industry” [71].

When NOx levels are measured electrochemically, NO and NO_2 can lead to opposing signals because NO is oxidized and NO_2 tends to be reduced. Moreover, it is preferred to obtain a ‘total’ NOx measurement instead of only one of the constituents. The latter can be achieved by catalytically equilibrating the feed with oxygen before contact with the sensor by coating an active zeolite layer on top or placing a active catalyst bed in front of the sensor. Both approaches have been demonstrated successfully with a Pt-Y zeolite as active catalyst [72,73]. Additional advantage of the filter bed is a reduction in the cross sensitivity with CO due to CO oxidation above 673 K.

In a similar manner Sahner *et al.* [74,75] utilized a Pt-ZSM-5 layer to reduce the cross-sensitivity of a hydrocarbon (propane) sensor towards CO, propene, H_2 and NO at 673 K. The zeolite layer was put on the sensor as a paste. The improved cross-sensitivity is attributed to selective oxidation of all considered components except propane. Trimboli *et al.* [76] demonstrated the same concept by using a Pt-Y zeolite for the CO oxidation, maintaining the sensitivity for propane.

The added value, variety of use and methods to apply zeolite coatings or films in sensor applications has convincingly been demonstrated. Although current trends focus on miniaturization of sensors and creating smaller zeolite crystals and thinner films, to decrease the response time of the sensor [77], often thick-film technology is sufficient to apply zeolite films for this type of application. Some sensor materials cannot withstand high temperatures necessary for template removal by air calcination. Recent work demonstrated that ozonication yields sufficient removal at lower temperatures (~470 K), extending the application of templated zeolites for thermo-sensitive sensors materials [78-80]. The long term stability has not been demonstrated but, considering the stability of zeolites in general, this is not expected to be a limiting factor. For the application of zeolite films in sensor applications a bright future is anticipated.

4 Current hurdles

It is evident that zeolite membranes can have added value in catalysis, but industrial applications are still lacking. Thus, the question remains what the major factors are that stand in the way of application. The following factors are considered troublesome and will be discussed in more detail:

1. Cost considerations
2. Synthesis of thin (< 1 μm) defect free and stable membranes
3. Scale-up and reproducibility
4. Cheap high-temperature sealing
5. Understanding of transport phenomena
6. Catalyst development
7. Reaction and membrane integration

4.1 Cost considerations

The estimated cost of a zeolite membrane is about € 1000-3000 m^{-2} [81-84] at this moment, including a full module design. Most costs are related to the module and support and only 10-20% to the membrane itself [81]. Although cost is the predominant factor regarding application, feasibility studies for zeolite membrane based processes are scarce. The cost that would make a zeolite membrane process profitable is strongly related to the targeted process. Meindersma and de Haan estimated that for an industrial-scale separation process of aromatic hydrocarbons a cost of € 200 m^{-2} would be profitable, in addition, a minimum selectivity of 40 and an aromatic hydrocarbon flux 25 times higher than reported are additional requirements. According to Tennison [83], detailed flow sheeting studies pointed out that very few processes could tolerate installed membrane costs of more than € 1000 m^{-2}. As an example, the dehydrogenation process of butane is mentioned where with the fluxes reported in the late 90s and with a hydrogen separation factor of 40 costs should be below € 1000 m^{-2} to make the process profitable. Although a recent report by Khajavi *et al.* [85] indicate that using sodalite membranes for water removal in a Fischer-Tropsch process a viable zeolite-membrane reactor based process could be within reach, the overall picture is that the current price level of zeolite membranes is too high for profitable application. On the other hand the energy savings and/or CO_2 emission reductions that might be achieved is an aspect that gains increasing importance and may shift the break-even price for membrane investment. Considering that the major part of the costs of supported membranes are related to the support leads to the conclusion that this is the part where significant cost reduction is required to permit widespread industrial application of zeolite membranes.

The considerations above apply to zeolite membranes as applied on the macro level (*e.g.* PBMR). Zeolite membranes applied on the particle level or smaller might lead to a more optimistic outlook since this type of application does neither involve expensive modules and supports nor expensive sealing material.

4.2 Synthesis of thin defect-free membranes

In zeolite membrane synthesis marvellous progress has been made in the last decades and, as shown in paragraph 1.2.2, high-quality thin membranes of a growing number of different zeolites can be produced. But, considering that zeolite membranes have a relative low flux, ‘ultra’ thin (< 1 μm) membranes are desired for a more widespread application. The group of Hedlund has been very active in this field and have been able to make high flux MFI membranes with a thickness of 0.5 μm in a very reproducible way [86], however, such a membrane thickness remains a lower limit and is not common practice. Thin MFI membranes on a titania support, to avoid incorporation of any destabilising Al from a support, were synthesized for butene isomer separation. The goal of high fluxes was achieved, but selectivity was moderate and decreased at higher pressures, relevant for practice [87].

4.3 Scale-up and reproducibility

For installation of large membrane areas module designs with high surface to volume ratios are desired. Geometries that are under consideration are: multi-tubular, monolithic (or multi-channel), capillaries and hollow fibres. Scaling up by a multi-tubular geometry is applied by Mitsubishi Chemicals (formerly BNRI) in their medium-scale isopropanol and large-scale ethanol dehydration plants (*e.g.* [10]) and is a demonstrated viable technology. Also Inocermic is involved in a new ethanol dehydration plant [21]. For high temperatures, sealing is an important issue and an interesting novel concept is the all-ceramic multi-tubular support. Although not demonstrated for zeolite membranes yet, successful H_2/N_2 separation experiments with a silica membrane on this type of support at 773 K and a pressure drop of 9.5 bar have been demonstrated for 1000 hours of operation [88].

Although hollow fibres are thought to be an excellent candidate to be used as support - they are cheap and have a very high surface area to volume (> 1000 m^2 m^{-3}) – very few reports on hollow-fibre supported zeolite membranes exist in the open literature. For zeolite membranes *ceramic* hollow fibres are preferred because of their mechanical and thermal stability. Recently, Alshebani *et al.* [89] obtained a high quality MFI membrane supported by an alumina hollow fibre via a pore-plugging synthesis. The fluxes and binary separation factors of a H_2 / *n*-butane mixture were comparable to high quality MFI membranes prepared on tubular supports. Zeolite membranes based on ceramic hollow fibres appear to be a promising option, moreover because ceramic hollow fibre modules are commercially available [90]

(Figure 5). Richter *et al.* [91] report the synthesis of MFI membranes supported by small tubes and capillaries. Reasonable selectivities, better than Knudsen selectivity, are demonstrated. Bowen *et al.* [92] made a B-MFI membrane on a monolithic support. The pervaporation fluxes and selectivities of several alcohol/water mixtures were comparable to similar tubular based B-MFI membranes, demonstrating the scale-up, although for pervaporation the quality requirements are much more forgiving. Kuhn *et al.* tested a multi-channel high silica MFI membrane for ethanol/water separation. The membrane was supplied by NGK Insulators and, also in this case, the multi-channel membrane measures up to its tubular counterparts [93] (Figure 5).

An important driver for zeolite membrane applications has been the commercialization of the NaA membranes for dehydration. However, for these membranes the quality required is not as high as compared to gas phase molecular sieving applications, since in the case of dehydration defects or imperfections are blocked by water adsorption, resulting in high selectivities, even if gas phase separations yield only Knudsen selectivity values. Natural gas purification by zeolite membranes (*e.g.* DD3R) seems to be a viable application [15,16][Chapter 2], and this application could strongly catalyze the development of large surface area gas permeation zeolite membranes.

Sometimes the reproducibility of zeolite membranes is questioned. But, taking into account the large surface areas that are produced for the mentioned application examples, for well-studied zeolite membrane syntheses this does not appear to be a limiting factor.

Figure 5. Ceramic hollow fibre module of Hyflux [90] (top left); ceramic multi-channel supports of Inopor GmbH [94](top right) and the multi-channel membrane design of NGK insulators (bottom).

4.4 High-temperature sealing

Sealing can be expensive when zeolite membranes are used at high temperatures. Cheap polymer sealings can be used up to around 400-500 K. Higher temperatures require much more expensive polymers or graphite. Brazed or glazed tube ends can withstand high temperatures, but suffer from mismatches in thermal expansion coefficients with the support and module which can lead to thermally induced stress. Innovative methods to simplify sealing are, for example, the synthesis of the membrane on a steel support [95] that allow welding of the support onto a module. An innovative and promising approach is the all-ceramic multi-tubular support [88,96] in which several tubes are connected to a dense alumina endplate by a glass-based sealant prior to the synthesis of the membrane. No additional sealing is required.

4.5 Transport phenomena

In order to design a zeolite-membrane-based process a good model description of the multi-component mass transport properties is required. Moreover, this will reduce the amount of practical work required in the development of zeolite membranes and membrane reactors. Concerning intra-crystalline mass transport a decent continuum approach is available within a Maxwell-Stefan framework for mass transport [97-101][Chapter 5]. The well-defined geometry of zeolites, however, gives rise to microscopic effects, like specific adsorption sites and non-isotropic diffusion, which become manifest at the macro scale. It remains challenging to incorporate these microscopic effects into a generalized model and to obtain an accurate multi-component prediction of a ‘real’ membrane.

In the case of supported membranes also the support can play an important role in the separation performance of the membrane in the gas as well as in the liquid phase [102-104]. Transport in these support pores can be accurately described by the ‘Dusty Gas Model’ [101,105] although it is put forward by Kerkhof and Geboers that their ‘Binary Friction Model’ is physically more correct [106].

Modelling on the reactor level, which is needed for design of the zeolite membrane reactor, could receive some more attention, since the number of studies in this particular field are few (*e.g.* [56,107]).

4.6 Catalyst development

An important aspect of a membrane reactor is the catalyst [108]. Replacing a conventional reactor by a membrane reactor can change the operating conditions considerably (*e.g.* operating temperature and/or concentration levels) which might be rather different than the catalyst originally was designed for. Furthermore, for a membrane reactor system with a high performance membrane, the catalyst can become the factor limiting the reactor’s effectiveness

[109]. When considering dehydrogenation reactions, an extractor type PBMR can lead to higher conversion by hydrogen removal, than a conventional fixed-bed reactor. Further, the operation temperature can be reduced without sacrificing product yield. But, such a temperature reduction leads to a reduced catalytic activity and the extraction of hydrogen can lead to increased coke formation. Thus, for this application, more active catalysts with reduced coke formation would be required to ultimately arrive at an optimal reactor system. The main message is that, with increasing membrane performance, it should not be overlooked that eventually another part of the system will limit the reactor performance and this can very well be the catalyst developed for normal steady state operation.

4.7 Reaction and membrane integration

A trivial point, which arises from the previous subparagraph and is without saying assumed throughout this chapter, is that the operational regime of the membrane and of the catalyst should overlap to be able combine to catalysis and membrane permeation. Furthermore, the performance of the catalyst and the membrane, in terms of productivity and permeability, respectively, should match and should be integrated in an appropriate way [110]. Otherwise either the catalyst or the membrane will be poorly utilized. In practice, the reactor space time yield (*STY*, mol m^{-3} s^{-1}) is matched with the membrane areal time yield (*ATY*, mol m^{-2} s^{-2}) by application of a support geometry with the required membrane surface area to volume ratio (*A/V*, m^2 m^{-3}). As pointed out by van de Graaf *et al.*, *A/V* values of porous ceramic membranes range from 20-5000 m^{-1}, which appears sufficient to match typical *STY*-values of 1-10 mol m^{-3} s^{-1} making application of zeolite membranes in catalysis feasible from this perspective [111].

Integration of the separation and reaction step has several advantages but an inherent downside of such a process intensification step is the loss of degrees of freedom for process design and process control (Figure 6).

4.8 Concluding remarks

The consideration that many zeolite types exist, with many tuneable properties (*e.g.* pore size and alumina content), leads to a wealth of options, but also to a high level of complexity. Due to this complexity and limited understanding of zeolite formation and permeation behaviour a lot of experimental effort is required in this field, slowing down developments towards successful application.

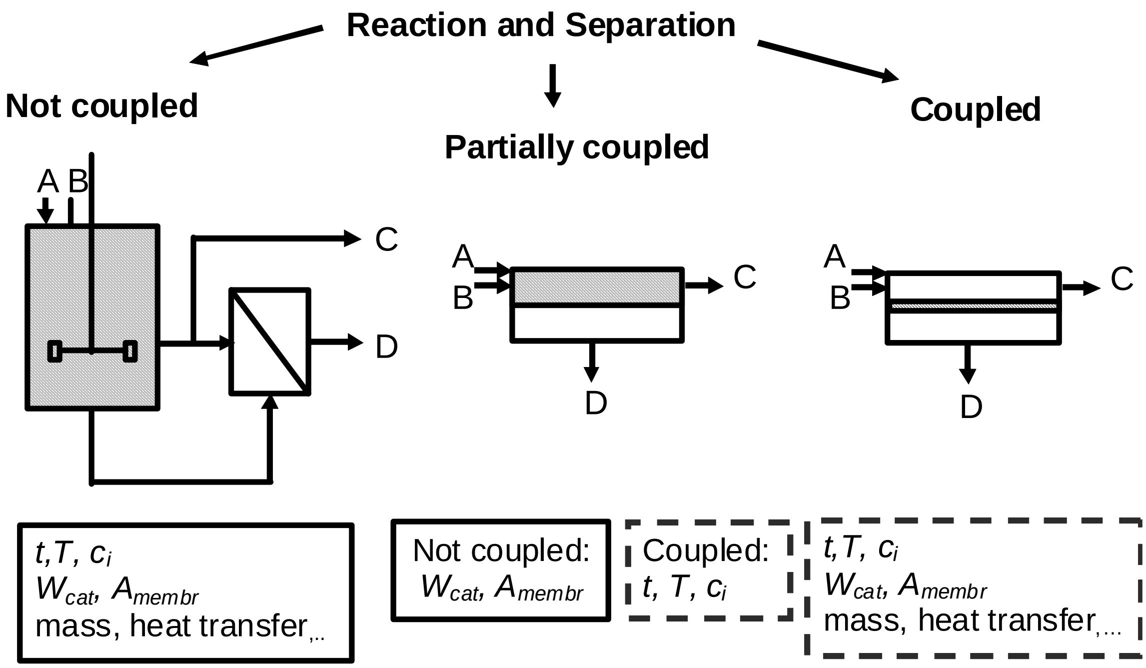

Figure 6. Combining reaction and separation steps leads to a loss in process design degrees of freedom.

A general remark regarding industrial implementation of any new technology is that the process industry is conservative and new technologies need to be well-demonstrated before they are accepted, particularly when high investment costs are involved. Moreover, application of a membrane reactor in an existing plant will not be straightforward since this membrane reactor will presumably be designed for a different conversion level than the original reactor, which will affect downstream processing. Therefore, introduction of a membrane reactor is not likely to be a simple change of reactor, but requires a considerable plant redesign. A completely new process lay-out has a better outlook but requires considerable investments. Rather membrane add-on units are expected to have a larger chance of introduction in existing plants to improve performance, debottlenecking or increasing capacity.

As is obvious, many potential hurdles discussed in the previous sections do not apply to application of zeolite membranes at the micro and particle level. Issues like scale-up and high-temperature sealing do not play a role here. Additionally, coated catalyst particles do not require a change of reactor, but only replacement of the catalyst. Application of zeolite membranes at these levels is therefore considered to be easier and their implementation will probably occur earlier.

References

[1] J. L. Falconer, R. D. Noble, and D. P. Sperry, Catalytic Membrane Reactors, in: Membrane Separations Technology; Principles and Applications, Noble, R. D. and Stern, S. A. (Eds), Ch. 14, **1995**, Elsevier, Amsterdam, 669.

[2] J. Sanchez and T.T.Tsotsis, Catalytic Membranes and Membrane Reactors, **2002**, Wiley-VCH, Weinheim.

[3] H. P. Hsieh, Inorganic Membranes for Separation and Reaction, **1996**, Elsevier, Amsterdam.

[4] A. Corma, *Journal of Catalysis*, 216, **2003**, 298.

[5] C. J. Plank, W. P. Hawthorne, and E. J. Rosinski, *Industrial & Engineering Chemistry Product Research and Development*, 3, **1964**, 165.

[6] International Zeolite Association, www.iza-structure.org/databases/, Visited **2009**.

[7] M. Taramasso, G. Perego, and B. Notari, Preparation of porous crystalline synthetic material comprised of silicon and titanium oxides, **1983**, US Patent 4,410,501.

[8] S. Kulprathipanja and J. Charoenphol, Mixed matrix membrane for separation of gases, **1986**, US Patent 6,726,744.

[9] H. Suzuki, Composite membrane having a surface layer of an ultrathin film of cage-shaped zeolite and processes for production thereof, **1987**, US Patent 4,699,892.

[10] Y. Morigami, M. Kondo, J. Abe, H. Kita, and K. Okamoto, *Separation and Purification Technology*, 25, **2001**, 251.

[11] W. J. W. Bakker, F. Kapteijn, J. Poppe, and J. A. Moulijn, *Journal of Membrane Science*, 117, **1996**, 57.

[12] K. Okamoto, H. Kita, K. Horii, K. Tanaka, and M. Kondo, *Industrial & Engineering Chemistry Research*, 40, **2001**, 163.

[13] M. Lassinantti, J. Hedlund, and J. Sterte, *Microporous and Mesoporous Materials*, 38, **2000**, 25.

[14] M. Matsukata, K. i. Sawamura, T. Shirai, M. Takada, Y. Sekine, and E. Kikuchi, *Journal of Membrane Science*, 316, **2008**, 18.

[15] T. Tomita, K. Nakayama, and H. Sakai, *Microporous and Mesoporous Materials*, 68, **2004**, 71.

[16] J. van den Bergh, W. Zhu, J. Gascon, J. A. Moulijn, and F. Kapteijn, *Journal of Membrane Science*, 316, **2008**, 35.

[17] S. G. Li, J. L. Falconer, and R. D. Noble, *Journal of Membrane Science*, 241, **2004**, 121.

[18] M. L. Maloncy, A. W. C. van den Berg, L. Gora, and J. C. Jansen, *Microporous and Mesoporous Materials*, 85, **2005**, 96.

[19] T. Matsufuji, S. Nakagawa, N. Nishiyama, M. Matsukata, and K. Ueyama, *Microporous and Mesoporous Materials*, 38, **2000**, 43.

[20] S. Khajavi, F. Kapteijn, and J. C. Jansen, *Journal of Membrane Science*, 299, **2007**, 63.

[21] J. Caro, M. Noack, and P. Kölsch, *Adsorption-Journal of the International Adsorption Society*, 11, **2005**, 215.

[22] O. de la Iglesia, R. Mallada, M. Menéndez, and J. Coronas, *Chemical Engineering Journal*, 131, **2007**, 35.

[23] U. Illgen, R. Schäfer, M. Noack, P. Kölsch, A. Kühnle, and J. Caro, *Catalysis Communications*, 2, **2001**, 339.

[24] S. A. S. Rezai and Y. Traa, *Journal of Membrane Science*, 319, **2008**, 279.

[25] L. Gora and J. C. Jansen, *Journal of Catalysis*, 230, **2005**, 269.

[26] A. Cruz-López, N. Guilhaume, S. Miachon, and J. A. Dalmon, *Catalysis Today*, 107-108, **2005**, 949.

[27] Y. Hasegawa, K. Kusakabe, and S. Morooka, *Journal of Membrane Science*, 190, **2001**, 1.

[28] T. Masuda, T. Asanuma, M. Shouji, S. R. Mukai, M. Kawase, and K. Hashimoto, *Chemical Engineering Science*, 58, **2003**, 649.

[29] H. J. Sloot, G. F. Versteeg, and W. P. M. Van Swaaij, *Chemical Engineering Science*, 45, **1990**, 2415.

[30] V. Diakov and A. Varma, *Chemical Engineering Science*, 57, **2002**, 1099.

[31] M. A. Al-Juaied, D. Lafarga, and A. Varma, *Chemical Engineering Science*, 56, **2001**, 395.

[32] N. van der Puil, E. J. Creyghton, E. C. Rodenburg, S. T. Sie, H. van Bekkum, and J. C. Jansen, *Journal of the Chemical Society, Faraday Transactions*, 92, **1996**, 4609.

[33] N. Nishiyama, K. Ichioka, D. H. Park, Y. Egashira, K. Ueyama, L. Gora, W. D. Zhu, F. Kapteijn, and J. A. Moulijn, *Industrial & Engineering Chemistry Research*, 43, **2004**, 1211.

[34] N. Nishiyama, K. Ichioka, M. Miyamoto, Y. Egashira, K. Ueyama, L. Gora, W. D. Zhu, F. Kapteijn, and J. A. Moulijn, *Microporous and Mesoporous Materials*, 83, **2005**, 244.

[35] Y. J. Zhong, L. Chen, M. F. Luo, Y. L. Xie, and W. D. Zhu, *Chemical Communications*, **2006**, 2911.

[36] H. C. Foley, D. S. Lafyatis, R. K. Mariwala, G. D. Sonnichsen, and L. D. Brake, *Chemical Engineering Science*, 49, **1994**, 4771.

[37] N. Nishiyama, M. Miyamoto, Y. Egashira, and K. Ueyama, *Chemical Communications*, **2001**, 1746.

[38] J. J. He, B. L. Xu, Y. Yoneyama, N. Nishiyama, and N. Tsubaki, *Chemistry Letters*, 34, **2005**, 148.

[39] J. J. He, Y. Yoneyama, B. L. Xu, N. Nishiyama, and N. Tsubaki, *Langmuir*, 21, **2005**, 1699.

[40] J. J. He, Z. L. Liu, Y. Yoneyama, N. Nishiyama, and N. Tsubaki, *Chemistry-A European Journal*, 12, **2006**, 8296.

[41] M. Miyamoto, T. Kamei, N. Nishiyama, Y. Egashira, and K. Ueyama, *Advanced Materials*, 17, **2005**, 1985.

[42] D. van Vu, M. Miyamoto, N. Nishiyama, Y. Egashira, and K. Ueyama, *Journal of Catalysis*, 243, **2006**, 389.

[43] D. van Vu, M. Miyamoto, N. Nishiyama, S. Ichikawa, Y. Egashira, and K. Ueyama, *Microporous and Mesoporous Materials*, 115, **2008**, 106.

[44] A. L. Yonkeu, V. Buschmann, G. Miehe, H. Fuess, A. M. Goossens, and J. A. Martens, *Crystal Engineering*, 4, **2001**, 253.

[45] K. R. Kloetstra, H. W. Zandbergen, J. C. Jansen, and H. van Bekkum, *Microporous Materials*, 6, **1996**, 287.

[46] J. J. Jafar, P. M. Budd, and R. Hughes, *Journal of Membrane Science*, 199, **2002**, 117.

[47] K. Tanaka, R. Yoshikawa, C. Ying, H. Kita, and K. i. Okamoto, *Catalysis Today*, 67, **2001**, 121.

[48] M. P. Bernal, J. Coronas, M. Menéndez, and J. Santamaría, *Chemical Engineering Science*, 57, **2002**, 1557.

[49] Y. Kiyozumi, Y. Nemoto, T. Nishide, T. Nagase, Y. Hasegawa, and F. Mizukami, *Microporous and Mesoporous Materials*, 116, **2008**, 485.

[50] S. Khajavi, J. C. Jansen, and F. Kapteijn, *Journal of Membrane Science*, 326, **2010**, 123.

[51] J. Kuhn, K. Yajima, T. Tomita, J. Gross, and F. Kapteijn, *Journal of Membrane Science*, 321, **2008**, 344.

[52] S. Khajavi, J. C. Jansen, and F. Kapteijn, *Journal of Membrane Science*, 326, **2009**, 153.

[53] S. Khajavi, J. C. Jansen, and F. Kapteijn, *Catalysis Today*, In Press, **2010**, doi:10.1016/j.cattod.2010.02.042.

[54] M. P. Rohde, G. Schaub, S. Khajavi, J. C. Jansen, and F. Kapteijn, *Microporous and Mesoporous Materials*, 115, **2008**, 123.

[55] P. Ciavarella, D. Casanave, H. Moueddeb, S. Miachon, K. Fiaty, and J.-A. Dalmon, *Catalysis Today*, 67, **2001**, 177.

[56] B. H. Jeong, K. I. Sotowa, and K. Kusakabe, *Journal of Membrane Science*, 224, **2003**, 151.

[57] Z. Xiongfu, L. Yongsheng, W. Jinqu, T. Huairong, and L. Changhou, *Separation and Purification Technology*, 25, **2001**, 269.

[58] C. Kong, J. Lu, J. Yang, and J. Wang, *Journal of Membrane Science*, 306, **2007**, 29.

[59] G. Q. Lu, J. C. Diniz da Costa, M. Duke, S. Giessler, R. Socolow, R. H. Williams, and T. Kreutz, *Journal of Colloid and Interface Science*, 314, **2007**, 589.

[60] J. Caro and M. Noack, *Microporous and Mesoporous Materials*, 115, **2008**, 215.

[61] N. Nishiyama, M. Yamaguchi, T. Katayama, Y. Hirota, M. Miyamoto, Y. Egashira, K. Ueyama, K. Nakanishi, T. Ohta, A. Mizusawa, and T. Satoh, *Journal of Membrane Science*, 306, **2007**, 349.

[62] L. van Dyk, L. Lorenzen, S. Miachon, and J. A. Dalmon, *Catalysis Today*, 104, **2005**, 274.

[63] S. Haag, M. Hanebuth, G. T. P. Mabande, A. Avhale, W. Schwieger, and R. Dittmeyer, *Microporous and Mesoporous Materials*, 96, **2006**, 168.

[64] A. M. Tarditi, G. I. Horowitz, and E. A. Lombardo, *Catalysis Letters*, 123, **2008**, 7.

[65] X. F. Zhang, E. S. M. Lai, R. Martin-Aranda, and K. L. Yeung, *Applied Catalysis A-General*, 261, **2004**, 109.

[66] S. M. Lai, C. P. Ng, R. Martin-Aranda, and K. L. Yeung, *Microporous and Mesoporous Materials*, 66, **2003**, 239.

[67] Y. S. S. Wan, K. L. Yeung, and A. Gavriilidis, *Applied Catalysis A: General*, 281, **2005**, 285.

[68] M. J. den Exter, H. van Bekkum, C. J. M. Rijn, F. Kapteijn, J. A. Moulijn, H. Schellevis, and C. I. N. Beenakker, *Zeolites*, 19, **1997**, 13.

[69] M. Vilaseca, J. Coronas, A. Cirera, A. Cornet, J. R. Morante, and J. Santamaría, *Sensors and Actuators B: Chemical*, 133, **2008**, 435.

[70] R. Moos, R. Müller, C. Plog, A. Knezevic, H. Leye, E. Irion, T. Braun, K. J. Marquardt, and K. Binder, *Sensors and Actuators B: Chemical*, 83, **2002**, 181.

[71] M. E. Franke, U. Simon, R. Moos, A. Knezevic, R. Müller, and C. Plog, *Physical Chemistry Chemical Physics*, 5, **2003**, 5195.

[72] J. C. Yang and P. K. Dutta, *Sensors and Actuators B: Chemical*, 123, **2007**, 929.

[73] N. F. Szabo and P. K. Dutta, *Sensors and Actuators B: Chemical*, 88, **2003**, 168.

[74] K. Sahner, D. Schönauer, P. Kuchinke, and R. Moos, *Sensors and Actuators B: Chemical*, 133, **2008**, 502.

[75] K. Sahner, R. Moos, M. Matam, J. J. Tunney, and M. Post, *Sensors and Actuators B: Chemical*, 108, **2005**, 102.

[76] J. Trimboli and P. K. Dutta, *Sensors and Actuators B: Chemical*, 102, **2004**, 132.

[77] E. Biemmi and T. Bein, *Langmuir*, 24, **2008**, 11196.

[78] J. Kuhn, J. Gascon, J. Gross, and F. Kapteijn, *Microporous and Mesoporous Materials*, 120, **2008**, 12.

[79] J. Kuhn, M. Motegh, J. Gross, and F. Kapteijn, *Microporous and Mesoporous Materials*, 120, **2008**, 35.

[80] L. Gora, J. Kuhn, T. Baimpos, V. Nikolakis, F. Kapteijn, and E. M. Serwicka, *Analyst*, 134, **2009**, 2118.

[81] J. Caro, M. Noack, P. Kolsch, and R. Schafer, *Microporous and Mesoporous Materials*, 38, **2000**, 3.

[82] G. W. Meindersma and A. B. de Haan, *Desalination*, 149, **2002**, 29.

[83] S. Tennison, *Membrane Technology*, 2000, **2000**, 4.

[84] J. Caro, Workshop on Zeolite Membranes, ICIM9, Lillehammer, **2006**.

[85] S. Khajavi, V. Wong, N. Dokhale, D. Patil, J. C. Jansen, and F. Kapteijn, Proceedings ICIM10, Tokyo, Fischer Tropsch Synthesis with in-situ water removal: industrial implementation of membranes and their economic feasibility, **2008**.

[86] J. Hedlund, J. Sterte, M. Anthonis, A. J. Bons, B. Carstensen, N. Corcoran, D. Cox, H. Deckman, W. De Gijnst, P. P. de Moor, F. Lai, J. McHenry, W. Mortier, J. Reinoso, and J. Peters, *Microporous and Mesoporous Materials*, 52, **2002**, 179.

[87] H. Voss, A. Diefenbacher, G. Schuch, H. Richter, I. Voigt, M. Noack, and J. Caro, *Journal of Membrane Science*, 329, **2009**, 11.

[88] Y. Yoshino, T. Suzuki, H. Taguchi, M. Nomura, S. i. Nakao, and N. Itoh, *Separation Science and Technology*, 43, **2008**, 3432.

[89] A. Alshebani, M. Pera-Titus, E. Landrivon, T. Schiestel, S. Miachon, and J. A. Dalmon, *Microporous and Mesoporous Materials*, 115, **2008**, 197.

[90] Website Hyflux, www.Hyflux.com, Visited **2010**.

[91] H. Richter, I. Voigt, G. Fischer, and P. Puhlfürß, *Separation and Purification Technology*, 32, **2003**, 133.

[92] T. C. Bowen, H. Kalipcilar, J. L. Falconer, and R. D. Noble, *Journal of Membrane Science*, 215, **2003**, 235.

[93] J. Kuhn, S. Sutanto, J. Gascon, J. Gross, and F. Kapteijn, *Journal of Membrane Science*, 339, **2009**, 261.

[94] Website Inopor, http://www.inopor.com/en/membranes_e.html, Visited **2008**.

[95] J. M. van de Graaf, F. Kapteijn, and J. A. Moulijn, *Chemical Engineering Science*, 54, **1999**, 1081.

[96] I. Voigt; G. Fischer; P. Puhlfürß; M. Stahn, and G. F. Tusel, Full Ceramic Modules for High Temperature Gas Separation and Pervaporation, **2000**.

[97] F. Kapteijn, J. A. Moulijn, and R. Krishna, *Chemical Engineering Science*, 55, **2000**, 2923.

[98] R. Krishna and R. Baur, *Separation and Purification Technology*, 33, **2003**, 213.

[99] J. van den Bergh, S. Ban, T. J. H. Vlugt, and F. Kapteijn, *Journal of Physical Chemistry C*, 113, **2009**, 17840.

[100] J. van den Bergh, S. Ban, T. J. H. Vlugt, and F. Kapteijn, *Journal of Physical Chemistry C*, 113, **2009**, 21856.

[101] F. Kapteijn, W. Zhu, J. A. Moulijn, and T. Q. Gardner, Zeolite Membranes: Modeling and Application, in: Structured Catalysts and Reactors, Cybulski, A. and Moulijn, J. A. (Eds), Ch. 20, **2005**, Taylor & Francis Group, Boca Raton, FL, 701.

[102] J. M. van de Graaf, E. van der Bijl, A. Stol, F. Kapteijn, and J. A. Moulijn, *Industrial & Engineering Chemistry Research*, 37, **1998**, 4071.

[103] F. de Bruijn, J. Gross, Ž. Olujic, P. Jansens, and F. Kapteijn, *Industrial & Engineering Chemistry Research*, 46, **2007**, 4091.

[104] F. T. de Bruijn, L. Sun, Z. Olujic, P. J. Jansens, and F. Kapteijn, *Journal of Membrane Science*, 223, **2003**, 141.

[105] M. O. Coppens, F. J. Keil, and R. Krishna, *Reviews in Chemical Engineering*, 16, **2000**, 71.

[106] P. J. A. M. Kerkhof and M. A. M. Geboers, *AIChE Journal*, 51, **2005**, 79.

[107] D. Casanave, P. Ciavarella, K. Fiaty, and J.-A. Dalmon, *Chemical Engineering Science*, 54, **1999**, 2807.

[108] S. Miachon and J. A. Dalmon, *Topics in Catalysis*, 29, **2004**, 59.

[109] L. van Dyk, S. Miachon, L. Lorenzen, M. Torres, K. Fiaty, and J.-A. Dalmon, *Catalysis Today*, 82, **2003**, 167.

[110] R. Dittmeyer, K. Svajda, and M. Reif, *Topics in Catalysis*, 29, **2004**, 3.

[111] J. M. van de Graaf, M. Zwiep, F. Kapteijn, and J. A. Moulijn, *Applied Catalysis A: General*, 178, **1999**, 225.

2

Separation and permeation characteristics of a DD3R zeolite membrane

Permeation of various light gases (carbon dioxide, nitrous oxide, methane, nitrogen, oxygen, argon, krypton, neon) and their equimolar mixtures through DD3R membranes have been investigated over a temperature range of 220 – 373 K and a feed pressure range of 101 – 400 kPa. Helium was used as sweep gas at atmospheric pressure. Adsorption isotherms were determined in the temperature range 195 – 298 K, and modelled by a single- and dual-site Langmuir model. The permeation flux is determined by the size of the molecule relative to the window opening of DD3R, and its adsorption behaviour. As a function of temperature, bulky molecules (*e.g.* methane) show activated permeation, weakly adsorbing molecules decreasing permeation behaviour and the permeance of strongly adsorbing molecules pass through a maximum. Counter-diffusion of the sweep gas (helium) ranged from almost zero up to the order of the feed gas permeation and was strongly influenced by the adsorption of the feed gas. DD3R membranes have excellent separation performance for carbon dioxide / methane mixtures (selectivity 100 – 3000), exhibit good selectivity for nitrogen / methane (20 - 45), carbon dioxide / air, nitrous oxide / air (20 - 400) and air / krypton (5 – 10) and only a modest

---

This chapter is based on the following publication:

J. van den Bergh, W. Zhu, J. Gascon, J.A. Moulijn and F. Kapteijn, Journal of Membrane Science, 316, **2008**, 35-45.

selectivity for oxygen / nitrogen (~2) separation. The selectivity of mixtures of a strongly and a weakly adsorbing component decreased with increasing temperature and feed pressure. The selectivity of mixtures of weakly adsorbing components was independent of feed pressure.

The permeation and separation characteristics of light gases through DD3R membranes can be explained by taking into account: (1) steric effects introduced by the window opening of DD3R leading to molecular sieving and activated transport, (2) competitive adsorption effects, as observed for mixtures involving strongly adsorbing gases, and (3) interactions between diffusing molecules in the cages of the zeolite.

1 Introduction

Membrane processes can be an alternative to energy demanding separation processes such as distillation and absorption and can enhance the conversion of equilibrium-limited reactions. Zeolite membranes are a special class of porous inorganic membranes with well-defined nano-pores due to their crystallinity. Zeolite membranes are considered more expensive than polymeric membranes and therefore their unique properties of size selectivity and thermal and chemical stability should be exploited for successful application [1]. Since each zeolite has its own specific properties (*e.g.* its pore dimensions) continuously new types of zeolites are looked for. The zeolite used in this study is DD3R (decadodesil 3R), also referred to as all-silica DDR, where DDR stands for the framework topology. DD3R is a micro-porous structure consisting of cages, each connected by three windows of 8-membered rings forming a 2-dimensional pore structure [2]. Small-pore-zeolite membranes have the potential to separate light gases based on molecular sieving effects. Such effects have been clearly demonstrated for 8-ring zeolites such as: SAPO-34 [3], zeolite T [4] and DD3R [5]. The advantage of DD3R over SAPO-34 and zeolite T would be the chemical and thermal stability because of its all-silica structure.

The characterization and first synthesis of DD3R were done by Gies [2]. Den Exter [6] optimized the synthesis procedure and scaled it up to batches of 20 g. Den Exter already showed via adsorption experiments that DD3R has potential to separate light hydrocarbons. Zhu *et al.* [7] found that the DD3R 8-ring window is capable of separating certain C_4-mixtures and propene / propane mixtures. Recently, Tomita *et al.* [5] have successfully synthesized a DD3R membrane and demonstrated the capability of the DD3R membrane to separate an equimolar carbon dioxide / methane mixture with high separation factors (100 – 200).

In this study the permeation and separation properties of an all-silica DD3R membrane have been investigated for various light gases and their mixtures as a function of temperature and feed pressure, and complemented by single component adsorption experiments for modelling purposes. Binary permeation experiments are essential to fully understand the capabilities of the membranes since only such experiments can reveal mixture adsorption [8,9] and diffusion

[10] effects. Since such effects are more pronounced when the occupancy in the zeolite is high, low temperature experiments (down to 220 K) were carried out to obtain such high loadings. To put them in perspective, these results are compared with another all-silica membrane, silicalite-1, and with predictions of molecular simulations [11].

2 Experimental

2.1 Adsorption measurements

A Micromeritics ASAP 2010 gas adsorption analyzer (stainless-steel version) was used to measure the adsorption isotherms of carbon dioxide, nitrous oxide, nitrogen, oxygen, argon, krypton and methane on DD3R in the pressure range from 0.002 to 120 kPa. The instrument was equipped with a turbo molecular vacuum pump and three different pressure transducers (0.13, 1.33, and 133 kPa, respectively) to enhance the sensitivity in different pressure ranges. The static-volumetric technique was used to determine the volume of the gas adsorbed at different partial pressures. The sample cell was loaded with 190.2 mg of DD3R crystals. Prior to the adsorption measurements the adsorbent particles were outgassed in situ in vacuum at 623 K for 16 h to remove any adsorbed impurities. The obtained dry sample weight was used in the calculation of isotherm data. Adsorption measurements were subsequently done at 195, 252, 273 and 298 K. The 195 K isotherm was measured using solid carbon dioxide in isopropylalcohol as coolant. For the adsorption measurements two different DD3R samples were used, which gave identical results. One sample was provided by Exxon Mobil, the other was synthesized in-house, following the method of den Exter [6].

2.2 Permeation measurements

The permeation experiments were carried out with an α-alumina supported disc-shaped membrane. The zeolite layer was approximately 5 μm thick and a permeable area of 4.10^{-5} m^2 was left after sealing with a silicon O-ring. The α-alumina support has an average pore diameter of 0.6 μm and is 1.5 mm thick.

The membrane permeation measurements were performed by the so-called Wicke-Kallenbach (WK) method (see [12] for more details), with helium as sweep gas. The feed gas flow rate was set to 100 ml min^{-1} and the sweep gas flow rate to 17.5 ml min^{-1}. The feed side pressure was varied from 101.3 to 500 kPa, the permeate side pressure was kept constant at 101.3 kPa. The temperature was varied from 220 to 373 K. Sub-ambient temperatures were achieved by adding solid carbon dioxide (dry ice) to the oven. The partial pressures in the permeate and retentate side were measured with a Ledamass Quadrupole Mass Analyzer.

All gases used have a purity of 0.9995 minimum.

3 Results & Discussion

3.1 Adsorption isotherms

Mass transport through zeolite membranes is seen as adsorptive diffusion (surface diffusion) [13-15], therefore adsorption data have been measured to be able to distinguish between adsorption and diffusion effects in the membrane permeation results. Figure 1 shows the adsorption isotherms of methane, carbon dioxide, nitrous oxide, nitrogen, oxygen, argon and krypton on DD3R crystals at 195, 252, 273 and 298 K. The data for both zeolite samples coincided well. The carbon dioxide and methane isotherms match very well with recently published adsorption data by Himeno *et al.* [16]. The adsorbed amount of neon was too low to be quantified accurately and neon can therefore be considered almost non-adsorbing on DD3R.

For most adsorption data the loading (q) could be described well as a function of the pressure (p) and temperature (T) by a classical single-site Langmuir isotherm. For the components with the highest loadings on the zeolite (carbon dioxide, nitrous oxide and krypton) a dual-site Langmuir isotherm with sites A and B was required (Equation 1). The enthalpy of adsorption (ΔH_{Ads}), the pre-exponential of the adsorption equilibrium constant (K_0) and the saturation loading in the zeolite (q^{sat}) have been extracted from combined fitting of all data. The estimated values of the adsorption parameters are summarized in Table 1.

$$q_i = q_i^{sat,A} \frac{K_i^A p_i}{1+K_i^A p_i} + q_i^{sat,B} \frac{K_i^B p_i}{1+K_i^B p_i}, \qquad K_i^n = K_{0,i}^n \exp\left(\frac{-\Delta H_i^n}{RT}\right) \tag{1}$$

The carbon dioxide and the nitrous oxide isotherms are almost identical, nicely illustrated by the similarity of the estimated parameters in Table 1. Notice that the carbon dioxide and nitrous oxide isotherms reach a much higher loading than the other components. Therefore, carbon dioxide and nitrous oxide are considered ‘strongly’ adsorbing with respect to the other gases studied, which are consequently referred to as ‘weakly’ adsorbing. The obtained order in adsorbed amount is: $CO_2 = N_2O > Kr > CH_4 > O_2 > Ar > N_2 >> Ne$.

Since each DD3R unit cell ($(SiO_2)_{120}$) has a molar weight of 7.308 kg mol^{-1} [17] and contains six cavities, the estimated saturation loading of carbon dioxide (4.39 mol kg^{-1}) corresponds to 5.35 molecules per cavity. This compares well to the nitrogen physisorption experiments of Himeno *et al.* [16] that yield a nitrogen saturation loading of 5.4 molecules per cavity (4.46 mol kg^{-1}). Only the estimated saturation loadings of carbon dioxide and nitrous oxide are considered a reasonable approximation of the true saturation loading. All other saturation capacities are based on too limited adsorption data and are considered under-predictions.

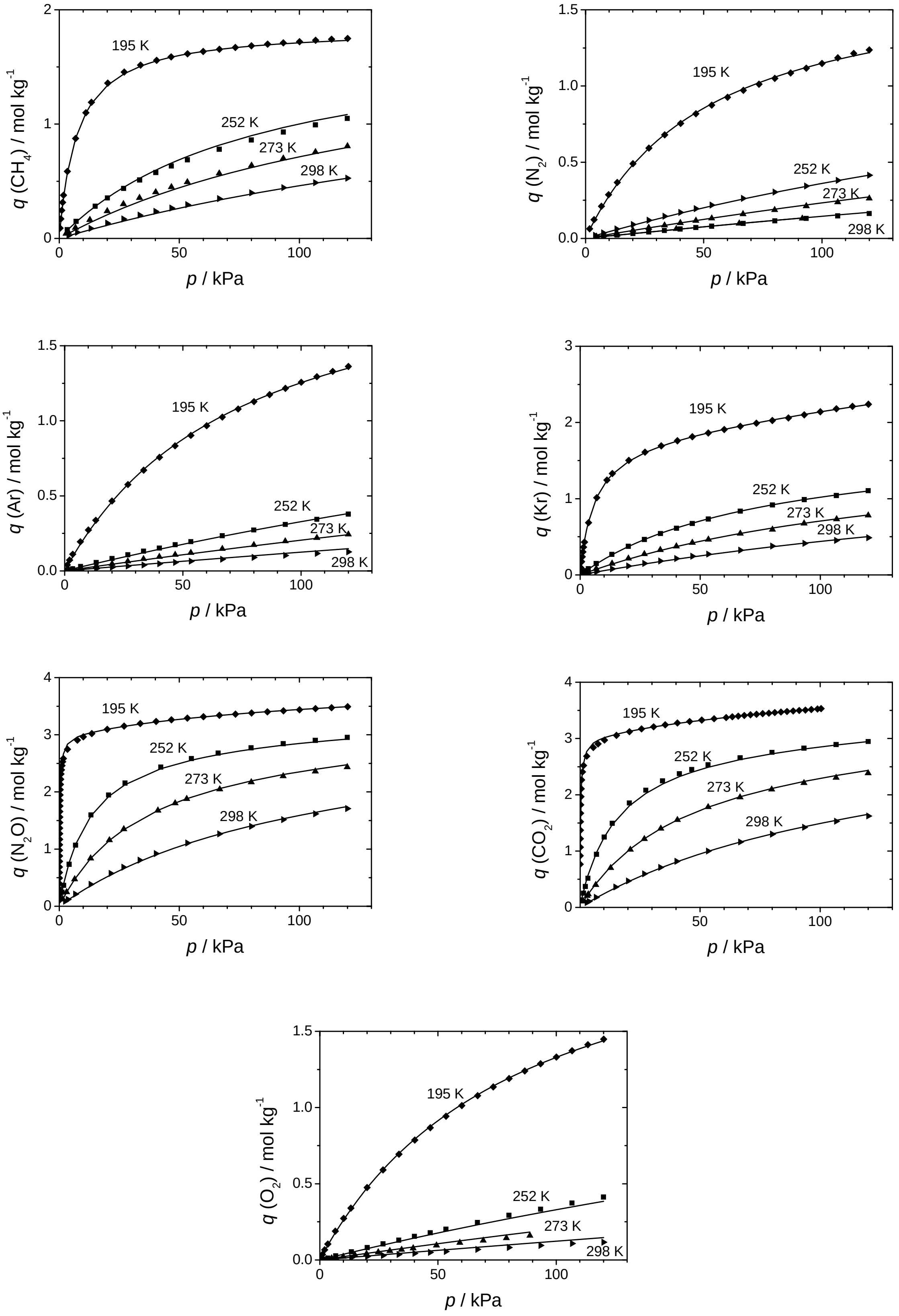

Figure 1. Adsorption isotherms of carbon dioxide, nitrous oxide methane, nitrogen, argon, krypton, neon and oxygen on DD3R crystals at 195, 252, 273 and 298 K. Lines represent results of a full data fit with a single- or dual-site Langmuir model (Equation 1).

Table 1. Adsorption parameters of the gases under investigation on DD3R crystals including their 95% confidence intervals. Modelled by Equation 1.

	T_c	$q^{sat,A}$	K_0^A	$-\Delta H_{Ads}^A$	$q^{sat,B}$	K_0^B	$-\Delta H_{Ads}^B$
	K	mol kg^{-1}	10^{-7} kPa^{-1}	kJ mol^{-1}	mol kg^{-1}	10^{-7} kPa^{-1}	kJ mol^{-1}
CO_2	304.2	3.02 ± 0.06	0.81 ± 0.17	28.5 ± 0.4	1.37 ± 1.21	408 ± 505	8.11 ± 2.1
N_2O	309.6	2.99 ± 0.06	0.95 ± 0.19	28.6 ± 0.4	1.06 ± 0.68	242 ± 360	9.30 ± 2.8
CH_4	190.6	1.84 ± 0.05	31.2 ± 8.7	17.3 ± 0.7	-	-	-
N_2	126.2	1.75 ± 0.02	28.3 ± 1.6	14.3 ± 0.1	-	-	-
Kr	209.4	1.74 ± 0.02	16.9 ± 0.69	18.8 ± 0.1	2.37 ± 0.02	0.0078 ± 0.1	24.3 ± 0.05
Ar	150.9	2.20 ± 0.04	17.2 ± 0.12	14.5 ± 0.1	-	-	-
O_2	154.6	2.44 ± 0.06	14.6 ± 0.12	14.6 ± 0.1	-	-	-
Ne	44.4	-	-	-	-	-	-

3.2 Single component permeation

The pure component permeation flux of carbon dioxide, nitrous oxide, methane, nitrogen, oxygen, krypton, argon and neon are presented as a function of temperature in Figure 2. The temperature dependency exhibits three different types of flux behaviour: (1) carbon dioxide and nitrous oxide show a maximum at low temperature, (2) methane increases monotonically with temperature, and (3) all other gases monotonically decrease with increasing temperature. The flux through a zeolite membrane is a function of the diffusivity of the component and the amount adsorbed in the zeolite. Diffusion in zeolites is an activated process and the diffusivity increases with temperature, but the amount adsorbed decreases with temperature. In situation (3) the flux decreases with temperature because the amount adsorbed decreases with temperature and, apparently, this effect dominates over the increasing activated diffusion. Additionally, carbon dioxide and nitrous oxide have a maximum at low temperatures. When decreasing the temperature the zeolite becomes saturated and the decrease of diffusivity starts to dominate due to the asymptotic approach of adsorption saturation. Methane (situation 2) does not show this behaviour, but it has been shown analytically [18] and experimentally for branched hydrocarbons with silicalite-1 membranes [19,20] that when the activation energy for diffusion is larger than the heat of adsorption, a monotonically increasing flux with temperature is found. The fact that the size of methane (kinetic diameter = 0.38 nm) is close to the window opening of DD3R (0.36 x 0.44 nm) indicates that a relative high activation energy for diffusion can be expected.

Mass transport through zeolite membranes can usually be modelled well by a Maxwell-Stefan formulation for surface diffusion [13,14,20]. Equation 2 represents the analytical solution for the flux (N) of a single component through a zeolite membrane when adsorption can be represented by a multi-site Langmuir isotherm.

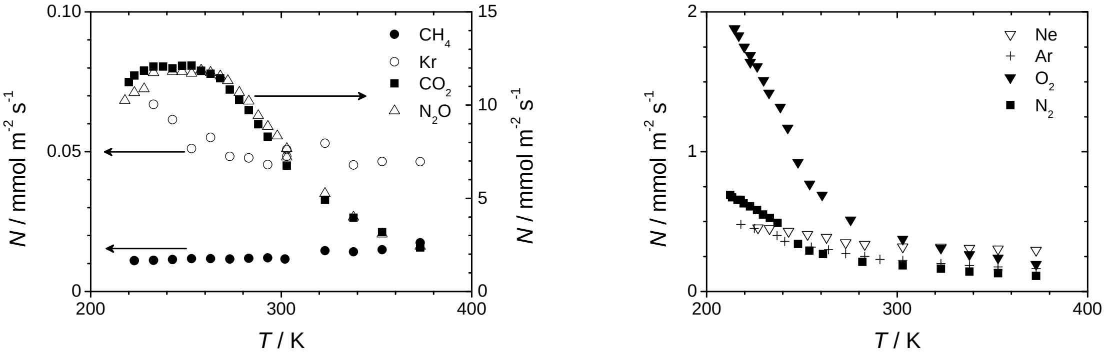

Figure 2. Single component flux of the investigated gases through a DD3R membrane as a function of the temperature. Feed and permeate pressure 101 kPa, sweep gas helium.

$$N_i = \frac{\rho}{\delta}\text{Đ}_i \sum_{n=1}^{n} q_i^{sat,n} \ln\left(\frac{1+K_i^n p_{i,ret}}{1+K_i^n p_{i,per}}\right), \qquad \text{Đ}_i = \text{Đ}_{0,i}\exp\left(\frac{-E_{A,diff,i}}{RT}\right) \tag{2}$$

ρ is the zeolite density, δ the membrane thickness and the Maxwell Stefan diffusivity (Đ) is dependent on the temperature leading to an activation energy for diffusion ($E_{A,diff}$) and a diffusivity pre-exponent (Đ_0). If the system is in the Henry regime (*i.e.* weak adsorption regime) and can be described by a single-site Langmuir isotherm, Equation 2 can be simplified to Equation 3

$$N_i = \frac{q_i^{sat}\rho}{\delta}\text{Đ}_{0,i}\exp\left(\frac{-E_{A,diff,i}}{RT}\right)K_i\left(p_{ret,i} - p_{per,i}\right) \tag{3}$$

in which now an apparent activation energy for the flux ($E_{A,app}$) can be distinguished:

$$E_{A,app,i} = E_{A,diff,i} + \Delta H_{Ads,i} \tag{4}$$

Plotting the back-calculated lumped diffusivity ($\rho\text{Đ}\delta^{-1}$) versus the reciprocal of the temperature shows that Equation 2 holds for all studied components (except neon) (Figure 3). The estimated values for the activation energy and the diffusivity pre-exponent are given in Table 2. The activation energy increases with increasing kinetic diameter, illustrating the steric effects of the 8-ring window opening. Although quite linear Arrhenius plots are shown in Figure 3, it must be emphasized that a loading dependency of the diffusivity (see *e.g.* [22]) is not explicitly considered in Equation 2, and, if present, is therefore contained in the diffusivity activation energy. Recently, a more detailed modelling study of carbon dioxide, methane and nitrogen permeation trough a DD3R membrane revealed strong loading effects of the diffusivity [21]. These results are in accordance with results of molecular dynamics studies [11,22].

Table 2. Kinetic diameter, pre-exponential of diffusivity, activation energy for diffusion and apparent permeation activation energy of the gases under investigation including their 95% confidence intervals. Modelled by Equation 2, DD3R framework density: 1714 kg m^{-3}, membrane thickness: 5.10^{-6} m.

	d_{kin}	$Đ_0$	$E_{A,diff}$	$E_{A,app}$
	nm	/ 10^{-10} m^2 s^{-1}	/ kJ mol^{-1}	/ kJ mol^{-1}
CO_2	0.33	1.9 ± 0.5	6.8 ± 0.7	-21.7
N_2O	0.33	2.2 ± 0.2	7.2 ± 0.2	-21.4
CH_4	0.38	0.47 ± 0.15	15.9 ± 0.9	-1.4
N_2	0.36	1.2 ± 0.5	7.0 ± 1.0	-7.3
Kr	0.37	0.76 ± 0.32	13.7 ± 1.0	-5.1
Ar	0.35	1.0 ± 0.2	9.7 ± 0.5	-4.8
O_2	0.35	0.38 ± 0.39	3.6 ± 3.2	-11.0
Ne	0.28	-	-	-2.2

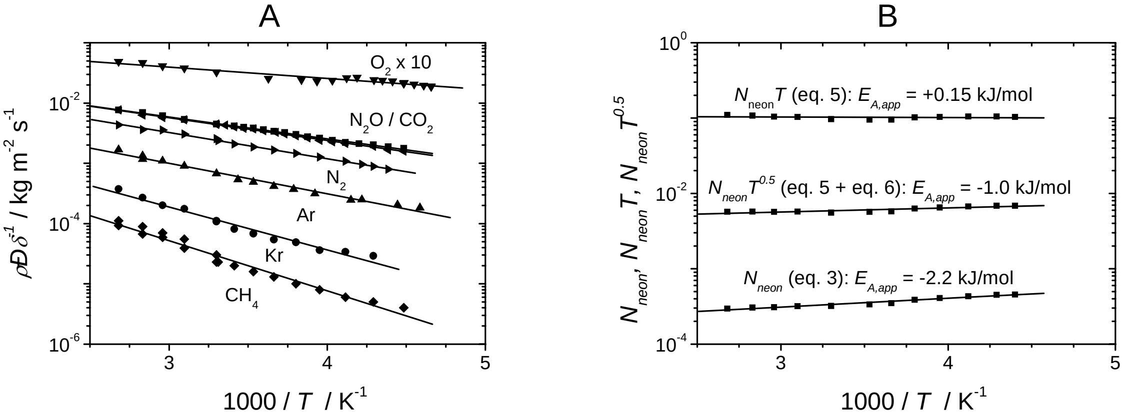

Figure 3. A: Lumped diffusivity ($\rho Đ \delta^{-1}$) as a function of 1000 T^{-1}. B: Neon permeation flux (Equation 3), neon flux multiplied with temperature (Equation 5) and neon flux multiplied with the square root of the temperature (Equation 5 & Equation 6) as a function of 1000 T^{-1}. Feed and permeate pressure 101 kPa, sweep gas helium.

For neon no adsorption data could be established and can be considered as a very weakly adsorbing gas. Plotting the flux against the reciprocal of the temperature (Figure 3B) suggests that the weak adsorption approximation of the surface diffusion equation (Equation 3) holds. The negative apparent activation energy can be due to a smaller activation energy for diffusion than the heat of adsorption. However, based on the presented data we cannot exclude that neon permeates in a non-adsorbed (gaseous) way. In this case mass transport of a gas through a zeolite can be expressed as:

$$N_i = \frac{1}{\delta}\frac{1}{RT}D_i\left(p_{ret,i} - p_{per,i}\right) \tag{5}$$

Where the diffusivity can be of the Knudsen type, which can have an activated part [23]:

$$D_i = \frac{d_0}{3}\sqrt{\frac{8RT}{\pi M_i}}\exp\left(-\frac{E_{A,gas,i}}{RT}\right). \tag{6}$$

Using Equation 5, the slightly increasing neon flux with decreasing temperature can be accounted for by an increased gas phase concentration (p/RT) as is revealed by plotting the product of the flux and temperature versus 1000 T^{-1} (Figure 3B). (Activated) Knudsen type diffusion can not be confirmed as plotting the flux times the square root of temperature (Equation 5 & Equation 6) versus 1000 T^{-1} (Figure 3B) indicates, since a negative activation energy is found. Considering the trends in activation energy with kinetic diameter in Table 2, a non–activated diffusion could indeed be the case for the small neon molecule. The apparent activation energy for permeation of all studied components is given in Table 2. The value of neon is derived from figure 3B, the other component parameters are calculated by Equation 4, where only the enthalpy of adsorption of site A is used in case of the dual-site Langmuir data.

The influence of the feed pressure on the single component fluxes is presented in Figure 4. All component fluxes increase proportionally with feed pressure, following Equation 3 except for carbon dioxide and nitrous oxide. The latter components strongly adsorb and permeation occurs outside the Henry regime.

Comparison of all fluxes as a function of their kinetic diameter reveals the strong steric effects induced by the DD3R window opening (Figure 5). Based on these molecular sieving effects ideal separation factors of over 100 are expected for carbon dioxide / methane separation, two for oxygen / nitrogen, while nitrous oxide and carbon dioxide would be inseparable. The permeation data compare well with earlier data of Tomita *et al.* [5]. The helium flux shown in Figure 5 is the back permeation flux of helium sweep gas in the neon experiment. Since the magnitude of this back-permeation flux is at least comparable and in most cases higher than the other component fluxes, this back-permeation flux might have affected the permeation results as well.

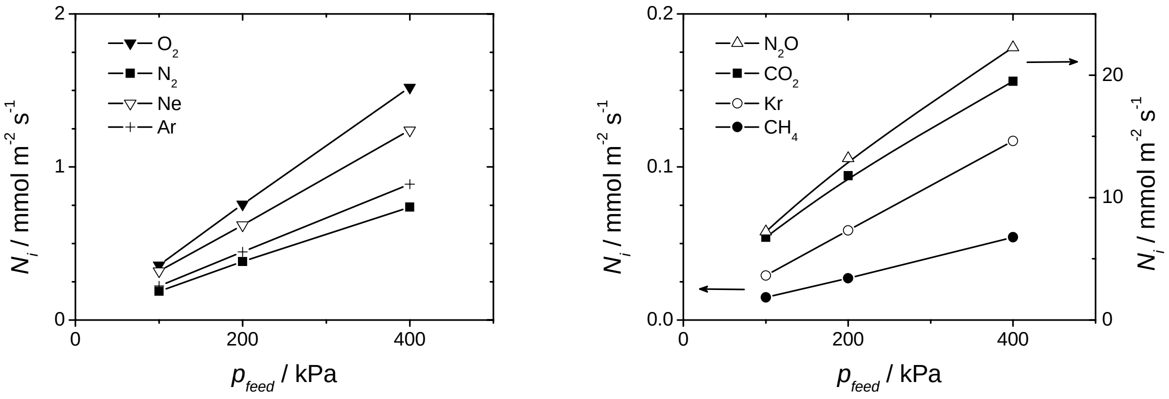

Figure 4. Single component flux of the investigated gases through a DD3R membrane as a function of the feed pressure at 303 K. Permeate pressure 101 kPa, sweep gas helium.

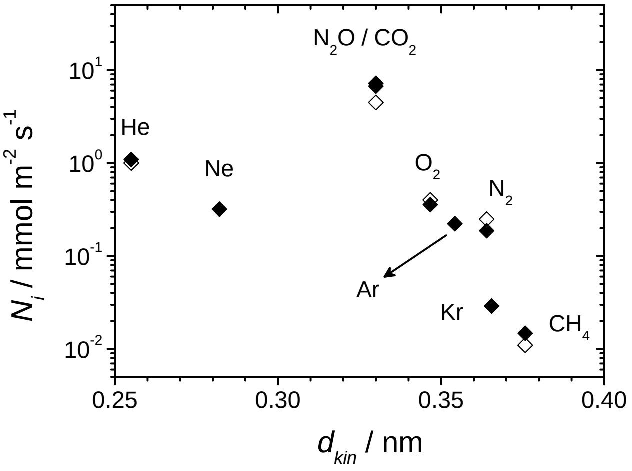

Figure 5. Single component flux of the investigated gases through a DD3R membrane as a function of the kinetic diameter of the molecule at 303 K(◆). Feed and permeate pressure 101 kPa, sweep gas helium. In case of helium, its back permeation flux is presented here when neon was used as feed gas. Data from [5](◇) were measured without sweep gas.

3.3 Back-permeation

To obtain more insight in the back-permeation of helium it was determined for different feed gases (Figure 6). Two situations are distinguished: ‘high’ loading (303 K, 400 kPa feed pressure) and ‘low’ loading (373 K, 101 kPa feed pressure). Figure 6A shows the typical results of a weakly adsorbing gas (argon) and a strongly adsorbing gas (nitrous oxide). The helium flux is slightly reduced with increased feed pressure of the other component. Nitrous oxide suppresses strongly the back permeation flux: the significant occupancy of nitrous oxide hinders helium counter permeation. In Figure 6B the back permeation of helium is presented for different feed gases, where the feed gases are arranged according to increasing feed side loading, from neon to nitrous oxide.

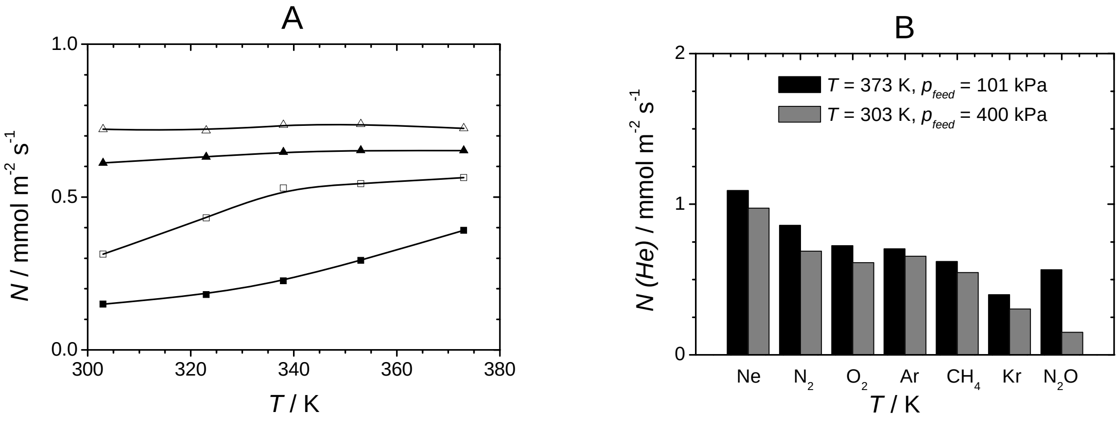

Figure 6. Back-permeation flux of helium. A: As a function of the temperature with argon (▲,△) and nitrous oxide (■,□) as feed gas. Feed pressure at 101 (open symbols) and 400 kPa (closed symbols). B: For different feed gases under 'high' and 'low' adsorption loading conditions. Components are arranged according to increasing adsorption loading.

The results in Figure 6B lead to the conclusion that the helium back permeation is very low for strongly adsorbing components and is the highest for the hardly adsorbed neon. Adsorption is the major factor controlling the back permeation of helium. Whether momentum transfer between diffusing molecules in the cages of the zeolite play a role is not clear though. It is argued based on molecular dynamic simulations that molecular jumps in cage-like structures can be assumed uncorrelated, at least for low loadings [11,24].

3.4 Mixture permeation

Figure 7 shows comparisons of single component permeance ($N_i / \left(p_{ret,i} - p_{per,i} \right)$) data at 101 kPa feed pressure with equimolar mixture permeance data at a total feed pressure of 101 kPa. The pure air permeance compared with air mixtures with nitrous oxide, carbon dioxide and krypton reveals the suppression of the air permeance due to the presence of a strongly adsorbing gas (Figure 7A). The presence of krypton has no observable influence on the air flux (and vice versa, not shown here), addition of carbon dioxide or nitrous oxide strongly reduces the air permeance below 275 K. Similar effects are found for methane. The methane permeance remains unaffected by the presence of nitrogen and is suppressed by carbon dioxide at low temperature (Figure 7B). The temperature where this adsorption suppression becomes manifest is similar as for the air mixtures; approximately below 275 K. It corresponds with occupancies of carbon dioxide and nitrous oxide at the membrane feed side of about 60 % and about 3 molecules per cage. The similarity of the carbon dioxide and nitrous oxide is illustrated once more in Figure 7C. The pure component permeances match those in an equimolar mixture, which one would not expect in first instance.

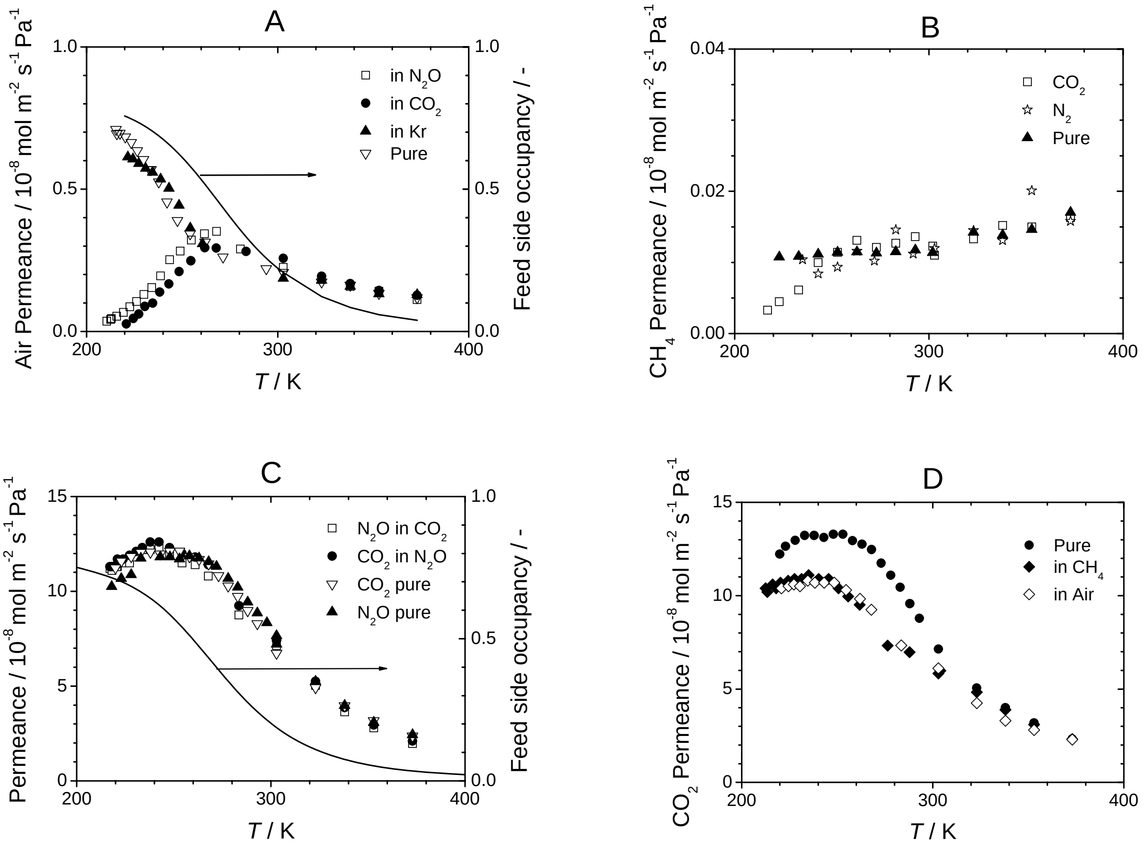

Figure 7. A: Permeance of pure air and in equimolar mixtures with carbon dioxide, krypton and nitrous oxide. B: Permeance of methane as pure component and in equimolar mixtures with nitrogen and carbon dioxide. C: Permeance of nitrous oxide and carbon dioxide in an equimolar mixture and as single component. D: Permeance of carbon dioxide as single component and in equimolar mixtures with air and methane. The continuous lines indicate the predicted occupancy of carbon dioxide at the feed side. All data is measured at a total feed pressure of 101 kPa with helium as sweep gas.

Usually the permeance of the strongly adsorbing components at 50 kPa would be higher than at 101 kPa, meaning that in the absence of mixture effect a higher permeance is expected in a mixture with other gases due to dilution. For the carbon dioxide / nitrous oxide mixture one could almost consider using nitrous oxide as tracer for carbon dioxide or vice versa. On the other hand, the presence of air and methane reduces the carbon dioxide permeance below 300 K (Figure 7D), already at feed side carbon dioxide occupancy of 25 % and higher. Hence, strong interaction effects play a role in these mixtures. Peculiar is that the effect of air and methane on the CO_2 permeance is exactly the same, whereas the fluxes of these components differ at least one order of magnitude.

3.5 Mixture selectivity

The selectivity of DD3R towards the mixtures under investigation is a very important factor with respect to application of the membrane. The selectivity as a function of the temperature and pressure are depicted in Figure 8. The selectivity decreases with increasing temperature and remains constant or decreases with increasing feed pressure. This decreasing trend occurs when one of the components is strongly adsorbing (nitrous oxide or carbon dioxide). In the case of the krypton / air mixture, a weak increasing trend of the selectivity is observed. The selectivity with respect to the relative strongly adsorbed krypton decreases, which is the same trend as found for the nitrous oxide / air, carbon dioxide / air and carbon dioxide / methane mixtures, but less pronounced, since krypton adsorbs significantly weaker than carbon dioxide and nitrous oxide. As already expected from the single component data, very high carbon dioxide selectivities are found for carbon dioxide / methane mixtures at 101 kPa feed pressure; ~500 at room temperature, >> 1000 below 250 K and still > 100 at 373 K. The separation factor of carbon dioxide and nitrous oxide to air is well above 20 and increases above 100 in the low temperature region. Additionally, the carbon dioxide flux is high in both cases. Air separation (oxygen / nitrogen) has a reasonable separation factor of two but a very low flux. The oxygen / nitrogen selectivity in the air / nitrous oxide and air / carbon dioxide mixture permeation is also two (not shown here). Air / krypton separation factors are 5-10, nitrogen / methane 20-45 and nitrous oxide / carbon dioxide is exactly 1.

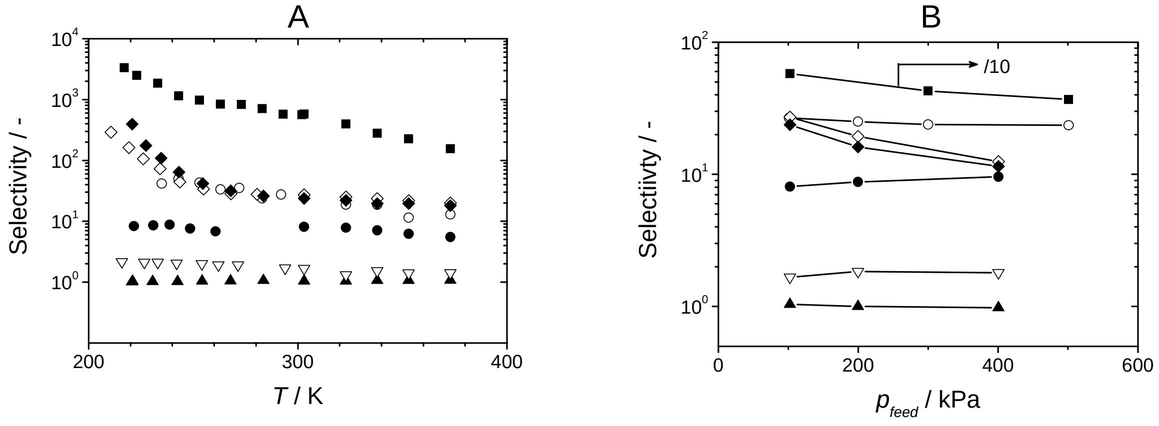

Figure 8. Selectivities of the investigated equimolar mixtures through the DD3R membrane as a function of the temperature (A) and total feed pressure (B). Isobaric data at constant total feed pressure of 101 kPa, isothermal data at 303 K, sweep gas He at 101 kPa. Legend: CO_2 / CH_4 (■), N_2 / CH_4 (○), CO_2 / Air (◆), N_2O / Air (◇), Air / Kr (●), O_2 / N_2 (▽), N_2O / CO_2 (▲).

For mixtures with strongly adsorbing components, the increased selectivity is attributed to selective adsorption. Comparison of the ideal permeation selectivity to the mixture selectivity clearly reveals this behaviour (Figure 9). At low temperatures the mixture selectivity is much higher than the ideal selectivity for the carbon dioxide mixtures. For the weakly adsorbed nitrogen and methane the mixture and ideal selectivities are the same, which is characteristic for all other mixtures without strongly adsorbing gases.

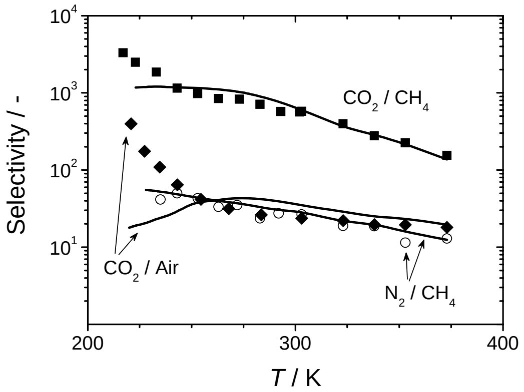

Figure 9. Comparison of the mixture selectivity (symbols) and the ‘ideal’ selectivity (lines) at a total feed pressure of 101 kPa for equimolar binary mixtures of carbon dioxide, methane and nitrogen. Ideal selectivity is based on single component flux data at a total feed pressure of 101 kPa.

3.6 Mixture adsorption prediction

Mixture mass transport through a zeolite membrane is the result of complex interplay of adsorption and diffusion effects. Therefore, it can be instructive to isolate the adsorption effects and compare these with the mixture permeation data.

Figure 10A-D display the amount adsorbed and adsorption selectivity of carbon dioxide, nitrogen, methane and mixtures thereof as a function of the temperature. The mixture properties are calculated with the Ideal Adsorbed Solution Theory (IAST) [25]. This theory allows prediction of mixture loadings based on single component adsorption isotherms and is generally assumed applicable to zeolite systems. Adsorption data from Table 1 are used as input data. Nitrogen is taken as model component for air. Figure 10A reveals that severe competitive adsorption effects are expected at temperatures below 275 - 300 K for carbon dioxide / air and carbon dioxide / methane mixtures. For the methane / nitrogen mixture little competitive effects are expected. All observations are in line with the permeation results, also the temperature range where the competitive effects occur in the permeation and adsorption data match quite well (Figures 7A, B and D). But the effects in the permeation data seem to appear at somewhat lower temperatures and the maximum in permeance are more pronounced.

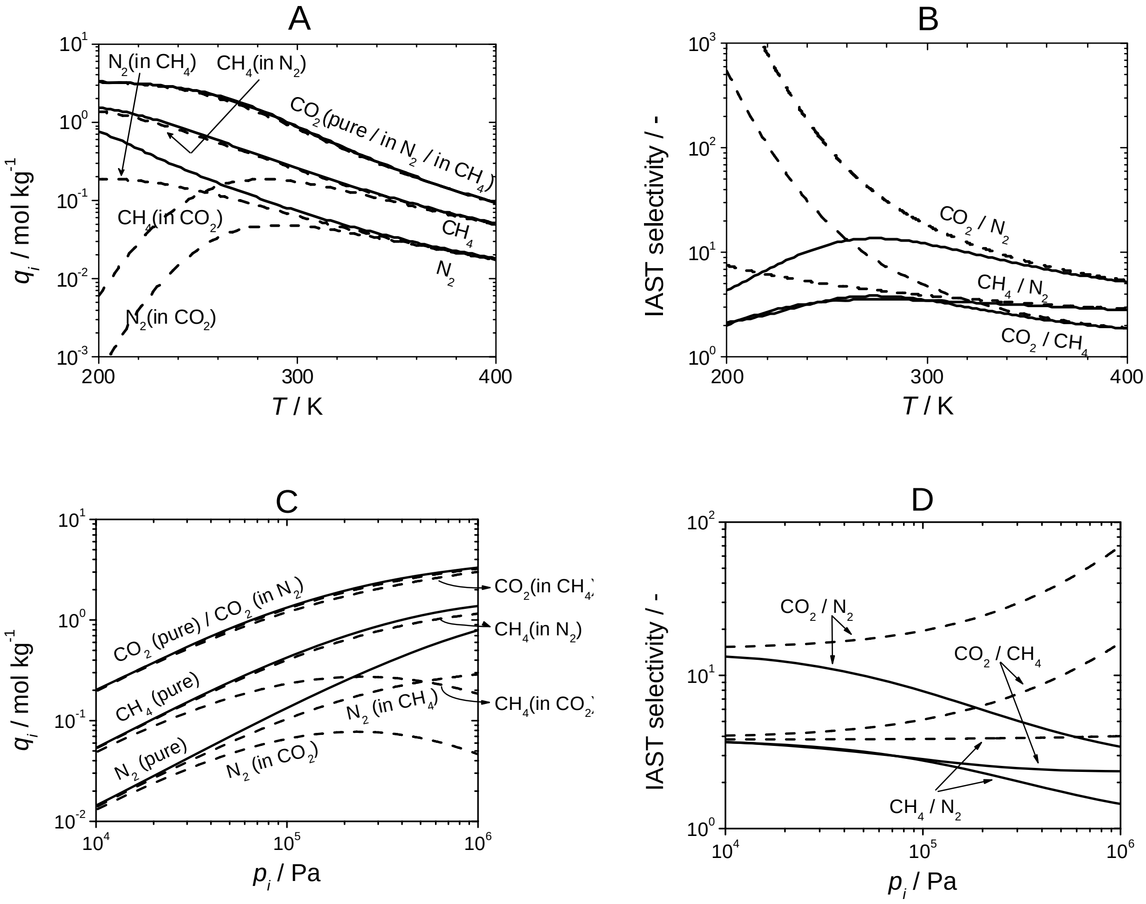

Figure 10. Comparison of amount adsorbed (A, C) and adsorption selectivity (B, D) of carbon dioxide, nitrogen and methane as pure components (solid lines) and in equimolar binary mixtures (dashed lines) as a function of temperature (p_i = 50 kPa) and of pressure (T = 303 K). Mixture loadings are predicted by the IAST.

The predicted loading of carbon dioxide is hardly affected by the presence of methane or nitrogen. This indicates that the effects of air and methane on the carbon dioxide permeance as shown in Figure 7D are most likely related to momentum transfer between these two species.

With increasing pressure competitive adsorption effects are expected, though not as strong as found with temperature variations (Figure 10C and D). The adsorption selectivity trend is opposite of the permeation behaviour (Figure 8B). The decreasing selectivity with pressure has also been found by molecular simulations and is explained by a strong loading dependence of the diffusivity of the individual components on the total loading [11,22,24,26]. This appears to be a property inherent to the cage-like structure of DD3R in which molecules residing in the cages exert repulsion forces on each other, increasing their diffusivity [27,28]. More concrete, this means that the presence of carbon dioxide increases the diffusivity of methane and air, resulting in a decrease of the mixture selectivity. This is also suggested by the selectivity data in Figure 9. A low temperature region is found ($T < 250$ K) where adsorption effects dominate, and an intermediate temperature region ($250 < T < 300$ for carbon dioxide / methane and $275 < T < 350$ for carbon dioxide / air) where the mixture selectivity is lower than the ideal selectivity.

4 Conclusions

Adsorption of the investigated gases in different DD3R samples could be modelled well by a single-site Langmuir isotherm for argon, oxygen, nitrogen and methane and a dual-site Langmuir isotherm for carbon dioxide, nitrous oxide and krypton.

Permeation is determined by the size of the molecule relative to the window opening of DD3R, and its adsorption behaviour. As a function of temperature, bulky molecules (methane) show activated permeation, weakly adsorbing molecules decreasing permeation behaviour and strongly adsorbing molecules pass through a maximum. Counter diffusion of the sweep gas (helium) ranged from almost zero up to the order of the feed gas permeation and was strongly influenced by the type of feed gas.

The DD3R membrane has excellent separation performance for carbon dioxide / methane mixtures (selectivity 100 – 3000), exhibit good selectivity for nitrogen / methane (20 - 45), carbon dioxide and nitrous oxide / air (20 - 400), and air / krypton (5 – 10) and only a modest selectivity for oxygen / nitrogen (~2) separation. The selectivity of mixtures of a strongly and a weakly adsorbing component decreased with increasing temperature and pressure. The selectivity of mixtures of weakly adsorbing components was independent of pressure.

The permeation and separation characteristics of permanent gases through DD3R membranes can be explained by taking into account: (1) steric effects introduced by the window opening of DD3R leading to molecular sieving and activated transport, (2) competitive adsorption effects, as observed for mixtures involving strongly adsorbing gases, and (3) interaction between diffusing molecules in the cages of the zeolite.

Acknowledgements

Exxon Mobil is gratefully acknowledged for supplying the crystals, NGK Insulators for supplying the membranes and Johan Groen and Sander Brouwer (TU Delft) for performing the adsorption experiments.

References

[1] J. Caro, M. Noack, and P. Kölsch, *Adsorption-Journal of the International Adsorption Society*, 11, **2005**, 215.

[2] H. Gies, *Zeitschrift fur Kristallographie*, 175, **1986**, 93.

[3] S. G. Li, J. L. Falconer, and R. D. Noble, *Abstracts of Papers of the American Chemical Society*, 227, **2004**, 350.

[4] Y. Cui, H. Kita, and K. Okamoto, *Journal of Materials Chemistry*, 14, **2004**, 924.

[5] T. Tomita, K. Nakayama, and H. Sakai, *Microporous and Mesoporous Materials*, 68, **2004**, 71.

[6] M. J. den Exter, J. C. Jansen, and H. van Bekkum, *Zeolites and Related Microporous Materials: State of the Art 1994*, 84, **1994**, 1159.

[7] W. Zhu, F. Kapteijn, and J. A. Moulijn, *Chemical Communications*, **1999**, 2453.

[8] F. Kapteijn, W. J. W. Bakker, J. van de Graaf, G. Zheng, J. Poppe, and J. A. Moulijn, *Catalysis Today*, 25, **1995**, 213.

[9] F. Kapteijn, J. van de Graaf, and J. A. Moulijn, *Journal of Molecular Catalysis A-Chemical*, 134, **1998**, 201.

[10] J. M. van de Graaf, F. Kapteijn, and J. A. Moulijn, *AIChE Journal*, 45, **1999**, 497.

[11] R. Krishna, J. M. van Baten, E. Garcia-Perez, and S. Calero, *Industrial & Engineering Chemistry Research*, 46, **2007**, 2974.

[12] J. M. van de Graaf, F. Kapteijn, and J. A. Moulijn, *Journal of Membrane Science*, 144, **1998**, 87.

[13] F. Kapteijn, J. A. Moulijn, and R. Krishna, *Chemical Engineering Science*, 55, **2000**, 2923.

[14] F. Kapteijn, W. Zhu, J. A. Moulijn, and T. Q. Gardner, Zeolite Membranes: Modeling and Application, in: Structured Catalysts and Reactors, Cybulski, A. and Moulijn, J. A. (Eds), Ch. 20, **2005**, Taylor & Francis Group, Boca Raton, FL, 701.

[15] R. Krishna and J. A. Wesselingh, *Chemical Engineering Science*, 52, **1997**, 861.

[16] S. Himeno, T. Tomita, K. Suzuki, and S. Yoshida, *Microporous and Mesoporous Materials*, 98, **2007**, 62.

[17] W. Zhu, Adsorption and Diffusion in Microporous Materials, PHD thesis, **2001**, Delft University of Technology, Delft.

[18] F. Kapteijn, J. M. van de Graaf, and J. A. Moulijn, *AIChE Journal*, 46, **2000**, 1096.

[19] W. J. W. Bakker, F. Kapteijn, J. Poppe, and J. A. Moulijn, *Journal of Membrane Science*, 117, **1996**, 57.

[20] W. J. W. Bakker, L. J. P. van den Broeke, F. Kapteijn, and J. A. Moulijn, *AIChE Journal*, 43, **1997**, 2203.

[21] J. van den Bergh, W. Zhu, J. C. Groen, F. Kapteijn, J. A. Moulijn, K. Yajima, K. Nakayama, T. Tomita, and S. Yoshida, *Studies in Surface Science and Catalysis*, 170 A, **2007**, 1021.

[22] R. Krishna, J. M. van Baten, E. Garcia-Perez, and S. Calero, *Chemical Physics Letters*, 429, **2006**, 219.

[23] J. M. van de Graaf, F. Kapteijn, and J. A. Moulijn, *Chemical Engineering Science*, 54, **1999**, 1081.

[24] S. Li, J. L. Falconer, R. D. Noble, and R. Krishna, *Industrial & Engineering Chemistry Research*, 46, **2006**, 3904.

[25] A. L. Myers and J. M. Prausnitz, *AIChE Journal*, 11, **1965**, 121.

[26] S. Li, J. L. Falconer, R. D. Noble, and R. Krishna, *Journal of Physical Chemistry C*, 111, **2007**, 5075.

[27] D. A. Reed and G. Ehrlich, *Surface Science*, 102, **1981**, 588.

[28] J. R. Xiao and J. Wei, *Chemical Engineering Science*, 47, **1992**, 1123.

3

High temperature permeation and separation characteristics of an all-silica DDR zeolite membrane

The permeation and separation characteristics of an all-silica DDR zeolite tubular membrane have been studied in the temperature range of 303 to 773 K and feed pressures up to 500 kPa. The permeation experiments are complemented by single component adsorption isotherms.

The permeance of He, H_2, CO_2, CO and N_2 monotonically decreases with increasing temperature. This behaviour could be described accurately for all components by a surface diffusion mechanism. Only in case of N_2 and CO small deviations are observed above 600 K. Isobutane is not able to enter the DDR pores and passes only through a very small number of defects in the membrane.

All single component permeances are about equal to the permeances of these components in a binary mixture. Only below 473 K the H_2 permeance in a mixture with CO_2 or isobutane is reduced in comparison with its single component permeance. The ideal H_2/CO and CO_2/CO selectivities range from 3 to 12 and 10 to 2 between 303 and 673 K, respectively. The mixture selectivities where always below 5 and much lower than the ideal selectivities because of non-differential operation along the membrane tube. The ideal H_2/isobutane selectivity is > 600 at 101 kPa feed pressure at all temperatures. The mixture selectivities at 101 kPa total feed pressure are ~ 400 in an equimolar binary mixture.

This chapter is based on the following publication:

J. van den Bergh, A.Tihaya and F. Kapteijn, Microporous and Mesoporous Materials, 132, **2010**, 137.

The high selectivities, high H_2 and CO_2 fluxes and stable membrane operation, also at high temperatures, makes this membrane a potential candidate for high temperature (reactive) separations that involve removal of H_2 and CO_2.

1 Introduction

Zeolites are crystalline aluminosillicates with well-defined pores of sub-nanometer dimensions. Advantages of this type of material are its high thermal and chemical stability and its molecular sieving ability allowing very specific size-selective separations. After the first reports of zeolite membranes in the late eighties the quality of zeolite membranes improved and in 2001 the first industrial scale application of a zeolite membrane was accomplished by Mitsui [1]. They developed a large scale pervaporation plant based on NaA zeolite membranes to dewater alcohols, producing 530 L h^{-1} of solvents.

The most studied zeolite membranes are of the MFI type. This medium pore 10-ring zeolite has a pore diameter of 0.55 nm. This cut-off diameter allows separation of xylenes [2] and linear from branched hydrocarbons [3]. A recent trend is to develop membranes based on small-pore 8-ring window zeolites that allow separation of light gases. An example of such a zeolite is DDR which consists of cages connected by 8-ring window openings of 0.36×0.44 nm. This type of zeolite has received considerable attention in recent years: DDR has been demonstrated to be very successful in propane/propene [4,5], CO_2/CH_4 [6-8][Chapter 2] and water/ethanol [9] separation. The good separation performance is based mainly on its molecular sieving abilities.

The objective of this chapter is to demonstrate the separation quality of a tubular DD3R membrane at high temperature. The abbreviation DD3R is commonly used to refer to all-silica DDR. Permeation results are presented up to 773 K for various light gases (He, H_2, CO_2, CO, N_2 and isobutane) and several binary mixtures thereof. Special attention is paid to the mass transport mechanism through this type of membrane at high temperatures, for this is currently under debate [10-14]. An important question regarding this matter is up to which extent adsorption takes place at these elevated temperatures. Therefore, adsorption experiments at elevated temperatures have been carried out to verify this.

The chapter is built up as follows. Firstly, the adsorption results are discussed (Section 3.1) and some remarks are made on the stability of the membrane and reproducibility of the permeation experiments (Section 3.2). Then the permeation results of isobutane are presented, a molecule that cannot enter the DDR pores and passes only through membrane defects (Section 3.3). The influence of pressure and temperature on the single component permeances are discussed in Section 3.4 and 3.5, respectively, while in the latter section also the mass transport mechanism is treated in detail. In Section 3.6 the estimated surface diffusivities are discussed and compared to literature data. The mixture permeation results and the obtained selectivities are given in Section 3.7 and 3.8, respectively. But, first we continue the introduction with background information on the current views on the mass transport mechanism across zeolite membranes, specifically at high temperatures.

1.1 Mass transport mechanism

Intra-crystalline transport through zeolite membranes is commonly referred to as surface diffusion or zeolitic diffusion, which is an interplay between diffusion and adsorption. The most promising approach to model this in our view is within the Maxwell-Stefan approach to mass transport [15]. For zeolitic systems dedicated model equations have been derived for single component and mixture systems [16-19].

The loading or adsorbed concentration (q_i) on zeolites is an essential part in modelling mass transport in zeolites. The loading of component *i* can be related to the partial pressure of component *i* (p_i) via a Langmuir adsorption isotherm:

$$q_i = q_i^{sat} \frac{K_i p_i}{1 + K_i p_i}, \qquad K_i = K_{0,i} \exp\left(\frac{-\Delta H_{Ads,i}}{RT} \right), \tag{1}$$

in which $q_\mathrm{i}^\mathrm{sat}$ represents the saturation loading and K_i the adsorption equilibrium constant. The latter is dependent on temperature via a van ‘t Hoff dependency yielding an adsorption enthalpy ($\Delta H_{\mathrm{Ads,i}}$) and pre-exponential adsorption equilibrium constant ($K_{0,\mathrm{i}}$). In case the loading on the zeolite is represented by a single-site Langmuir isotherm the analytical solution of the Maxwell-Stefan equations to describe the flux (N_i) of a single component *i* through the membrane is [18]:

$$N_i = \frac{\rho}{\delta} \cdot \text{Đ}_i \cdot q_i^{sat} \cdot \ln\left(\frac{1 + K_i \cdot p_{ret,i}}{1 + K_i \cdot p_{per,i}} \right), \qquad \text{Đ}_i = \text{Đ}_{0,i} \cdot \exp\left(\frac{-E_{A,diff,i}^{S}}{R \cdot T} \right). \tag{2}$$

δ is the membrane thickness, ρ the zeolite density and Đ_i the Maxwell-Stefan diffusivity of component *i* in the zeolite. The diffusivity has an Arrhenius type temperature dependency leading to an activation energy for surface diffusion ($E_{A,dif,i}^{S}$) and a pre-exponential of the diffusivity ($\text{Đ}_{0,i}$). The flux is also dependent on the permeate (p_{per}) and retentate (p_{ret}) pressure. Note that in this case mass transport is related to the total concentration of the component in the zeolite. However, adsorption in zeolites can be segregated [20] and it has been shown recently that accounting for this effect leads to an improved description of the mass transport in zeolites [21,22][Chapter 5].

In case that adsorption is weak, the adsorption isotherm can be expressed by Henry’s law ($q_i = q_i^{sat} K_i p_i$) and Equation (2) can be simplified into:

$$N_i = \frac{q_i^{sat} \cdot \rho}{\delta} Đ_i \cdot K_i \cdot \left(p_{ret,i} - p_{per,i} \right). \tag{3}$$

The combination of the diffusivity and the adsorption equilibrium constant yields an apparent activation energy:

$$E_{A,app,i}^{S} = E_{A,diff,i}^{S} + \Delta H_{Ads,i}. \tag{4}$$

The temperature dependency that can be expected based on the surface diffusion mechanism is dependent on the apparent activation energy [23]. If the apparent activation energy is positive ($E_{A,diff,i}^{S} > -\Delta H_{Ads,i}$) a continuously increasing flux with increasing temperature would be observed. However, in most cases $E_{A,diff,i}^{S} < -\Delta H_{Ads,i}$ and then, starting from very low temperatures, the flux first increases with increasing temperature, passes through a maximum and then continuously decreases.

The latter dependency has been confirmed by Bakker *et al.* [24] and van de Graaf *et al.* [11,25] who measured a series of gases through MFI membranes. However, at high temperatures the decreasing trend changes into an increasing flux with increasing temperature for many components, particularly for weakly adsorbing components.

To explain these results the so-called gas translation diffusion mechanism proposed by Xiao and Wei [26,27] was used. In the case that (almost) no adsorption occurs molecules retain their gaseous nature inside the zeolite and the flux can be expressed as follows:

$$N_i = \frac{1}{\delta} \frac{1}{RT} \frac{\alpha}{z} \sqrt{\frac{8RT}{\pi M_i}} \exp\left(-\frac{E_{A,diff,i}^{G}}{RT} \right) \left(p_{ret,i} - p_{per,i} \right). \tag{5}$$

z represents the coordination number (which would be three in case of DDR), α the distance between adjacent sites and M_i the molar mass of component *i*. In this case an activation energy for gaseous diffusion ($E_{A,diff,i}^{G}$) is found. This activation energy arises from a potential difference between a site (*e.g.* a cavity) and a steric barrier that separates two sites (*e.g.* a window opening). This type of diffusion is sometimes also referred to as activated gaseous or activated Knudsen diffusion. A full description of the flux dependency on the temperature could now be obtained by considering surface and gas translation diffusion as parallel processes [11,24].

When considerable amounts are adsorbed on the zeolite, surface diffusion will be the dominant transport mechanism. However, the permeation mechanism at elevated temperatures, when little or no adsorption occurs is subject of debate. Recently, two groups have published high temperature membrane permeation results that give cause to reconsideration of the permeation mechanism at these conditions [12-14]. Kanezashi *et al.* [12,13] propose that indeed the governing mechanism at high temperatures is of the gas translation type. The activation energy of the gas translation is related to the molecule/pore diameter ratio, as already proposed by Xiao and Wei [26,27]: with increasing molecule/pore diameter ratio an increasing activation energy for diffusion is expected. Kanezashi and Lin [12] reported a continuously decreasing H_2, He, CO and CO_2 flux with increasing temperature through a MFI membrane up to 773 K. Their membrane consisted of relatively small crystals (200-400 nm). The molecule/pore diameter ratio is relatively small in this system leading to a very low activation energy for gas translation diffusion. The estimated activation energy for diffusion was that low that a Knudsen type diffusion could explain the observed flux-temperature dependency. However, in case of H_2, He, and CO permeation experiments up to 773 K through an all-silica DDR membrane, increasing fluxes with increasing temperature were found at elevated temperatures [13]. These results are opposite to the results for the same components through MFI membranes. This difference is explained by a larger molecule/pore diameter ratio in case of DDR, which leads to a higher activation energy for diffusion and, consequently, an apparent activated flux behaviour.

A different interpretation is proposed by Miachon *et al.* [14] based on permeation results suggesting that the governing mass transport mechanism is surface diffusion, even at high temperatures. They measured H_2 permeation through a pore-plugging MFI membrane (zeolite crystals inside support, no film on top of the support) up to 873 K and observed a continuously decreasing flux with increasing temperature. They could describe their results accurately with a surface diffusion mechanism over the complete temperature range. The flux increase at high temperature in, for example, the work of Van de Graaf *et al.* [11] was attributed to the thermal expansion mismatch of the support and zeolite membrane. With increasing temperature the support expands and the zeolite crystals shrink, thereby creating defects that led to the flux increase. The absence of these effects in their own permeation measurements is due to the small crystals that are present inside the support that would minimize the formation of defects upon temperature increase. The surface diffusion mechanism appeared also valid for permeation of N_2 and a series of linear, light hydrocarbons through MFI membranes up to high temperature (723 K).

2 Experimental

2.1 Adsorption experiments

Adsorption experiments of CO, CO_2 and H_2 have been performed on all-silica DD3R crystals. The crystals have been synthesized in-house, using the method of den Exter [5,28,29]. A Micromeretics ASAP 2010 gas adsorption analyzer has been used to measure the adsorption isotherms (volumetric), more details on the equipment and followed procedure are provided elsewhere [7][Chapter 2].

In case of the very weak adsorbing H_2 the isotherms have been measured at low temperatures (77.4, 195 and 253 K). In case of CO and CO_2 also isotherms at high temperature (up to 373 K for CO and up to 473 K for CO_2) were measured to obtain insight into the adsorption behaviour at these elevated temperatures

2.2 Membrane permeation experiments

Membrane permeation experiments were carried out on a tubular DD3R zeolite membrane provided by NGK Insulators [30]. The membrane is of the same batch as used by Kuhn *et al.* [9] who also show SEM pictures of the membrane. A ~1-2 μm thick zeolite layer is present on the outside of a 150 mm long α-alumina tube. The outer diameter of the tube is 12 mm. The support consists of three layers of different pore size (0.2, 1 and 5 micron) and thickness (13, 70 and 1750 micron, respectively). The composite membrane was sealed in a stainless-steel module using graphite O-rings leaving 120 mm effective tube length and 0.0045 m^2 membrane area.

Before experiments the membrane was flushed with He at 373 K overnight to remove adsorbed materials. The permeation experiments were carried out in two separate series; in between the membrane was stored at ambient conditions for four months. During the first series single component permeation of He, H_2, CO_2 and CO and equimolar binary mixture permeation of CO_2/H_2, CO_2/CO and CO/H_2 mixtures were studied under pressure drop conditions (no sweep gas). The permeate pressure was always at atmospheric pressure. The feed pressure was varied between 200 and 500 kPa and the temperature between 303 and 673 K. Total feed flow rate was 250 ml min^{-1} (STP) for all experiments.

In the second series single component permeation of H_2, and isobutane and equimolar binary mixture permeation of H_2/isobutane mixtures were studied using nitrogen as sweep gas. Single component He permeances were measured in the pressure drop mode (no sweep gas). The permeate pressure was always at atmospheric pressure. The feed pressure was varied between 101 and 300 kPa and the temperature between 303 and 773 K. In case of the He and H_2 single component experiments both the feed and sweep gas flow rate were set to 200 ml min^{-1} (STP). The experiments involving isobutane were performed at a feed and sweep gas flow rate of 100 ml min^{-1} (STP).

All experiments were carried out in counter-current mode. The retentate and permeate flows were determined using a soap-film meter. The compositions of both flows were determined by GC analysis. In the case of isobutane a FID detector and for all other components a TCD detector was used. For H_2 detection Ar was used as carrier gas.

Because of the tubular geometry of the membrane, the composition of the feed and sweep flow can change along the tube length. Therefore, the permeance is calculated using a logarithmic-mean pressure difference [31]. In case of counter-current operation this is expressed as:

$$\left(\Delta p_i\right)_{lm} = \frac{\left(p_i^{feed} - p_i^{perm}\right) - \left(p_i^{ret} - p_i^{sweep}\right)}{\ln\left(\dfrac{p_i^{feed} - p_i^{perm}}{p_i^{ret} - p_i^{sweep}}\right)}. \tag{6}$$

3 Results and Discussion

3.1 Adsorption results

Figure 1 shows the equilibrium adsorption isotherms of CO_2, CO and H_2 on all-silica DD3R crystals up to 120 kPa. The lines represent model fit results with a single-site Langmuir isotherm (Equation (1)). For all components a good description of the adsorption data is obtained. The estimated adsorption equilibrium constants are listed in Table 1. In case of H_2 a relatively poor fit of the data is obtained. This can be due to the very broad temperature range covered, and moreover, due to the low amount adsorbed of H_2 the quality of the data is not optimal. Note that the estimated saturation loading should be considered primarily as a model fit parameter, it underestimates the total saturation loading.

The amount adsorbed at 100 kPa and 298 K is used to compare the adsorbates to each other (Table 1). Also the previously determined [7](Chapter 2) adsorption isotherms of N_2, O_2, Ar, Kr and CH_4 are taken into consideration. Now the following order in amount adsorbed under these conditions is found: $CO_2 >> Kr \approx CH_4 > CO > N_2 \approx O_2 \approx Ar > H_2$. Isobutane is too large to fit into the DDR pore and is taken as non-adsorbing. CO_2 will be referred to from now on as strong adsorbing, CO and N_2 as weak adsorbing and H_2 as very weak adsorbing component on DD3R. This order is also reflected in the maximum temperature at which still reliable adsorption data could be obtained. In case of CO_2 at 573 K and CO at 473 K still 0.035 and 0.009 mol kg^{-1} have been measured at 120 kPa, respectively. However, the full isotherms are omitted because of insufficient accuracy of the data.

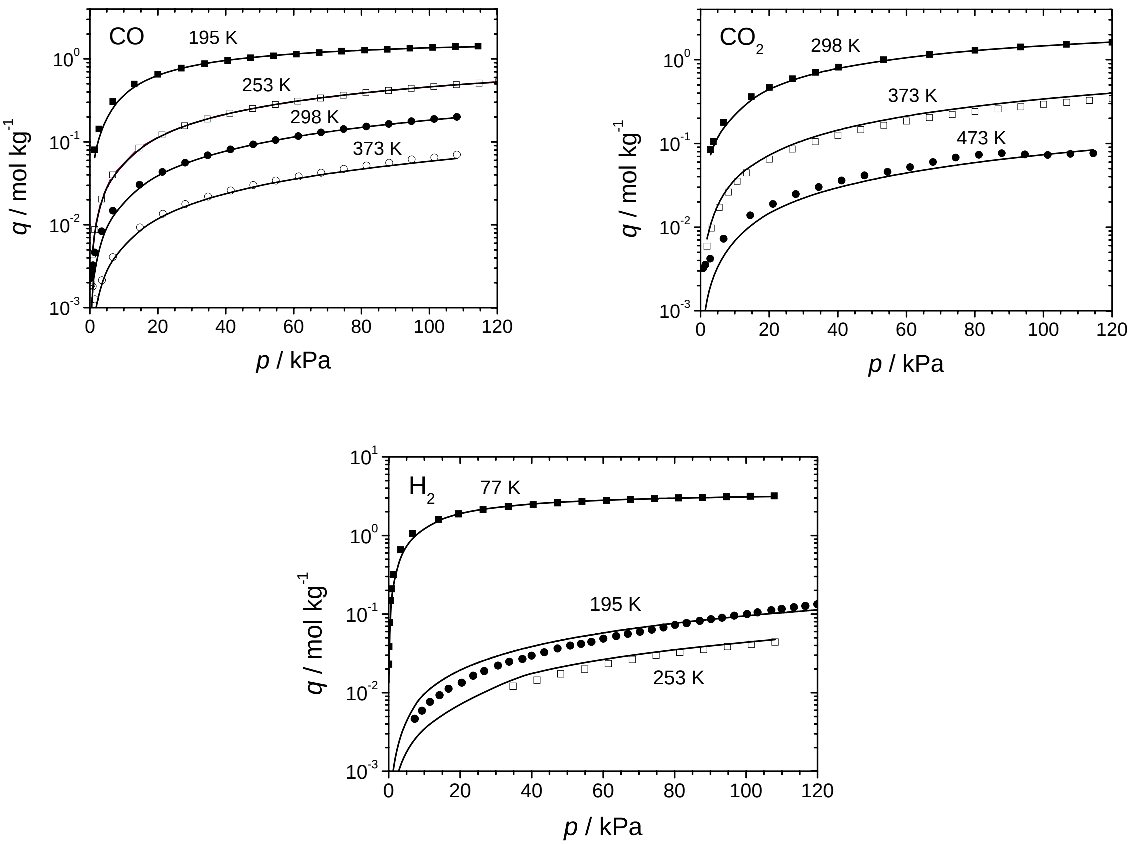

Figure 1. Adsorption isotherms of CO, CO_2 and H_2 on all-silica DD3R crystals. Lines represent model fit results of a single-site Langmuir isotherm.

Table 1. Single-site Langmuir adsorption parameters of CO_2, CO and H_2 on DD3R crystals. Including the adsorption enthalpies of N_2, Ar, Kr and CH_4 determined previously [7](Chapter 2) and the adsorption enthalpies of a series of light gases on silicalite-1 (MFI) [24].

	q (100 kPa, 298 K) mol kg^{-1}	q^{sat} mol kg^{-1}	K_0 kPa^{-1}	ΔH_{ads} kJ mol^{-1}	ΔH_{ads} (MFI)^b kJ mol^{-1}
CO_2	1.47	3.46	$5.26\cdot10^{-7}$	-23.7	-24.0
CO	0.19	1.89	$2.58\cdot10^{-6}$	-14.9	-17.9 ^{c}
H_2	0.10 (253 K)	3.66	$8.22\cdot10^{-6}$	- 5.6	- 5.9
O_2	0.13	-	-	-14.6 ^{a}	-
N_2	0.15	1.75 ^{a}	$2.83\cdot10^{-6\,a}$	-14.3 ^{a}	-13.8
Ar	0.13	-	-	-14.5 ^{a}	-13.2
Kr	0.40	-	-	-18.8 ^{a}	-19.3
CH_4	0.45	-	-	-17.3 ^{a}	-22.6

^{a} Data taken from [7]; ^{b} Data taken from [24]; ^{c} Determined from membrane permeation data.

A comparison is made of the estimated adsorption enthalpies on the all-silica DDR and literature adsorption enthalpies of the same gases on silicalite-1 (all-silica MFI zeolite) (Table 1). These results are in good agreement indicating that the temperature dependency of adsorption of these all-silica materials is very similar.

An intriguing question is how much actually adsorbs at high temperature, *i.e.* what is the excess amount adsorbed. To evaluate this, a comparison of the adsorbed concentration to the concentration in an ideal gas under the same conditions is calculated. Note that in the volumetric adsorption experiments the amount adsorbed is calculated using the (assumed) non-adsorbing He gas as a reference. This means that the determined loadings represent an excess amount adsorbed. The adsorbed concentration is expressed based on the total accessible volume of the DD3R crystals. Zhu *et al.* [32] report an apparent density of DD3R crystals of 1714 kg m^{-3} and an accessible pore volume of 0.15 dm^3 kg^{-1} based on N_2 physisorption. This leads to an accessible porosity of 0.26. This value is used to estimate the adsorbed amount per volume unit of zeolite. Figure 2 shows the adsorbed to ideal gas concentration of CO_2, CO, N_2 and H_2 at 101 kPa as a function of the temperature. A significant concentration enrichment relative to the corresponding gas concentration is found. The temperature at which the ratio of the adsorbed and gas phase concentration equals 10 is 275, 450, 450 and 600 K for H_2, N_2, CO and CO_2, respectively.

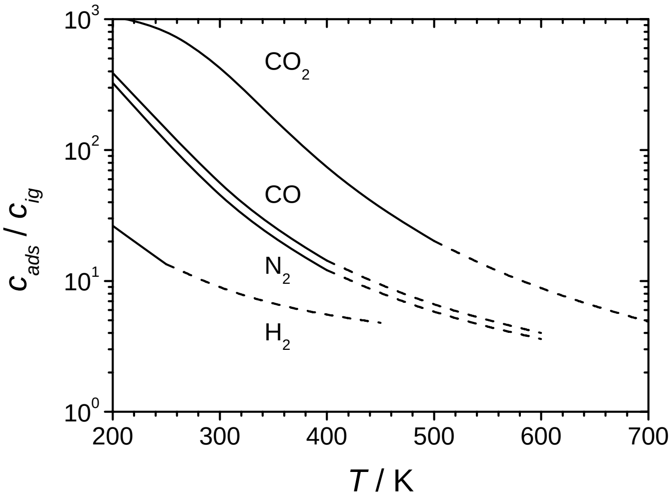

Figure 2. Ratio of the adsorbed concentration in DDR and ideal gas concentration at the same temperature of CO_2, CO, N_2 and H_2 at 101 kPa as a function of the temperature. Adsorbed concentrations are calculated using the Langmuir adsorption parameters given in Table 1. Dashed lines represent data extrapolated outside the experimental data region.

3.2 Reproducibility of permeation experiments

After pre-treatment of the membrane at 373 K under He overnight the reproducibility of the permeation experiments has been studied by a series of He membrane permeation experiments. Figure 3 shows the He permeance at a feed pressure of 300 kPa as a function of the temperature. These data have been collected at the start of the second series of experiments, directly after pretreating the membrane overnight with He at 373 K. A stepwise temperature cycle has been made from 373 K to 773 K and back to 303 K. A difference in the permeance has been found: the He permeance is higher in the cooling branch. When performing a second cycle this difference is not observed anymore and the permeance is stable, at the top branch. Although stable membrane performance is obtained after the first temperature cycle, when the membrane is stored under ambient conditions for several months similar behaviour is observed: only after the first full temperature cycle stable membrane operation is obtained. Possibly the hysteresis is related to the removal of some residue of the synthesis or some settling effect of the crystals upon temperature increase. The first explanation does not seem very likely since in this case the hysteresis is expected to disappear permanently after the first temperature cycle. Moreover, the membrane has been calcined prior to use at high temperatures (~1073 K for 4 hr [30]). An alternative explanation could be hydrolysis of the membrane surface, which imposes a surface barrier leading to a lower flux. Upon heat treatment the hydroxyl groups are removed, however when stored in open air the surface is able to rehydrolyse.

Throughout the membrane experiments control experiments of He indicated a stable membrane operation for several months of operation, including long term (~ 5 days) high temperature operation and numerous (>10) full temperature cycles.

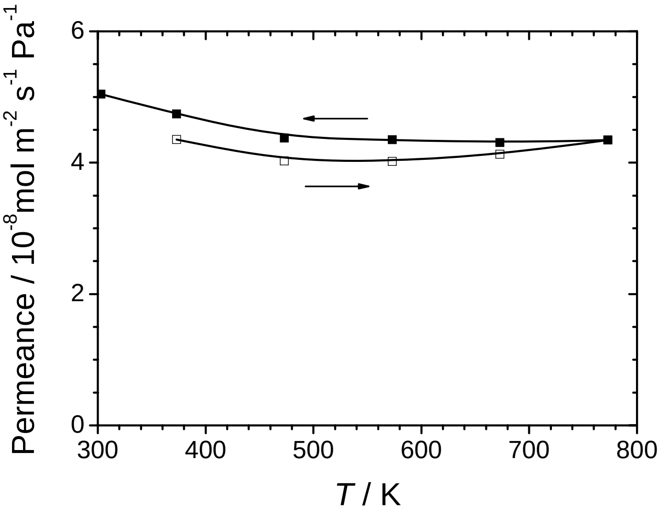

Figure 3. He permeance through a DD3R zeolite membrane as a function of the temperature. First the temperature was increased stepwise from 373 to 773 K (open symbols) then it was reduced to 303 K (closed symbols). Feed pressure is 300 kPa, no sweep gas used.

3.3 Isobutane permeation

Because isobutane is not able to enter the zeolite pores its permeation behaviour is discussed separately. The defect flow of isobutane is expected to be through pores that result in Knudsen and/or viscous flow [18,33]. Mathematically this can be expressed for a single component system as:

$$N_i = -\frac{1}{RT}\left(D_{Kn,i}^{eff} + \frac{\overline{p}B_0^{eff}}{\eta_i} \right)\frac{\Delta p_i}{\delta}, \tag{7}$$

where η represents the viscosity and $\overline{p}_i$ the average pressure of component *i* in the membrane layer. The effective Knudsen diffusivity and effective permeability (for cylindrical pores) are defined as:

$$D_{Kn,i}^{eff} = \frac{\varepsilon}{\tau}\frac{d_0}{3}\sqrt{\frac{8RT}{\pi M_i}}, \qquad B_0^{eff} = \frac{\varepsilon}{\tau}\frac{d_0^2}{32}. \tag{8}$$

ε, τ and d_0 represent the membrane defect porosity, tortuosity and pore size, respectively. Note that the driving force for Knudsen flow is the partial pressure drop and in case of viscous flow the total pressure drop over the membrane layer.

The isobutane permeance through the DD3R membrane is shown in Figure 4. The isobutane permeance is ~ $1\cdot10^{-10}$ mol m^{-2} s^{-1} Pa^{-1}. This is more than two orders of magnitude lower than the He permeance (~ $4\cdot10^{-8}$ mol m^{-2} s^{-1} Pa^{-1}). Considering that isobutane permeates only through the defects leads to the conclusion that this membrane contains very few defects. Moreover, the flux shows a continuously decreasing permeance with increasing temperature that indicates that no significant number of defects is created or are enlarged upon temperature increase. At 101 kPa feed pressure the absolute pressure drop over the membrane is zero, leading to only Knudsen flow. When the pressure is increased, also the permeance increases indicating a viscous flow contribution. A good model fit is obtained by a combined Knudsen/viscous flow model (Equation (7)) using two fitting parameters ($B_0^{eff}\delta^{-1}$ and $\varepsilon\tau^{-1}d_0\delta^{-1}$) (Figure 4). At 200 kPa feed pressure the viscous flow contribution at a feed pressure of 200 kPa is estimated to be 28 and 11 % of the total flow at 300 and 773 K, respectively.

An estimation of the flow of CO_2, CO, H_2 and N_2 through defects in the DD3R membrane is made by accounting for the molar mass dependency of the Knudsen flow (*cf.* Equation (8)). The viscous flow contribution is neglected because the defect flow in case of isobutane is dominated by Knudsen diffusion and this will be even more pronounced for the other components due to their lower molecular mass compared to isobutane. The relative defect flow contribution is expected to be the highest at low permeances, which are found at the highest investigated temperature (773 K) for all components. The estimated defect flow contribution to the total permeance at 773 K for CO_2, N_2, H_2 is only 1 % and for CO 3 %. Therefore, the defect flow contribution is neglected in the analysis of the single component behaviour.

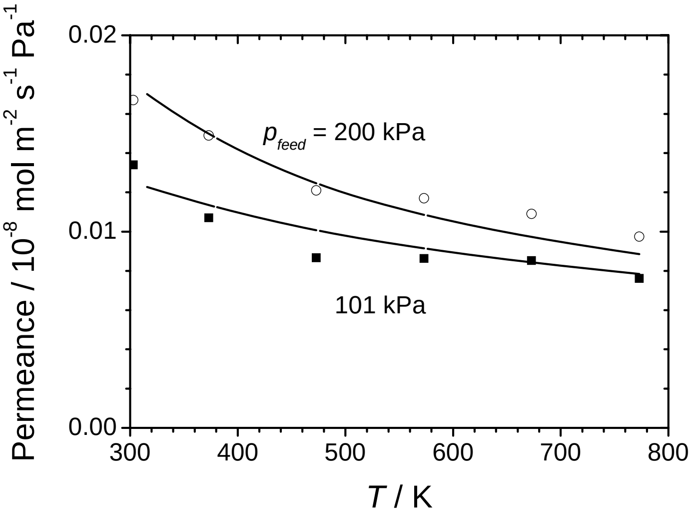

Figure 4. Isobutane permeance through defects of the DD3R membrane at feed pressures of 101 and 200 kPa and N_2 as sweep gas. Lines represent model fit results assuming a combination of viscous and Knudsen flow.

3.4 Pressure dependency of single component permeances

The membrane permeation flux of CO_2, CO, H_2 and N_2 has been measured up to feed pressures of 500 kPa at temperatures from 300 up to 773 K. The permeance can be dependent on the feed pressure in case that either viscous flow or surface diffusion of a relative strong adsorbing component takes place. Viscous flow can be excluded for CO_2, N_2, H_2 and CO permeation through the membrane. Previously, DD3R membrane experiments of a series of gases (CO_2, N_2O, Kr, CH_4, N_2, O_2, Ar and Ne) have been conducted in a temperature range of 220 to 373 K and a feed pressure range of 101 to 400 kPa [7](Chapter 2). From these results it was concluded that only the relative strongly adsorbing molecules CO_2 and N_2O showed a decreasing permeance with increasing feed pressure, whereas all other gases showed a constant permeance as a function of the feed pressure. These results are confirmed in the current study: only in case of CO_2 at 300 K and to a lesser extent at 373 K a small permeance decrease with increasing feed pressure is observed, all other gases showed a constant permeance as a function of the feed pressure. So, all these gases permeate as weakly adsorbing gases via a surface diffusion mechanism or a type of gaseous diffusion mechanism. Considering earlier results [7](Chapter 2) and the adsorption properties (Section 3.1) this pressure independent permeance could be expected.

3.5 Temperature dependency of single component permeances

The permeance of isobutane, CO_2, CO, H_2, He and N_2 are presented as a function of the temperature in Figure 5. Included are permeances of CO_2, N_2 and CH_4 on a disc-shaped DD3R membrane [7](Chapter 2) to extend the temperature range. These data are multiplied with a factor 6 to make them coincide with the current data. This difference in permeance can be related to the membrane thickness: the tubular membrane has a thickness of approximately 1-2 μm and the disc membrane of about 5 μm. Isobutane permeates through membrane defects predominantly via a Knudsen mechanism leading to a decreasing permeance with increasing temperature. The CH_4 permeance increases slightly with increasing temperature. This CH_4 permeance follows a surface diffusion type temperature dependency [7](Chapter 2). The slight increase of the permeance implies a slightly positive apparent activation energy for diffusion. Because the size of CH_4 is very close to the size of the window of DDR a relative high activation energy for diffusion is found, even larger than the adsorption enthalpy resulting in a positive apparent activation energy [23].

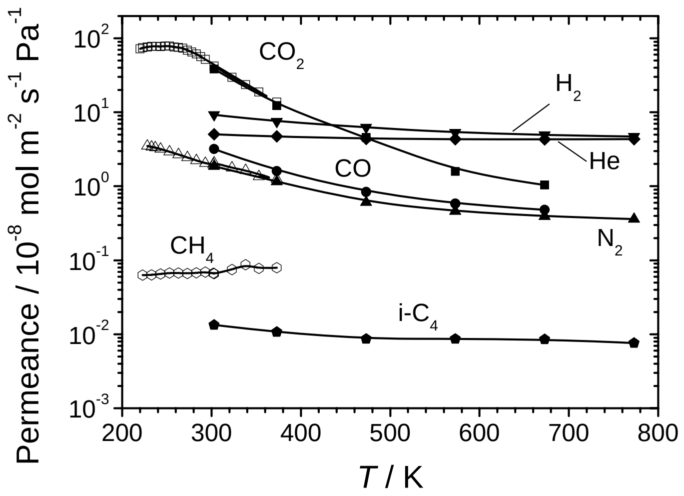

Figure 5. Permeance of CO_2, H_2, He, CO, N_2, CH_4 and isobutane through the DD3R membrane as a function of the temperature. Open symbols represent previously measured data on a disc-shaped DD3R membrane [7](Chapter 2) using He as sweep gas. This permeance data is multiplied by a factor 6. The H_2 and N_2 data in the current study (closed symbols) represent counter-current permeation data using H_2 as feed and N_2 as sweep gas. The CO_2, CO and He permeances are measured using the pressure drop method with a pressure drop of 100 kPa. Isobutane is measured using a feed gas pressure of 101 kPa and sweep gas pressure of 101 kPa.

CO_2 shows an increasing permeance with increasing temperature, passes through a maximum and then monotonically decreases with increasing temperature. This behaviour can be explained by a surface diffusion mechanism [23]. With increasing temperature the diffusivity increases whereas the loading in the zeolite decreases. Starting at low temperature, the zeolite is close to saturated and an increase in permeance is observed due to an increase of the diffusivity. With increasing temperature the loading decreases leading to a decreasing permeance with increasing temperature. In between a maximum is found. Note that in this case adsorption dominates the permeance behaviour (*i.e.* $E^{S}_{A,diff,i} < -\Delta H_{Ads,i}$) whereas in the case of CH_4 diffusion slightly dominates.

All other components show continuously decreasing permeances with increasing temperature. At relatively low temperatures this decreasing trend can be explained by the surface diffusion model since in this region the amount adsorbed on the zeolite is significant. To investigate the validity of this mechanism at higher temperatures the permeance is plotted versus the reciprocal of the temperature in Figure 6. If the permeance can be described by the surface diffusion mechanism in the Henry regime (Equation (3)) linear plots should be obtained. At temperatures up to 473 this appears to be valid for all components. For CO, H_2 and N_2 a fit of the permeances at 303, 373 and 473 to Equation (3) is made. In case of the strong adsorbing CO_2 a fit based on the permeances at all temperatures is made. The estimated diffusivity parameters are discussed in more detail in the next section.

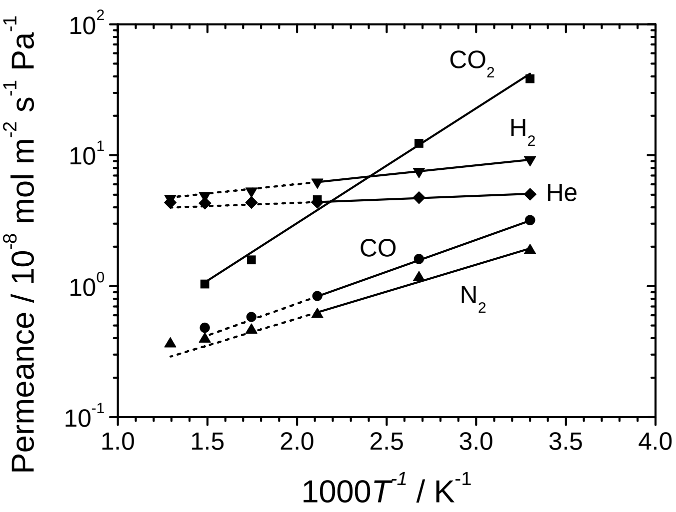

Figure 6. Permeance of CO_2, CO, H_2, N_2 and He through a DD3R membrane versus 1000/*T*. Solid lines represent model fit results assuming a surface diffusion model. Dashed lines are extrapolations. Details on the operating conditions are given in the caption of Figure 5.

Our permeation results deviate from the work of Kanezashi *et al.* [13] who also measured the permeance of CO_2, CO, H_2 and He through a DD3R membrane from room temperature up to 773 K. They report a monotonically decreasing permeance of CO_2, which is in agreement with our results. But the permeances of CO, H_2 and He first decrease with increasing temperature, pass through a minimum and then increase with increasing temperature. Clearly the difference between the two DDR type membranes cannot be explained from an intrinsic zeolite mass transport mechanism. A possible explanation could be that the flux increase at higher temperatures observed by Kanezashi *et al.* is due to shrinkage of the zeolite crystals with increasing temperature. Their membrane is built up from crystals of about 5 μm, whereas our membrane has a crystal size of 0.5-1 μm. This could explain why the flux increase is not observed in our membrane permeation results. The thermal expansion coefficient of DDR determined in a temperature range of 492-1185 K is about -3·10^{-6} $\Delta l \cdot l^{-1} K^{-1}$ in all three dimensions [34,35]. This is about half the thermal expansion coefficient of MFI. The thermal expansion coefficient of alumina is 8.5·10^{-6} $\Delta l \cdot l^{-1} K^{-1}$ [14]. The membrane of Kanezashi *et al.* would be closed at the synthesis temperature of 428 K. At 773 K intracrystalline defects of about 20 nm could be theoretically formed, in case of 5 μm crystals. In case of 1 μm crystals this would be a factor 5 lower: 4 nm. Note that in the data of Kanezashi *et al.* the minimum permeance is found at the membrane synthesis temperature, which is an indication that from this point on defects open up. Careful analysis of our own permeation data reveals that in case of the He and Isobutane permeance also a change in permeation behavior as a function of the temperature is observed between 373 and 473 K (Figure 3 and Figure 4). Also here the membrane appears to behave differently above the synthesis temperature (428 K) although not as pronounced as in the case of Kanezashi *et al.*

Figure 6 shows that at higher temperatures deviations from surface diffusion behaviour are observed in case of N_2, CO and He. Several explanations can be thought of, although none of these explanations are conclusive based on the current experimental data. Firstly, the assumption that the adsorbed concentration is described accurately by the Langmuir adsorption equilibrium constant over the considered temperature range can be violated. In other words: to be able to falsify if surface diffusion is the governing mass transport mechanism an accurate description of the amount adsorbed at all studied conditions is required. Secondly, the deviations can be due to opening of defects that lead to a slight defect flux contribution to the total flux. Up to which extent this additional defect flow becomes manifest is dependent on the ratio of this defect flux and the total flux. Considering that the defect flux is proportional to the Knudsen diffusivity (*cf.* Equation (8)) then the ratio of this defect flux and the total flux would be proportional to $\left(N_i \sqrt{M_i}\right)^{-1}$. Evaluated at 673 K it appears that this ratio is expected to be three times larger for N_2 and CO compared to CO_2, H_2 and He. So, also in this case this effect is expected to be the most pronounced for N_2 and CO, which is in accordance with experimental results. Thirdly, these deviations could be due to a transport mechanism shift from surface diffusion to gas translation diffusion. In addition to the gas translation model an activated transport mechanism can also be expected from the surface diffusion model. This Maxwell-Stefan model relates the flux to a concentration of component *i* (c_i) a surface diffusivity and a gradient of the natural logarithm of the partial pressure of component *i*. The adsorbed phase concentration can be interpreted as a concentration enrichment compared to the gas phase concentration. If then the total concentration in the zeolite is assumed to consist of the excess amount adsorbed ($q_{ads,i}^{exc}$) and the gas phase concentration (p_i / RT) the following expression to describe the flux can be found:

$$N_i = -c_i Đ_i^S \nabla \ln p_i = -\left(\rho q_{ads,i}^{exc} + \frac{p_i}{RT} \right) Đ_i^S \nabla \ln p_i \, . \tag{9}$$

In the low concentration (Henry) regime the adsorbed phase concentration is significantly higher than the ideal gas concentration leading to Equation (3). In the case that adsorption gradually vanishes the concentration in the zeolite approaches the gas phase concentration and in this limit a kind of activated gas diffusion is found:

$$N_i = -\frac{Đ_i}{RT} \nabla p_i \, . \tag{10}$$

The reason that the deviations from the surface diffusion mechanism become manifest predominantly for CO and N_2 can be explained as follows. The CO_2 flux will still be dominated by surface diffusion at the studied conditions due to its strong adsorbing nature. The activation energy for diffusion is expected to increase with molecule size [26]. Therefore, the larger CO and N_2 molecules are expected to show a stronger activated behaviour compared to the smaller He and H_2 molecules, which is in accordance with the experimental results.

3.6 Surface diffusivity parameters

The estimated apparent activation energy for diffusion, the activation energy for surface diffusion, the pre-exponent of the surface diffusion coefficient and the surface diffusivity at 300 K are given in Table 2. The activation energy for surface diffusion is found by subtraction of the adsorption enthalpy (Table 1) from the apparent activation energy (Equation (4)). The pre-exponent of the surface diffusion coefficient is calculated from Equation (3) assuming a DD3R framework density of 1714 kg m^{-3}, a membrane thickness of $1.5 \cdot 10^{-6}$ m (assuming that only the film layer on top of the support is responsible for the mass transport resistance) and the adsorption saturation loading and pre-exponent of the adsorption equilibrium constant given in Table 1. Additionally, the previously determined diffusivity parameters from the disc-shaped DD3R membrane are added to this table. A one to one relation between the size of a molecule and the activation energy for diffusion is not expected because the activation energy is dependent on both steric (window to molecule size) *and* adsorption effects. However, the relatively small H_2 molecule has a very low activation energy for surface diffusion compared to the other components, and CH_4 and Kr, with their size close to that of the DDR window, have a high activation energy for surface diffusion.

Table 2. Molecule dimensions, pre-exponential of the surface diffusivity, apparent activation energy and activation energy for surface diffusion of a series of light gases in DD3R. Diffusion parameters are estimated from the membrane permeation results.

	d_m [b] nm	$Đ^S(303K)$ $m^2\ s^{-1}$	$Đ_0^S$ $m^2\ s^{-1}$	$E_{A,app}$ $kJ\ mol^{-1}$	$E_{A,diff}^S$ $kJ\ mol^{-1}$
CO_2	0.303 × 0.535	$1.7 \cdot 10^{-11}$	$2.56 \cdot 10^{-10}$	-16.8	6.9
CO_2 [a]	0.303 × 0.535	$1.3 \cdot 10^{-11}$	$1.9 \cdot 10^{-10}$	-21.7	6.8
CO	0.356 (C) × 4.41 [c] 0.30 (O) × 4.41 [c]	$4.1 \cdot 10^{-11}$	$3.77 \cdot 10^{-10}$	-9.3	5.6
H_2	0.28	$5.1 \cdot 10^{-9}$	$1.49 \cdot 10^{-8}$	-2.9	2.7
He	0.228	-	-	-1.0	-
N_2	0.332 × 4.42	$3.2 \cdot 10^{-11}$	$4.11 \cdot 10^{-10}$	-7.9	6.4
N_2 [a]	0.332 × 4.42	$7.4 \cdot 10^{-11}$	$1.2 \cdot 10^{-10}$	-7.3	7.0
O_2 [a]	0.309 × 4.29 [d]	$9.1 \cdot 10^{-12}$	$0.38 \cdot 10^{-10}$	-11.0	3.6
Ar [a]	0.342	$2.1 \cdot 10^{-12}$	$1.0 \cdot 10^{-10}$	-4.8	9.7
Kr [a]	0.364	$3.3 \cdot 10^{-13}$	$0.76 \cdot 10^{-10}$	-5.1	13.7
CH_4 [a]	0.372	$8.5 \cdot 10^{-14}$	$0.47 \cdot 10^{-10}$	-1.4	15.9

[a] Diffusivity data taken from [7](Chapter 2); [b] Molecular dimensions, based on atom-atom Lennard-Jones parameters and bond lengths of the molecules, data taken from [36]; [c] Data taken from [37]; [d] Data taken from [38].

A plot of the surface diffusivity at 300 K versus the molecule's shortest dimension of several light gases in DDR is shown in Figure 7. The dimension considered is based on the Lennard-Jones parameter σ for the individual atoms of the molecule. In this way a distinction between the length and width of a molecule is made leading to a more appropriate measure to evaluate the window to molecule size. Often Lennard-Jones parameters estimated from viscosity data assuming spherical molecules are used to characterize the molecule size. Here, we follow Krishna and van Baten [36] from whom also most parameters are obtained (Table 2). Figure 7 shows a nice correlation between a decreasing diffusivity and increasing molecular diameter. CO_2 and CO seem to break the trend. Note that in case of CO the molecule is not symmetric: the diameter based on the carbon atom is significantly larger than based on the oxygen atom (Table 2). In the plot the largest diameter is considered.

Experimental data on diffusivities in DDR are rare. Hedin *et al.* and Chance *et al.* have determined the self diffusivity of CO_2 and CH_4 at low loading at 301 K using PFG-NMR in ZSM-58 crystals (Si/Al ratio 190) [39,40]. For CH_4 and CO_2, the diffusivities are $1.6 \cdot 10^{-12}$ and $1.0 \cdot 10^{-10}$ $m^2\ s^{-1}$, respectively. Corcoran and Chance presented diffusivities of CO_2, CH_4 and N_2 at 300 K determined by frequency response (FR) measurements of $4 \cdot 10^{-11}$, $2 \cdot 10^{-13}$ and $3 \cdot 10^{-11}$, respectively [41].

The diffusivities calculated from the membrane permeation data for CH_4 and CO_2 at 300 K are $8.5 \cdot 10^{-14}$ and $1.7 \cdot 10^{-11}$ m^2 s^{-1}, respectively. It appears that the membrane diffusivities are about one order of magnitude lower than the PFG-NMR data and are in fair agreement with the FR data. Since in the case of PFG-NMR diffusivities are measured at very short length scales, the difference in diffusivities could point in the direction of additional diffusion barriers in case of the membrane and the FR measurements. These could be surface barriers or intra-crystalline grain boundaries as have been revealed for various zeolite crystals (*e.g.* [42-44]).

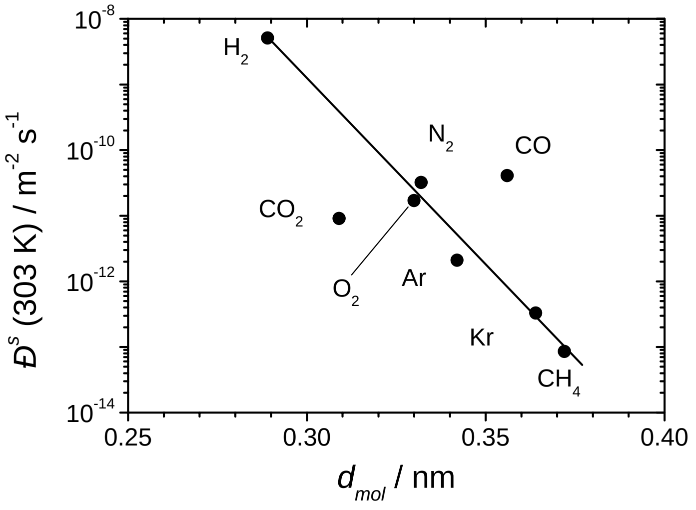

Figure 7. Surface diffusivity of light gases in DD3R at 303 K as a function of the molecule's shortest dimension as specified in Table 2.

3.7 Mixture permeances

Single component permeation through the DD3R membrane is determined by interaction of the component with the zeolite. In case of surface diffusion two effects play a role: adsorption on the zeolite and 'friction' with the zeolite characterized by its diffusivity. When another species is introduced to the system two additional effects could be observed: competitive adsorption and 'friction' effects between the two different species that can lead to 'speeding up' of the slower and 'slowing down' of the faster species. Both effects are expected to become manifest only when the occupancy in the zeolite is significant. In our previous work [7](Chapter 2) competitive adsorption effects have only been observed for CO_2-containing mixtures below room temperature and also 'friction' between the different species seemed to be completely absent.

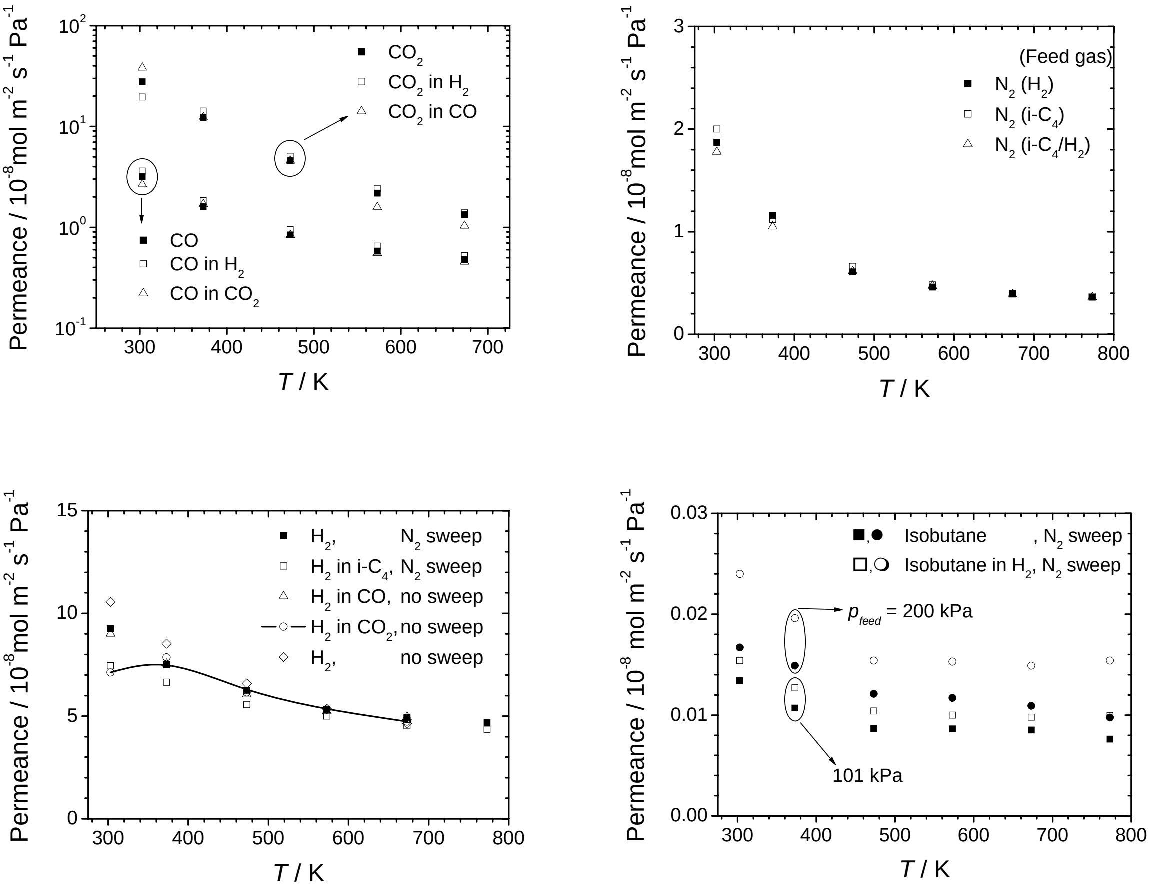

Figure 8. Pure component and mixture permeance of CO_2, CO, H_2, N_2 and isobutane through the tubular DD3R membrane. The line in the bottom left graph is added to guide the eye. All data are considered at a total pressure drop of 100 kPa over the membrane. In case of the H_2/isobutane mixture also the data at a feed pressure of 101 kPa and no absolute pressure drop are shown.

Figure 8 shows the permeance of CO_2, H_2, CO, N_2 and isobutane as single component and in mixtures. As explained in detail in the experimental section and indicated in the figure, some experiments are performed in pressure drop and other in sweep gas mode. In case of N_2 the permeance obtained from a unary permeation experiment in pressure drop mode is compared to the N_2 sweep gas back-permeance with various feed gases. In general the single component permeances are very close to the permeances of the same component in a mixture. Focussing especially on CO_2, CO and N_2 no significant differences are observed. This indicates that the permeances are independent of the other components in the system. No competitive adsorption effects or ‘friction’ between components is observed. The unary H_2 permeance seems to be higher compared to its permeance in the mixtures, particularly at lower temperatures. At temperatures above 500 K all H_2 permeances become equal. The most significant reduction is observed for the mixtures of H_2 with CO_2 or isobutane. In case of the CO_2 mixture even a maximum in the H_2 permeance is observed. This maximum is also observed for experiments with the same mixture at different feed pressures. The permeance of the very weakly adsorbing H_2 is reduced by adsorption of CO_2. These effects become more manifest at lower temperatures resulting in a decreasing H_2 permeance. The same effect is observed for CO_2/air and CO_2/CH_4 mixtures in our previous study [21] at lower temperatures. This can be understood by realizing that N_2, O_2 and CH_4 are more strongly adsorbing than H_2. The reduced H_2 permeance in the mixture with isobutane could be due to surface adsorption of isobutane leading to blocking of H_2 molecules to enter the zeolite crystals. Also in this case the permeance reduction will be larger at lower temperatures due to a stronger surface adsorption. Reduction of the H_2 permeance due to interaction with isobutane in the defect pores is not likely since it is estimated that only 1% of the H_2 passes through the defects. The isobutane permeance in a mixture with H_2 seems to be higher than its permeance in a unary configuration. Since the diffusion mechanism in the defects seems to be of the Knudsen type, molecule-wall interactions will dominate this process and no significant 'friction' effects between the different species are expected. The increased isobutane permeance could be an indication that the membrane quality changes slightly in time.

3.8 Ideal and mixture selectivity

From the single component permeances a so-called ideal selectivity can be calculated:

$$\alpha_{i,j}^{ideal} = \frac{Permeance_i}{Permeance_j}. \tag{11}$$

This selectivity can also be evaluated for mixtures. The so-called mixture selectivity is based on mixture permeation data and is defined from a unit operation perspective based on the fractions (x) of component i and j that enter and leave the membrane:

$$\alpha_{i,j}^{mix} = \left(\frac{x_j}{x_i}\right)_{feed}\left(\frac{x_i}{x_j}\right)_{permeate}. \tag{12}$$

An important difference between the two selectivities is that the mixture selectivity is evaluated under actual mixture conditions, including the effect of competitive adsorption and interactions between species. However, in our case the single component and mixture permeances are fairly equal for many components indicating that in most cases competitive adsorption and 'friction' effects between species play no significant role. Moreover, the permeance is independent of the feed pressure, except for CO_2 below 373 K. But, also in this case comparing the two selectivities is not straightforward. Equation (11) can be rewritten as:

$$\alpha_{i,j}^{ideal} = \frac{\left(\Delta p_j\right)_{lm}}{\left(\Delta p_i\right)_{lm}}\frac{N_i}{N_j} = \frac{\left(\Delta p_j\right)_{lm}}{\left(\Delta p_i\right)_{lm}}\left(\frac{x_i}{x_j}\right)_{permeate}, \tag{13}$$

where the pressure difference is calculated based on a log mean pressure difference as defined in the experimental section. In case an equimolar binary mixture is fed the difference between the two selectivity definitions is that the ideal selectivity is corrected for the partial pressure difference over the membrane for each component, which can be interpreted as a correction for the driving force that is present for each species. The ideal selectivity represents in this case a measure for the intrinsic separation quality of the membrane while the mixture selectivity is dependent on the feed and sweep gas flow rates. During membrane permeation the concentration of the component with the highest permeance will become higher in the permeate side and will be reduced at the feed side, leading to a reduced driving force and consequently a reduced flux. Therefore, the mixture selectivity will be lower than the ideal selectivity in this case obtained under non-differential operation. For example, when an equimolar mixture of H_2 and isobutane is fed, the retentate molar fractions of these components at 303 K and a total feed pressure of 200 kPa are 0.31 and 0.58, respectively. The remaining part of the retentate consists of back-permeated N_2.

The mixture and ideal selectivities for a number of binary mixtures are shown in Figure 9. All selectivities are calculated from data with an absolute pressure drop of 100 kPa over the membrane. The ideal selectivity is always higher than the mixture selectivity, when expressed as the ratio of the component with the highest and the lowest permeance, due to non-differential operation: the fraction of the component with the highest permeance will become higher in the permeate side and will be reduced in the feed side, leading to a reduced driving force and consequently a reduced flux and mixture selectivity. Although shown here only for the H_2/isobutane mixture, the mixture selectivity decreases with increasing total feed pressure for all mixtures since in this case the driving force for the component with the highest permeance is decreased the most. Because the ideal selectivity reflects the intrinsic separation properties of the membrane best, this value will be used predominantly in the discussions.

The ideal selectivity is directly calculated from the single component permeances. The H_2 permeance decreases less with increasing temperature compared to CO_2, CO and N_2 leading to an increasing H_2 selectivity with increasing temperature for the corresponding mixtures. In case of He the opposite holds and a decreasing H_2/He selectivity trend with increasing temperature is found. In case of isobutane, the selectivity is close to independent of the temperature, only a slight selectivity decrease is observed with increasing temperature. For the mixture selectivity the same trends are observed except for the H_2/isobutane selectivity. For these mixtures a slight increase of the mixture selectivity with increasing temperature is observed between 303 and 473 K, whereas the ideal selectivity shows a slight decrease in this region. This difference is attributed to the reduced H_2 permeance in the mixture due to adsorbed isobutane that is removed at higher temperatures. Note that at 400 K the CO_2/H_2 selectivity is reversed.

The maximum H_2/CO and CO_2/CO selectivities found are ~10 and 12, respectively. However, these maximum selectivities are either found at high (H_2) or at low (CO_2) temperature and hence a constant average product (CO_2 + H_2) to reactant (CO) selectivity of around 6-7 is found over the complete temperature range. Clearly the performance of the membrane in the water gas shift reaction is strongly dependent on the water permeance [45], which has not been considered in this study.

As expected from the single component isobutane membrane permeation results, very high H_2/isobutane ideal selectivities are found: above 600 at 101 kPa and above 400 at 200 kPa feed pressure over the complete temperature range. Since both the flux of H_2 through the zeolite layer and the Knudsen diffusion of isobutane through the defects are proportional with the pressure, the decrease in ideal selectivity with increasing total feed pressure is due to the viscous flow contribution of isobutane through the defects. Application of this membrane in the dehydrogenation of isobutane in a membrane reactor is a viable option. Almost complete retention of the hydrocarbons seems possible when removing H_2 from the reaction mixture with the DD3R membrane.

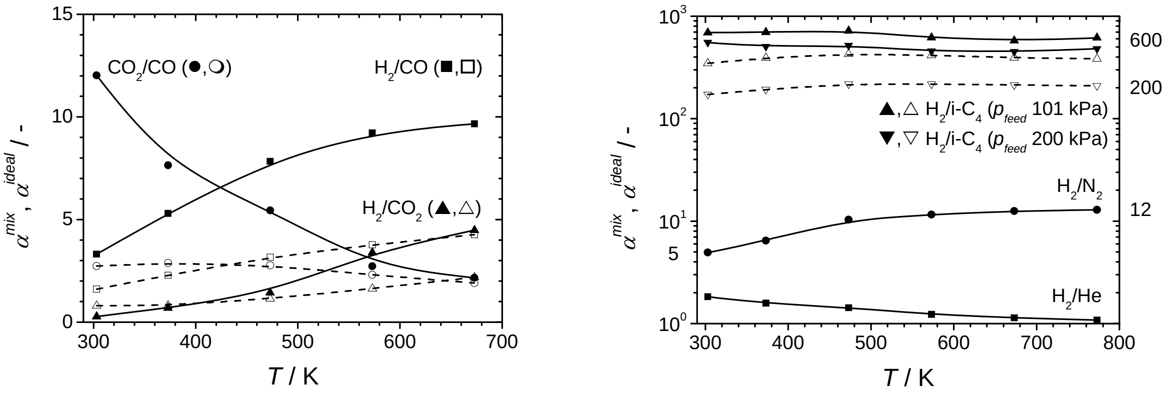

Figure 9. Mixture and ideal selectivities of the DD3R membrane. Closed symbols and solid lines represent ideal selectivities, dashed lines and open symbols mixture selectivities under non-differential operation. The lines are added to guide the eye. All data are considered at a total pressure drop of 100 kPa over the membrane. In case of the H_2/isobutane mixture also the data at a feed pressure of 101 kPa without absolute pressure drop are shown.

4 Conclusions

The He, H_2, CO, CO_2 and N_2 permeances through an all-silica DD3R zeolite tubular membrane decrease monotonically with increasing temperature. A surface diffusion mechanism describes the observed temperature dependency of the permeance best. No indication for the presence of activated gaseous diffusion (gas translation diffusion) has been observed. Adsorption experiments up to 573 K revealed that indeed significant concentration enrichment in the zeolites compared to the gas phase concentration occurs for CO_2, CO and N_2. The estimated Maxwell-Stefan surface diffusivity at 303 K decreases strongly with increasing molecular size of the components: steric effects induced by the DDR window have a large influence on the diffusivity. A comparison of the estimated diffusivities of CO_2 and CH_4 with literature diffusivities determined by PFG-NRM points to the presence of surface or intra-crystalline barriers in case of the membrane.

The low isobutane single component permeance ($\sim 1\times10^{-10}$ mol m^{-2} s^{-1} Pa^{-1}) is attributed to viscous and Knudsen flow through defects. The permeance of H_2, CO, CO_2, N_2 and isobutane is not significantly different in a mixture compared to the single component permeance. This indicates that no competitive adsorption or ‘speeding up’ or ‘slowing down’ effects between species play a significant role. In two cases differences between the mixture and single component permeances are observed. The H_2 permeance in a mixture with isobutane or CO_2 at temperatures below 473 K is lower than its single component permeance. This is attributed to the strong adsorption of CO_2 in the zeolite and adsorption at the external membrane surface for isobutane, respectively.

The ideal selectivities are always higher than the mixture selectivities, mainly because the component with the highest permeance reduces its own driving force along the membrane tube due to this higher permeance and non-differential operation. The H_2/CO and CO_2/CO ideal selectivities are 3 and 12 at 303 K and 2 and 10 at 673 K. The H_2/isobutane ideal selectivity is > 600 at 101 kPa feed pressure and > 450 at 200 kPa feed pressure over the complete temperature range. The mixture selectivities are ~ 400 and ~ 200 in an equimolar binary mixture at 101 and 200 kPa total feed pressure. Considering these H_2/isobutane selectivities and the low permeance of CH_4 found in our previous study makes this membrane very suitable to be applied for high temperature dehydrogenation of hydrocarbons.

A stable membrane operation has been achieved for several months of operation, including long term (~ 5 days) high temperature operation and numerous (>10) full temperature cycles. Combining this with the high selectivities makes the DD3R membrane a potential candidate for application in high temperature (reactive) separations that involve removal of H_2 and/or CO_2.

Acknowledgements

NGK Insulators is gratefully acknowledged for supplying the membrane, Nicla Vicinanza for performing part of the membrane permeation experiments and Sander Brouwer for performing part of the adsorption experiments.

References

[1] Y. Morigami, M. Kondo, J. Abe, H. Kita, and K. Okamoto, *Separation and Purification Technology*, 25, **2001**, 251.

[2] Z. Lai, G. Bonilla, I. Diaz, J. G. Nery, K. Sujaoti, M. A. Amat, E. Kokkoli, O. Terasaki, R. W. Thompson, M. Tsapatsis, and D. G. Vlachos, *Science*, 300, **2003**, 456.

[3] L. Gora and J. C. Jansen, *Journal of Catalysis*, 230, **2005**, 269.

[4] W. Zhu, F. Kapteijn, and J. A. Moulijn, *Chemical Communications*, **1999**, 2453.

[5] J. Gascon, W. Blom, A. van Miltenburg, A. Ferreira, R. Berger, and F. Kapteijn, *Microporous and Mesoporous Materials*, 115, **2008**, 585.

[6] T. Tomita, K. Nakayama, and H. Sakai, *Microporous and Mesoporous Materials*, 68, **2004**, 71.

[7] J. van den Bergh, W. Zhu, J. Gascon, J. A. Moulijn, and F. Kapteijn, *Journal of Membrane Science*, 316, **2008**, 35.

[8] J. van den Bergh, W. Zhu, F. Kapteijn, J. A. Moulijn, K. Yajima, K. Nakayama, T. Tomita, and S. Yoshida, *Research on Chemical Intermediates*, 34, **2008**, 467.

[9] J. Kuhn, K. Yajima, T. Tomita, J. Gross, and F. Kapteijn, *Journal of Membrane Science*, 321, **2008**, 344.

[10] W. J. W. Bakker, F. Kapteijn, J. Poppe, and J. A. Moulijn, *Journal of Membrane Science*, 117, **1996**, 57.

[11] J. M. van de Graaf, F. Kapteijn, and J. A. Moulijn, *Chemical Engineering Science*, 54, **1999**, 1081.

[12] M. Kanezashi and Y. S. Lin, *Journal of Physical Chemistry C*, 113, **2009**, 3767.

[13] M. Kanezashi, J. O'Brien-Abraham, Y. S. Lin, and K. Suzuki, *AIChE Journal*, 54, **2008**, 1478.

[14] S. Miachon, P. Ciavarella, L. van Dyk, I. Kumakiri, K. Fiaty, Y. Schuurman, and J. A. Dalmon, *Journal of Membrane Science*, 298, **2007**, 71.

[15] R. Krishna and J. A. Wesselingh, *Chemical Engineering Science*, 52, **1997**, 861.

[16] F. Kapteijn, J. A. Moulijn, and R. Krishna, *Chemical Engineering Science*, 55, **2000**, 2923.

[17] R. Krishna and L. J. P. van den Broeke, *Chemical Engineering Journal and the Biochemical Engineering Journal*, 57, **1995**, 155.

[18] F. Kapteijn, W. Zhu, J. A. Moulijn, and T. Q. Gardner, Zeolite Membranes: Modeling and Application, in: Structured Catalysts and Reactors, Cybulski, A. and Moulijn, J. A. (Eds), Ch. 20, **2005**, Taylor & Francis Group, Boca Raton, FL, 701.

[19] F. Kapteijn, W. J. W. Bakker, J. van de Graaf, G. Zheng, J. Poppe, and J. A. Moulijn, *Catalysis Today*, 25, **1995**, 213.

[20] R. Krishna and J. M. van Baten, *Separation and Purification Technology*, 61, **2008**, 414.

[21] J. van den Bergh, S. Ban, T. J. H. Vlugt, and F. Kapteijn, *Journal of Physical Chemistry C*, 113, **2009**, 17840.

[22] J. van den Bergh, S. Ban, T. J. H. Vlugt, and F. Kapteijn, *Journal of Physical Chemistry C*, 113, **2009**, 21856.

[23] F. Kapteijn, J. M. van de Graaf, and J. A. Moulijn, *AIChE Journal*, 46, **2000**, 1096.

[24] W. J. W. Bakker, L. J. P. van den Broeke, F. Kapteijn, and J. A. Moulijn, *AIChE Journal*, 43, **1997**, 2203.

[25] J. M. van de Graaf, F. Kapteijn, and J. A. Moulijn, *Microporous and Mesoporous Materials*, 35-6, **2000**, 267.

[26] J. R. Xiao and J. Wei, *Chemical Engineering Science*, 47, **1992**, 1123.

[27] J. R. Xiao and J. Wei, *Chemical Engineering Science*, 47, **1992**, 1143.

[28] M. J. den Exter, J. C. Jansen, and H. van Bekkum, *Zeolites and Related Microporous Materials: State of the Art 1994*, 84, **1994**, 1159.

[29] J. Kuhn, J. Gascon, J. Gross, and F. Kapteijn, *Microporous and Mesoporous Materials*, 120, **2008**, 12.

[30] S. Himeno, T. Tomita, K. Suzuki, K. Nakayama, K. Yajima, and S. Yoshida, *Industrial & Engineering Chemistry Research*, 46, **2007**, 6989.

[31] M. Mulder, Basic Principles of Membrane Technology, **1990**, Kluwer, Dordrecht.

[32] W. Zhu, F. Kapteijn, J. A. Moulijn, M. C. den Exter, and J. C. Jansen, *Langmuir*, 16, **2000**, 3322.

[33] G. R. Gavalas, *Industrial & Engineering Chemistry Research*, 47, **2008**, 5797.

[34] P. Lightfoot, D. A. Woodcock, M. J. Maple, L. A. Villaescusa, and P. A. Wright, *Journal of Materials Chemistry*, 11, **2001**, 212.

[35] S. H. Park, W. G. Kuntsleve, H. Graetsch, and H. Gies, *Studies in Surface Science and Catalysis*, 105, **1997**, 1989.

[36] R. Krishna and J. M. van Baten, *Microporous and Mesoporous Materials*, 109, **2008**, 91.

[37] J.-P. Bouanich, *Journal of Quantitative Spectroscopy and Radiative Transfer*, 47, **1992**, 243.

[38] R. Krishna and J. M. van Baten, *Microporous and Mesoporous Materials*, 125, **2009**, 126.

[39] N. Hedin, G. J. DeMartin, W. J. Roth, K. G. Strohmaier, and S. C. Reyes, *Microporous and Mesoporous Materials*, 109, **2008**, 327.

[40] S. E. Jee and D. S. Sholl, *Journal of the American Chemical Society*, 131, **2009**, 7896.

[41] N. Corcoran and R. Chance, Poster 151 at: Diffusion Fundamentals I, Leipzig, **2005**.

[42] J. Kärger, P. Kortunov, S. Vasenkov, L. Heinke, D. R. Shah, R. A. Rakoczy, Y. Traa, and J. Weitkamp, *Angewandte Chemie-International Edition*, 45, **2006**, 7846.

[43] M. H. F. Kox, E. Stavitski, J. C. Groen, J. Perez-Ramirez, F. Kapteijn, and B. M. Weckhuysen, *Chemistry-A European Journal*, 14, **2008**, 1718.

[44] L. Zhang, C. Chmelik, A. N. C. van Laak, J. Kärger, P. E. de Jongh, and K. P. de Jong, *Chemical Communications*, **2009**, 6424.

[45] J. Kuhn, J. M. Castillo-Sanchez, J. Gascon, S. Calero, D. Dubbeldam, T. J. H. Vlugt, F. Kapteijn, and J. Gross, *The Journal of Physical Chemistry C*, 113, **2009**, 14290.

4

Isobutane dehydrogenation in a DD3R zeolite membrane reactor

Dehydrogenation of isobutane has been studied in a DD3R zeolite membrane reactor (MR) at 712 and 762 K, using pure isobutane at 101 kPa as feed gas and N_2 as sweep gas. Clear advantage of using the small-pore zeolite DD3R is that it offers an absolute separation of H_2 from isobutane by a molecular sieving mechanism. Experiments in a conventional packed bed reactor served as benchmark. Cr_2O_3 on Al_2O_3 is used as catalyst.

The DD3R membrane showed an excellent H_2/isobutane permselectivity (> 500 @ 773 K)) and a reasonable H_2 permeance (~ $4.5 \cdot 10^{-8}$ mol m^{-2} s^{-1} Pa). At low residence times isobutene yields 50% above the equilibrium are found. At 762 K and 0.13 $kg_{feed}kg_{cat}^{-1}h^{-1}$, the isobutene yield in the membrane reactor is 0.41, where the equilibrium yield is ~ 0.28. The increased performance is attributed to removal of H_2 from the reaction zone by the membrane, up to 85 % at the lowest space velocity. The removal of H_2 mildly promotes coke formation, suppresses hydrogenolysis reactions and appears to slightly reduce the catalyst activity. The membrane permeation parameters and reaction rate constants have been estimated independently from membrane permeation and packed bed reactor (PBR) experiments, respectively. From these parameters the behaviour of the MR can be simulated well. Two important dimensionless parameters determine the MR performance primarily, the Damköhler (*Da*) and membrane Péclet number (Pe_δ). For a significant improvement of the MR

This chapter is based on the following publication:

J. van den Bergh, C. Gücüyener, J. Gascon and F. Kapteijn, *Journal of membrane science*, submitted, **2010**.

performance as compared to a PBR $Da \geq 10$ and $Pe_\delta \leq 0.1$. $DaPe_\delta$ should be ≈ 1 to optimally utilize both catalyst and membrane. In the current MR unit both the hydrogen removal capacity and catalyst activity stand in the way of successful application. Using a more active catalyst *and* a more favourable area to volume ratio could greatly improve the MR performance. Operation at a higher feed pressure could also be a possible solution. Since membranes with higher fluxes are already available, the limited catalyst activity and stability under relative low temperature and H_2 lean conditions are the most important limiting factors regarding application of MRs in dehydrogenation reactions at reduced temperatures.

1 Introduction

Alkane dehydrogenation reactions are industrially very relevant, but they are also a class of reactions where the conversion can be (severely) equilibrium-limited at practical conditions [1]. Low conversions lead to a large flow of alkane/alkene mixtures that needs to be separated and recycled. Particularly the separation of alkanes/alkenes is very energy intensive [2]. An approach to increase the single-pass conversion is by using a membrane reactor (MR). By *in situ* removal of the product H_2 an apparent equilibrium shift can be accomplished. Moreover, if the equilibrium conversion based on the feed conditions does not limit the single pass conversion, the operating temperature could be decreased and pure H_2 can be obtained. An additional advantage of a lower operating temperature could be suppression of coke formation [3]. Clearly, the membrane should be suitable in terms of H_2 to hydrocarbon selectivity, H_2 permeance and stability. Therefore, many types of membranes [4] have been investigated for this type of application. Isobutane dehydrogenation, for example, has been studied using γ-alumina [5], zeolite MFI [5-9], Pd/Ag [10-12], Pd [9,13], dense silica [14] and carbon molecular sieve [15] membranes. Comparison of the achieved improvements of the different MR is difficult, since the operating conditions vary considerably. However, the general outcome is that in all cases an apparent equilibrium conversion could be obtained due to H_2 removal by the membrane. Eventually, the flux, selectivity, stability and price of the membrane will determine the viability of each type of MR. For several types of membranes the H_2/hydrocarbon selectivity and H_2 permeance are compared in Table 1. It is clear that Pd-based membranes stand out because they combine a very high H_2 selectivity with a high H_2 permeance. But, palladium membranes are relatively expensive, simply due to the high palladium price [8], and may be unstable [16]. Although zeolite membranes are also quite expensive [Chapter 1], they could be more advantageous in terms of stability. However, the currently studied medium-pore zeolite MFI has pores larger than both isobutane and H_2, which leads to only modest separation factors. Although infinite selectivity is not essential to obtain an improved reactor performance, the amount of hydrocarbons retained in the feed does determine the maximum level of conversion increase that can be obtained [17] and an infinite H_2 to hydrocarbon selectivity has the clear advantage of obtaining a pure H_2 flow at the sweep side of the reactor. Moreover, in case of relative large pores not only reactant loss is an issue, but also a significant dilution of the feed gas by counter-permeation of the sweep gas can occur [5,8]. This can be prevented, or at least minimized, by choosing a smaller-pore membrane that combines the stability of a zeolite membrane with the absolute H_2/isobutane selectivity found for Pd-based membranes. A zeolite MR with such properties could be much more viable compared to the zeolites studied so far.

An example of such a zeolite is DD3R which consists of cages connected by 8-ring window openings of 0.36 × 0.44 nm. This type of zeolite has received considerable attention in recent years: DDR has been demonstrated to be very successful in propane/propene [18,19], CO_2/CH_4 [20-22] and water/ethanol [23] separations. Recently, we have demonstrated that this membrane shows a very high H_2/isobutane selectivity (> 500, Table 1), which is maintained up to high temperatures [24](Chapter 3).

Table 1. H_2 permeance and selectivity of various membranes used in the isobutane dehydrogenation reaction.

Membrane	Thickness micron	Pore size nm	H_2 permeance 10^{-7} mol m^{-2} s^{-1} Pa^{-1}	Selectivity (H_2/Isobutane)	Reference
γ-alumina	3	3	160 (723 K)	4 (723 K)^a	[5]
Zeolite MFI	n.a.^{b}	0.55	11 (723 K)	30 (723 K)^a	[5]
Zeolite MFI	60	0.55	1.1 (773 K)	70 (773)^c	[8]
Zeolite MFI	n.a.^{b}	0.55	5 (~725 K)	10 (~725 K)^c	[9]
Dense silica	0.1	n.a.^{b}	0.2 (773K)	80-300^a	[14]
PdAg	10	dense	9	1200 (H_2/N_2)	[10]
PdAg	6	dense	40(723 K)	Infinite	[12]
Pd	5	dense	30 (~725 K)	60 (~725 K)^a	[9]
DD3R	1-2	0.38×0.44	0.45 (773 K)	>500 (773 K)^a	[24]

^{a} Permselectivity; ^{b} n.a. : information not available; ^{c} Mixture selectivity

The aim of this paper is to demonstrate and evaluate the performance of a DD3R zeolite membrane in dehydrogenation reactions using the catalytic dehydrogenation of isobutane in a packed bed membrane reactor configuration as a model example. First, the permeation and separation properties of the membrane are discussed. Then the MR is evaluated in terms of isobutene yield, selectivity, catalyst activity and stability. Experiments in a conventional packed bed reactor are used as a benchmark for the MR results. A detailed model of the MR is used to support interpretation of the results. Finally, an analysis is made on the controlling processes in the MR performance by a characteristic times evaluation.

2 Experimental

2.1 Membrane experiments

Membrane permeation experiments were carried out using a tubular DD3R zeolite membrane provided by NGK Insulators [25]. The membrane is of the same type as used by Kuhn *et al.* [23]. A ~1-2 μm thick zeolite layer is present on the outside of a 150 mm long α-alumina tube. The outer diameter of the tube is 12 mm. The support consists of three layers of different pore size (0.2, 1 and 5 micrometer) and thickness (13, 70 and 1750 micrometer, respectively). The composite membrane was sealed in a stainless-steel module using graphite O-rings leaving 120 mm effective tube length and 0.0045 m^2 membrane area (Figure 1). The inner diameter of the shell is 40 mm. Although the membrane tube is closed at one end, countercurrent plug-flow-like operation is obtained by feeding the gas from the closed end through a feed tube sticking inside the membrane tube as shown in Figure 1. Single component permeation of H_2, and isobutane and equimolar binary mixture permeation of H_2/isobutane mixtures were studied using nitrogen as sweep gas. Single component He permeances were measured in the pressure drop mode (no sweep gas). The permeate pressure was always at atmospheric pressure. The feed pressure was 101 kPa in case of the experiments with sweep gas and 200 kPa in case of pressure drop experiments, the temperature was varied between 303 and 773 K. In case of the He and H_2 single component experiments both the feed and sweep gas flow rate were set to 200 ml min^{-1} (STP). The experiments involving isobutane were performed at a feed and sweep gas flow rate of 100 ml min^{-1} (STP). All experiments were carried out in countercurrent mode. The retentate and permeate flows were determined using a soap film meter. The compositions of both flows were determined by GC analysis. In the case of isobutane a FID detector and for all other components a TCD detector was used. For H_2 detection Ar was used as carrier gas.

2.2 (Membrane) reactor experiments

The same membrane used for the permeation studies has been used in the membrane reactor (MR) experiments. The effective tube length available for permeation was 95 mm. Now the tube is packed with 4.1 g of chromia-alumina catalyst (Cr_2O_3/Al_2O_3), Harshaw (nowadays BASF Nederland) Cr-0211-T, 5/32" (Cr_2O_3, 18.0 %; ZrO_2, 0.25 %; Al_2O_3, 82.0 %). The catalyst was crushed and sieved to obtain particles with a diameter between 0.7 and 1.0 mm. The tube is packed with catalyst over the length of the permeable membrane area. Quartz wool was placed before and after the catalyst bed. The temperature was measured in the feed tube that sticks through the catalyst bed. The pressure was measured before and after the packed bed. Pure isobutane at 101 kPa was fed in the range of 3.7 to 57 ml min^{-1} (STP) at 762 and 712 K with a countercurrent N_2 sweep gas flow rate of 100 ml min^{-1} (STP) at 101 kPa.

The catalyst was regenerated overnight at the reaction temperature under a 2 % O_2 in N_2 flow. The retentate and permeate flows and compositions are measured as described in Section 2.1. As a benchmark for the membrane reactor results, experiments with an impermeable stainless-steel tube in the module instead of the DD3R membrane were performed. The same flow rates and catalyst loading as in case of the membrane were used. These experiments are referred to as packed bed reactor (PBR) experiments.

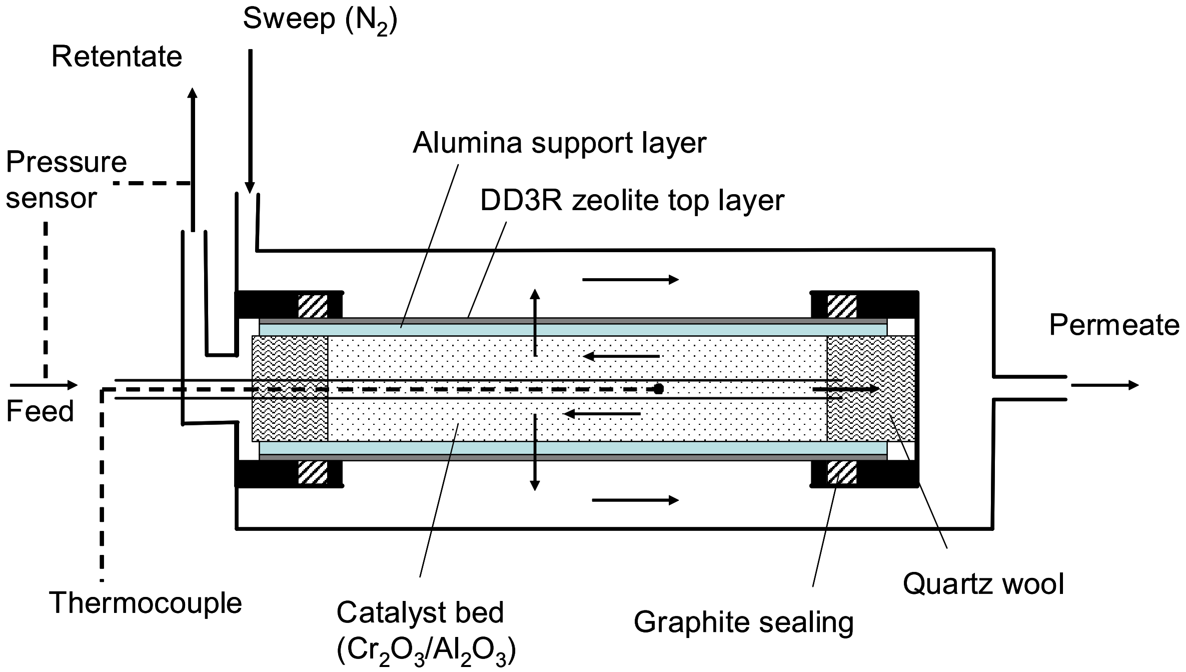

Figure 1. Schematic drawing of the membrane reactor module. Arrows indicate the flow directions in the module.

The isobutene yield (Y_E) is normally defined based on the in and outgoing molar flow rates (F) of isobutane (A) and isobutene (E):

$$Y_E = \frac{F_E^{out}}{F_A^{in}}. \tag{1}$$

However, this requires a very accurate estimate of the in and outgoing volumetric flow rates which appears difficult, particularly at low Weight Hourly Space Velocity (*WHSV*). Therefore, the yield is calculated based on merely the outgoing flows and compositions (x) according to:

$$Y_E = \frac{F_{tot}^{perm} x_E^{perm} + F_{tot}^{ret} x_E^{ret}}{F_{tot}^{perm}\sum_{i=1}^{4}\frac{i}{4}\left(x_{Ci}^{perm}\right) + F_{tot}^{ret}\sum_{i=1}^{4}\frac{i}{4}\left(x_{Ci}^{perm}\right)}. \tag{2}$$

Here subscript *Ci* represents the different hydrocarbons grouped according to their carbon number: C1 (methane), C2 (ethane and ethane) etc.. Also in this calculation procedure determination of the volumetric flows play a role, but since the amount of hydrocarbons in the permeate flow is very low, the influence of the flow rates on the estimated yield is minimal. By considering only the outgoing flows the formation of coke is neglected.
The conversion of isobutane is defined in a similar way:

$$X = 1 - \frac{F_{tot}^{perm} x_A^{perm} + F_{tot}^{ret} x_A^{ret}}{F_{tot}^{perm} \sum_{i=1}^{4} \frac{i}{4}\left(x_{Ci}^{perm}\right) + F_{tot}^{ret} \sum_{i=1}^{4} \frac{i}{4}\left(x_{Ci}^{ret}\right)} \tag{3}$$

and the selectivity (*S*) towards isobutene as:

$$S_E = \frac{Y_E}{X} . \tag{4}$$

2.3 Membrane reactor modelling

For a quantitative interpretation of the membrane reactor results a model has been set up [4,26]. In the formulation of the model equations dimensionless numbers are introduced that characterize the MR's performance. The model includes convection and diffusion at the membrane tube and shell side, exchange of moles between the shell and tube side via the membrane and reaction in the catalyst bed held in the tube (Figure 2). Radial dispersion, pressure drop over the packed bed and temperature gradients are neglected. The latter two assumptions have been validated by pressure and temperature measurements.

Let us now consider the above mentioned transport phenomena separately. The diffusive flux (N_i^{diff}) of component *i* in the shell and tube side is represented by

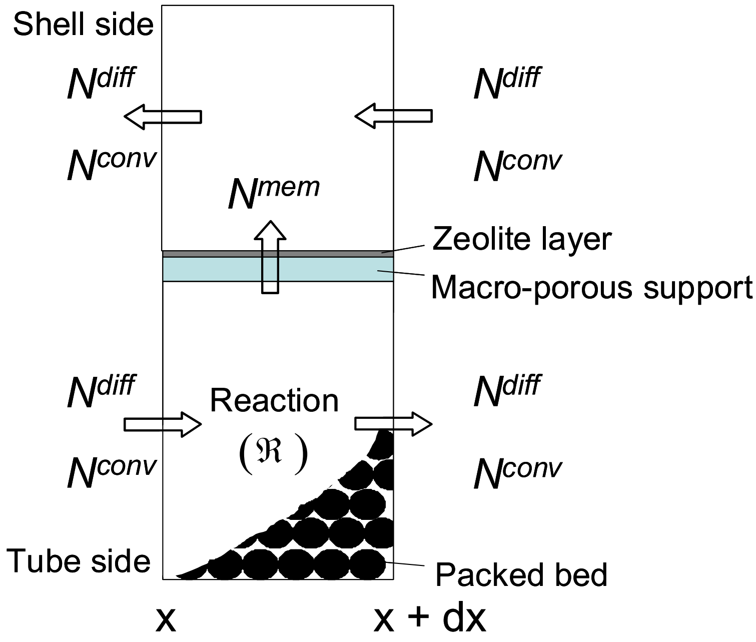

Figure 2. Schematic representation of the MR and all processes that are considered in the model: Convection (*conv*) and diffusion (*diff*) in the shell and tube side, reaction in the tube and exchange of molecule across the membrane (*mem*) between the shell and tube side. All mass transport processes are indicated as fluxes (*N*).

Fick's law:

$$N_i^{diff} = -D_i^{g,eff} \frac{dc_i}{dx}, \tag{5}$$

where now an effective gas diffusion coefficient $D_i^{g,eff}$, concentration c and space x is found. The convective flux of each component at the shell and tube side is given by the product of the gas velocity (u) and its concentration:

$$N_i^{conv} = uc_i. \tag{6}$$

The flux through the membrane is assumed to be determined completely by the zeolite layer; mass transport resistance in the support is neglected. Following earlier analysis of the membrane permeation data [24](Chapter 3) it is assumed that isobutane flux through the membrane is only due to Knudsen diffusion through membrane defects. Mathematically this flux can be expressed as:

$$N_i^{mem} = \frac{D_{Kn,i}^{eff}}{\delta^{mem}} \frac{\left(p_i^T - p_i^S\right)}{RT}, \qquad D_{Kn,i}^{eff} = \frac{\varepsilon}{\tau} \frac{d_0}{3} \sqrt{\frac{8RT}{\pi M_i}} \tag{7}$$

Where p, M, δ^{mem}, ε, τ and d_0 represent the pressure, molar mass, membrane thickness, membrane defect porosity, tortuosity and pore size, respectively. The superscripts S and T refer to shell and tube side properties, respectively. Also viscous flow plays a role [24](Chapter 3), but this contribution can be neglected because in the current case only situations without an absolute pressure drop over the membrane are considered. The unknown properties in Equation (7) are lumped:

$$\frac{\varepsilon}{\tau} \frac{d_0}{\delta^{mem}} \tag{8}$$

and have been fitted to the isobutane permeation data. The diffusivity of isobutene is based on the isobutane diffusivity corrected for the molar mass dependency expected from the Knudsen diffusion mechanism (Equation (7)). The permeation data of N_2 and H_2 are assumed to follow a surface diffusion mechanism [24,27](Chapter 3). In case that mass transport occurs in a very weak adsorption regime the flux across the membrane can be expressed as:

$$N_i^{mem} = \frac{q_i^{sat} \rho}{\delta^{mem}} Đ_i K_i \left(p_i^T - p_i^S\right). \tag{9}$$

q^{sat} is the maximum loading in the zeolite and ρ the zeolite density. The Maxwell Stefan diffusivity ($Đ$) and adsorption equilibrium constant (K) have the following temperature dependency:

$$K_i = K_{0,i}\exp\left(\frac{-\Delta H_{Ads,i}}{RT}\right) \qquad Đ_i = Đ_{0,i}\cdot\exp\left(\frac{-E_{A,diff,i}}{RT}\right). \tag{10}$$

This yields the pre-exponential of the adsorption equilibrium constant (K_0), enthalpy of adsorption (ΔH_{Ads}), the pre-exponential of the Maxwell Stefan diffusivity ($Đ_0$) and the activation energy of the diffusivity ($E_{A,diff}$).

Equation (9) can also be presented in a slightly different form, which is more convenient when expressing the equations in a dimensionless form later on:

$$N_i^{mem} = \frac{D_i^{mem}}{\delta^{mem}}\frac{\left(p_i^T - p_i^S\right)}{RT}, \qquad \frac{D_i^{mem}}{\delta^{mem}} = RT\frac{\rho q_i^{sat} K_{0,i}\, Đ_{0,i}}{\delta^{mem}}\exp\left(\frac{-E_{A,i}^{app}}{RT}\right). \tag{11}$$

The apparent activation energy for diffusion is defined as:

$$E_A^{app} = E_{A,diff} + \Delta H_{Ads}. \tag{12}$$

The lumped parameter $\rho q_i^{sat} K_{0,i}\, Đ_{0,i}\left(\delta^{mem}\right)^{-1}$ and E_A^{app} have been estimated from the H_2 and N_2 permeation data. Note that Equation (11) is also valid to predict the permeance in a mixture since the single component and mixture permeances are the same for the considered mixtures at high temperatures across the DD3R membrane [24][Chapter 3].

The reaction rate in the packed bed is described by a Langmuir Hinshelwood type rate equation [28], assuming that isobutane adsorption is the rate-limiting step:

$$\Re\left[\frac{mol}{kg_{cat}s}\right] = \frac{kp_A\left(1 - \frac{p_E p_H}{p_A K_{eq}}\right)}{1 + \frac{p_E}{K_E} + \frac{p_H}{K_H}}. \tag{13}$$

Here we can distinguish the partial pressures and adsorption equilibrium constants (K_i) of isobutane (i=A), isobutene (E) and hydrogen (H). K_{eq} represents the overall reaction equilibrium constant.

A molar balance for each component over a slice dz in axial direction ($z = x/L_{tube}$, L_{tube} = permeable tube length) of the isobaric membrane reactor tube side (Figure 2) leads to:

$$\begin{aligned}0 = \frac{\pi d_{tube}^2}{4}\left(\frac{p_{tot}^T}{RT}\right)\frac{\delta x_i^T u^T}{\delta z} - \frac{\pi d_{tube}^2}{4}\left(\frac{p_{tot}^T}{RT}\right)\frac{D_i^{g,eff}}{L_{tube}}\frac{d^2 x_i^T}{dz^2} - \nu_i \Re m_{cat} \\ + L_{tube}\pi d_{tube}\frac{D_i^{mem}}{\delta_{mem}}\frac{1}{RT}\left(p_i^T - p_i^S\right)\end{aligned} \quad . \tag{14}$$

And on the shell side:

$$\begin{aligned}0 = \frac{\pi(d_{shell}^2 - d_{tube}^2)}{4}\left(\frac{p_{tot}^S}{RT}\right)\frac{\delta x_i^S u^S}{\delta z} - \frac{\pi(d_{shell}^2 - d_{tube}^2)}{4}\left(\frac{p_{tot}^S}{RT}\right)\frac{D_i^{g,eff}}{L_{tube}}\frac{d^2 x_i^S}{dz^2} \\ - L_{tube}\pi d_{tube}\frac{D_i^{mem}}{\delta_{mem}}\frac{1}{RT}\left(p_i^T - p_i^S\right)\end{aligned} \quad . \tag{15}$$

Here m_{cat} and v represent the catalyst mass and stoichiometric coefficient, respectively. Now we introduce a dimensionless flow rate ϑ, a Péclet number with respect to the diffusive and convective flux in the packed bed (Pe_L), the Damköhler number (Da) and a Péclet number with respect to the convective flux in the packed bed and membrane flux (Pe_δ). Note that the Péclet numbers are based on the properties of H_2 since this characterizes the system best. Da is defined assuming first order kinetics in isobutane to arrive at a concentration independent dimensionless number.

$$\begin{aligned}&\vartheta^T = \frac{u^T}{u_0^T},\ Pe_L^{\mathrm{T}} = \frac{L_{tube}u_0^T}{D_H^{g,eff}},\ Da = \frac{4RTkm_{cat}}{u_0^T \pi d_{tube}^2},\ Pe_\delta^{\mathrm{T}} = \frac{\delta^{mem}u_0^T}{4D_H^{mem}}\frac{d_{tube}}{L_{tube}} \\ &\vartheta^S = \frac{u^S}{u_0^S},\ Pe_L^{\mathrm{S}} = \frac{L_{tube}u_0^S}{D_H^{g,eff}},\ Pe_\delta^{\mathrm{S}} = \frac{\delta^{mem}u_0^S}{4D_H^{mem}}\frac{\left(d_{shell} - d_{tube}\right)}{L_{tube}}\end{aligned} \tag{16}$$

In addition to these dimensionless numbers the $DaPe_\delta$ number [29], a type of Damköhler number describing the ratio of reaction rate and membrane flux is defined:

$$DaPe_\delta = \frac{k\delta^{mem}d_{tube}}{D_H^{mem}}. \tag{17}$$

In the case the tube and shell side have the same pressure Equation (14) can be written as:

$$0 = x_i^T\frac{\delta\vartheta^T}{\delta z} + \vartheta^T\frac{\delta x_i^T}{\delta z} - \left(\frac{D_i^{g,eff,T}}{D_H^{g,eff,T}}\right)\frac{1}{Pe_L^T}\frac{d^2 x_i^T}{dz^2} - \frac{\nu_i\Re}{p_{tot}^T k}Da + \left(\frac{D_i^{mem}}{D_H^{mem}}\right)\frac{1}{Pe_\delta^F}\left(x_i^T - x_i^S\right) \tag{18}$$

and Equation (15) can be cast into:

$$0 = x_i^S \frac{\delta \vartheta^S}{\delta z} + \vartheta^S \frac{\delta x_i^S}{\delta z} - \left(\frac{D_i^{g,eff,S}}{D_H^{g,eff,S}} \right) \frac{1}{Pe_L^S} \frac{d^2 x_i^S}{dz^2} - \left(\frac{D_i^{mem}}{D_H^{mem}} \right) \frac{1}{Pe_\delta^S} \left(x_i^T - x_i^S \right). \tag{19}$$

The final set of equations that constitutes the membrane reactor model comprises Equations (18) and (19) repeated for each component together with two equations that ensure that the sum of all fractions in the feed and sweep side equals 1:

$$1 = \sum_{i=1}^{n} x_i^T, \quad 1 = \sum_{i=1}^{n} x_i^S . \tag{20}$$

This system of equations has been solved in Athena Visual Studio [30] as a boundary value problem using orthogonal collocation. The system is modelled as a closed system using Danckwerts type boundary conditions:

$$\begin{array}{ll}
z = 0, \text{ Tube side} & z = 1, \text{ Tube side} \\
x_{i,0}^T = x_i^T - \left(\frac{D_i^{g,eff,T}}{D_H^{g,eff,T}} \right) \frac{1}{Pe_L^T} \frac{dx_i^T}{dz} & \frac{dx_i^T}{dz} = 0 \\
\vartheta^T = 1 & \frac{d\vartheta^T}{dz} = 0 \\
z = 0, \text{ Shell side} & z = 1, \text{ Shell side} \\
\frac{dx_i^S}{dz} = 0 & x_{i,0}^S = x_i^S - \left(\frac{D_i^{g,eff,S}}{D_H^{g,eff,S}} \right) \frac{1}{Pe_L^S} \frac{dx_i^S}{dz} \\
\frac{d\vartheta^S}{dz} = 0 & \vartheta^S = 1
\end{array} \tag{21}$$

3 Results and discussion

3.1 Membrane permeation

The performance of the DD3R membrane up to 773 K has been studied previously [24][Chapter 3]. The fluxes of He, N_2, H_2 and isobutane from this study are shown in Figure 3. The fluxes of N_2 and H_2 have been modelled assuming that the mass transport across the membrane is governed by intra-crystalline surface diffusion (Equation (11)), isobutane is modelled assuming permeation through defects by a Knudsen diffusion mechanism (Equation (7)). More details on the models can be found in Section 2.3, while the permeation results have been discussed in detail in Ref. [24][Chapter 3]. The model fit parameters that apply are listed in Table 2.

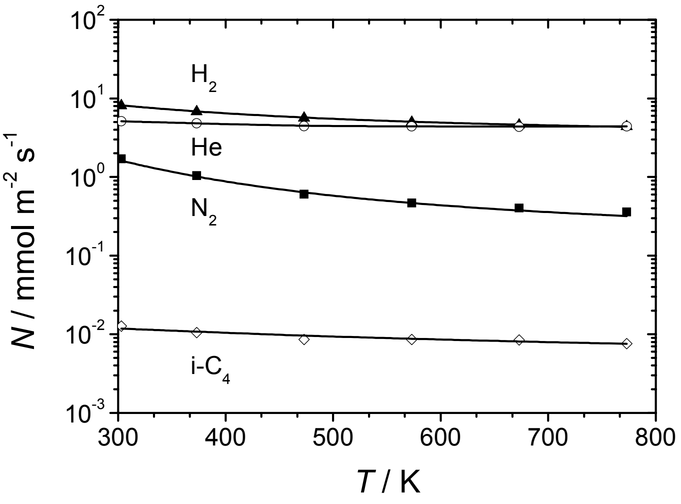

Figure 3. Permeance of H_2, He, N_2 and isobutane through the DD3R membrane as a function of the temperature. The H_2 and N_2 data in the current study (closed symbols) represent counter-current permeation data using H_2 as feed and N_2 as sweep gas. The He permeances are measured using the pressure drop method with a pressure drop of 100 kPa. Isobutane is measured using a feed gas pressure of 101 kPa and sweep gas (N_2) pressure of 101 kPa. Lines represent model fit results, except in case of He where the drawn line is to guide the eye.

Table 2. Estimated values from model fitting for membrane permeation and reaction rate parameters.

	Membrane transport parameters	Units
Isobutane	$\frac{\varepsilon}{\tau}\frac{d_0}{\delta^{mem}} = 2.7 \cdot 10^{-9}$	–
N_2	$D^{mem}\left(\delta^{mem}\right)^{-1} = RT \cdot 1.12 \cdot 10^{-9}\exp(7000/RT)$	m s^{-1}
H_2	$D^{mem}\left(\delta^{mem}\right)^{-1} = RT \cdot 2.88 \cdot 10^{-8}\exp(2880/RT)$	m s^{-1}

Reaction rate parameters		Units
Happel [28]	Fitted parameters	
$k = 5.1 \cdot 10^{-03}\exp\left(-\frac{74822}{RT}\right)$	$k = 1.2 \cdot 10^{-03}\exp\left(-\frac{67509}{RT}\right)$	$mol \cdot kg_{cat}^{-1}s^{-1}Pa^{-1}$
$K_{eq} = 1.4 \cdot 10^{+12}\exp\left(-\frac{121638}{RT}\right)$	$K_{eq} = 1.8 \cdot 10^{+12}\exp\left(-\frac{121638}{RT}\right)$	Pa^{-1}
$K_E = 2.1 \cdot 10^{-10}\exp\left(\frac{74822}{RT}\right)$	$K_E = 2.1 \cdot 10^{-10}\exp\left(\frac{74822}{RT}\right)$	Pa^{-1}
$K_H = 4.2 \cdot 10^{-12}\exp\left(\frac{100738}{RT}\right)$	$K_H = 4.2 \cdot 10^{-12}\exp\left(\frac{100738}{RT}\right)$	Pa^{-1}

The isobutane flux is very low because it cannot enter the DDR pore and passes only through a small number of defects in the membrane. As compared to the medium-pore zeolite MFI, the H_2 permeance of DD3R is about one order of magnitude lower (Table 1). It appears that by reducing the pore size also the permeance is reduced.

Both the H_2 and isobutane flux show a slightly decreasing flux with increasing temperature. This leads to an almost constant ideal selectivity of more than 500 over the complete temperature range, as shown in Figure 4. The ideal selectivity (α^{ideal}) is based on the single component permeances:

$$\alpha_{ij}^{ideal} = \frac{Permeance_i}{Permeance_j} = \frac{N_i}{N_j}\frac{\left(p_j^{retentate} - p_j^{sweep}\right)}{\left(p_i^{retentate} - p_i^{sweep}\right)}. \tag{22}$$

The mixture selectivity (α_{ij}^{mix}) is based on mixture permeation results and is defined as:

$$\alpha_{ij}^{mix} = \left(\frac{x_j}{x_i}\right)^{feed} \left(\frac{x_i}{x_j}\right)^{permeate}. \tag{23}$$

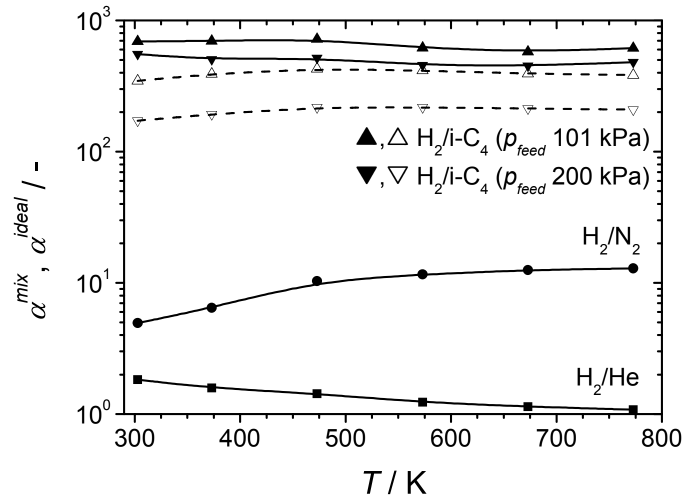

Figure 4. Mixture and ideal selectivities of the DD3R membrane. Closed symbols and solid lines represent ideal selectivities, dashed lines and open symbols mixture selectivities under non-differential operation. The lines are added to guide the eye. All data are considered at a total pressure drop of 100 kPa over the membrane. In case of the H_2/isobutane mixture also the data at a feed pressure of 101 kPa without pressure drop over the membrane are shown.

The H_2/isobutane mixture selectivity is slightly lower than the ideal selectivity due to non-differential effects: the faster permeating H_2 reduces its driving force for permeation by increasing its partial pressure in the permeate and reducing its partial pressure in the feed side [24][Chapter 3]. The H_2/isobutane selectivities also decrease slightly with increasing pressure due to a viscous flow contribution to the isobutane flux in case of an absolute pressure drop over the membrane. The H_2/N_2 (~11, 773 K) is much higher than the H_2/He (~1, 773K) ideal selectivity. This makes N_2 the preferred choice as sweep gas in terms of minimal feed dilution by counter-permeation of the sweep gas.

3.2 Packed bed (membrane) reactor

3.2.1 Asymmetry and packing effects

Compared to the membrane results in the previous section the membrane tube is filled with catalyst particles and the feed gases are fed from the inside of the tube (from the support side) instead of from the outside of the tube (from the zeolite layer side). If the support resistance can be ignored no difference in permeance should be observed if the gas is permeating from the support or from the zeolite layer side [31]. To ensure that the permeation data are suitable input to model the MR performance, an experiment has been performed with the packed bed membrane reactor at 303 K and 101 kPa using an equimolar H_2/isobutane mixture passing through the tube side and N_2 as sweep gas passing through the shell side. The H_2 and N_2 permeances are the same as in the membrane permeation experiments, while the isobutane permeance is a factor 2 lower.

3.2.2 Isobutene yield

Figure 5 shows the isobutene yield in the PBR and MR at 762 and 712 K, together with model fit results of the PBR and model predictions of the MR. The MR and PBR have been modelled using the reactor model as described in Section 2.3, where in case of the PBR the membrane fluxes are set to zero. The gas phase diffusivities are predicted using the correlation of Füller *et al.* [32], accounting for the packed bed porosity and tortuosity, which are assumed to be 0.4 and 1.5, respectively. The reaction rate kinetic constants have been estimated by model fitting of the packed bed yield data. The rate constants of Happel *et al.* [28] have been used as starting point because these have been determined on a similar catalyst (Cr_2O_3/Al_2O_3) in a suitable temperature range (650-762 K). The pre-exponential and activation energy of the rate constant have been estimated. Additionally, the pre-exponential of the reaction equilibrium constant has been fitted to reconcile the model and experimental equilibrium yields. The H_2 and isobutene adsorption equilibrium constants have been kept constant. The original constant values of Happel *et al.* and the model fit results of the current study are listed in Table 2. Note that the estimated values and the original ones of Happel *et al.* are in good agreement.

The PBR conversion data show an increase in yield with increasing temperature due to an increased catalyst activity and an increased equilibrium conversion. At low *WHSV*, *i.e.* long contact times, the PBR yield approaches the equilibrium yield. The model fit results describe the PB data well.

The MR yields coincide with the PBR yields at high *WHSV* and at low *WHSV* the yields of the MR are significantly higher than the PBR and equilibrium yield. The MR model predictions are in fairly good agreement with the experimental MR data, but the yields appear to be slightly overpredicted. An explanation could be that the catalyst activity is decreased in case of the MR due to H_2 removal from the reaction zone, which is not accounted for in the current model. This effect has also been observed by Casanave *et al.* [6]. An indication of this behaviour can also be found from the comparison of the PBR and MR yield data at 712 K where the MR yield is slightly lower than the PBR yield, whereas model predictions always indicate a higher MR yield due to removal of H_2 from the reaction zone. However, the difference between the simulated and experimental yields could also be due to model assumptions like not accounting for radial dispersion. Moreover, the conversion level for which the kinetic constants have been estimated does not match the level for which the prediction is made at low WHSV. The reduced activity could therefore also be due to inhibition by the product isobutene, which is underestimated in the rate equation. Airaksinen *et al.* [33] estimated for instance an isobutene adsorption equilibrium constant 8 times as high as the value we used in our study. But, by fitting the rate constant using a higher isobutene equilibrium adsorption constant from the PBR data does not lead to significantly different results.

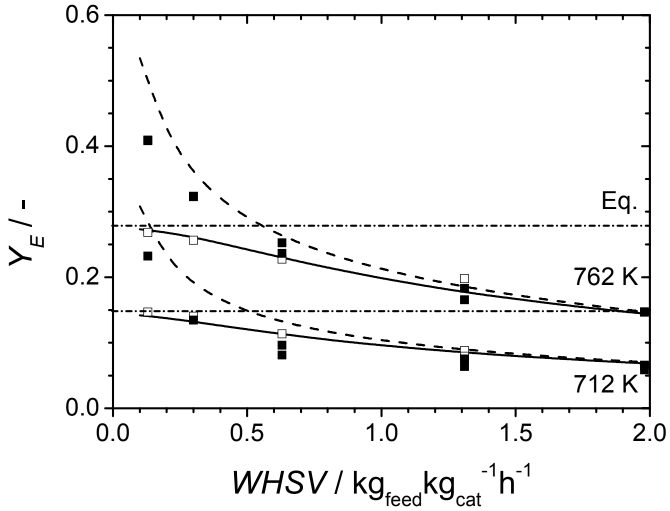

Figure 5. Isobutene yield in a packed bed (open symbols) and membrane reactor (closed symbols) at 762 and 712 K as s function of the *WHSV*. Pure isobutane is fed at 101 kPa, N_2 is used as sweep gas in counter-current mode. Solid, dashed and dash-dot lines represent PBR model fit results, MR model predictions and the equilibrium conversion, respectively.

The fraction of H_2 present in the retentate in case of the MR and PBR is shown in Figure 6. This figure clearly illustrates that due to removal of H_2 from the reaction zone at low *WHSV* the MR outperforms the PBR. Whereas at high *WHSV* the membrane H_2 flux is not sufficient to remove a significant amount of H_2 and the MR and PBR performances are equal. It is also evident that the H_2 concentration reduction in the tube side of the MR compared to the PBR is that significant that if the catalyst activity is reduced when the hydrogen concentration is reduced this effect will become manifest at *WHSV* values < 1 h^{-1}.

Note that also at low *WHSV*s the hydrocarbon retention in the feed side is very high due to the excellent H_2/isobutane selectivity of the membrane. Even at a *WHSV* of 0.13 h^{-1} < 2 % of the isobutane and isobutene leave the MR from the permeate side, > 98 % is retained in the feed side.

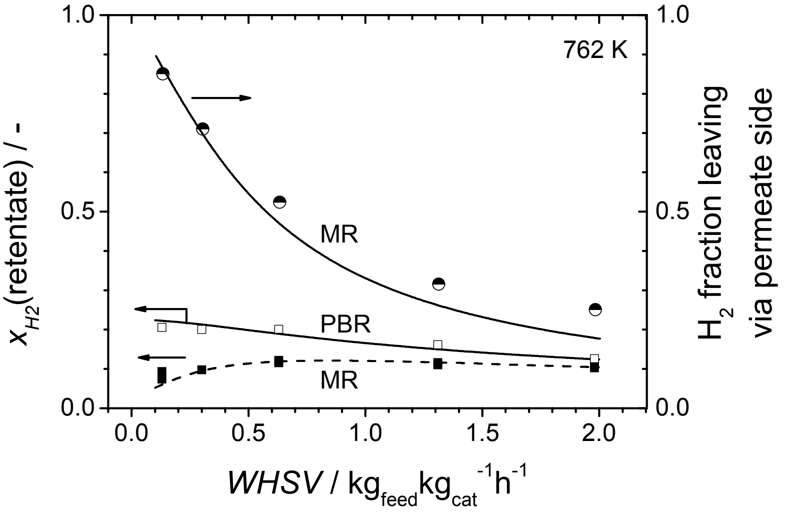

Figure 6. Fraction of H_2 in the retentate of the PBR and MR at 762 K as a function of the *WHSV*. Points are experimental data, lines are modelling results.

3.2.3 Selectivity

Besides isobutene also side products like coke or lower hydrocarbons can be formed. When coke is formed the amount of H_2 will be higher than the amount of isobutene in the reactor effluent. In case of the PBR experiments no excess of H_2 to isobutene could be detected. Although difficult to calculate accurately, there appears to be a significant excess of H_2 in case of the membrane reactor up to 10-15% at 762 K and low *WHSV*s. In case that for each mol isobutane converted to coke four mol of H_2 are formed and, accounting for the amount of H_2 consumed in the hydrogenolysis reactions, this leads to a selectivity towards coke of ~ 3 % at *WHSV* = 0.13 h^{-1} . These results indicate that indeed due to H_2 removal coke formation is mildly promoted, particularly at long residence times.

The selectivity towards isobutene (Equation (4) and (2)) with respect to lower hydrocarbons in the MR is compared to the selectivity in the PBR at 712 and 762 K (Figure 7). At high *WHSV* the selectivity is high, > 0.96 for all cases. Upon increasing the residence time in the reactor more lower-hydrocarbons are formed. Also at higher temperature more by-products are formed. In all cases the major part of the by-products constitutes of methane and propane/propene (Figure 8). Propane/propene and methane are present in almost equimolar amounts; only a modest excess of methane is present. This is expected since these are the products of hydrogenolysis of isobutane and isobutene. The amount ethane/ethene formed is very low. A comparison of the selectivity in the PBR and MR reveals that hydrogenolysis reactions are suppressed in the MR, probably due to removal of H_2 from the reaction zone. This has also been found in other studies [10,13,14].

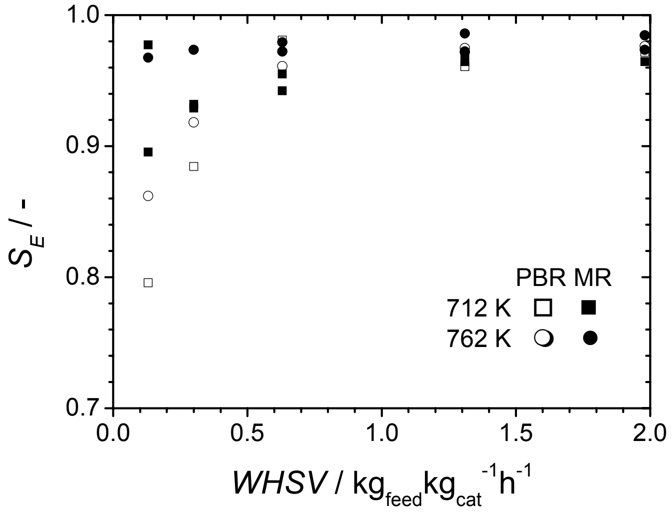

Figure 7. Selectivity of the isobutane dehydrogenation reaction towards isobutene in the PBR and MR at 712 and 762 K as a function of the *WHSV*.

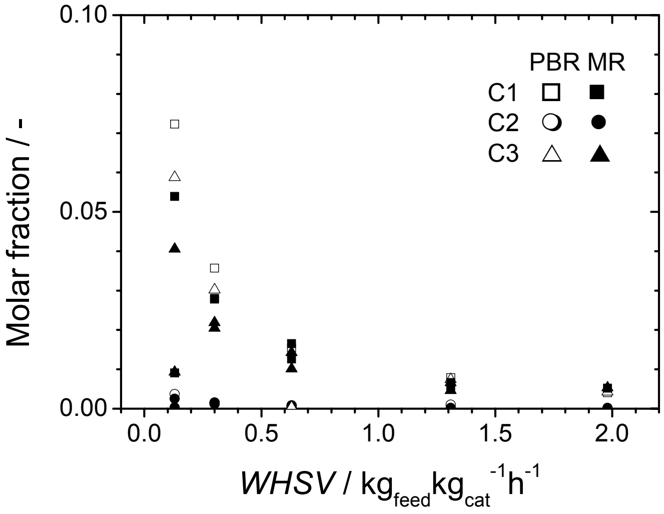

Figure 8. Molar fraction of C1 (methane), C2 (ethane and ethane) and C3 (propane and propene) of all hydrocarbons that leave the MR and PBR at 762 K.

3.2.4 Catalyst and membrane stability.

Although it appears that the catalyst activity in the MR is lower compared to the PBR (Section 3.2.2), no signs of very rapid catalyst deactivation in time have been observed. An experimental run at 762 K is shown in Figure 9. Initially, a *WHSV* of 0.3 h^{-1} has been set. Note that at these conditions a significant amount of H_2 is removed from the reaction zone (Figure 6) and that the conversion is above the equilibrium conversion (Figure 9). Firstly, the catalyst shows a high activity, leading to a conversion of 0.4, then the conversion drops quickly, passes through a minimum and becomes constant after 2 hours of operation. The initial high conversion is due to oxidation of part of the feed by the pre-oxidized catalyst.

Changing the *WHSV* leads to a new steady state conversion quickly. After 7 h of operation the steady state conversion at 0.3 h^{-1} after 2 h could be reproduced. Although the total number over turnovers is not very high, a stable MR operation without significant catalyst deactivation for several hours is observed under H_2 lean conditions.

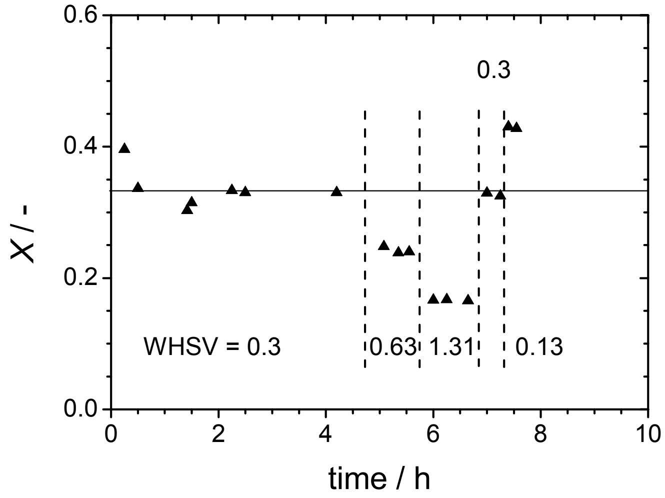

Figure 9. Isobutane conversion as a function of time on stream in the MR at 762 K. During operation time the *WHSV* was changed from 0.3 to 0.63 to 1.31 to 0.3 and 0.13 h^{-1}.

Prior to the MR experiments the membrane has been exposed to high temperature conditions for the permeation experiments for several months (~ 6) including > 10 temperature heating up and cooling down cycles [24][Chapter 3]. The MR experiments added another 3 months of operation at high temperature (> 700 K). Of this period ~ 25 working days of dehydrogenation experiments have been carried with the same number of overnight regenerations. In this period 5 heating up and cooling down cycles have been performed. The isobutane fraction in the permeate has been around $6 \cdot 10^{-4}$ to $1 \cdot 10^{-3}$ during all MR experiments. No significant increase of this fraction has been observed which indicates a stable membrane performance.

3.2.5 Feed dilution effects

In Section 3.2.2 the good performance of the MR has been attributed to the removal of H_2 from the reaction zone. Counter permeation of the sweep gas (N_2), however, can lead to dilution of the feed which can also contribute to an increased conversion [5,8] because the equilibrium conversion is higher at lower partial pressures. Figure 10 shows the fraction of N_2 in the retentate due to counter permeation. Due to the longer residence time at the feed side the fraction of N_2 increases with decreasing *WHSV* up to almost 0.3 at a *WHSV* of 0.13 $kg_{feed}\ kg_{cat}^{-1}\ h^{-1}$. Note that this value represents the upper limit of the N_2 concentration in the tube.
To investigate the influence of the feed dilution on the yield, the MR conversion is simulated for several cases (Figure 10): 1) experimental conditions: full model as considered in the previous sections, 2) No feed dilution: no N_2 flux across the membrane, 3) No H_2 flux across the membrane and 4) Completely impermeable membrane, *i.e.* a PBR. As shown previously (Figure 5), the PBR approaches the equilibrium yield at low *WHSV* (Figure 10). When no hydrogen is removed, but the feed is diluted due to N_2 counter permeation (case 3) the conversion becomes significantly higher than the equilibrium. Now a modest conversion increase due to dilution is found. The MR conversions with (case 1) and without (case 2) sweep gas counter permeation are exactly the same. Clearly the effect of feed dilution on the isobutene yield under experimental conditions is minimal. The effect of feed dilution will only be of importance when the reactor operates close to the local thermodynamic equilibrium, which is not the case under the current conditions. The latter claim is verified by an evaluation of the retentate composition. The equilibrium constant and the reactant and product fractions are under equilibrium conditions related by:

$$K_{eq} = p_{tot} \left\{ \frac{x_H x_E}{x_A} \right\}_{eq} \quad . \tag{24}$$

The right hand side of the equation, evaluated for the retentate composition at 0.1 h^{-1} and 762 K, is 6351 Pa, which is about 1.5 times lower than the equilibrium value of 9320 Pa (left hand side).

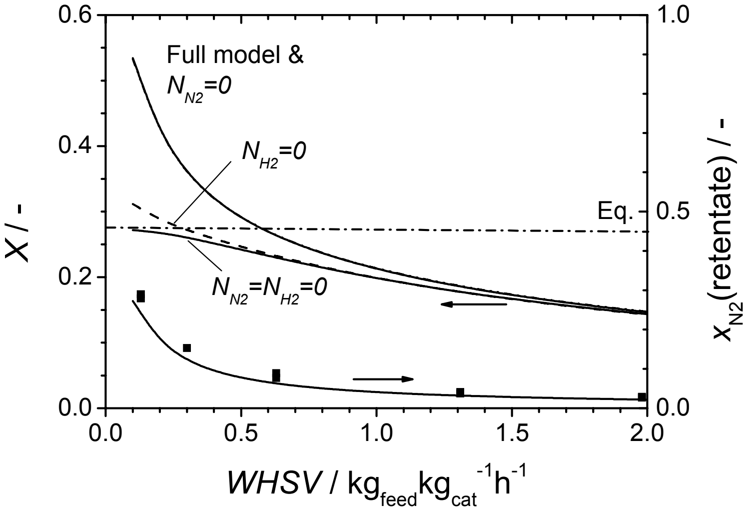

Figure 10. Effect of feed dilution by counter-permeation of sweep gas on the membrane reactor conversion. Lines represent model simulations of the reactor reflecting the MR experiments (Full model) and simulations assuming that the membrane is impermeable to the sweep gas (N_{N2} = 0), impermeable to H_2 (N_{H2} = 0) and impermeable to both H_2 and N_2 ($N_{H2} = N_{N2} = 0$). The right axis represents the fraction of N_2 in the retentate. The line represents simulation results of the full model, points are experimental data. The membrane reactor operates at 101 kPa pure isobutane feed, 762 K and 100 ml min^{-1} sweep gas (N_2) in counter-current mode.

3.2.6 Performance evaluation

The MR is evaluated further based on the dimensionless numbers introduced in Section 2.3. If we neglect axial and radial dispersion, three processes need to be balanced to obtain an optimal MR performance [34,35][Chapter 1]. In terms of characteristic times these are: residence time, reaction time and a time related to hydrogen removal by the membrane. Combining these characteristic times leads to three different ratios: *Da* (residence time / reaction time), Pe_δ (time for H_2 removal / residence time) and $DaPe_\delta$ (time for H_2 removal / reaction time) (details in Section 2.3). The values of these dimensionless numbers for the MR are given in Table 3 at 762 and 712 K and different *WHSV*s. *Da* increases with increasing temperature due to the activated nature of the rate constant. At low *WHSV* the residence time is long compared to the reaction time and a high conversion is expected and obtained (Figure 5). As a rule of thumb *Da* is related to the conversion as [36]: if $Da < 0.1$ then $X < 0.1$ and if $Da > 10$ then $X > 0.9$. Our results follow this rule of thumb well considering that our conversion scales from 0 to the equilibrium conversion. Pe_δ is almost independent of temperature because the membrane permeation of H_2 is only slightly dependent on the temperature (Figure 3). At $WHSV = 1.0$ h^{-1} the residence time and time required for H_2 removal are of the same order ($Pe_\delta \approx 1$). This is illustrated nicely in Figure 6, where indeed at this *WHSV* a considerable amount of H_2 is produced and removed from the reaction zone. Moving to lower *WHSV*s the residence time increases, whereas the characteristic time for H_2

removal remains constant, leading to an improved H_2 removal and reaction performance. Finally, $DaPe_\delta$ increases with increasing temperature since the characteristic time for reaction is reduced and the time for H_2 removal remains close to constant. The value of $DaPe_\delta$ is close to one, which indicates that in the current design the catalyst activity and membrane performance are balanced quite well. However, since the MR outperforms the PBR only at low *WHSV*s the appropriate conclusion is that both are not optimal regarding application of this MR. Note that compared to other type of MRs the H_2 permeance of the DD3R membrane is relatively low (Table 1). In those studies typically the catalyst activity is the factor limiting the MR performance [9,10,13].

Table 3. Dimensionless numbers relating residence time and reaction time (*Da*), time to remove H_2 and residence time (Pe_δ), and time to remove H_2 and reaction time ($Da\ Pe_\delta$).

WHSV	T / K	*Da*	Pe_δ	$Da_L Pe_\delta$
0.1	762	5.31	0.12	0.63
0.3	762	1.77	0.36	0.63
1.0	762	0.53	1.19	0.63
0.1	712	2.54	0.12	0.29
0.3	712	0.85	0.35	0.29
1.0	712	0.25	1.16	0.29

To demonstrate that both the catalyst and membrane limit the performance the MR is simulated considering the cases that: 1) *Da* is 10 times higher; 2) Pe_δ is 10 times lower and 3) that both *Da* is 10 times higher and Pe_δ is 10 times lower. The simulated conversions are compared to the original MR performance (Figure 11).

Increasing the H_2 removal rate ($Pe_\delta\downarrow$) lead to a very modest conversion improvement, clearly the catalyst activity hampers an improved MR performance. If only the catalyst activity is increased ($Da\uparrow$), the reactor approaches its equilibrium conversion already at a much higher *WHSV*, but the membrane permeation flux is too low to obtain conversions significantly above the equilibrium at high *WHSV*s. If both the reaction activity and H_2 membrane removal rate are increased by a factor 10 ($Da\uparrow$ and $Pe_\delta\downarrow$), the conversion is strongly increased, as expected. Alternatively, the space velocity can be reduced by a factor 10, but then axial dispersion will become increasingly important with a negative impact on the plug flow reactor behaviour. For further reading on the influence on other operational aspects of MR in dehydrogenation reactions see for instance [17,37].

Several options could be applied to improve the MR's performance. *Da* can be increased by using a more active catalyst [38], or using a higher operating temperature (although a higher temperature would lead to a higher coking rate at the catalyst). A decrease of Pe_δ (Equation (16)) can be achieved by removing more H_2 through application of a thinner DDR membrane, a different membrane with a higher permeance or by choosing a higher membrane area to reactor volume ratio. This latter area to volume ratio can be greatly increased by choosing a smaller tube or hollow fibrous support [34,39]. Note that Da can be increased and Pe_δ decreased efficiently by increasing the feed pressure since this will lead to a decreased gas velocity at a given $WHSV$, a higher reaction rate and a higher permeation flux. A potential downside of this approach can be that the increased hydrocarbon partial pressures could lead to a reduced catalyst selectivity or activity.

Note that van de Graaf *et al.* [34] have discussed their MR performance by comparing the membrane Areal Time Yield (ATY) and Space Time Yield (STY). In order to balance the two yields the area to volume ratio (A/V) can be changed. A clear connection between their and the present approach exists since:

$$DaPe_\delta \approx \frac{STY}{ATY}\frac{V}{A} = \frac{STY}{ATY}\frac{d_{tube}}{4}. \tag{25}$$

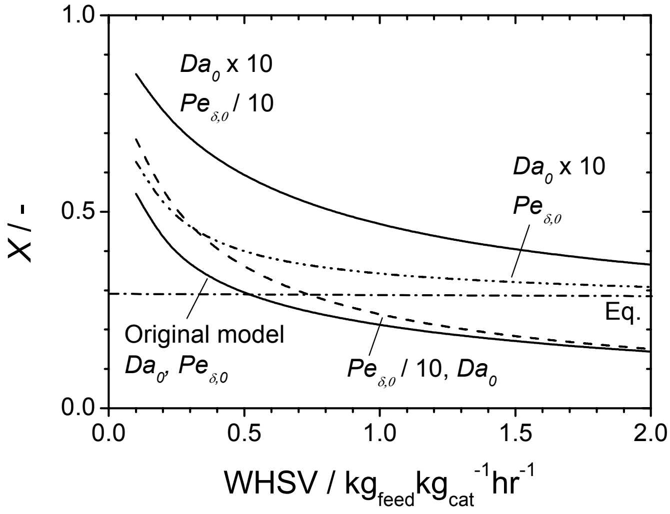

Figure 11. Effect of variations of Da and Pe_δ on the MR conversion. Lines represent MR simulations at 762 K and 101 kPa total feed pressure, using 100 ml min^{-1} (STP) N_2 as sweep gas in countercurrent operation at 101 kPa. Starting from the original Da_0 and $Pe_{\delta,0}$ values simulations using a 10 times higher Da or a 10 times lower Pe_δ or a combination of the two have been performed.

Another issue for application of this type of reactor is that it seems that removal of H_2 leads to a lower activity (Section 3.2.2) and more coke formation. As shown in Figure 6 the H_2 fraction in the retentate needs to be strongly reduced to obtain high conversions. Since in this reaction only H_2 is removed and isobutene is retained the H_2 fraction needs to be very low to achieve very high conversions due to the reaction equilibrium constant (*cf.* Equation (24)).

The ultimate viability of the MR should be based on an economical evaluation and clear insights in the effects of very H_2 lean conditions on the catalyst performance. However, from the current results it can be concluded that the minimum requirements of a MR to obtain a significant conversion improvement compared to a PBR are: $Da \geq 10$ and $Pe_{\delta} \leq 0.1$, while $DaPe_{\delta}$ should be ≈ 1 to optimally utilize both catalyst and membrane activity.

Note that since membranes with higher fluxes are already available, it is the limited catalyst activity and stability under relative low temperature and H_2 lean conditions that is an important limiting factor regarding application of MRs in dehydrogenation reactions [38].

4 Conclusions

A DD3R zeolite membrane has been successfully applied as H_2 selective membrane in the dehydrogenation reaction of isobutane in a packed bed membrane reactor (MR) configuration. Experiments with a conventional packed bed reactor (PBR) served as benchmark. The membrane shows an excellent H_2/isobutane permselectivity (>500 @ 773 K)) and a reasonable H_2 permeance (~ $4.5 \cdot 10^{-8}$ mol m^{-2} s^{-1} Pa). The high selectivity is due to molecular sieving: isobutane cannot enter the pores of DD3R and passes only through membrane defects. At low *WHSV*s isobutene yields above the equilibrium yield based on feed conditions could be obtained. At 762 K and 0.13 $kg_{feed}kg_{cat}^{-1}h^{-1}$, the isobutene yield in the MR is 0.41, where the equilibrium and PBR yields are only ~0.28, an increase of about 50%. This increased yield is attributed to removal of H_2 from the reaction zone by the membrane, up to 85% at the lowest space velocity. Although some counter permeation of the sweep gas N_2 occurs, this dilution effect does not contribute significantly to the yield increase of the MR. The activity of the catalyst in the MR seems modestly reduced compared to the PBR, but no indications of faster deactivation of the catalyst are observed under H_2 lean conditions. A constant very high hydrocarbon retention in the reaction zone indicated that the membrane quality remained constant throughout all experiments.

Compared to the PBR the selectivity in the MR towards coke seems to be mildly increased due to the lower H_2 partial pressure in the reactor, although the selectivity towards coke is still low: < 5 %. The selectivity towards methane and propane/propene is somewhat lower in the MR. By keeping the H_2 concentration in the reactor low, cracking hydrogenolysis reactions are mildly suppressed.

An isothermal membrane reactor model captures the experimental results well. The membrane permeation parameters and reaction rate constants have been estimated independently from membrane permeation and PBR experiments, respectively.

An analysis of the major characteristic times describing the system, the residence time in the reactor, reaction time and time required for H_2 removal by the membrane, expressed as ratios in two dimensionless parameters *Da* and Pe_{δ}, revealed that in the current MR design the catalyst activity and H_2 removal rate are nicely balanced ($DaPe_{\delta} \approx 1$), but both limit the overall performance. Improvements of the current design are possible by choosing a more active catalyst, or higher operating temperature, and a membrane support with a higher surface area per unit reactor volume. Also operation at higher feed pressure could boost the

MR's performance. $Da \geq 10$ and $Pe_\delta \leq 0.1$. are proposed as minimal requirements of a MR to show a significantly improved performance compared to a PBR. $DaPe_\delta$ should be ≈ 1 to optimally utilize both catalyst and membrane activity. Since membranes with higher fluxes are already available, it is the limited catalyst activity and stability under relative low temperature and H_2 lean conditions that is an important limiting factor regarding application of MRs in dehydrogenation reactions [38].

Acknowledgements

NGK Insulators is gratefully acknowledged for providing the membrane. Isabelle Aerts and Anna Tihaya are gratefully acknowledged for their contribution to the model development and membrane reactor experiments, respectively.

References

[1] B. M. Weckhuysen and R. A. Schoonheydt, *Catalysis Today*, 51, **1999**, 223.

[2] J. A. Moulijn, M.Makkee, and A.van Diepen, Chemical process technology, **2001**, Wiley, New York.

[3] R. Schafer, M. Noack, P. Kolsch, M. Stohr, and J. Caro, *Catalysis Today*, 82, **2003**, 15.

[4] J. Sanchez and T.T.Tsotsis, Catalytic Membranes and Membrane Reactors, **2002**, Wiley-VCH, Weinheim.

[5] D. Casanave, A. Giroir-Fendler, J. Sanchez, R. Loutaty, and J. A. Dalmon, *Catalysis Today*, 25, **1995**, 309.

[6] D. Casanave, P. Ciavarella, K. Fiaty, and J.-A. Dalmon, *Chemical Engineering Science*, 54, **1999**, 2807.

[7] P. Ciavarella, D. Casanave, H. Moueddeb, S. Miachon, K. Fiaty, and J.-A. Dalmon, *Catalysis Today*, 67, **2001**, 177.

[8] U. Illgen, R. Schäfer, M. Noack, P. Kölsch, A. Kühnle, and J. Caro, *Catalysis Communications*, 2, **2001**, 339.

[9] L. van Dyk, S. Miachon, L. Lorenzen, M. Torres, K. Fiaty, and J.-A. Dalmon, *Catalysis Today*, 82, **2003**, 167.

[10] W. Q. Liang and R. Hughes, *Catalysis Today*, 104, **2005**, 238.

[11] M. Sheintuch and R. M. Dessau, *Chemical Engineering Science*, 51, **1996**, 535.

[12] Y. L. Guo, G. Z. Lu, Y. S. Wang, and R. Wang, *Separation and Purification Technology*, 32, **2003**, 271.

[13] T. Matsuda, I. Koike, N. Kubo, and E. Kikuchi, *Applied Catalysis A-General*, 96, **1993**, 3.

[14] T. Ioannides and G. R. Gavalas, *Journal of Membrane Science*, 77, **1993**, 207.

[15] G. Sznejer and M. Sheintuch, *Chemical Engineering Science*, 59, **2004**, 2013.

[16] J. P. Collins, R. W. Schwartz, R. Sehgal, T. L. Ward, C. J. Brinker, G. P. Hagen, and C. A. Udovich, *Industrial & Engineering Chemistry Research*, 35, **1996**, 4398.

[17] Y. V. Gokhale, R. D. Noble, and J. L. Falconer, *Journal of Membrane Science*, 103, **1995**, 235.

[18] W. Zhu, F. Kapteijn, and J. A. Moulijn, *Chemical Communications*, **1999**, 2453.

[19] J. Gascon, W. Blom, A. van Miltenburg, A. Ferreira, R. Berger, and F. Kapteijn, *Microporous and Mesoporous Materials*, 115, **2008**, 585.

[20] T. Tomita, K. Nakayama, and H. Sakai, *Microporous and Mesoporous Materials*, 68, **2004**, 71.

[21] J. van den Bergh, W. Zhu, J. Gascon, J. A. Moulijn, and F. Kapteijn, *Journal of Membrane Science*, 316, **2008**, 35.

[22] J. van den Bergh, W. Zhu, F. Kapteijn, J. A. Moulijn, K. Yajima, K. Nakayama, T. Tomita, and S. Yoshida, *Research on Chemical Intermediates*, 34, **2008**, 467.

[23] J. Kuhn, K. Yajima, T. Tomita, J. Gross, and F. Kapteijn, *Journal of Membrane Science*, 321, **2008**, 344.

[24] J. van den Bergh, A. Tihaya, and F. Kapteijn, *Microporous and Mesoporous Materials*, 132, **2010**, 137.

[25] S. Himeno, T. Tomita, K. Suzuki, K. Nakayama, K. Yajima, and S. Yoshida, *Industrial & Engineering Chemistry Research*, 46, **2007**, 6989.

[26] A. Seidel-Morgenstern (Ed.), Membrane reactors, **2010**, Wiley, Weinheim.

[27] F. Kapteijn, W. Zhu, J. A. Moulijn, and T. Q. Gardner, Zeolite Membranes: Modeling and Application, in: Structured Catalysts and Reactors, Cybulski, A. and Moulijn, J. A. (Eds), Ch. 20, **2005**, Taylor & Francis Group, Boca Raton, FL, 701.

[28] J. Happel, K. Kamholz, D. Walsh, and V. Strangio, *Industrial & Engineering Chemistry Fundamentals*, 12, **1973**, 263.

[29] S. Battersby, P. W. Teixeira, J. Beltramini, M. C. Duke, V. Rudolph, and J. C. niz da Costa, *Catalysis Today*, 116, **2006**, 12.

[30] Website Athena Visual studio, http://www.athenavisual.com/, Visited **2010**.

[31] J. M. van de Graaf, E. van der Bijl, A. Stol, F. Kapteijn, and J. A. Moulijn, *Industrial & Engineering Chemistry Research*, 37, **1998**, 4071.

[32] W. N. Fueller, P. D. Schettler, and J. C. Giddings, *Industrial & Engineering Chemistry Research*, 58, **1966**, 19.

[33] S. M. K. Airaksinen, M. E. Harlin, and A. O. I. Krause, *Industrial & Engineering Chemistry Research*, 41, **2002**, 5619.

[34] J. M. van de Graaf, M. Zwiep, F. Kapteijn, and J. A. Moulijn, *Applied Catalysis A: General*, 178, **1999**, 225.

[35] J. van den Bergh, N. Nishiyama, and F. Kapteijn, Zeolite membranes in catalysis; what is new and how bright is the future?, in: Novel concepts in catalysis and chemical

Reactors, Cybulski, A., Moulijn, J. A., and Stankiewicz, A. (Eds), Ch. 10, **2010**, Wiley, New York, 211.

[36] H. S. Fogler, Elements of chemical reaction engineering, **2006**, Pearson Education, New York.

[37] S. A. S. Rezai and Y. Traa, *Journal of Membrane Science*, 319, **2008**, 279.

[38] S. Miachon and J. A. Dalmon, *Topics in Catalysis*, 29, **2004**, 59.

[39] R. Dittmeyer, K. Svajda, and M. Reif, *Topics in Catalysis*, 29, **2004**, 3.

5

The Relevant Site Model

Together with excellent separation results a remarkable strong loading dependency of diffusion of light gases in DD3R is found. It is well-known that the diffusivity in zeolites is dependent on the loading, but simulation and experimental data point out that for small pore 8-ring zeolites very strong loading dependencies of diffusion are quite common. This strong loading dependency complicates modelling of permeation behaviour of such zeolite membranes, which is required for module design. The most promising model available, the so-called Reed Ehrlich approach, turned out only modestly successful to model CH_4/CO_2 and CH_4/N_2 mixture permeation across an all-silica DDR membrane.

Therefore, a new model has been introduced in this thesis to describe the loading dependency of diffusion in zeolites (**Chapter 5A**). The model is formulated around the idea of segregated adsorption in cage-like zeolites, *i.e.* that molecules are located either in the cage or in the window. Only the molecules located at the window site are able to make a successful jump to another cage. This so-called Relevant Site Model (RSM) is based on the Maxwell-Stefan framework for mass transport but includes one extra parameter that describes the adsorption properties of the ‘relevant site’. Key feature of the RSM as applied to mixtures is that competitive adsorption effects and ‘speeding up and slowing down’ (momentum exchange) effects between guest molecules are related to the relevant site loading instead of the overall loading, two quantities that can be very different. In addition to the RSM the concept of free space relevant for diffusion has been introduced. Because the diffusivity often approaches very small values when the loading in the zeolite approaches its saturation loading a ‘confinement’ factor is introduced to indicate the available free space. Now it is argued that due to, for example, side pockets or positional rearrangements not all free space is relevant for diffusion. A method has been put forward to account for these effects in modelling work.

Application to zeolite DDR

Firstly, the RSM has been applied to a set of single component diffusivity data of CO_2 and N_2 in DD3R computed using molecular dynamic (MD) simulations (**Chapter 5B**). The RSM describes the Maxwell Stefan diffusivity data very well up to saturation. The observed diffusivity loading dependency is explained from the relative low window site occupancy that is typically much lower than the total occupancy at lower loadings. The RSM is successfully extended to non-isothermal diffusivity data of CO_2 and N_2 in DDR. Relating intermolecular correlation effects (momentum exchange) to the relevant site occupancy instead of the total occupancy leads to a quantitative prediction of the observed correlation effects and, consequently, the self diffusivity. Analysis of the N_2 data suggests positional rearrangements in the DDR cages in a certain loading range. These effects have been incorporated in the model successfully using the concept of free space relevant for diffusion.

Then, the RSM has been subjected to an extensive set of diffusivity data of N_2/CO_2 and Ne/Ar mixtures in zeolite DDR, directly computed using molecular dynamics (**Chapter 5C**). A large part of the considered data has been taken from literature. It has been shown that the RSM provides excellent mixture diffusivity predictions from single component diffusivity data. The results are comparable to the ‘Reed-Ehrlich’ approach as put forward by Krishna and co-workers. A clear improvement by the RSM is found in the case of the N_2 diffusivity in N_2/CO_2 mixtures, attributed to the specific window blocking effect by CO_2 which is inherently incorporated in the RSM by relating adsorption to the relevant (window) site.

Extension to other zeolites

After the successful application of the RSM to describe the loading dependency of diffusion in zeolite DDR it has also been successfully applied to a variety of light gases (CH_4, CO_2, Ar and Ne) and binary mixtures thereof in other zeolite topologies, DDR, CHA, MFI and FAU, utilizing the extensive diffusivity dataset published by Krishna and van Baten for this variety of zeolite-guest systems (*e.g.* R. Krishna and J. M. van Baten, *Chemical Engineering Science*, 63, 2008, 3120, supporting information)(**Chapter 5D**). From the RS approach a measure for the level of adsorption segregation is derived: the ratio of the RS and total occupancy. The predicted level of adsorption segregation correlates well with the level of confinement of a molecule at the RS: the molecule diameter to zeolite pore diameter. Moreover, the predicted degree of adsorption segregation of the studied light gases in DDR is in good agreement with molecular simulations results, indicating the physical meaningfulness of the estimated RS adsorption parameters. The binary mixture diffusivity modelling points out that in case of the small-pore zeolites (DDR and CHA) the data is described best with equal RS saturation loadings for both components. For the large-pore zeolite FAU the ratio of the RS saturation loadings equals that of the bulk saturation loadings. The geometry of the RS strongly influences the RS saturation loading: in case of the small-pore zeolites the RS (= window site) is restricted to only one molecule but when the RS becomes larger more than one molecule can be adsorbed.

Application to DD3R membrane permeation data

Having demonstrated the usefulness of the RSM using simulated diffusivities, the model has been applied to membrane permeation data (**Chapter 5E**). Single component (CO_2, CH_4 and N_2) and equimolar binary mixture (CO_2/CH_4, N_2/CH_4 and CO_2/Air) permeation data across a disc-shaped all-silica DDR zeolite membrane have been the subject of a thorough modelling study over a challenging broad temperature (220-373 K) and feed pressure (101-1500 kPa) range. Also here a comparison to the Reed Ehrlich approach is made.

Both the RSM as the RE approach yield an excellent model fit of the single component permeation data. However, for both models the N_2 and CH_4 single component permeation data did not allow an accurate estimation of the model fit parameters. Both models can lead to a good prediction of comparable quality of the mixture permeation data based on the single component model fit parameters. The RE approach is very sensitive towards the model input parameters and the estimated mixture loading, which both can be very hard to determine accurately in practice. The RSM does not suffer from both these issues, which is an evident advantage with respect to application of this model.

Reconciliation with dynamically corrected transition state theory

The RSM closely resembles the well-known concept of dynamically corrected Transition State Theory (dcTST) which is often used in molecular simulations to study the dynamics of rare events. Therefore, we investigated this connection in detail (**Chapter 5F**). It turns out that the ratio of the RS and total loading and a factor containing the exchange effects and free space available for diffusion in the RSM are directly related to those in dcTST, *i.e.* the probability that a molecule is on top of the free energy barrier and the transmission coefficient κ. Therefore, the RSM provides a direct link between properties at the molecular scale and the macroscopic Maxwell-Stefan diffusion coefficient.

5A

The Relevant Site Model: Theory

Here, the relevant site model foundations are introduced together with the concept of free space relevant for diffusion.

This chapter is based on the following publications:

J. van den Bergh, S. Ban, T. J. H. Vlugt, and F. Kapteijn, *Journal of Physical Chemistry C*, 113, **2009**, 17840.

J. van den Bergh, S. Ban, T. J. H. Vlugt, and F. Kapteijn, *Journal of Physical Chemistry C*, 113, **2009**, 21856.

J. van den Bergh, S. Ban, T. J. H. Vlugt, and F. Kapteijn, *Separation and Purification Technology*, 73, **2010,** 151.

1 Introduction

This chapter deals with loading dependency of diffusion in zeolites. Diffusion plays an important role in the use of zeolites in catalysis, and separation processes based on adsorption and zeolite membranes [1]. Zeolites are commonly used as catalyst and adsorbent for a long time. In the field of zeolite membranes currently only a few applications exist but several new applications are anticipated [2]. An example of a potential new application is the purification of natural gas (CO_2 / CH_4 separation), where for several 8-ring zeolite membranes very high separation factors and fluxes have been demonstrated (DD3R [3-7][Chapter 2], Zeolite T [8] and SAPO 34 [9,10]), breaking through the so-called Robeson upper limit of polymeric membranes [11].

Together with excellent separation results a remarkable strong loading dependency of diffusion of light gases in the above mentioned topologies is found. It is well-known that the diffusivity in zeolites is dependent on the loading, but simulation and experimental data point out that for small-pore 8-ring zeolites very strong loading dependencies of diffusion are quite common [12-14]. This strong loading dependency complicates modelling of permeation behaviour of such zeolite membranes, which is required for module design.

Recently, Krishna and co-workers have put forward a method to capture the loading dependency of diffusion within a Maxwell-Stefan framework for mass transport [15]. In Section 2.1 their approach is discussed in more detail. This approach yielded concentration dependent diffusivities in good agreement with experimental data generated by MD simulations of several zeolite topologies and was also successfully applied to model single component and mixture membrane permeation data of SAPO-34 membranes [16,17]. Two crucial assumptions are made in this approach regarding the mixture modelling: 1) The self- and Maxwell-Stefan diffusivity of an individual component in a mixture with a certain total loading is the same as for this component in a single component situation with a loading equivalent to the total loading (‘total loading assumption’); 2) Correlation effects are neglected, *i.e.* speeding up and slowing down effects are not accounted for. The latter assumption is justified by the observation that in many cases almost no correlation effects appear to be present [18].

This approach was only modestly successful to model CH_4/CO_2 and CH_4/N_2 mixture permeation through an all-silica DDR membrane [5]. There are several aspects that may be responsible for this. Firstly, in DDR distinct segregated adsorption was observed [19] which causes a poor mixture adsorption prediction by the Ideal Adsorbed Solution Theory (IAST) [20,21] and may introduce specific blocking effects by molecules that prefer to reside in the window sites of DDR. Secondly, correlation effects in mixtures are neglected in the current approach, but speeding up and slowing down effects are observed in binary permeation across MFI and SAPO-34 membranes and no adequate method to account for this is available [22]. The most important assumption, however, is the ‘total loading’ assumption, which follows from the idea that intermolecular repulsions are the origin of the observed loading dependency of diffusion.

In this chapter a new model is introduced to describe and explain the observed loading dependency of the diffusivity from a different perspective. This ‘Relevant Site Model’ (RSM) starts from the idea of segregated adsorption, *i.e.* that molecules are located either in the cage or at the window of the DDR cages [19,22]. Only molecules located at the window site of DDR are assumed to be able to make a successful jump to the next cage. Therefore, by abandoning the idea that molecular repulsions are the origin of the observed loading dependency, as in the Reed-Ehrlich approach, a new formulation for mass transport is derived that gives opportunities to improve current modelling approaches when extended to mixtures. In a sense our model shows parallels to the work of Coppens and Iyengar [23] who emphasize that site heterogeneity in zeolites should be accounted for within the Maxwell-Stefan formulation for mass transport.

A second concept that will be introduced deals with the effective free space in the zeolite that is available for mass transport. It will be argued that the free space based on the total loading, as derived from the adsorption isotherm, is not a proper measure in many cases. Therefore, a free space relevant for mass transport is introduced.

2 Theory

The diffusivity in zeolites can be a strong function of the amount adsorbed on the zeolite [12-14]. Particularly zeolite topologies consisting of cages connected by windows show strong and peculiar loading dependencies, especially for molecules that are strongly confined in the window opening [24]. In this case a strong increase of the diffusivity is observed with increasing loading, passing through a maximum and decreasing to very low values when approaching saturation loading [12]. The RSM is introduced to account for these effects; the foundations of the RSM are introduced below.

2.1 Maxwell Stefan approach to mass transfer

The RSM is based on the Maxwell-Stefan (MS) approach to mass transport for diffusion in zeolites [25-27]. In the MS approach the fundamental driving force for mass transport under isothermal conditions is considered to be a gradient in chemical potential ($\nabla\mu_i$) of component *i*. This driving force is balanced with ‘friction’ that a component with a certain velocity (u_i) has with the zeolite and with other species in the system. The interaction, or ‘friction’, with the zeolite is characterised by the MS diffusivity $Đ_i$ and the interaction with other components with the exchange diffusivity $Đ_{ij}$. The latter interactions, or correlation effects as they will be referred to from now on, can be interpreted by ‘friction’ between molecules that can lead to 'speeding up' and 'slowing down' effects of one component by the other in a mixture. θ_i is the occupancy of *i* and is defined as the ratio of its loading and its saturation loading (q_i / q_i^{sat}).

$$-\nabla\mu_i = RT\frac{u_i}{Đ_i} + \sum_{j=1}^{n}\theta_j RT\frac{u_i - u_j}{Đ_{ij}}, \quad i = 1, 2, \ldots n\,. \tag{1}$$

Introducing the flux (*N*) in terms of the loading on the zeolite (*q*) and zeolite density (*ρ*):

$$N_i \equiv \rho q_i u_i \tag{2}$$

and relating the fugacity (*f*) to the chemical potential via:

$$\mu_i = \mu_i^o + RT\ln f_i \tag{3}$$

leads to a final expression to describe the flux in a multi-component zeolite-guest system:

$$-\rho\theta_i\nabla\ln f_i = \sum_{j=1}^{n}\frac{q_j N_i - q_i N_j}{q_i^{sat} q_j^{sat} Đ_{ij}} + \frac{N_i}{q_i^{sat} Đ_i}, \quad i = 1, 2, \ldots n\,. \tag{4}$$

2.1.1 Relation transport and self diffusivity

The MS diffusivity describes the collective motion of molecules. The diffusion process of individual molecules is called self diffusion, which also takes place in absence of a concentration gradient. Paschek and Krishna have derived a relation between the corrected and self diffusivity of a single component system from Equation (4) by considering this a pseudo mixture of tagged (t) and untagged species [28]. When a case of self-diffusion is considered it holds that:

$$\nabla\theta_i + \nabla\theta_i^t = 0 \quad \text{and} \quad N_i + N_i^t = 0\,. \tag{5}$$

When the restrictions from Equation (5) are imposed to Equation (4) it follows that the self and transport diffusivities can be related through the following equation:

$$\frac{1}{D_{self,i}} = \frac{1}{Đ_i} + \frac{\theta_i}{Đ_{ii}}\,. \tag{6}$$

It is then argued that the difference between the self and transport diffusivity arises from correlation effects that component *i* has with itself that are characterized by the so-called self exchange diffusivity ($Đ_{ii}$) [28]. It follows from Equation (6) that correlation effects are very low when either the loading is very low or the self exchange diffusivity is very large. This concept has been extended to mixtures as follows:

$$\frac{1}{D_{self,i}} = \frac{1}{\text{Đ}_i} + \sum_{j=1}^{n} \frac{\theta_j}{\text{Đ}_{ij}}, \quad i = 1, 2 \ldots n\,. \tag{7}$$

2.1.2 Estimation of the exchange coefficient Đ_{ij}

To make a prediction of the fluxes based on the single component diffusivities using Equation (4) the exchange coefficient needs to be estimated. A common approach is to use a logarithmic interpolation using the single component diffusivities and mixture occupancies:

$$\text{Đ}_{ij} = \left(\text{Đ}_i\right)^{(\theta_i/(\theta_i+\theta_j))} \left(\text{Đ}_j\right)^{(\theta_j/(\theta_i+\theta_j))}\,. \tag{8}$$

However, an approach including also the saturation loadings and self exchange coefficients appears to yield more accurate results [29]:

$$q_j^{sat}\,\text{Đ}_{ij} = \left[q_j^{sat}\,\text{Đ}_{ii}\right]^{(q_i/(q_i+q_j))} \left[q_i^{sat}\,\text{Đ}_{jj}\right]^{(q_j/(q_i+q_j))} = q_i^{sat}\,\text{Đ}_{ji} \qquad . \tag{9}$$

The occupancy dependency of the self-exchange diffusivities ($\text{Đ}_{ii}, \text{Đ}_{jj}$) is captured by the following empirical relation [29], introducing two fitting parameters (*a* and *b*) that are fitted to single component MS and self diffusivity data:

$$\frac{\text{Đ}_{ii}}{\text{Đ}_i} = a_i \exp\left(-b_i\theta_i\right). \tag{10}$$

For experimental studies Equation (9) is less relevant than Equation (8) since typically only the self or transport diffusivity is known, not both.

2.1.3 Mixture adsorption

To calculate the mixture loadings usually the so-called Ideal Adsorbed Solution Theory (IAST) is used [20,25,30]. This approach allows prediction of mixture loadings based on single component isotherms. An advantage of this method is that it accounts for differences in saturation loading. This approach has proven successful in many cases, however, appears to fail when adsorption becomes inhomogeneous [21]. If the saturation loadings of the components in the mixture are equal, an extended Langmuir isotherm can also be applied:

$$\theta_i = \frac{K_i f_i}{1+\sum_{i=1}^{n} K_i f_i}, \quad i = 1, 2, \dots n, \tag{11}$$

In which K_i is the adsorption equilibrium constant.

2.1.4 Reed Ehrlich approach

Krishna and co-workers have introduced an approach to account for the observed loading dependency of the diffusivity. This approach is quite successful in many cases [24,31,32]. The origin of the observed loading dependency in this approach is assumed to be inter-molecular repulsions, which can lead to a decrease in the energy barrier for diffusion. Quantitatively the loading dependency is expressed in a model originally developed by Reed and Ehrlich [15,33,34]:

$$\begin{aligned} &\text{Đ}_i = \text{Đ}_i(0) \cdot \frac{\left(1+\varepsilon_i\right)^{z-1}}{\left(1+\varepsilon_i/\phi_i\right)^{z}}, \quad \phi_i = \exp\left(\delta E_{A,i}/RT\right) \\ &\varepsilon_i = \frac{\left(\beta_i - 1 + 2\theta_i\right)\phi_i}{2\left(1-\theta_i\right)}, \qquad \beta_i = \sqrt{1-4\theta_i\left(1-\theta_i\right)\left(1-1/\phi_i\right)} \end{aligned} . \tag{12}$$

The model is based on a square lattice of evenly spaced adsorption sites separated by energy barriers. When a neighbouring site is occupied a repulsive effect can be experienced that leads to a reduction of the energy barrier to hop to another site. However, when a neighbouring site is occupied the number of vacant sites are reduced, which has a negative effect on the diffusivity. When all neighbouring sites are occupied the diffusivity will become zero. $\delta E_{A,i}$ represents the reduction in energy barrier per nearest neighbour. The number of nearest neighbours is given by z. Equation (12) is valid for a single component system. However, when applied to mixtures, the diffusivity Đ_i is evaluated using equation (12) at the total mixture occupancy: the total loading assumption [15].

2.2 Relevant Site Model

2.2.1 Basic concepts

The RSM model is based on the Maxwell-Stefan approach to mass transport, however, a distinction is made between the total loading (q) and the relevant site (RS) loading (q^*). This difference implies segregated adsorption, which is a phenomenon frequently observed in zeolites. A classical example is adsorption of alkanes in MFI where a distinction between channels and intersections is made [30,35,36]. But segregated adsorption has also been observed in zeolite CHA, DDR and ERI [37].

The main assumption in the RSM is that mass transport is determined by the RS: transport at the RS is rate controlling. As a case study DDR is selected [38,39], a zeolite consisting of cages connected by window openings. Krishna and van Baten [37] have shown that adsorption in DDR is segregated; a distinction between window sites and cage sites can be made. Molecules can reside in the cage or in the window region.

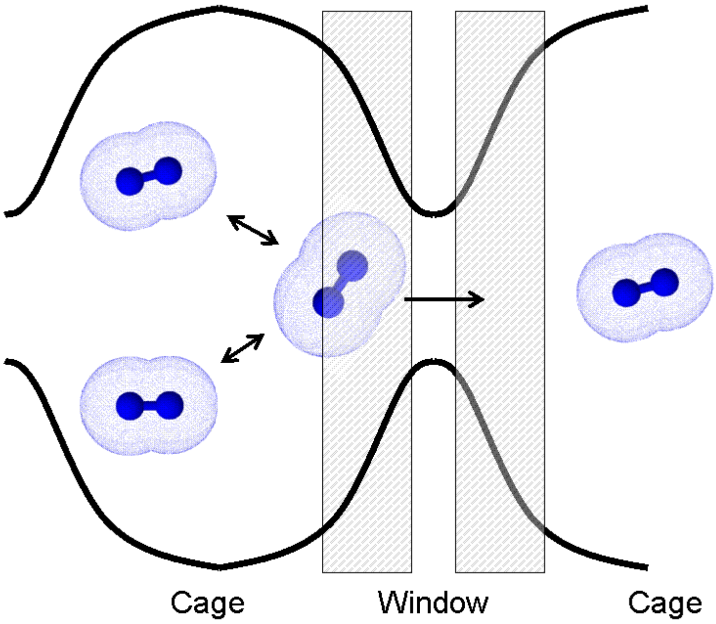

Figure 1. Schematic representation of a molecule located at a window site, in equilibrium with molecules present in the cage.

In the RSM it is assumed that only the molecules in the window region are able to make a successful jump to the next cage (Figure 1). Since it is now assumed that the diffusivity is determined by molecules that reside at the RS, Equation (1) can be expressed in terms of the RS properties:

$$-\nabla\mu_i = RT\frac{u_i^*}{Đ_i^*} + \sum_{j=1}^{n}\theta_j^* RT\frac{u_i^* - u_j^*}{Đ_{ij}^*}, \quad i = 1, 2, \ldots n\,. \tag{13}$$

All RS related properties are denoted with an asterisk. The flux of component i is defined as the product of its average velocity at the RS (u_i^*), the zeolite density (ρ) and the loading at the RS (q_i^*):

$$N_i \equiv \rho q_i^* u_i^*\,. \tag{14}$$

Equation (13) can then be cast into:

$$-\rho\theta_i^* \frac{\nabla\mu_i}{RT} = \sum_{j=1}^{n} \frac{q_j^* N_i - q_i^* N_j}{q_i^{sat,*} q_j^{sat,*} Đ_{ij}^*} + \frac{N_i}{q_i^{sat,*} Đ_i^*}, \quad i = 1, 2, ...n. \tag{15}$$

By inverting Equation (15) the following expression for the fluxes is obtained:

$$(N) = -\frac{\rho}{RT}\left[B^*\right]^{-1}\left[q^*\right](\nabla\mu), \tag{16}$$

where matrix $\boldsymbol{q}^*$ is an n×n matrix with diagonal elements $q_1^*, q_2^*, ..., q_n^*$ and all off-diagonal elements are zero. The elements of matrix $\boldsymbol{B}^*$ are given by:

$$B_{ii}^* = \frac{1}{Đ_i^*} + \sum_{\substack{j=1 \\ j \neq i}}^{n} \frac{q_j^*}{q_j^{sat,*} Đ_{ij}^*} \quad \text{and} \quad B_{ij}^* = -\frac{q_j^*}{q_j^{sat,*} Đ_{ij}^*}. \tag{17}$$

Finally, it is assumed that the RS diffusivity is proportional to the amount of free space available and relevant for diffusion ($1-\theta^{\#}$).

$$Đ_i^* = Đ_i^*(0)\left(1-\theta^{\#}\right) \tag{18}$$

This concept is explained in more detail in Section 2.3, but in the case that all free space is relevant for diffusion the so-called strong confinement scenario is found:

$$Đ_i^* = Đ_i^*(0)\left(1-\theta\right). \tag{19}$$

The total occupancy in a mixture can be defined as:

$$\theta = \sum_{i=1}^{n} \theta_i = \sum_{i=1}^{n} \frac{q_i}{q_i^{sat}}. \tag{20}$$

2.2.2 Relation RS self and transport diffusivities

In section 2.1.1 a relation between the transport and self diffusivity has been derived based on total loading properties (Equations (5-7)). When the same derivation is repeated assuming that all correlation effects are related to the RS, since this represents the part of the system that controls the mobility, a RS analogue of Equation (7) is obtained:

$$\frac{1}{D_{self,i}^*} = \frac{1}{Đ_i^*} + \sum_{j=1}^{n} \frac{\theta_j^*}{Đ_{ij}^*}, \quad i = 1, 2...n. \tag{21}$$

Paschek *et al.* proposed to assume the self exchange coefficient to be equal to the Maxwell-Stefan diffusivity ($Đ_{ii}=Đ_i$), which is a practical solution [28]. This approach was successful for a very limited number of cases but is in general not useful to predict self diffusivities from Maxwell-Stefan diffusivities. Now, we propose the following relation between the RS transport diffusivity and the RS exchange diffusivity:

$$Đ_{ii}^{*}= a_i \cdot Đ_i^{*}, \tag{22}$$

in which a_i represents an extra model fit parameter. It is shown in Chapters 4B-4D that for small-pore cage-like zeolites like DDR and CHA a_i equals 1. In this case $D_{self,i}^{*}$ and $Đ_i^{*}$ are directly related through the relevant site occupancy:

$$D_{self,i}^{*} = \frac{Đ_i^{*}}{1+\theta_i^{*}}. \tag{23}$$

2.2.3 Estimation of the RS exchange diffusivity

The RS exchange diffusivity ($Đ_{ij}^{*}$) can be estimated using the Vignes logarithmic interpolation [29], based on the self exchange diffusivities, RS saturation loadings and the fraction (x) of components i and j at the RS (*cf.* Section 2.1.2):

$$q_j^{sat*}Đ_{ij}^{*}=\left[q_j^{sat*}Đ_{ii}^{*}\right]^{x_i^*}\left[q_i^{sat*}Đ_{jj}^{*}\right]^{x_j^*} = q_i^{sat*}Đ_{ji}^{*}, \qquad x_i^* = q_i^*/(q_i^*+q_j^*). \tag{24}$$

In case that the saturation loadings of the considered components are equal and $Đ_{ii}^{*}=Đ_i^{*}$ Equation (24) simplifies into:

$$Đ_{ij}^{*}=\left[Đ_i^{*}\right]^{x_i^*}\left[Đ_j^{*}\right]^{x_j^*} =Đ_{ji}^{*}, \qquad x_i^* = q_i^*/(q_i^*+q_j^*) \qquad . \tag{25}$$

The complicating part with respect to application of the model in its current form is that the RS saturation loadings are not known. Fortunately, Equation (24) can be rewritten showing that the RS exchange diffusivities $Đ_{ij}^{*}$ and $Đ_{ji}^{*}$ are only a function of the *ratio* of the RS saturation loadings and the RS fraction and not of the absolute values of the saturation loadings:

$$Đ_{ij}^{*}=\left[\frac{q_i^{sat*}}{q_j^{sat*}}\right]^{x_j^*}\left[Đ_{ii}^{*}\right]^{x_i^*}\left[Đ_{jj}^{*}\right]^{x_j^*} = \frac{q_i^{sat*}}{q_j^{sat*}}Đ_{ji}^{*}. \tag{26}$$

Since the fraction is a function of the total RS loading it may seem that the RS exchange diffusivities are still dependent on the absolute value of the RS loading. However, in the case that the mixture loadings *i* and *j* are calculated with the IAST from single-site Langmuir isotherms the calculated fraction of component *i* on the RS is only dependent on RS occupancies and the ratio of the RS saturation loadings and not on the absolute value of the RS saturation loading.

2.2.4 Relation RSM and diffusivities based on total loading

This section describes how the RS diffusivities and diffusivities based on the total loading relate. This is very relevant since the diffusivity is commonly defined based on the total loading in experimental and computer simulation studies. We will work out this relation by considering diffusivities as calculated from molecular dynamic (MD) simulations.

The MS approach to mass transport can be directly related to MD simulation results. It is most convenient to start from an Onsager type representation of Equation (16) where the fluxes are expressed as linear functions of the driving force:

$$(N) = -[L](\nabla\mu). \qquad (27)$$

The Onsager reciprocal relations demand that matrix ***L*** is symmetric [40]. In order to relate Equation (27) to the MS diffusivity usually a modified Onsager matrix **Δ** is introduced based on the *total* loading:

$$(N) = -\frac{\rho}{RT}[\Delta][q](\nabla\mu). \qquad (28)$$

Where ***q*** is an n×n matrix with diagonal elements $q_1, q_2, ..., q_n$ and all off-diagonal elements are zero. The elements of matrix **Δ** can be directly calculated from MD simulations through [24]:

$$\Delta_{ij} = \frac{1}{N_j}\lim_{\Delta t\to\infty}\frac{1}{\Delta t}\left\langle\left(\sum_{l=1}^{N_i}\left(r_{l,i}(t+\Delta t)-r_{l,i}(t)\right)\right)\left(\sum_{k=1}^{N_j}\left(r_{k,j}(t+\Delta t)-r_{k,j}(t)\right)\right)\right\rangle, \qquad (29)$$

where N_j represents the number of molecules *j*, $r_{l,i}$ and $r_{k,i}$ indicate the position of the individual molecules *l* and *k* of each individual molecule of species *i* and *j*, respectively. The self diffusivity of component *i* can be calculated directly via [41]:

$$D_{Self,i} = \frac{1}{N_i}\lim_{\Delta t\to\infty}\frac{1}{\Delta t}\left\langle\sum_{l=1}^{N_i}\left(r_{l,i}(t+\Delta t)-r_{l,i}(t)\right)^2\right\rangle. \qquad (30)$$

However, to relate the Onsager matrix ***L*** (Equation (27)), to the MS formulation based on the RS (Equation (16)) it is convenient to introduce a modified Onsager matrix $\boldsymbol{\Delta}^*$, based on the RS loading:

$$(N) = -\frac{\rho}{RT}\left[\Delta^*\right]\left[q^*\right](\nabla\mu). \tag{31}$$

Since in this case

$$\left[B^*\right]^{-1} = \left[\Delta^*\right], \tag{32}$$

the elements of matrix Δ^* for a binary system can be related to the RS diffusivities through:

$$\left[\Delta^*\right] = \begin{bmatrix} \dfrac{\text{Đ}_1^*\left(1+\dfrac{\theta_1^*\text{Đ}_2^*}{\text{Đ}_{21}^*}\right)}{1+\dfrac{\theta_1^*\text{Đ}_2^*}{\text{Đ}_{21}^*}+\dfrac{\theta_2^*\text{Đ}_1^*}{\text{Đ}_{12}^*}} & \dfrac{\text{Đ}_1^*\dfrac{\theta_1^*\text{Đ}_2^*}{\text{Đ}_{12}^*}}{1+\dfrac{\theta_1^*\text{Đ}_2^*}{\text{Đ}_{21}^*}+\dfrac{\theta_2^*\text{Đ}_1^*}{\text{Đ}_{12}^*}} \\ \dfrac{\text{Đ}_2^*\dfrac{\theta_2^*\text{Đ}_1^*}{\text{Đ}_{21}^*}}{1+\dfrac{\theta_1^*\text{Đ}_2^*}{\text{Đ}_{21}^*}+\dfrac{\theta_2^*\text{Đ}_1^*}{\text{Đ}_{12}^*}} & \dfrac{\text{Đ}_2^*\left(1+\dfrac{\theta_2^*\text{Đ}_1^*}{\text{Đ}_{12}^*}\right)}{1+\dfrac{\theta_1^*\text{Đ}_2^*}{\text{Đ}_{21}^*}+\dfrac{\theta_2^*\text{Đ}_1^*}{\text{Đ}_{12}^*}} \end{bmatrix}. \tag{33}$$

A comparison of the definition of the matrix $\boldsymbol{\Delta}$ as based on the total loading (Equation (28)) and based on the RS loading (Equation (31) leads to the following relation between the two:

$$[\Delta] = \left[\Delta^*\right]\left[q^*\right][q]^{-1}. \tag{34}$$

The diagonal elements of matrix $\boldsymbol{\Delta}$ are found by multiplication of the diagonal elements of matrix $\boldsymbol{\Delta}^*$ with the ratio q_i^*/q_i. This ratio represents the fraction of adsorbed molecules that is assumed to contribute to mass transport. Note that a clear parallel to transition state theory (TST) is found. In Chapter 5F the relation between the RSM and TST is investigated in more detail. In case of a single component system Equation (34) leads to the following relation between the transport diffusivity based on the total and RS loading:

$$\text{Đ}_i = \text{Đ}_i^*\frac{q_i^*}{q_i}. \tag{35}$$

Next it will be argued that the self diffusivity based on the total loading is also obtained by multiplication of the self diffusivity based on the RS loading by the ratio (q_i^*/q_i). The self diffusivity is based on the mean square displacement of individual molecules. As shown in Equation (30) this is based on the individual displacements of *all* molecules of species *i* (N_i). Now a RS self diffusivity is defined based on only the molecules located at a RS (N_i^*).

$$D_{Self,i}^* = \frac{1}{N_i^*} \lim_{\Delta t \to \infty} \frac{1}{\Delta t} \left\langle \sum_{l^*=1}^{N_i^*} \left(r_{l^*,i}\left(t + \Delta t\right) - r_{l^*,i}\left(t\right) \right)^2 \right\rangle . \tag{36}$$

The assumption of the RSM is that only molecules located at the RS contribute to mass transport. Consequently, the summation in Equation (36), based on the RS, equals the summation in Equation (30), which is based on the total loading. In this case the following relation is obtained after comparing Equation (36) and (30):

$$D_{Self,i} = D_{Self,i}^* \frac{q_i^*}{q_i} . \tag{37}$$

Note that treating the definition of the elements of matrix $\mathbf{\Delta}$, as defined in Equation (29), in a similar manner as done for the self diffusivity described above one arrives at the same relation as presented in Equation (34).

2.2.5 Application of the RSM to single component systems

In order to apply the RSM the RS diffusivity and loading need to be estimated from diffusivity based on the total loading. Therefore it is proposed to relate the relevant site loading (q_i^*) to the fugacity via a single-site Langmuir isotherm in which K_i^* represents the relevant site adsorption equilibrium constant:

$$q_i^* = \frac{q_i^{sat*} K_i^* f_i}{1 + K_i^* f_i} . \tag{38}$$

Combining Equation (18), (35) and (38) yields the following expression for the diffusivity based on the total loading in terms of RS properties:

$$Đ_i = Đ_i^*(0)\left(1-\theta^\#\right)\frac{q_i^*}{q_i} = q_i^{sat*} Đ_i^*(0)\frac{\left(1-\theta^\#\right)}{q_i}\frac{K_i^* f_i}{1+K_i^* f_i} . \tag{39}$$

So, the diffusivity follows the ‘strong confinement’ scenario and normalization is required with respect to the fraction of molecules at the relevant site (q_i^*/q_i). Note this means that this fraction of molecules is considered to be rate determining. Provided that the adsorption isotherm of the system is known and all free space is relevant for diffusion the observed loading dependency of the diffusivity based on the total loading can be used to estimate the relevant site adsorption constant (K_i^*) and a lumped diffusivity parameter ($q_i^{sat*}Đ_i^*(0)$). Note that in the limit $f_i \to 0,\ \ q_i \to q_i^{sat}K_i f_i$, and $Đ_i$ is given by:

$$Đ_i(0) = Đ_i^*(0)\frac{q_i^{sat*}}{q_i^{sat}}\frac{K_i^*}{K_i}. \tag{40}$$

A Van ‘t Hoff temperature dependency of the RS adsorption constants and Arrhenius type activated diffusion of the RS diffusivity is now assumed:

$$Đ_i^*(0) = Đ_{i,0}^*(0)\exp\left(\frac{-E_{A,i}^*}{RT}\right), \qquad K_i^* = K_{i,0}^*\exp\left(\frac{-\Delta H_i^*}{RT}\right). \tag{41}$$

Now the zero loading pre-exponential of the RS diffusivity ($Đ_{i,0}^*(0)$), activation energy of the RS diffusivity ($E_{A,i}^*$), the pre-exponential of the RS adsorption equilibrium constant ($K_{i,0}^*$) and the RS adsorption enthalpy (ΔH_i^*) are found. In this case Equation (40) simplifies into:

$$Đ_i = Đ_i^*(0)\frac{q_i^{sat*}}{q_i^{sat}}\frac{K_{i,0}^*}{K_{i,0}}\exp\left(\frac{-\left(E_{A,i}^* + \Delta H_i^* - \Delta H_i\right)}{RT}\right) \tag{42}$$

and the flux under these conditions can be expressed as:

$$N_i = -\rho Đ_i^*(0) q_i^{sat*} K_{i,0}^*\exp\left(\frac{-\left(E_{A,i} + \Delta H_i^*\right)}{RT}\right)\nabla f_i. \tag{43}$$

In this situation the temperature dependency of diffusion and adsorption cannot be distinguished anymore and an apparent activation energy for diffusion ($E_{A,app,i}^*$) is found:

$$E_{A,app,i}^* = E_{A,diff,i}^* + \Delta H_{ads,i}^*. \tag{44}$$

It follows from Equation (39) that the loading dependency of the diffusivity based on the total loading, and generally presented in literature, is dependent on the adsorption constant of the relevant site *and* on the single component adsorption isotherm. Some typical profiles that can be expected from Equation (39) are presented in Figure 2. Two reference systems are considered: 1) a system where the total adsorption is described by a single-site Langmuir isotherm and 2) a system that is described by a dual-site Langmuir isotherm with $K_i^A = 100K_i^B$ and $q_i^{sat,A} = q_i^{sat,B}$. The dependency of the normalized diffusivity of these two systems on the relevant site adsorption constant is shown in Figure 2. The normalized

Maxwell-Stefan diffusivity follows from Equation (39) and (40), assuming that all free space is relevant for diffusion (Equation (19)):

$$\frac{\text{Đ}_i}{\text{Đ}_i(0)} = \left(1-\theta\right)\frac{\theta_i^*}{\theta_i}\frac{K_i}{K_i^*}\,. \tag{45}$$

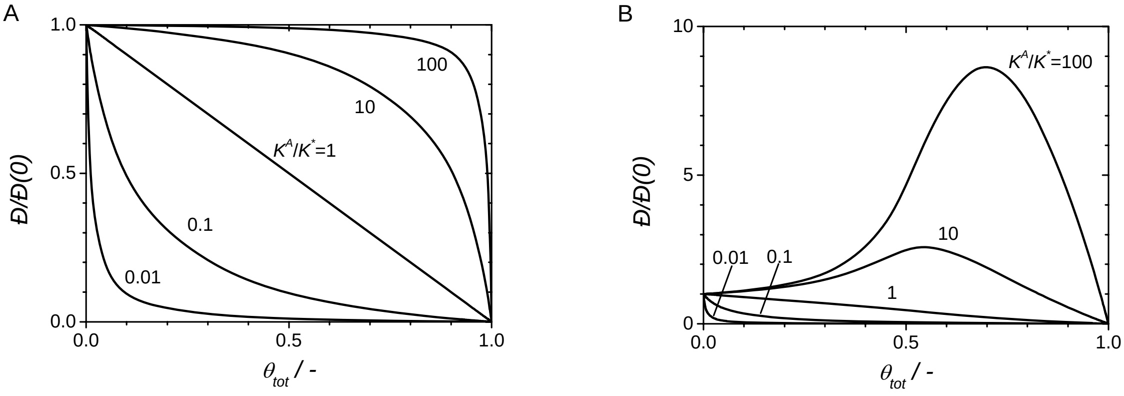

Figure 2. Influence of the relevant site parameter (K^*) on the normalized diffusivity for the case that the adsorption isotherm is described by a single-site Langmuir isotherm (A) and by a dual-site Langmuir isotherm (B) with $K_i^A = 100K_i^B$ and $q_i^{sat,A} = q_i^{sat,B}$.

When the relevant site occupancy equals the total occupancy (*i.e.* the case that $K^* = K^A$), the diffusivity follows the 'strong confinement' scenario ($\text{Đ}_i = \text{Đ}_i^*(0)\left(1-\theta_i\right)$). When the relevant site occupancy is higher than the total occupancy (*i.e.* in the case that $K^* > K^A$), for both systems the diffusivity is always lower than the strong confinement scenario. When the occupancy of the relevant site is lower than the total occupancy the diffusivity is found to be (much) higher than in the strong confinement scenario. The predicted normalized diffusivities for the single-site Langmuir system are restricted to a maximum value of one. For weak adsorption at the RS the diffusivity may stay fairly constant over a wide occupancy range. The normalized diffusivities in case two (dual-site Langmuir) can be much higher than one, a consequence of the dual-site adsorption isotherm. Note that the top curve in Figure 2B represents the situation where $K^* = K^B$.

The normalized diffusivity profile for $K^* < K^A$ is commonly observed for light gases in small-pore zeolites. From the RS perspective this can be understood as follows (*cf.* Equation (45)):

- starting from low loading an increase in diffusivity is observed because the fraction of mobile molecules increases, $\text{Đ} \propto \left(\theta_i^*/\theta_i\right)$
- in the limit of saturation the zeolite becomes completely occupied and diffusivity drops to a very low value, $\text{Đ} \propto \left(1-\theta\right)$
- for intermediate loading a maximum is found.

2.2.6 Application of the RSM to multi-component systems

In order to apply the RSM in mixture systems through Equation (15) or (21) a prediction of the mixture loadings at the RS are required. If the saturation loadings are equal an extended Langmuir isotherm applies:

$$\theta_i^* = \frac{K_i^* f_i^*}{1 + \sum_{i=1}^{n} K_i^* f_i}, \quad i = 1, 2, \ldots n. \tag{46}$$

If the saturation loadings are not equal the IAST is a more appropriate choice (*cf.* Section 2.1.3). Note that competitive adsorption effects are considered specifically at the RS, which can be very different compared to competitive adsorption effects at the total loading level. All other relations to make a mixture prediction based on known (estimated) single component RS diffusivities and adsorption constants are given in the previous sections.

In the case of equal RS saturation loadings a simple analytical solution of the RS transport diffusivity can be obtained. If the saturation loadings are equal consequently $Đ_{12}^* = Đ_{21}^*$ because the Onsager matrix needs to be symmetrical. This equal saturation loading assumption will be valid when molecules are very confined at the RS and only one molecule fits at the RS. For DDR this appears to be the case [39][Chapter 5C]. Subsequently, a description of the MS diffusivities based on the total loading in a binary mixture in terms of the total and RS occupancies and RS diffusivities can be derived. First note that the total loading analogues of matrix $\boldsymbol{B}^*$ and $\boldsymbol{\Delta}^*$ (matrix $\boldsymbol{B}$ and $\boldsymbol{\Delta}$) are simply Equations (17) and (33) without the asterisks and are related via: $\left[B\right]^{-1} = \left[\Delta\right]$. The diffusivity based on the total loading can be calculated from matrix $\boldsymbol{\Delta}$ via matrix $\boldsymbol{B}$. Matrix $\boldsymbol{\Delta}$ is found by substituting Equation (33) into Equation (34).

$$Đ_1 = q^{sat,*} Đ_1^* \frac{\theta_1^*}{q_1} \left(\frac{1}{1 + \theta_2^* \dfrac{Đ_1^*}{Đ_{12}^*} \left(1 - \dfrac{\theta_1^*}{\theta_2^*} \dfrac{\theta_2}{\theta_1} \right)} \right) \tag{47}$$

$$Đ_2 = q^{sat,*} Đ_2^* \frac{\theta_2^*}{q_2} \left(\frac{1}{1 + \theta_1^* \dfrac{Đ_2^*}{Đ_{12}^*} \left(1 - \dfrac{\theta_2^*}{\theta_1^*} \dfrac{\theta_1}{\theta_2} \right)} \right) \tag{48}$$

Note that also in this case the RS diffusivities are a function of the free space relevant for diffusion (Equation (18)).

2.3 Free space relevant for diffusion

In general self- and transport diffusivities appear to decrease to very low values when the loading approaches saturation. This led to the hypothesis that the diffusivity should be corrected for the free space that is available for diffusion. This can be accounted for in modelling by of the strong confinement scenario (Equation (19)) where the diffusivity decreases proportionally with total loading. Now a distinction is made between the free space that plays a role in the diffusion process and the total free space available for adsorption as determined from the isotherm. Hence, the central question is whether the total free space is the proper parameter to be used in the description for mass transport.

Adsorption isotherms can often be described well by multi-site Langmuir (MSL) isotherms. In some cases these different sites can be reconciled with distinct locations in the zeolite. A well-known example of this is siting of alkanes, for instance butane and hexane, in zeolite MFI. Steps or inflections in the isotherms can be ascribed to the difference in channel and intersection locations [30,35,36]. In the case of cage-like zeolites the isotherms can be described well by three-site Langmuir isotherms (see *e.g.* [12]), but the physical meaning of the extracted adsorption parameters of *all three* sites is not fully understood yet. A distinction between molecules residing in the cage or window of the cage has been made [37], but no other sites can be distinguished clearly. It could be that several sites exist inside the cage, or that the inflections in the isotherm are induced by intermolecular repulsion effects. An alternative reason for an inflection can be that molecules re-arrange inside the zeolite with increasing occupancy, *e.g.* as for the commensurate freezing of n-hexane in silicalite-1 [35,42] and N_2 and Ar adsorption in the same zeolite at 77 K [43,44]. In the case of Ar in silicalite-1 it has recently been shown that a step in the isotherm that was believed to be caused by a liquid to solid phase transition is actually a consequence of the flexibility of the zeolite [45].

Consider now a micro-porous system in which the adsorption is described by a three-site Langmuir isotherm (site A, B and C). Three possible configurations are depicted in Figure 3 to which this isotherm can correspond:

1. All three sites are located in series ABCABC
2. Two sites form a direct pathway for diffusion (A and B), site C is an adjacent site: a side-pocket, but no direct transport from site C to another site C is possible
3. An example of a re-arrangement in a cage-like zeolite, other examples of rearrangements can be easily thought of. Firstly, molecules move from site C to a group of sites A, which represents a cage. At a certain point, when the loading is increased, a rearrangement occurs where now a situation of six instead of five available sites is found. The ‘site B’ in the isotherm represents this rearrangement.

What free space is relevant for mass transport for each situation? It seems obvious that in case 1 all sites are part of the ‘active pathway’ for mass transport and the total saturation loading is expected to provide an appropriate measure for the available free space for mass transport. In situation 2 site C should not affect the diffusivity since it is merely a side-pocket. In this case it can be argued that the occupancy relevant for mass transport should be based on the sites A and B only. The third case is somewhat more complex. Considering the left pictorial of the third case leads to the conclusion that this system will be completely saturated when sites A and C are occupied. However, above a certain pressure an extra molecule can be squeezed in due to a rearrangement. The question is, if in the case when the system is still in its A-configuration (maximum 5 sites per cavity), the saturation capacity of the cage should be accounted for as the capacity at infinite pressure (B-configuration, maximum 6 molecules per cavity). It is now proposed that the total cage capacity of six sites should not be used to calculate the available free space. The cage will firstly fill up to 5 molecules in its A-configuration. In this situation the system behaves according to this: *i.e.* the maximum occupancy is 5/5, when 5 molecules are present and no free space is available. If subsequently an extra molecule is squeezed in, the system is pushed into its B-configuration. In this situation the occupancy is 6/6, which is the same level of occupancy as a saturated A-configuration system. To conclude, in case 3 the ‘site’ that represents the rearrangement should not be accounted for when calculating the available free space relevant for mass transport.

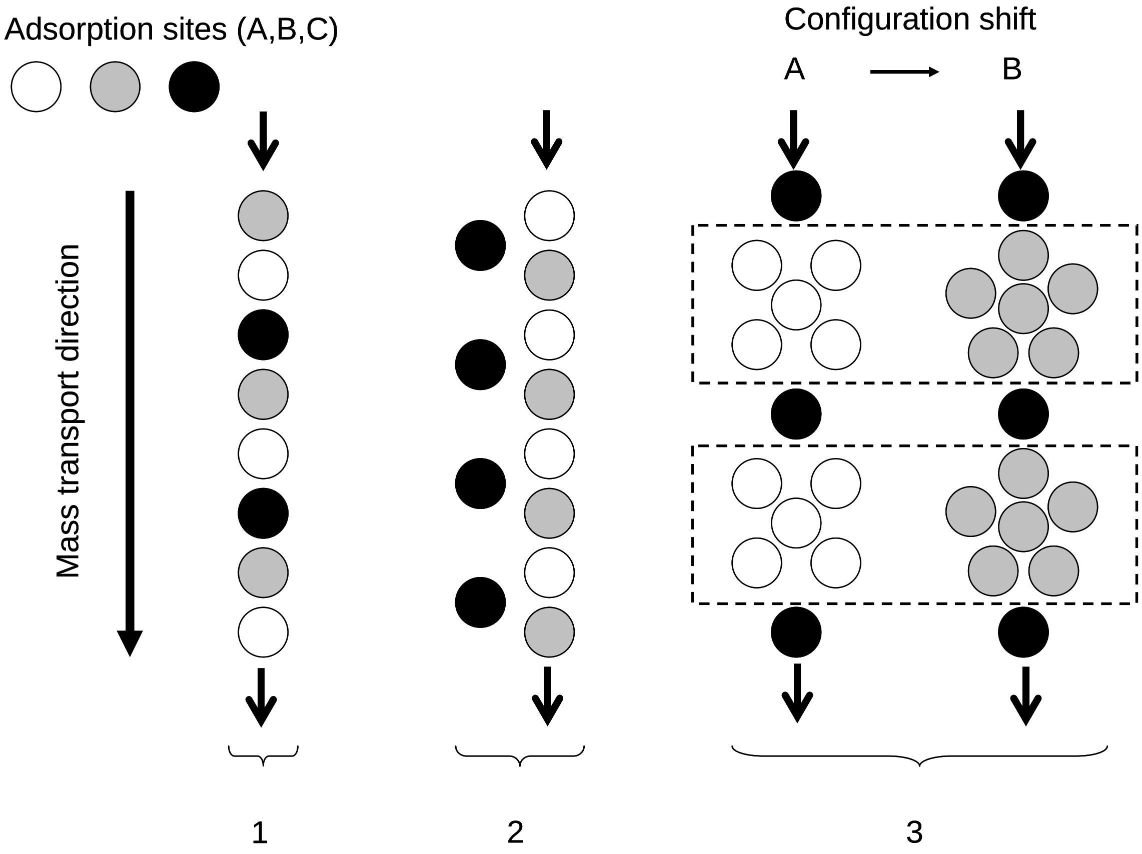

Figure 3. Schematic of possible arrangements of adsorption sites in a structured micro-porous material.

In Figure 3, case 3, as the rearrangement is very local the shift from situation A to B occurs gradually: cage per cage. However, other configurations can be thought of in which the rearrangement cannot occur at a local level, but requires a complete system rearrangement (Figure 4). This hypothetical system is built up from sites A and B which are slightly overlapping which make simultaneous occupation of both sites impossible. At lower pressures site A is preferred and filled up completely to saturation, although the saturation capacity of B is higher. Above a certain pressure the system will rearrange to its B-configuration allowing a higher uptake.

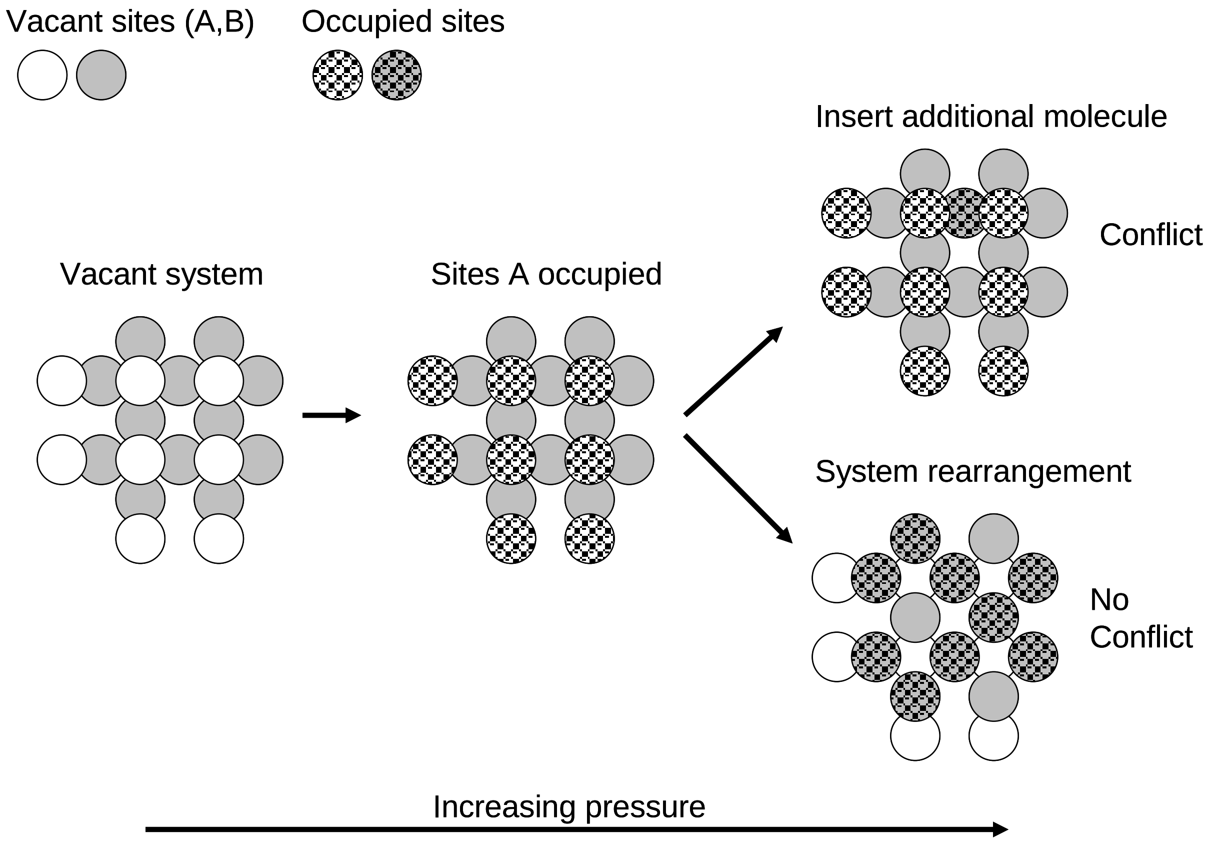

Figure 4. Schematic representation of an arrangement of adsorption sites A and B that can lead to a total system rearrangement.

The consequence of this consideration is that in some cases certain contributions or steps in the isotherms do not represent space relevant for mass transport and should be neglected. The effect of this is now illustrated for a system that is described by a three-site Langmuir isotherm. The vacant space should be the space relevant for mass transport, as denoted by ($^{\#}$):

$$Đ_i^* = Đ_i^*(0)\left(1-\theta^{\#}\right). \tag{49}$$

Four different cases are distinguished in Figure 5, in each case the free space relevant for mass transport is based on a different part of the adsorption isotherm; details are given in

Table 1. If the free space can be described accurately by the complete isotherm a type I dependency is found, which described the classical strong confinement scenario. In the case that one of the three “adsorption sites” does not represent free space for diffusion, *e.g.* a rearrangement or a side-pocket, one of type II-IV curves can arise. Depending on whether the first, second or third site (of decreasing adsorption strength) should be omitted regarding the actual free space for diffusion calculation, type II, III or IV curves are found, respectively. In all three cases a plateau in diffusivity is found in the occupancy region where the site is filled up that does not contribute to the free space for diffusion. With increasing difference of adsorption constants, *i.e.* the adsorption steps become increasingly separated in the isotherm, the transitions in the diffusivity curves become more pronounced.

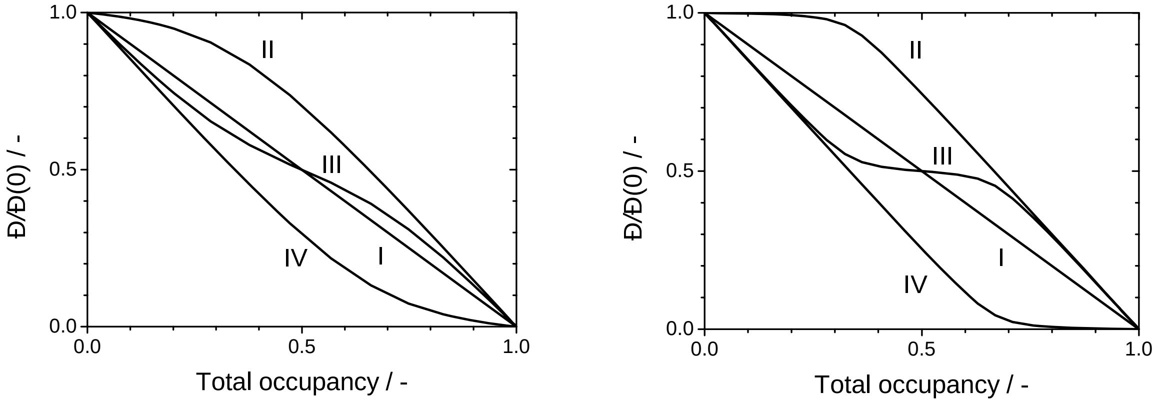

Figure 5. The influence of the amount of free space relevant for mass transport on the normalized diffusivities as a function of the total occupancy. The data is described with a three-site Langmuir isotherm. $q^{sat,A} = q^{sat,B} = q^{sat,C}$. Left figure: $K^A = 10\ K^B = 100\ K^C$. Right figure: $K^A = 100\ K^B = 10\ 000\ K^C$. More details on the definition of the four cases is presented in Table 1.

Table 1. Four cases depicted in Figure 5 when the occupancies of the available space for diffusion is based on different sites in the adsorption isotherm.

	$\theta_i^\#$	Physical meaning	Relation to Figure 3
I	$\theta_i^\# = \dfrac{q_i^A + q_i^B + q_i^C}{q_i^{sat,A} + q_i^{sat,B} + q_i^{sat,C}} = \theta_i$	All sites are relevant for diffusion.	Case 1
II	$\theta_i^\# = \dfrac{q_i^B + q_i^C}{q_i^{sat,B} + q_i^{sat,C}}$	Site A can be a side-pocket, for example.	Case 2
III	$\theta_i^\# = \dfrac{q_i^A + q_i^C}{q_i^{sat,A} + q_i^{sat,C}}$	Site B can be a side-pocket, or represent a rearrangement.	Case 2 or 3
IV	$\theta_i^\# = \dfrac{q_i^A + q_i^B}{q_i^{sat,A} + q_i^{sat,B}}$	Site C can be a side-pocket, or represent a rearrangement.	Case 2 or 3

To account for the suggested phenomenon it is proposed to disregard the part of the isotherm that represents free space irrelevant for diffusion. For a single component system the free space relevant for diffusion can be expressed as:

$$1-\theta^{\#}=1-\frac{\sum_{k=A}\left(\frac{q^{sat,k}K^{k}f}{1+K^{k}f}\right)-\frac{q^{sat,ID}K^{ID}f}{1+K^{ID}f}}{\sum_{k=A}\left(q^{sat,k}\right)-q^{sat,ID}}. \tag{50}$$

Where the multi-site Langmuir isotherm consist of sites A, B,… The additional loading associated with the space irrelevant for diffusion (ID) is described by a single-site Langmuir isotherm with a certain saturation loading ($q^{sat,ID}$) and adsorption equilibrium constant (K^{ID}). Note that in the case that $\theta^{\#}$ equals θ, *i.e.* the total free space in the zeolite is relevant for diffusion, the classical strong confinement scenario is found (Equation (19)).

3 Conclusions

A new model has been introduced to describe the loading dependency of diffusion in zeolites, as an alternative to the Reed-Ehrlich approach. The model is formulated around the idea of segregated adsorption in cage-like zeolites, *i.e.* molecules are located either in the cage or in the window site region and that only the molecules located at the window site are considered to be able to make a successful jump to another cage. This so-called Relevant Site Model (RSM) is based on the Maxwell-Stefan framework for mass transport but includes one extra fitting parameter that describes the adsorption properties of the ‘relevant site’. Key feature of the RSM as applied to mixtures is that exchange effects (‘friction’ between molecules) and competitive adsorption effects are related to the RS occupancy and not to the total occupancy.
Analysis of the meaning of the free space relevant for diffusion yielded a concept to account for possible rearrangements or free space not relevant for diffusion within the RSM.
The next chapters focus on demonstrating the feasibility and advantages of this model.

References

[1] M. O. Coppens, F. J. Keil, and R. Krishna, *Reviews in Chemical Engineering*, 16, **2000**, 71.

[2] J. Caro and M. Noack, *Microporous and Mesoporous Materials*, 115, **2008**, 215.

[3] J. van den Bergh, W. Zhu, J. Gascon, J. A. Moulijn, and F. Kapteijn, *Journal of Membrane Science*, 316, **2008**, 35.

[4] J. van den Bergh, W. Zhu, F. Kapteijn, J. A. Moulijn, K. Yajima, K. Nakayama, T. Tomita, and S. Yoshida, *Research on Chemical Intermediates*, 34, **2008**, 467.

[5] J. van den Bergh, W. Zhu, J. C. Groen, F. Kapteijn, J. A. Moulijn, K. Yajima, K. Nakayama, T. Tomita, and S. Yoshida, *Studies in Surface Science and Catalysis*, 170 A, **2007**, 1021.

[6] S. Himeno, T. Tomita, K. Suzuki, K. Nakayama, K. Yajima, and S. Yoshida, *Industrial & Engineering Chemistry Research*, 46, **2007**, 6989.

[7] T. Tomita, K. Nakayama, and H. Sakai, *Microporous and Mesoporous Materials*, 68, **2004**, 71.

[8] Y. Cui, H. Kita, and K. Okamoto, *Journal of Materials Chemistry*, 14, **2004**, 924.

[9] S. G. Li, J. G. Martinek, J. L. Falconer, R. D. Noble, and T. Q. Gardner, *Industrial & Engineering Chemistry Research*, 44, **2005**, 3220.

[10] S. G. Li, J. L. Falconer, and R. D. Noble, *Abstracts of Papers of the American Chemical Society*, 227, **2004**, 350.

[11] L. M. Robeson, *Journal of Membrane Science*, 320, **2008**, 390.

[12] R. Krishna and J. M. van Baten, *Microporous and Mesoporous Materials*, 109, **2008**, 91.

[13] E. Beerdsen, D. Dubbeldam, and B. Smit, *Journal of Physical Chemistry B*, 110, **2006**, 22754.

[14] A. I. Skoulidas and D. S. Sholl, *Journal of Physical Chemistry A*, 107, **2003**, 10132.

[15] R. Krishna, D. Paschek, and R. Baur, *Microporous and Mesoporous Materials*, 76, **2004**, 233.

[16] S. Li, J. L. Falconer, R. D. Noble, and R. Krishna, *Journal of Physical Chemistry C*, 111, **2007**, 5075.

[17] S. Li, J. L. Falconer, R. D. Noble, and R. Krishna, *Industrial & Engineering Chemistry Research*, 46, **2006**, 3904.

[18] R. Krishna, J. M. van Baten, E. Garcia-Perez, and S. Calero, *Chemical Physics Letters*, 429, **2006**, 219.

[19] R. Krishna and J. M. van Baten, *Chemical Physics Letters*, 446, **2007**, 344.

[20] A. L. Myers and J. M. Prausnitz, *AIChE Journal*, 11, **1965**, 121.

[21] M. Murthi and R. Q. Snurr, *Langmuir*, 20, **2004**, 2489.

[22] R. Krishna, S. Li, J. M. van Baten, J. L. Falconer, and R. D. Noble, *Separation and Purification Technology*, 60, **2008**, 230.

[23] M. O. Coppens and V. Iyengar, *Nanotechnology*, 16, **2005**, 442.

[24] R. Krishna and J. M. van Baten, *Chemical Engineering Science*, 63, **2008**, 3120.

[25] F. Kapteijn, J. A. Moulijn, and R. Krishna, *Chemical Engineering Science*, 55, **2000**, 2923.

[26] R. Krishna and J. A. Wesselingh, *Chemical Engineering Science*, 52, **1997**, 861.

[27] F. Kapteijn, W. Zhu, J. A. Moulijn, and T. Q. Gardner, Zeolite Membranes: Modeling and Application, in: Structured Catalysts and Reactors, Cybulski, A. and Moulijn, J. A. (Eds), Ch. 20, **2005**, Taylor & Francis Group, Boca Raton, FL, 701.

[28] D. Paschek and R. Krishna, *Chemical Physics Letters*, 333, **2001**, 278.

[29] A. I. Skoulidas, D. S. Sholl, and R. Krishna, *Langmuir*, 19, **2003**, 7977.

[30] R. Krishna, B. Smit, and T. J. H. Vlugt, *The Journal of Physical Chemistry A*, 102, **1998**, 7727.

[31] R. Krishna and J. M. van Baten, *Chemical Engineering Science*, 64, **2009**, 3159.

[32] R. Krishna and J. M. van Baten, *Chemical Engineering Science*, 64, **2009**, 870.

[33] D. A. Reed and G. Ehrlich, *Surface Science*, 102, **1981**, 588.

[34] R. Krishna, J. M. van Baten, E. Garcia-Perez, and S. Calero, *Industrial & Engineering Chemistry Research*, 46, **2007**, 2974.

[35] T. J. H. Vlugt, R. Krishna, and B. Smit, *Journal of Physical Chemistry B*, 103, **1999**, 1102.

[36] T. J. H. Vlugt, W. Zhu, F. Kapteijn, J. A. Moulijn, B. Smit, and R. Krishna, *Journal of the American Chemical Society*, 120, **1998**, 5599.

[37] R. Krishna and J. M. van Baten, *Separation and Purification Technology*, 61, **2008**, 414.

[38] J. van den Bergh, S. Ban, T. J. H. Vlugt, and F. Kapteijn, *Journal of Physical Chemistry C*, 113, **2009**, 17840.

[39] J. van den Bergh, S. Ban, T. J. H. Vlugt, and F. Kapteijn, *Journal of Physical Chemistry C*, 113, **2009**, 21856.

[40] S. Kjelstrup and D.Bedeaux, Non-equilibrium thermodynamics of heterogeneous systems, **2008**, World Scientific Publishing Co., Singapore.

[41] D. Dubbeldam and R. Q. Snurr, *Molecular Simulation*, 33, **2007**, 305.

[42] B. Smit and T. L. M. Maesen, *Nature*, 374, **1995**, 42.

[43] P. L. Llewellyn, J. P. Coulomb, Y. Grillet, J. Patarin, H. Lauter, H. Reichert, and J. Rouquerol, *Langmuir*, 9, **1993**, 1846.

[44] P. L. Llewellyn, J. P. Coulomb, Y. Grillet, J. Patarin, G. Andre, and J. Rouquerol, *Langmuir*, 9, **1993**, 1852.

[45] E. Garcia-Perez, J. B. Parra, C. O. Ania, D. Dubbeldam, T. J. H. Vlugt, J. M. Castillo, P. J. Merkling, and S. Calero, *The Journal of Physical Chemistry C*, 112, **2008**, 9976.

5B

The Relevant Site Model: Single components in DDR

The relevant site model (RSM) is applied to diffusivity data of N_2 and CO_2 in the 8-ring cage-type zeolite DDR. The RSM describes diffusivity data of N_2 and CO_2 in DDR very well up to saturation. The observed diffusivity loading dependency is explained from the relative low window site occupancy that is typically much lower than the total occupancy at lower loadings. The model is successfully extended to non-isothermal diffusivity data of CO_2 and N_2. Relating intermolecular correlation effects to the relevant site occupancy instead of the total occupancy leads to a quantitative prediction of the observed correlation effects and, consequently, the self diffusivity. Analysis of the N_2 data suggests positional rearrangements in the DDR cages in a certain loading range. These effects have been incorporated in the model successfully.

This chapter is based on the following publication:

J. van den Bergh, S. Ban, T. J. H. Vlugt, and F. Kapteijn, *Journal of Physical Chemistry C*, 113, **2009**, 17840.

1. Introduction

In Chapter 5A the motivation for and a detailed derivation of the Relevant Site Model (RSM) is given. The aim of the current chapter is to illustrate the application of the RSM by an analysis of single component diffusivity data of N_2 and CO_2 in DDR, as generated by Molecular Dynamics (MD). Thermodynamic properties such as adsorption isotherms are computed using Monte Carlo simulations in the grand-canonical ensemble. Specific attention is paid to the concept of free space relevant for diffusion and the temperature dependency of the RS diffusivity and RS adsorption constant.

Next the key equations from Chapter 5A relevant for the current chapter are repeated. Note that all RS properties are denoted with an asterisks. The following relation has been derived to describe the Maxwell-Stefan (MS) diffusivity based on the total loading ($Đ_i$) in terms of the RS lumped diffusivity ($q_i^{sat*} Đ_i^*(0)$), RS adsorption equilibrium constant (K_i^*), RS occupancy (θ^*), free space relevant for diffusion ($1-\theta^{\#}$), fugacity (f_i) and total loading (q_i):

$$Đ_i = q_i^{sat*} Đ_i^*(0) \frac{\left(1-\theta^{\#}\right)}{q_i} \theta^*, \qquad \theta^* = \frac{K_i^* f_i}{1+K_i^* f_i}. \tag{1}$$

Moreover, in case that the RS self exchange diffusivity equals the MS diffusivity, the RS self diffusivity ($D_{self,i}^*$) is related to the RS MS diffusivity according to:

$$D_{self,i}^* = \frac{Đ_i^*}{1+\theta_i^*}. \tag{2}$$

The self diffusivity based on the total loading and the RS self diffusivity are related through:

$$D_{Self,i} = D_{Self,i}^* \frac{q_i^*}{q_i}. \tag{3}$$

2. Experimental

To compute adsorption isotherms of CO_2 and N_2 Monte Carlo (MC) simulations in the grand-canonical (GC) ensemble (μVT) were used [1-3]. In these simulations, a fixed chemical potential (or fugacity) of the sorbent is imposed, resulting in a certain average number of sorbate molecules adsorbed in the zeolite. The zeolite is modelled as a rigid structure [4] with atomic positions taken from the Atlas of Zeolite Structures [5]. We only consider all-silica frameworks, *i.e.* no non-framework atoms or ions are present. The sorbate-zeolite and sorbate-sorbate interactions are modelled by the sum of Lennard-Jones (LJ) and Coulombic interactions. LJ interactions were truncated and shifted at 12 Å and Coulombic interactions were handled using the Ewald summation with a relative precision of 10^{-5}. CO_2 and N_2 are modelled as rigid molecules, the C-O and N-N bond lengths are 1.16 en 1.098 Å, respectively. For DDR-type zeolite, the inaccessible cages are artificially blocked using the procedure outlined by Jakobtorweihen *et al.* [6]. For more information on the force field and simulation details, we refer to [7].

The self- and Maxwell-Stefan diffusion coefficients are computed from equilibrium Molecular Dynamics (MD) simulations in the NVE ensemble using the same force field as for the adsorption calculations. Again, the zeolite is considered as a rigid structure. A time step of 0.001 ps was used to integrate the equations of motion. The starting positions of the sorbate molecules are taken from well-equilibrated MC simulations. Diffusivities are calculated from the mean-square displacements of either the particles or the centre of mass of a certain component, computed using the order-n algorithm of [8]. We refer the reader to [9-11] for details on how to extract diffusivities from equilibrium MD simulations. Simulations of typically 20 ns are needed to compute these diffusivities.

3. Results and Discussion

3.1 Isothermal N_2 and CO_2 data

To validate the RSM MD diffusivity data of N_2 and CO_2 on all silica DDR at 300, 373, 473 and 573 K are considered. In addition GCMC simulations were carried out to determine the adsorption isotherms up to saturation (Figure 1). The simulated adsorption isotherm data have been fitted with a three-site Langmuir isotherm. Additionally, the simulated N_2 data have also been fitted with a four-site Langmuir isotherm, which will become useful in a later stage. The estimated adsorption parameters are presented in Table 1. A comparison of the simulated and experimentally available adsorption isotherms [12][Chapter 2] shows that in general good agreement is found. The simulated CO_2 loading is somewhat higher at higher pressure and the N_2 data appear to be slightly shifted along the pressure axis.

Figure 2 shows the MS diffusivities of N_2 and CO_2 at various temperatures as a function of the loading on DDR. The N_2 data clearly represent a maximum in diffusivity as a function of loading on the zeolite. For CO_2 a slight maximum appears at 573 K. The lines in Figure 2 represent the model fit results of the RSM (Equation (1)) using a non-linear least squares method. Diffusivity data are fit for each individual temperature yielding a relevant site adsorption constant (K_i^*) and a lumped diffusivity parameter ($q_i^{sat*} Đ_i^*(0)$) for each temperature, which are listed in Table 2. The diffusivities of both components are described well by the RSM approach. The CO_2 data are described accurately; for N_2 the trend is well captured but the match is modest.

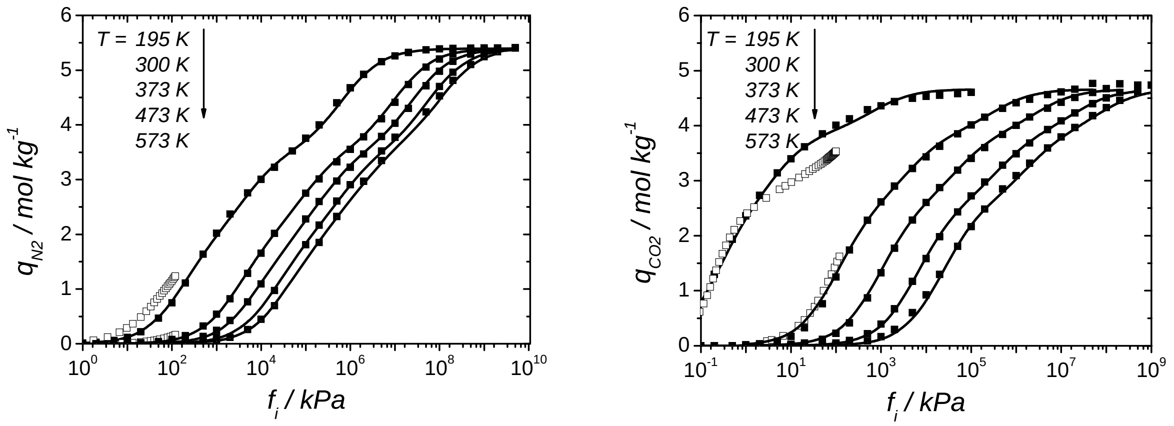

Figure 1. Adsorption isotherms of N_2 and CO_2 on DDR at 195, 300, 373, 473 and 573 K. Closed symbols represent GCMC simulated data, lines represent model fit results with a three-site Langmuir model and the open symbols represent experimental adsorption data on DD3R at 195 and 298 K respectively [12].

Table 1. Resulting parameters and their 95% confidence interval of a model fit with a three- and four-site Langmuir isotherm to the simulated CO_2 and N_2 adsorption data on DDR.

	Unit	CO_2		N_2 (I)		N_2 (II)	
$q^{sat,tot}$	mol kg^{-1}	4.66		5.39		5.40	
$q^{sat,A}$	mol kg^{-1}	2.63	± 0.08	2.01	± 0.08	0.85	± 0.29
K_0^A	kPa^{-1}	$1.18 \cdot 10^{-7}$	$\pm 0.15 \cdot 10^{-7}$	$1.52 \cdot 10^{-6}$	$\pm 0.17 \cdot 10^{-6}$	$5.03 \cdot 10^{-6}$	$\pm 2.46 \cdot 10^{-6}$
ΔH_{Ads}^A	kJ mol^{-1} K^{-1}	-28.1	± 0.27	-13.4	± 0.21	-12.4	± 0.66
$q^{sat,B}$	mol kg^{-1}	1.27	± 0.08	1.54	± 0.06	1.61	± 0.29
K_0^B	kPa^{-1}	$7.33 \cdot 10^{-10}$	$\pm 2.25 \cdot 10^{-10}$	$4.40 \cdot 10^{-8}$	$\pm 0.75 \cdot 10^{-8}$	$3.86 \cdot 10^{-7}$	$\pm 1.08 \cdot 10^{-7}$
ΔH_{Ads}^B	kJ mol^{-1} K^{-1}	-31.4	± 0.54	-13.7	± 0.26	-14.2	± 0.38
$q^{sat,C}$	mol kg^{-1}	0.76	± 0.07	1.84	± 0.04	1.20	[a]
K_0^C	kPa^{-1}	$3.09 \cdot 10^{-11}$	$\pm 1.21 \cdot 10^{-11}$	$7.76 \cdot 10^{-10}$	$\pm 0.72 \cdot 10^{-10}$	$2.68 \cdot 10^{-8}$	$\pm 0.51 \cdot 10^{-8}$
ΔH_{Ads}^C	kJ mol^{-1} K^{-1}	-28.7	± 0.84	-12.2	± 0.20	-13.2	± 0.30
$q^{sat,D}$	mol kg^{-1}					1.74	± 0.04
K_0^D	kPa^{-1}					$6.94 \cdot 10^{-10}$	$\pm 0.60 \cdot 10^{-10}$
ΔH_{Ads}^D	kJ mol^{-1} K^{-1}					-12.2	± 0.18

[a] Fixed value

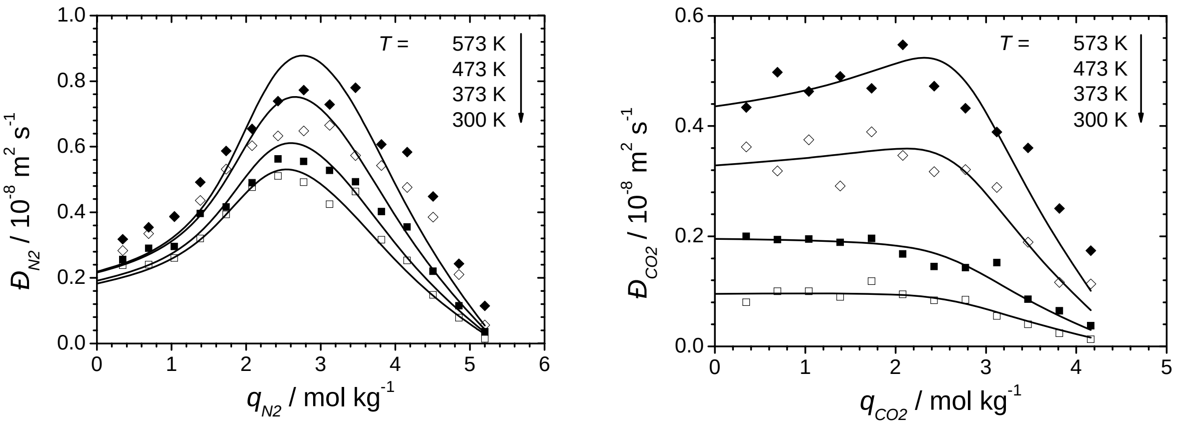

Figure 2. Maxwell-Stefan diffusivities of N_2 (left) and CO_2 (right) on DDR at 300, 373, 473 and 573 K. Lines represent model fit results with the RSM (Equation (1)).

Table 2. Resulting parameters of a model fit of the RSM to MD diffusivity data of N_2 and CO_2 in DDR.

Comp.	T	K^*	K_0^*	ΔH^*_{Ads}	$q^{sat*}Đ(0)^*$	$q^{sat*}Đ(0)^*_0$	E_A^*	$q^{sat,tot}$
	K	kPa^{-1}	10^{-8} kPa^{-1}	kJ mol^{-1} K^{-1}	10^{-8} mol kg^{-1} m^2 s^{-1}	mol kg^{-1} m^2 s^{-1}	kJ mol^{-1} K^{-1}	mol kg^{-1}
CO_2	300	$(3.77 \pm 0.93)\cdot 10^{-3}$	3.67	-28.6	0.63 ± 0.10	$25.7\cdot 10^{-8}$	9.37	4.66
	373	$(4.62 \pm 0.91)\cdot 10^{-4}$			1.16 ± 0.15			4.66
	473	$(5.18 \pm 1.1)\cdot 10^{-5}$			2.55 ± 0.35			4.66
	573	$(1.28 \pm 0.30)\cdot 10^{-5}$			3.91 ± 0.61			4.66
N_2	300	$(3.10 \pm 0.51)\cdot 10^{-5}$	5.75	-15.7	3.94 ± 0.33	$14.9\cdot 10^{-8}$	3.59	5.4
	373	$(9.46 \pm 2.13)\cdot 10^{-6}$			4.74 ± 0.55			5.4
	473	$(3.34 \pm 1.14)\cdot 10^{-6}$			6.07 ± 1.02			5.4
	573	$(1.49 \pm 0.51)\cdot 10^{-6}$			7.60 ± 1.30			5.4
N_2[a]	300	$(3.67 \pm 0.53)\cdot 10^{-5}$	8.95	-15.0	3.81 ± 0.27	$13.0\cdot 10^{-8}$	3.16	4.2
	373	$(1.14 \pm 0.11)\cdot 10^{-5}$			4.54 ± 0.20			4.2
	473	$(4.13 \pm 0.80)\cdot 10^{-6}$			5.76 ± 0.54			4.2
	573	$(2.07 \pm 0.44)\cdot 10^{-6}$			6.94 ± 0.75			4.2

[a] Accounted for free space available for diffusion

Our simulated adsorption and diffusivity data at 300 K and of Krishna and van Baten [13] are the same, as is expected since the used methods and force fields are identical.

Figure 3 shows the back-calculated lumped relevant site diffusivity ($q_i^{sat*}\text{Đ}_i^*$) as a function of the total loading for N_2 and CO_2. The data are all normalized with respect to the value at zero loading ($q_i^{sat*}\text{Đ}_i^*(0)$, Table 2). The relevant site diffusivity of CO_2 decreases linearly with increasing loading. The relevant site diffusivity of N_2, however, shows a structural mismatch. Recalling the discussion on the free space relevant for mass transport it is evident that the shape of the N_2 data clearly fits the type III trend (Figure 5, Chapter 5A). Considering the cage-like DDR topology, the N_2 diffusivity could be explained by a rearrangement inside the cages, as has been observed for N_2 adsorption in silicalite-1 [37].

The next step is to account for this effect in the modelling. Based on Figure 3, the rearrangement is described by an adsorption process with a capacity of around 1.2 mol kg^{-1}, which starts to become apparent at a loading of ~2.5 mol kg^{-1}. An adsorption corresponding to this capacity cannot be identified from the fitted 3-site Langmuir isotherm (Table 1). Therefore, a four-site Langmuir isotherm was fitted to the data satisfying the existence of the 'rearrangement site'. The estimated parameters are given in Table 1. Now the N_2 diffusivity data are fitted with the RSM using the four-site Langmuir isotherm and accounting for the 'rearrangement' effect. The latter is done by calculating the occupancy only based on site A, B and D. Figure 4 clearly shows that taking into account the effective free volume for diffusion leads to a significant improvement in fitting the Maxwell-Stefan diffusivities of N_2.

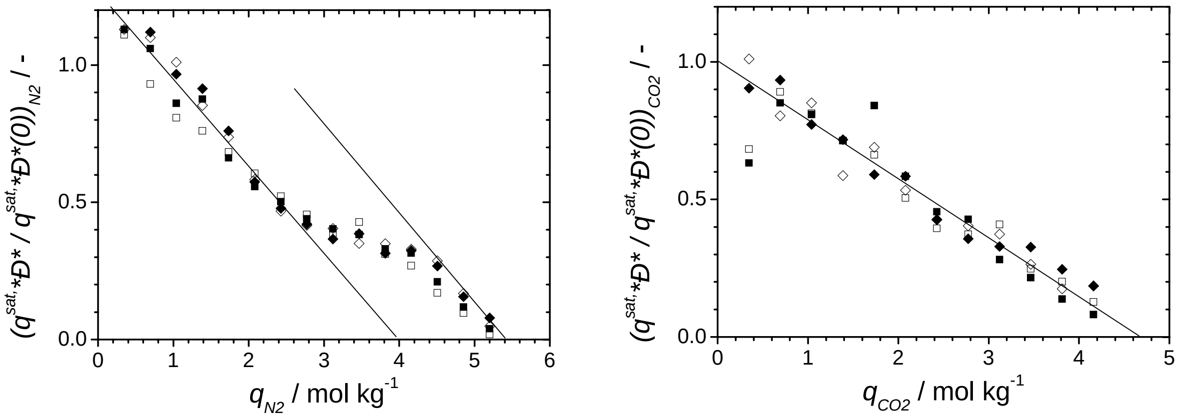

Figure 3. Normalized relevant site diffusivity of N_2 (left) and CO_2 (right) at 300 (□), 373 (■), 473 (◇) and 573 K (◆). Lines in the N_2 graphs are a guide to the eye, in the CO_2 figure the line represents the model fit results.

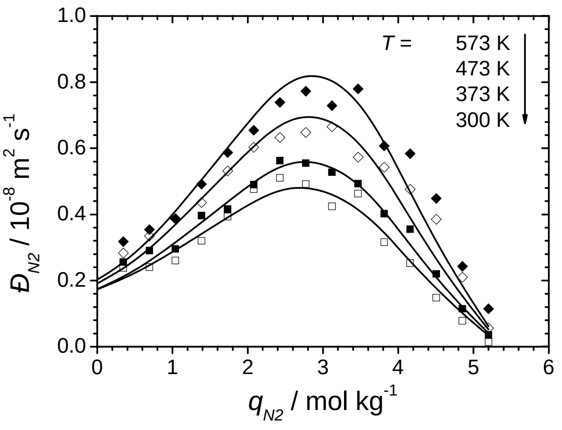

Figure 4. Maxwell-Stefan diffusivities of N_2 at 300, 373, 473 and 573 K. Lines represent model fit results with the RSM (Equation (1)) accounting for the effective free space available for diffusion.

3.2 Temperature dependency

The foregoing analysis was concerned with isothermal diffusivity data. Extending the temperature dependency of the RSM should be straightforward. The relevant site adsorption constant is assumed to follow a Van‘t Hoff- and the relevant site diffusivity parameter an Arrhenius temperature dependency. An Arrhenius plot of the relevant site adsorption constant (K^*) and the diffusivity parameter ($q_i^{sat*} Đ_i^*(0)$) is presented in Figure 5, the corresponding parameter values are listed in Table 2. In the case of N_2 the data including the vacancy correction are used. A consistent extension of the RSM to non-isothermal data is obtained for both components demonstrated by the very linear Arrhenius plots. The RS adsorption enthalpy of CO_2 and N_2 are very close to the adsorption enthalpies obtained from the adsorption isotherm data. The diffusivity of N_2 is only slightly activated compared to CO_2. Note that in the RSM a loading independent activation energy for diffusion is obtained.

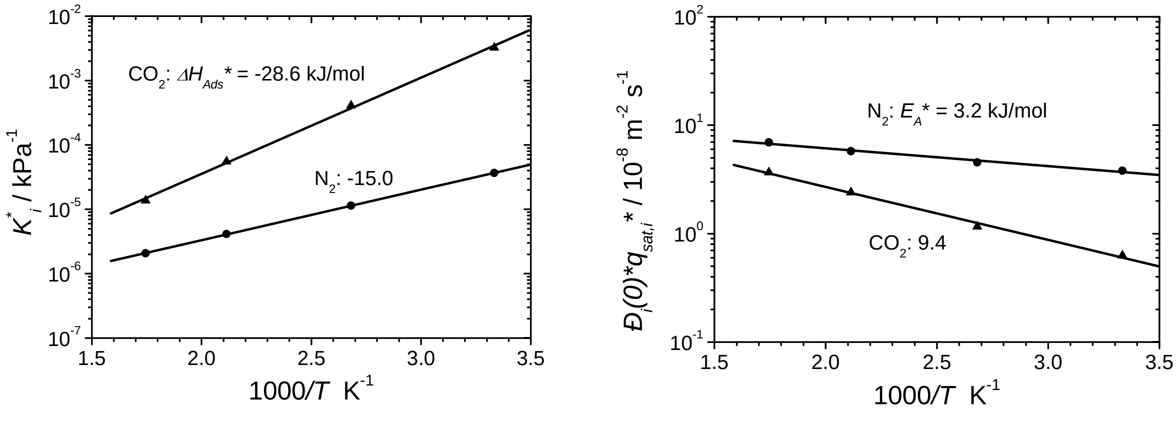

Figure 5. Arrhenius plots of the relevant site adsorption constant and lumped diffusivity parameter of N_2 and CO_2 on DDR.

3.3 Location of the relevant adsorption sites

When the relevant site is a physically meaningful property, is it then possible to locate this site in the adsorption isotherm? On forehand this will be difficult since the window and cage sites are not completely isolated regions [7]. The isotherms exhibit several inflection points. Although these isotherms are fitted by a three-site Langmuir isotherm it cannot be concluded that CO_2 and N_2 adsorb according to a three- or four-site adsorption model. Comparison of the values of the RS adsorption constants with those of the simulated isotherms does not lead to an exact match. But the values of the CO_2 and N_2 RS adsorption constants are close to those of the first and second site of their adsorption isotherms, respectively.

3.4 Self and transport diffusivity correlation

It has been proposed to relate the Maxwell-Stefan diffusivity and the self diffusivity through the relevant site (Chapter 5A). In this way the correlation effects, assumed responsible for the difference between the two diffusivities, are related to the relevant site and a prediction of the self diffusivity based on the MS diffusivity can be made. The self diffusivity is directly calculated from Equation (2) and (3), the Maxwell-Stefan diffusivity is calculated from Equation (1) using the estimated RS lumped diffusivity parameter and RS adsorption constant from Table 2. In the case of N_2 the effective free space for mass transport is used.

The predicted self diffusivities of N_2 and CO_2 are shown in Figure 6 together with the self diffusivities as simulated by MD. When Figure 2 and Figure 6 are compared it is clear that the self diffusivity values differ significantly from the MS diffusivities: the maximum in the N_2 data is shifted from ~2.8 (MS) to ~2.2 mol kg^{-1} (self) and the MS diffusivities are significantly higher; also in the case of CO_2 the MS diffusivities are significantly higher and the maximum that is observed for the MS diffusivity data does not appear in the self diffusivity data. In spite of these clear differences, an accurate prediction of the self diffusivities can be made by the RSM at all studied temperatures. The fact that a good prediction is made indicates that the correlation effects are well captured in this way.

It has been observed by Krishna and van Baten [13] that correlation effects in cage-like topologies (*e.g.* DDR, CHA and LTA) are very small for molecules that are relatively large compared to the window diameter. This conclusion is based on the observation that the ratio of the self exchange coefficient and MS diffusivity, based on the total occupancy, is large. N_2 in DDR is an example of such a case. A physical explanation of the absence of correlation effects in such confined systems is that molecules squeeze one by one through the windows and consequently have little chance of interacting in this case. However, in the RSM this is accounted for by the fact that these molecules have a window occupancy that is much lower than the total occupancy. Therefore, at the given occupancy the correlation effects are small, but, this is only the apparent behaviour since the cause of the observed low correlation effects is the very low window occupancy.

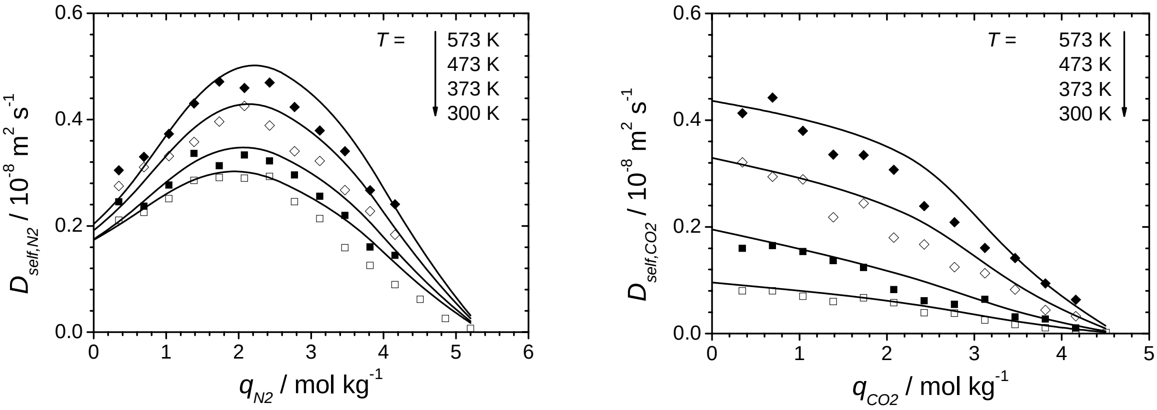

Figure 6. Self diffusivities of N_2 (left) and CO_2 (right) at 300, 373, 473 and 573 K. Lines represent model predictions (Equation (2) and (3)) including accounting for the effective occupancy in the case of N_2.

3.5 Literature results in perspective

Krishna and van Baten have investigated the diffusivity behaviour of various light gases in a broad range of zeolite topologies [13]. An important observation is that the strong loading dependency of the diffusivity, as discussed in the current paper, is strongly related to the 'degree of confinement' of a molecule in the zeolite. The maximum in the diffusivity as a function of the loading is only observed for strongly confined molecules, *i.e.* relative large molecules in small-pore zeolites. The loading dependency in CHA, DDR and LTA becomes stronger with increasing molecular diameter. Given the foundations of the RSM this can be understood as follows. With increasing molecular size the probability of finding this molecule in the window region is lower, which in essence means that the site becomes a weaker adsorption site. This causes a heterogeneous distribution of molecules throughout the zeolite (segregated adsorption). These effects are stronger when the molecule is more confined in the window. If then the window site determines the mass transport rate, an apparent loading dependency is found when the diffusivity is related to the total loading instead of the RS loading.

Krishna and van Baten observed that with increasing degree of confinement the apparent correlation effects are reduced and are almost absent in the case of very strong confinement. As already argued before, this can be explained from the relative low window site loading. Where significant correlation effects are expected at the given total occupancy, they are not from the perspective of the window site occupancy. Molecules with a relative low degree of confinement in DDR and CHA (He, Ne, H_2 and CO_2) are relatively homogeneously distributed, no strong loading effects are observed and the correlation effects are reasonably characterized by the total occupancy. CH_4 and Kr are strongly confined in DDR and CHA and show a very strong loading dependent diffusivity due to the very low window site loading, which is also responsible for the very small apparent correlation effects. In larger topologies all mentioned molecules are relative weakly confined and consequently the aforementioned phenomena are less prominent.

3.6 Comparison with Reed Ehrlich approach

To evaluate the RSM a comparison is made with respect to the Reed Ehrlich (RE) approach, currently the most successful approach to account for the observed loading dependency of diffusion. Both methods are capable of fitting the diffusivity profiles up to saturation with comparable results. The discussion on which approach requires the least fitting parameters is not straightforward. It appears that in most cases the RE model involves three fitting parameters [14] ($Đ_i(0)$ and $\phi_i = A_i \exp\left(B_i \theta_i\right)$ while the RSM requires only two ($q_i^{sat*} Đ_i^*(0)$ and K^*). However, in the case of CO_2 in DDR, ϕ_i can be taken as a single parameter reducing the model fit parameters to two [14]. Additionally, it can be argued that the zero-loading diffusivity is not a true fitting parameter since it can be directly found from the data, but this holds for both approaches. Moreover, the total saturation loading can be considered a fitting parameter, but this value can be derived with good result from the saturation value given by the adsorption isotherm.

In contrast to the extra fitting parameter required for the RE approach in many cases, it appears that in some cases in the RSM approach a correction for the free space available for diffusion needs to be made. It is interpreted, however, that this analysis gives additional insight in phenomena (*e.g.* rearrangement, dead volume) that may take place.

An additional difference between the two approaches is found when the models are extended to non-isothermal data. A recent publication of Krishna and van Baten [15] yielded an activation energy for diffusion that is dependent on the loading using the RE approach, whereas in the RSM approach a loading independent activation energy is obtained, as shown in this paper.

The major advantage of the RSM is found in the prediction of the self diffusivity. Within the RE approach the self exchange coefficient, relating the self and MS diffusivity, is merely an observable, within the RS concept these correlation effects can be predicted. The prediction of these correlation effects arises from the fundamental difference how the two approaches explain the observed loading dependency of diffusion, on the one hand molecular repulsions (RE) and on the other hand segregated adsorption (RSM). The new formulation for mass transport that is derived gives opportunities to improve current modelling approaches when extended to mixtures.

Evaluating, the presented RSM provides an engineering description of diffusional transport in zeolites based on the molecular modelling results that include details of the zeolite topologies in the adsorption isotherms and diffusivities. Considering the zeolite as an isotropic medium it still contains the details of its topology. Experimental data on diffusion and adsorption may further serve to calibrate the parameters for the real system under investigation.

The current research efforts focus on application of the RSM to other topologies and extension to mixture diffusivity data.

4 Conclusions

The relevant site model (RSM) is validated by analysis of a set of N_2 and CO_2 diffusivity data in zeolite DDR up to saturation loading, obtained by molecular dynamics simulations. The strong loading dependency of N_2 in DDR is explained by a very weak window adsorption, much weaker than the first adsorption step found in the adsorption isotherm. Simulations of CO_2 and N_2 in DDR at different temperatures up to saturation loading showed that the RSM can be consistently extended to non-isothermal diffusivity data.

The N_2 diffusivity data suggests positional rearrangement inside the DDR cages in a certain loading range. Accounting for these effects by considering that these rearrangements do not represent relevant free space for diffusion leads to a good model description of the diffusivity data of N_2 in combination with the RSM.

The correlation effects in DDR are related to the relevant site occupancy instead of the total occupancy. The assumption that the self exchange coefficient is equal to the Maxwell-Stefan diffusion coefficient leads to a good quantitative prediction of the self diffusivity within the RSM formulation. The observed very low correlation effects in DDR for N_2 are explained by the relatively low window site occupancy, which controls diffusional transport.

References

[1] B. Smit, *Molecular Physics*, 85, **1995**, 153.

[2] B. Smit, *Journal of Physical Chemistry*, 99, **1995**, 5597.

[3] T. J. H. Vlugt, R. Krishna, and B. Smit, *Journal of Physical Chemistry B*, 103, **1999**, 1102.

[4] T. J. H. Vlugt and M. Schenk, *Journal of Physical Chemistry B*, 106, **2002**, 12757.

[5] C. Baerlocher, L.B.McCusker, and D.H.Olson, Atlas of Zeolite Framework Types, **2007**, Elsevier, Amsterdam.

[6] S. Jakobtorweihen, N. Hansen, and F. J. Keil, *Molecular Physics*, 103, **2005**, 471.

[7] R. Krishna and J. M. van Baten, *Chemical Physics Letters*, 446, **2007**, 344.

[8] D. Frenkel and B.Smit, Understanding Molecular Simulation: from Algorithms to Applications 2nd ed., **2002**, Academic Press, San Diego.

[9] R. Krishna and J. M. van Baten, *Journal of Physical Chemistry B*, 109, **2005**, 6386.

[10] D. Dubbeldam and R. Q. Snurr, *Molecular Simulation*, 33, **2007**, 305.

[11] R. Krishna and J. M. van Baten, *Chemical Engineering Science*, 64, **2009**, 870.

[12] J. van den Bergh, W. Zhu, J. Gascon, J. A. Moulijn, and F. Kapteijn, *Journal of Membrane Science*, 316, **2008**, 35.

[13] R. Krishna and J. M. van Baten, *Microporous and Mesoporous Materials*, 109, **2008**, 91.

[14] R. Krishna and J. M. van Baten, *Chemical Engineering Science*, 63, **2008**, 3120.

[15] R. Krishna and J. M. van Baten, *Microporous and Mesoporous Materials*, 125, **2009**, 126.

5C

The Relevant Site Model:
Extension to binary mixtures in DDR

The Relevant Site Model (RSM) introduced in Chapter 5A is applied to mixtures. Analysis of an extensive set of diffusivity data of N_2/CO_2 and Ne/Ar mixtures in zeolite DDR, directly computed using molecular dynamics shows that the RSM provides excellent mixture diffusivity predictions from single component data. The results are comparable to the 'Reed-Ehrlich' approach as put forward by Krishna and co-workers (*e.g. SepPurTech*, 61, **2008**, 414). Although the model predictions are comparable, the two approaches are fundamentally different since in the Reed-Ehrlich approach the loading dependency of diffusion is described by inter-molecular repulsions. A clear improvement by the RSM is found in the case of the N_2 diffusivity in N_2/CO_2 mixtures, attributed to the specific window blocking effect by CO_2 and inherently incorporated in the RSM by relating (competitive) adsorption to the relevant (=window) site.

This chapter is based on the following publication:

J. van den Bergh, S. Ban, T. J. H. Vlugt, and F. Kapteijn, *Journal of Physical Chemistry C*, 113, **2009**, 21856.

1 Introduction

In Chapter 5A we have introduced the so-called relevant site model (RSM) which explains the observed loading dependencies of the Maxwell-Stefan diffusivity from adsorption heterogeneity. This model was demonstrated for single component systems as an alternative to the so-called Reed-Ehrlich (RE) approach in Chapter 5B. In the RE approach the loading dependencies are explained from inter-molecular repulsions. Both approaches are discussed in detail in Section 2.1 and 2.2 of Chapter 5A, respectively. The RE approach, as applied by Krishna and co-workers [1-7], has been applied to describe single component and mixture diffusivities in zeolites on a phenomenological basis. A considerable number of successful applications of this approach have been demonstrated. The RSM was introduced because the RE approach fails to describe membrane permeances of CO_2/CH_4 mixtures in DDR [8]. Furthermore, CO_2 containing mixtures in DDR suffer from segregated adsorption effects which are not properly accounted for in the Reed-Ehrlich approach [6]. Since the RSM is formulated around the central idea of segregated adsorption this gives opportunities to improve current models for describing the loading dependency of diffusivities.

Our initial work on the RSM showed very promising results regarding the modelling of diffusivities of N_2 and CO_2 single component systems in DDR (Chapter 5B). The aim of the current chapter is to extend the RSM to mixtures. For the basic principles of the Maxwell Stefan theory for mixtures and the derivation of the RSM the reader is referred to Chapter 5A. As a case study N_2/CO_2 and Ne/Ar mixture diffusivity data in DDR obtained by molecular dynamics (MD) are used to verify the quality of the RSM model predictions. Most MD data are taken from literature [9]. Also a comparison is made between the RSM and the RE approach, because we regard the latter as the most successful phenomenological modelling approach currently available.

2 Simulation technique

Molecular Dynamics (MD) simulations [10-12] are used to calculate the self and Maxwell-Stefan (MS) diffusivities of adsorbed guest molecules in zeolites. The velocity Verlet algorithm [13] was used with a time step of 0.5 fs. The temperature was controlled by a Nosé-Hoover thermostat [11]. The initial configuration of guest molecules was taken from the final configuration of a Monte Carlo simulation in the NVT ensemble. For simplicity, we used a rigid zeolite framework. Interactions between guest molecules and the zeolite hosts consist of Lennard-Jones and electrostatic interactions. The latter are computed using the Ewald summation. For a detailed description of the force field we refer the reader to Ref. [3]. The self and MS diffusivities are computed from mean square displacements of guest molecules, see the supporting info of Ref. [3] for details. These displacements are computed using an order-n algorithm [11,14]. For DDR-type zeolite, only diffusion in x and y directions is taken into account, as the pore structure is two-dimensional [15].

Simulations of an n-component system in the grand-canonical (μVT) ensemble can be used to compute the adsorption isotherm, *i.e.* the average loading $\langle N_i \rangle$ of component i with chemical potential μ_i or fugacity f_i (i =1,n). In general, $\langle N_i \rangle$ will depend on all μ_1, μ_2, · · · μ_n. For a detailed description on computing adsorption isotherms, we refer the reader to [16,17]. For given loadings $N_1^{\star}, N_2^{\star}, \cdots, N_n^{\star}$ we used simulations in the grand-canonical ensemble to "back-calculate" the corresponding fugacities of literature data. We use partial derivatives of the average loading with respect to the chemical potential to iteratively determine the chemical potentials $\mu_1, \mu_2, \ldots, \mu_n$ corresponding to the given loadings $N_1^{\star}, N_2^{\star}, \cdots, N_n^{\star}$:

$$\frac{\partial\langle N_i\rangle}{\partial\mu_j}=\frac{1}{k_BT}\left[\langle N_iN_j\rangle-\langle N_i\rangle\langle N_j\rangle\right]. \tag{1}$$

For more details on how to back-calculate the corresponding fugacities of the adsorbed components, see Ref. [18].

Alternatively, the Ideal Adsorption Solution Theory (IAST) [19] can be used to estimate the corresponding fugacities for a given mixture loading. The IAST allows a prediction of the mixture adsorption properties (loading or fugacity) based on the single component adsorption isotherms. This approach has proven successful in many cases, however, appears to fail when adsorption becomes inhomogeneous [20]. Recently, Krishna and van Baten have shown that this is also the case for CO_2/N_2 mixtures of equal fugacity in DDR [6]. Therefore, the IAST predictions are compared to Grand Canonical Monte Carlo (GCMC) data, as described in the next paragraph, to estimate the uncertainty that is introduced by using the IAST.

3. Results and discussion

A prediction of diffusivity data of N_2/CO_2 and Ne/Ar mixtures in DDR at 300 K is made. Most of the considered binary mixture diffusivity data is taken from Krishna and van Baten [9]. In the current study MD simulations have been used to compute mixture diffusivities for a CO_2/N_2 mixture at equal fugacity, which is at conditions relevant for CO_2/N_2 separations.

3.1 Single components

The RS single component lumped diffusivity parameter and adsorption equilibrium constant are fitted to single component MS diffusivity data. Figure 1 shows the MD single component diffusivity data of CO_2, N_2, Ar and Ne in DDR at 300 K taken from [9]. Lines represent RSM fitting results of the MS diffusivity data together with a prediction of the self diffusivity, assuming that $Đ_{ii}^{*}=Đ_{i}^{*}$, (*i.e.* $a_i=1$), as described in Section 2.3 of Chapter 5A. The adsorption parameters used [9,21][Chapter 4B] and the estimated RS adsorption constant and lumped diffusivity parameters are presented in Table 1. In this table also the fitted RS parameters of CO_2 and N_2 in DDR from [21][Chapter 5B] are presented. Note that in the case of N_2 a rearrangement is considered, as described in Section 2.4 of Chapter 5A, which has an effect on the available free space for diffusion. The rearrangement site parameters are taken from Chapter 5B.

For all components a very good fit of the MS diffusivity data with the RSM and an accurate prediction of the self diffusivity are obtained. The prediction of the self diffusivity indicates that the correlation effects (‘friction’) are well-captured by the RSM when assuming that $Đ_{ii}^{*}=Đ_{i}^{*}$. This provides a solid basis to move to the prediction of mixture diffusivities. With correlation effects the ‘friction’ effects between molecules are meant, as described by the (self) exchange diffusivity ($Đ_{ii}^{*}$, $Đ_{ij}^{*}$).

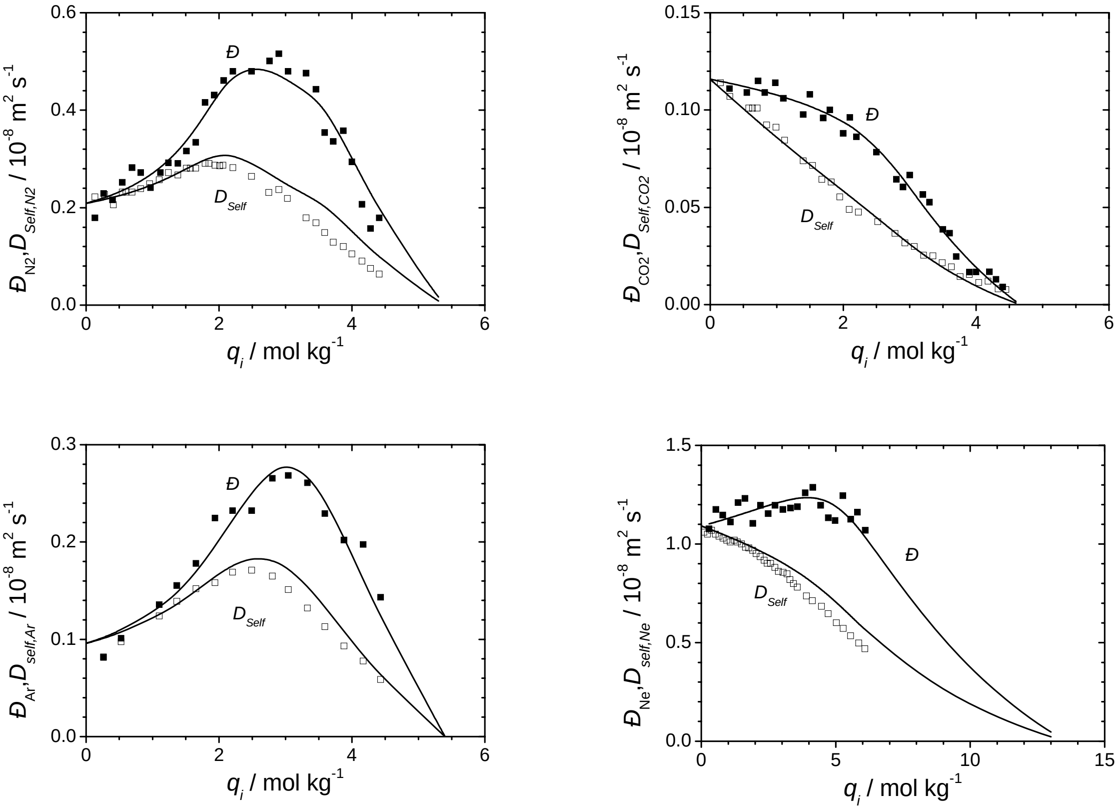

Figure 1. MD diffusivity data of CO_2, N_2, Ar and Ne in all-silica DDR at 300 K [9]. Lines represent modelling results of the RSM, parameter estimates are presented in Table 1. In the case of N_2 rearrangement of molecules in the cages is accounted for.

Table 1. Adsorption isotherm parameters used and estimated single component RS diffusivity and adsorption parameters of CO_2, N_2, Ne and Ar in DDR at 300 K.

		CO_2 [a]	N_2 [a]	CO_2 [b]	N_2 [b]	Ne [c]	Ar [c]
Estimated parameters							
$q^{sat*}Đ^{*}(0)$	$\left[mol\cdot kg^{-1}m^{2}s^{-1}\right]$	0.63	3.81	0.54	3.81	13.7	3.16
K^{*}	$\left[kPa^{-1}\right]$	$3.77\cdot10^{-3}$	$3.67\cdot10^{-5}$	$5.34\cdot10^{-3}$	$3.66\cdot10^{-5}$	$9.87\cdot10^{-6}$	$2.06\cdot10^{-5}$
$q^{sat,ID}$	$\left[mol\cdot kg^{-1}\right]$	-	1.20	-	1.20	-	-
K^{ID}	$\left[kPa^{-1}\right]$	-	$5.49\cdot10^{-6}$	-	$5.49\cdot10^{-6}$	-	-
Adsorption constants							
$q^{sat,A}$	$\left[mol\cdot kg^{-1}\right]$	2.63	2.01	2.63	2.01	5.00	2.1
K^{A}	$\left[kPa^{-1}\right]$	$9.38\cdot10^{-3}$	$3.22\cdot10^{-4}$	$9.38\cdot10^{-3}$	$3.22\cdot10^{-4}$	$2.39\cdot10^{-5}$	$3.06\cdot10^{-4}$
$q^{sat,B}$	$\left[mol\cdot kg^{-1}\right]$	1.27	1.54	1.27	1.54	4.10	1.3
K^{B}	$\left[kPa^{-1}\right]$	$2.17\cdot10^{-4}$	$1.04\cdot10^{-5}$	$2.17\cdot10^{-4}$	$1.04\cdot10^{-5}$	$1.03\cdot10^{-6}$	$2.58\cdot10^{-5}$
$q^{sat,C}$	$\left[mol\cdot kg^{-1}\right]$	0.73	1.84	0.73	1.84	4.47	2.0
K^{C}	$\left[kPa^{-1}\right]$	$3.01\cdot10^{-6}$	$1.05\cdot10^{-7}$	$3.01\cdot10^{-6}$	$1.05\cdot10^{-7}$	$2.00\cdot10^{-8}$	$1.11\cdot10^{-6}$

[a] Estimated parameters and adsorption constants taken directly from Chapter 4B; [b] RS parameters estimated in this work using diffusivity data of Ref. [9] and adsorption constants from Chapter 4B; [c] RS parameters estimated in this work using diffusivity data and adsorption constants from Ref. [9].

3.2 Mixtures

In order to make a prediction of the mixture diffusivities using the RSM the loadings of the adsorbed guest molecules and their fugacities need to be known. Two methods have been used to calculate these properties: IAST and GCMC simulations. The GCMC data are used to verify the accuracy of the IAST predictions.

The CO_2 and N_2 loadings used in our MD simulations are presented in Figure 2 together with GCMC results of a mixture of equal fugacity and a prediction of the IAST using the single component adsorption isotherms given in Table 1. Note that in the case of the MD simulation data points the N_2 partial pressures are approximations, since due to the low number of N_2

molecules in the simulation box the exact mixture fugacities would correspond to a non-integer number of N_2 molecules. The IAST underpredicts the N_2 loading and slightly overpredicts the CO_2 loading (dashed lines).

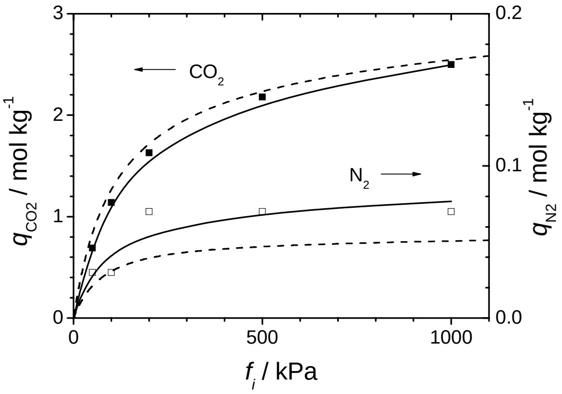

Figure 2. Adsorption isotherms of a mixture of CO_2 and N_2 in DDR at 300 K in a mixture at equal fugacity of each component. Points represent loadings used in MD simulations, solid lines represent GCMC results and dashed lines represent IAST predictions.

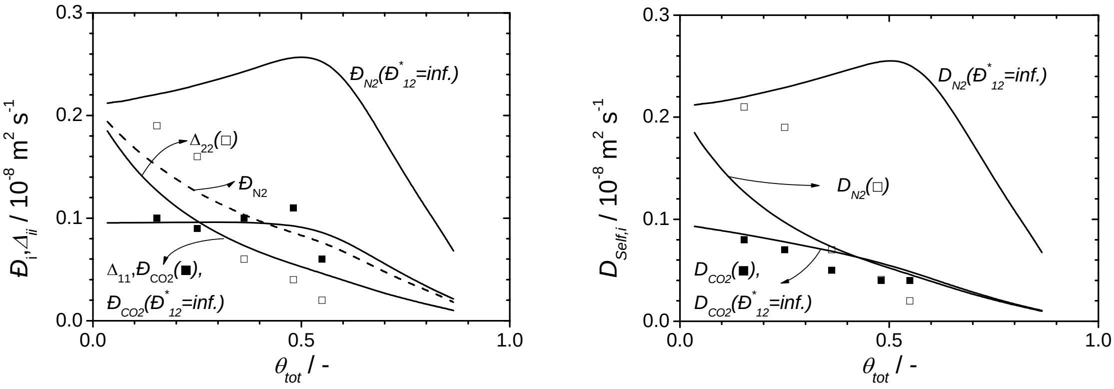

Figure 3. N_2 and CO_2 self and MS diffusivities in DDR in a mixture with equal fugacities. Points are MD simulation results, lines represent RSM model predictions for several scenarios as indicated in the figure and described in more detail in the text.

Figure 3 shows the simulated MS and self-diffusivities together with the RSM model predictions using the single component diffusivities and RS parameters from Chapter 5B. The mixture diffusivity predictions are generated using the procedure as outlined in Section 2.2 of Chapter 5A. Note that the RS saturation loadings of both components in the mixture are assumed equal, which leads to a simplified equation to calculate the RS exchange diffusivity ($Đ_{ij}^*$) and allows the use of an extended Langmuir isotherm to calculate the RS mixture occupancies. Also a model prediction is made neglecting exchange effects ($Đ_{ij}^* = \infty$, no ‘friction’ between guest molecules) and a prediction of the diagonal elements of the matrix Δ including interaction effects. The free space relevant for diffusion is calculated assuming a N_2 saturation loading of 4.2 mol kg^{-1}, thereby considering that 1.2 mol kg^{-1} of the total saturation loading is due to rearrangements, which is assumed not to represent space relevant for diffusion (Chapter 5B, Table 1). Furthermore, the N_2 loading is so low that no rearrangements are expected to occur. The loadings were estimated using the IAST. Prediction of diffusivities using the exact GCMC loading and fugacity dataset as shown in Figure 2 lead to very similar results and are not shown here.

The non-diagonal elements of the matrix Δ were found zero in the MD calculations leading to $Đ_i = \Delta_{ii}$ because no correlation effects are observed. The CO_2 mixture diffusivities closely match the single component diffusivities, which is logical since the mixture constitutes predominantly of CO_2. The N_2 mixture diffusivities differ markedly from the single component results: the maximum at intermediate loading is not observed and the diffusivities are much lower.

Both the CO_2 self and MS diffusivities are accurately predicted by the RSM. Moreover, the values obtained for $Đ_i$, Δ_{ii} and the scenario neglecting exchange all coincide. In the case of N_2 the model prediction follows the trend of the diffusivity data well. A small difference between $Đ_i$ and Δ_{ii} is predicted. The fact that the RSM prediction of $Đ_i$ and Δ_{ii} are very close in the case of N_2 indicates that indeed the interaction effects are small based on the total loading. This explains why these effects are difficult to observe in the MD simulations. Although small, neglecting the interaction effects ($Đ^*_{ij} = \infty$) leads to poor predictions that follow the trend of the single component data. Therefore, interaction effects should be accounted for in the RSM for N_2 in the mixture with CO_2. CO_2 is strongly dominating the diffusional behaviour due to its high occupancy of the RS.

For the dataset of Krishna and van Baten [9] for CO_2/N_2 and Ne/Ar mixtures in DDR the back-calculated fugacities by the IAST, using the pure component adsorption isotherms, are compared with GCMC back-calculated results for the CO_2/N_2 mixtures in Figure 4. The fugacities are predicted with good accuracy by the IAST and no severe errors are introduced for the studied conditions.

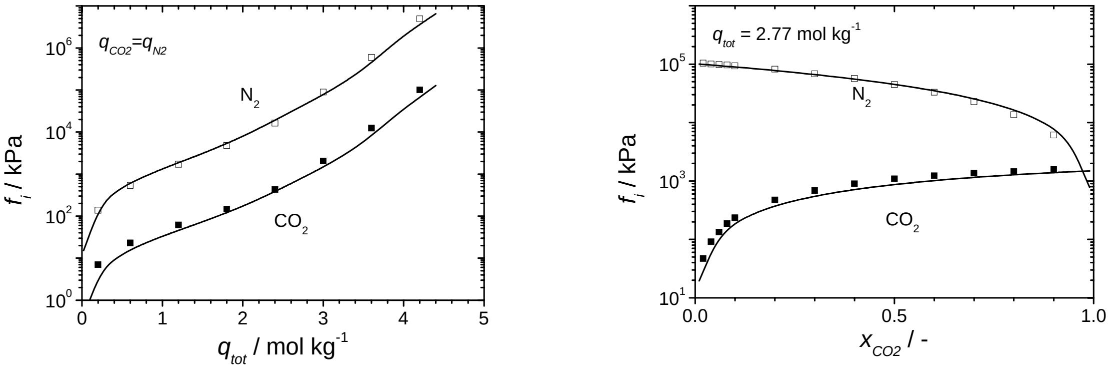

Figure 4. Fugacities of N_2 and CO_2 in DDR at 300 K in equal loading mixtures (left) and at various compositions at a constant total loading of 2.77 mol kg^{-1} (right). Lines represent IAST predictions, points are back-calculated by GCMC simulations.

Figure 5 and Figure 6 show the mixture self diffusivities and elements of matrix Δ_{ii} calculated using MD simulations from [9]. The lines represent RSM predictions and model predictions using the Reed-Ehrlich approach presented by Krishna and van Baten [9], as described in Section 2.1 of Chapter 5A. In the case of the Ne/Ar mixture also an α_{12} term is presented to characterize the off-diagonal elements of the Onsager matrix [3]:

$$\alpha_{12} = \frac{L_{12}}{\sqrt{L_{11}L_{22}}}. \qquad (2)$$

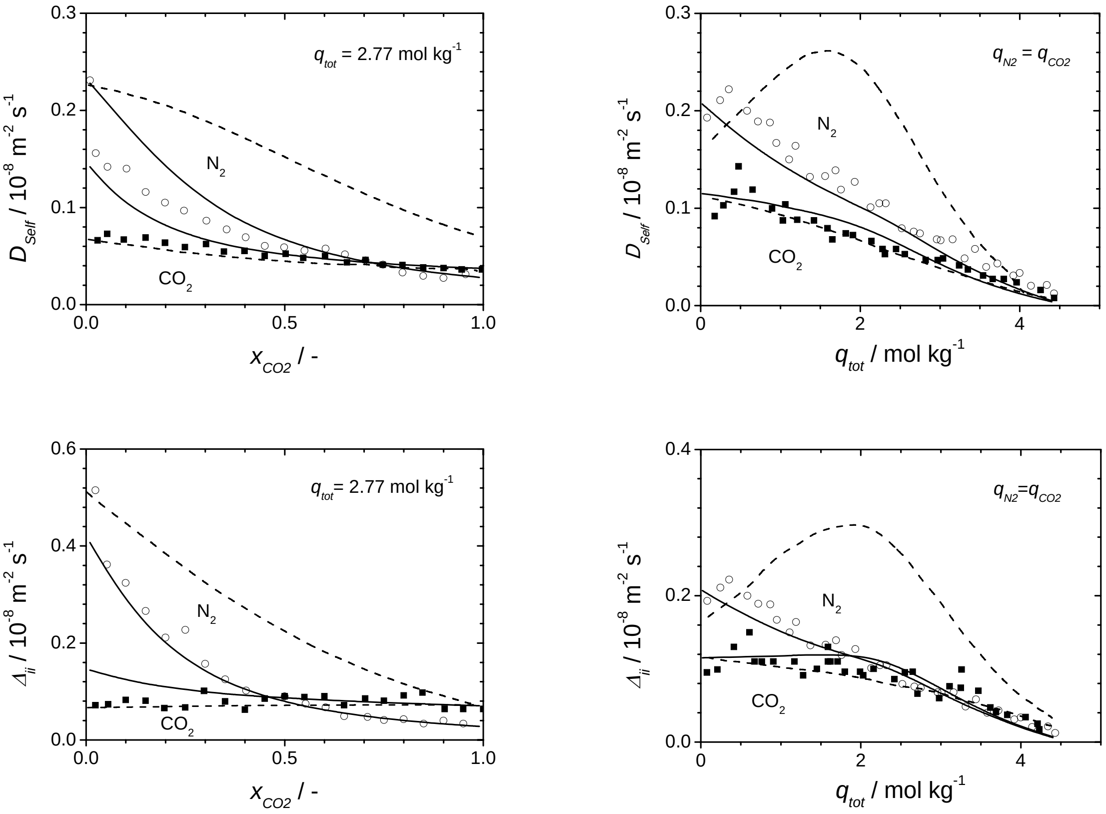

Figure 5. CO_2 and N_2 diffusivities (D_{Self} and Δ_{ii}) in mixtures in DDR as a function of different compositions at constant total loading (left) and as a function of total loading at equal composition (right). The data points, solid lines and dashed lines represent MD simulations results from [9], RSM predictions and model predictions of the 'Reed Ehrlich' approach given in [9], respectively.

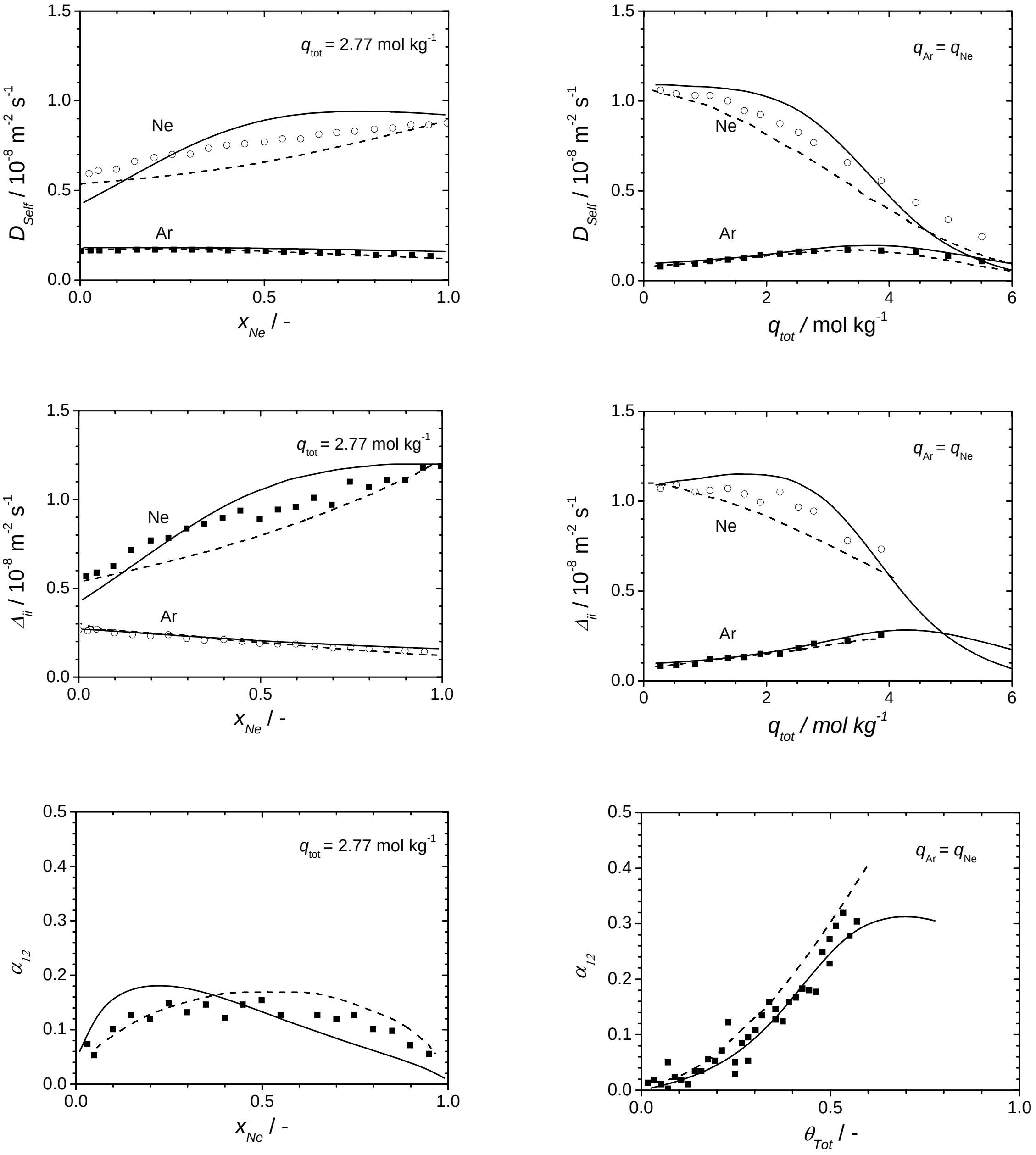

Figure 6. Ar and Ne diffusivities (D_{Self} and Δ_{ii}) and α_{12} in mixtures in DDR as a function of composition at constant total loading (left) and as a function of total loading at equal composition (right). The data points, solid lines and dashed lines represent MD simulations results from [9], RSM predictions and model predictions of the 'Reed Ehrlich' approach given in [9], respectively.

For the RSM predictions the diffusivity parameter values estimated from the single component diffusivity data of Krishna and van Baten (Table 1) are used. The total occupancy is calculated again using a saturation loading of 4.2 mol kg^{-1} for N_2. However, in the current dataset considerable N_2 loadings occur where part of the loading may represent rearrangements and should not be considered to calculate the free space available for diffusion. The highest N_2 loading in the considered mixtures is 2.77 mol kg $^{-1}$ and at single component conditions 0.4 mol kg^{-1} of this loading is ascribed to rearrangement effects. Moreover, in the case where the CO_2 fraction is reduced, more and more cages will consist of purely N_2 where rearrangements are expected. It is unclear up to what extent rearrangements occur in the mixture. It is now assumed that at a given N_2 loading in the mixture the same number N_2 molecules rearrange as found at this N_2 loading under single component conditions. This assumption will at least be valid in the case where the CO_2 fraction is the lowest, the situation where the N_2 loading is the highest in our case. The validity of this assumption is questionable when both N_2 and CO_2 loadings are high (> 2 mol kg^{-1}) which is not the case in our dataset. Now, the N_2 loading used to calculate the free space for diffusion is based on the loading of N_2 in the mixture after subtracting the loading that is assigned to rearrangement effects. The latter is calculated from the single component isotherm at the N_2 loading in the mixture.

Comparing the RSM predictions to the MD data of all mixtures (Figure 5 and Figure 6) leads to the general conclusion that a good prediction of the mixture data is obtained. A comparison of the RSM predictions to the Reed-Ehrlich predictions show that for the Ne/Ar mixtures very similar results are obtained: the Ar diffusivities are predicted very accurately and the Ne predictions show some small deviations.

In case of the N_2/CO_2 mixtures differences between the two approaches are found. The N_2 diffusivities are much better predicted by the RSM. It should be noted that the poor prediction of the N_2 is not typical for the Reed-Ehrlich approach, in many cases good results are obtained. These poor predictions appear to occur in CO_2 containing mixtures in cage-like zeolites, where segregated adsorption is found [6]. The origin of the over-prediction of the N_2 diffusivities is ascribed to window blocking of N_2 by CO_2 molecules that prefer to reside in the windows [6,22]. These effects are not accounted for in the Reed-Ehrlich approach. In case of the RSM mass transport is related to the window sites and competitive adsorption effects are also considered at the RS. In this way these window blocking effects are incorporated in the RSM approach leading to an improved prediction. The CO_2 fraction in the adsorbed mixture at equal loading is about 0.5, whereas at the RS it is around 0.7 to 0.8, clearly revealing preferential adsorption of CO_2 at the window site.

With decreasing CO_2 fraction the CO_2 diffusivity is increasingly over-predicted by the RSM, whereas an accurate prediction is found by the Reed-Ehrlich approach. Since the loading is given and the fugacities are accurately predicted (Figure 4) the error can be related to either an overprediction of the RS occupancy of CO_2 or to an overestimated exchange diffusivity.

Both can be due to the assumption of equal saturation loadings on the RS. If the saturation loadings are not equal, the extended Langmuir will yield an inaccurate prediction of the occupancy. A lower CO_2 or a higher N_2 RS adsorption equilibrium constant also results in a lower CO_2 occupancy. However, obtaining significantly higher or lower RS adsorption equilibrium constants from the single component data is not possible.

This discrepancy is likely related to the exchange effects because in the region where the model fails for CO_2 $Đ_{ij}^{*}$ increases strongly, up to $Đ_{N_2}^{*}$ in the limit of pure N_2. Whereas under all other conditions $Đ_{ij}^{*}$ is much lower, close to $Đ_{CO_2}^{*}$, due to the excess of CO_2 at the RS (Figure 7). The physical reason for this discrepancy could be due to N_2 rearrangements that are expected to occur increasingly at low CO_2 fractions. Possibly these rearrangements have an additional negative effect on the CO_2 diffusivity.

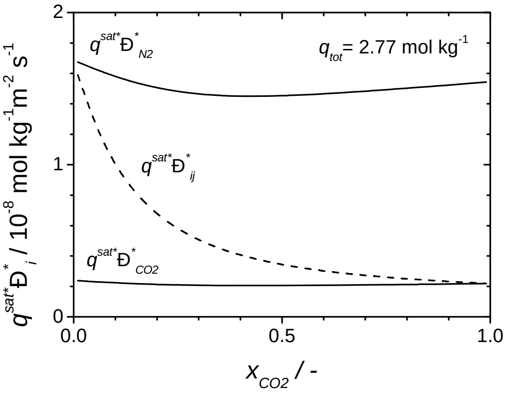

Figure 7. Lumped RS diffusivity parameter $q^{sat*}Đ_i^{*}$ for CO_2 and N_2 and the corresponding exchange diffusivity as a function of the CO_2 fraction.

3.3 Further application of the RSM

For the small-pore cage-like zeolite DDR the RSM is a suitable approach to describe mixture diffusivity, purely based on single component diffusivity data and single component adsorption isotherms. Future research will focus on the application to other topologies. The reason that the RSM works well in the case of DDR is that apparently the diffusion process can be simplified by the description of a single site (the RS) being rate controlling. It seems plausible that the RSM would also apply to other small-pore cage-like zeolites like chabasite (CHA), erionite (ERI), zeolite A (LTA) and Nu-3 (LEV) because of their similarity in topology with DDR.

Moving towards topologies where the diffusion is not controlled by a single site or where diffusion is anisotropic, the RSM may fail. However, these aspects are not incorporated in other phenomenological approaches either. Any zeolite system would have some degree of adsorption heterogeneity that gives opportunities for the RSM to realize improvements.

Sources of segregated adsorption can be of topological nature (*e.g.* cage-window, channel-intersection), but also due to framework composition (*e.g.* Si-Al ratio) or non-framework counter ions present in the system. Note that in the case that the adsorption is completely homogeneous the RSM occupancy becomes equal to the total occupancy and the model simplifies into the standard MS model applied to zeolites.

‘Friction’ between components in DDR can be captured well by relating them to the RS occupancy. It appears also that $Đ^*_{ii}=Đ^*_i$ in the case of DDR. This implies that the total friction between molecules is determined by ‘friction’ at the RS. This can be understood by realizing that, because the window site is rate controlling, the intra-cage hopping frequency is much higher than the hopping frequency from a window to the next cage. And, because the cages are large enough for molecules to pass each other inside the cages, a sort of well-mixed system is found in the cage where correlation effects are absent. The assumption that $Đ^*_{ii}=Đ^*_i$ will probably become invalid if more than one site becomes rate controlling, or if molecules have difficulties passing each other in between the rate controlling sites. In the latter case the (self-) exchange diffusivity will be overestimated when based solely on the RS.

The concept of free space relevant for diffusion should be considered in other systems. Several zeolitic systems have side-pockets where molecules may adsorb but that should be considered as a *cul de sac* for transport (*e.g.* MOR). For several zeolites specific arrangements of molecules inside the zeolite have been reported, depending on the loading. Examples of the latter case are, for example, *n*-butane and *n*-hexane (commensurate freezing [16,23]) and isobutane in MFI [24] and alkanes in $AlPO_4$ [25]. Rearrangements and dead volumes may lead to effects on the diffusivity that can be explained within the concept of free space relevant for diffusion.

4 Conclusions

The Relevant Site Model (RSM), previously successfully demonstrated to capture observed loading dependencies of single component diffusivities in zeolite DDR, has been extended to mixtures. The RSM treats diffusion in zeolites within the MS framework for mass transport, assuming that a specific ‘relevant’ site is rate controlling. Loading dependencies of diffusion are explained from segregated adsorption: the adsorption properties of the RS can be very different from the overall adsorption properties. Key feature of the RSM as applied to mixtures is that exchange effects (‘friction’ between molecules) and competitive adsorption effects are related to the RS occupancy and not to the total occupancy.

Single component MD diffusivity data of Ne, Ar, N_2 and CO_2 in DDR, could be described well by the RSM up to saturation loading. Moreover, using the RSM an accurate prediction could be made of the self diffusivity for all components by relating the self-exchange effects to the RS and assuming that the RS self-exchange diffusivity equals the RS MS diffusivity.

The RSM led to a good prediction of an extensive set of binary Ne/Ar and N_2/CO_2 mixture diffusivities using the estimated single component RS diffusivity and RS adsorption constants. The RSM and the alternative Reed-Ehrlich approach perform in most cases equally well. The N_2 diffusivities in the mixture, however, are much better described by the RSM. The main reason for this is that CO_2 prefers to adsorb in the window region of DDR thereby hindering N_2 [6]. These effects are not captured in the Reed-Ehrlich approach but they are in the RSM that incorporates adsorption at the RS in DDR, which is the window site.

Finally, for the challenging N_2/CO_2 mixture in DDR the RSM leads to improved mixture diffusivity predictions as compared to the current state of the art approach.

References

[1] R. Krishna and J. M. van Baten, *Chemical Engineering Science*, 64, **2009**, 870.

[2] R. Krishna and J. M. van Baten, *Chemical Engineering Science*, 64, **2009**, 3159.

[3] R. Krishna and J. M. van Baten, *Chemical Engineering Science*, 63, **2008**, 3120.

[4] S. Li, J. L. Falconer, R. D. Noble, and R. Krishna, *Journal of Physical Chemistry C*, 111, **2007**, 5075.

[5] R. Krishna, J. M. van Baten, E. Garcia-Perez, and S. Calero, *Industrial & Engineering Chemistry Research*, 46, **2007**, 2974.

[6] R. Krishna and J. M. van Baten, *Chemical Physics Letters*, 446, **2007**, 344.

[7] R. Krishna, D. Paschek, and R. Baur, *Microporous and Mesoporous Materials*, 76, **2004**, 233.

[8] J. van den Bergh, W. Zhu, J. C. Groen, F. Kapteijn, J. A. Moulijn, K. Yajima, K. Nakayama, T. Tomita, and S. Yoshida, *Studies in Surface Science and Catalysis*, 170 A, **2007**, 1021.

[9] R. Krishna and J. M. van Baten, *Chemical Engineering Science*, 63, **2008**, 3120, supporting information.

[10] D. C. Rapaport, The art of molecular dynamics simulation, **2004**, Cambridge University Press, Cambridge.

[11] D. Frenkel and B.Smit, Understanding Molecular Simulation: from Algorithms to Applications 2nd ed., **2002**, Academic Press, San Diego.

[12] M. P. Allen and D.J.Tildesley, Computer simulation of liquids, **1987**, Clarendon Press, Oxford.

[13] W. C. Swope, H. C. Andersen, P. H. Berens, and K. R. Wilson, *Journal of Chemical Physics*, 76, **1982**, 637.

[14] D. Dubbeldam, D. C. Ford, D. E. Ellis, and R. Q. Snurr, *Molecular Simulation*, 35, **2009**, 1084.

[15] Ch. Bearlocher and L. B. McCusker, Database of Zeolite Structures: www.iza-structure.org/databases/, Visited **8/2009**.

[16] T. J. H. Vlugt, R. Krishna, and B. Smit, *Journal of Physical Chemistry B*, 103, **1999**, 1102.

[17] D. Dubbeldam, S. Calero, T. J. H. Vlugt, R. Krishna, T. L. M. Maesen, and B. Smit, *Journal of Physical Chemistry B*, 108, **2004**, 12301.

[18] T. J. H. Vlugt and B. Dünweg, *Journal of Chemical Physics*, 115, **2001**, 8731.

[19] A. L. Myers and J. M. Prausnitz, *AIChE Journal*, 11, **1965**, 121.

[20] M. Murthi and R. Q. Snurr, *Langmuir*, 20, **2004**, 2489.

[21] J. van den Bergh, S. Ban, T. J. H. Vlugt, and F. Kapteijn, *Journal of Physical Chemistry C*, 113, **2009**, 17840.

[22] R. Krishna and J. M. van Baten, *Separation and Purification Technology*, 61, **2008**, 414.

[23] B. Smit and T. L. M. Maesen, *Nature*, 374, **1995**, 42.

[24] T. J. H. Vlugt, W. Zhu, F. Kapteijn, J. A. Moulijn, B. Smit, and R. Krishna, *Journal of the American Chemical Society*, 120, **1998**, 5599.

[25] T. Maris, T. J. H. Vlugt, and B. Smit, *Journal of Physical Chemistry B*, 102, **1998**, 7183.

5D

The Relevant Site Model: Application to light gases and their mixtures in zeolites DDR, CHA, MFI and FAU

The recently introduced Relevant Site Model (RSM) (Chapter 5A) to describe the loading dependency of diffusion in zeolite DDR is successfully extended to a variety of light gases (CH_4, CO_2, Ar and Ne) and binary mixtures thereof in other zeolite topologies, DDR, CHA, MFI and FAU, utilizing the extensive diffusivity dataset published by Krishna and van Baten for this variety of zeolite-guest systems (*e.g. ChemEngSci*, **2008**, *63*, 3120, supplementary material).

From the RSM approach a measure for the level of adsorption segregation is derived: the ratio of the RS and total occupancy. The predicted level of adsorption segregation correlates well with the level of confinement of a molecule at the RS: the molecule diameter to zeolite pore diameter. The predicted degree of adsorption segregation of the studied light gases in DDR is in good agreement with molecular simulations results, indicating the physical meaningfulness of the estimated RS adsorption parameters. The small-pore zeolite (DDR and CHA) data is described best with equal RS saturation loadings for both components. For the large pore zeolite FAU the ratio of the RS saturation loadings equals that of the bulk saturation loadings. The geometry of the RS strongly influences the RS saturation loading: in case of the small-pore zeolites the RS (= window site) is restricted to only one molecule but when the RS becomes larger more than one molecule can be adsorbed.

This chapter is based on the following publication:

J. van den Bergh, S. Ban, T. J. H. Vlugt, and F. Kapteijn, *Separation and Purification Technology*, 73, **2010**, 151.

1 Introduction

In this chapter the application of the RSM to zeolite topologies other than DDR are investigated. The vast majority of the considered single component diffusivity data and all mixture diffusivity data used are taken from Krishna and van Baten [1].

In Chapter 5C the RSM has been applied assuming equal RS saturation loadings for each component [2]. Here, the RS is applied to systems with unequal saturation loadings. The model is used to describe the loading dependency of the single component MS diffusivity of a series of light gases (CO_2, CH_4, Ar and Ne) in zeolites of quite different topologies (CHA, MFI and FAU). Previous modelling results of CO_2, N_2, Ar and Ne in DDR are also included in the discussion. Specific attention is paid to CH_4 in DDR for which new MS and self diffusivities are calculated as a function of the loading by Molecular Dynamic (MD) simulations at 300, 373, 473 and 573 K. Moreover, the corresponding adsorption isotherms of CH_4 in DDR are computed using Grand Canonical Monte Carlo (GCMC) simulations.

The estimated single component diffusivity parameters are used to predict the self and MS diffusivities of several binary equimolar mixtures (CO_2/Ne, Ar/Ne, CO_2/Ar and CH_4/Ar) in zeolites CHA, MFI and FAU.

2 Simulation technique

To compute adsorption isotherms of CH_4, Monte Carlo (MC) simulations in the grand-canonical (GC) ensemble (μVT) were used [3-5]. In these simulations, a fixed chemical potential (or fugacity) of the sorbent is imposed, resulting in a certain average number of sorbate molecules adsorbed in the zeolite. The zeolite is modelled as a rigid structure [6] with atomic positions taken from the Atlas of Zeolite Structures [7]. We only consider all-silica frameworks, *i.e.* no non-framework atoms or cations are present. The sorbate-zeolite and sorbate-sorbate interactions are modelled by the sum of Lennard-Jones (LJ). LJ interactions were truncated and shifted at 12Å. Methane is modelled as a chargeless united atom with parameters taken from [8]. For more information on the force field and simulation details, we refer the reader to [9].

The self- and Maxwell-Stefan diffusivities are computed from equilibrium Molecular Dynamics (MD) simulations in the *NVE* ensemble using the same force field as for the adsorption calculations. Again, the zeolite is considered as a rigid structure. A time step of 0.001 ps was used to integrate the equations of motion. The starting positions of the sorbate molecules are taken from well-equilibrated MC simulations. Diffusivities are calculated from the mean-square displacements computed using the order-n algorithm of [10,11]. We refer the reader to [12,13] for details on how to extract diffusivities from equilibrium MD simulations. Simulations of at least 20 ns are needed to be in the regime of diffusion to calculate the diffusivities [14].

3 Results and discussion:

A set of single component and mixture diffusivity data, obtained by MD simulations, is used to test the RSM in zeolites DDR, CHA, MFI and FAU. The diffusivity data is taken from Krishna and van Baten [1], except for CO_2 and N_2 in DDR, which is taken from our previous work [15][Chapter 5B], and the CH_4 diffusivity data in DDR. The latter data are calculated as part of the current work.

3.1 Description of considered zeolites

The diffusivity of several light gases is considered in all-silica zeolites DDR, CHA MFI and FAU. DDR and CHA are small-pore zeolites with 8-ring window openings of approximately 0.4 nm. DDR has a two-dimensional and CHA a three dimensional pore network consisting of cages connected by narrow window openings. MFI is a medium pore zeolite with a three-dimensional pore network of intersecting channels. The channels have an approximate diameter 0.55 nm. FAU is a large-pore zeolite built up from cages connected by windows that form a 3-dimensional pore network. The pore size of FAU is about 0.74 nm. In MFI and CHA diffusion is anisotropic; the pore connectivity of DDR, FAU can only result in isotropic diffusion. For more detailed spatial representations of the zeolites the reader is referred to the official website of the International Zeolite Association [16].

3.2 CH_4 diffusion and adsorption in DDR

The computed adsorption isotherms of CH_4 in DDR at 195, 300, 373, 473 and 573 K are presented in Figure 1 together with a combined three-site Langmuir model fit. The estimated adsorption parameters are given in Table 1. Figure 2 shows the diffusivity data of CH_4 MS in DDR at 300, 373, 473 and 573 K. The lines represent RSM model fits at each individual temperature with the exception of the data at 300 K. The computation of the diffusivity of CH_4 required long simulations (>20 ns) because the diffusivity is very low. This is particularly the case at 300 K. Therefore, the line at 300 K is not the result of a model fit. A prediction of this data is made using the estimated activation energy and pre-exponent of the diffusion coefficient estimated from the 373, 473 and 573 K data. The data fits include only data with loadings equal or higher than 1.0 mol kg^{-1}. The estimated parameter values are listed in Table 2.

A comparison of the self- and MS diffusivities of CH_4 in DDR at 373 K is shown in Figure 3. These data are typical for all CH_4 data: the MS- and self diffusivities are very close to each other indicating very low apparent ‘friction’ effects. The adjective apparent is used here to indicate the difference between ‘friction’ effects as observed (based on the total loading) and ‘intrinsic’ ‘friction’ effects related to the RS. Good results have been obtained by relating the MS- and self diffusivity through the RS self exchange diffusivity (Section 2.2.2, Chapter 5A).

For CO_2, N_2, Ar and Ne in DDR an excellent prediction of the self diffusivity was found assuming that $Đ_{ii}^{*}=Đ_{i}^{*}$ [2,15][Chapter 5B and 5C]. A prediction of the self diffusivity data of CH_4 is presented in Figure 3, using the same assumption. This shows that indeed the difference between the two diffusivities is expected to be very small based on the RSM prediction.

The loading dependence of the diffusivity of CH_4 in DDR can be understood as follows. CH_4 is strongly sterically hindered in the window site because it has about the same size as the DDR window, leading to segregated adsorption. Due to the steric effects, CH_4 is only very weakly adsorbed in the window, as reflected by the very low RS adsorption equilibrium constants, leading to the strong apparent loading dependency of diffusion. Moreover, the apparent 'friction' effects are very low because the RS occupancy, which determines these correlation effects, is very low compared to the total occupancy.

The Arrhenius plots of the RS diffusivities and RS adsorption equilibrium constants estimated at each individual temperature are given in Figure 4 and Table 2. As shown previously for CO_2 and N_2 [15][Chapter 5B], also for CH_4 a loading *independent* RS activation energy and adsorption enthalpy are found. The RS activation energy of diffusion of CH_4 (27.2 kJ mol^{-1}) is much higher than that of N_2 (3.2 kJ mol^{-1}) and CO_2 (9.4 kJ mol^{-1}). Clearly the bulkier CH_4 has a much higher energy barrier to overcome due to the narrow window opening. The apparent diffusion activation energy ($E_{A}^{app*}=E_{A,diff}^{*}+\Delta H_{Ads}^{*}$) of CH_4, N_2 and CO_2 are 7.3, -11.8 and -19.2 kJ mol^{-1}, respectively. These results are in qualitative agreement with observed temperature dependencies of CH_4, N_2 and CO_2 fluxes through a DD3R zeolite membrane: The CH_4 flux increases slightly with increasing temperature, the N_2 flux decreases with increasing temperature, and the CO_2 flux decreases strongly with increasing temperature due to the differences in absolute magnitude of the adsorption enthalpy and intrinsic activation energy of the diffusivity [17][Chapter 2].

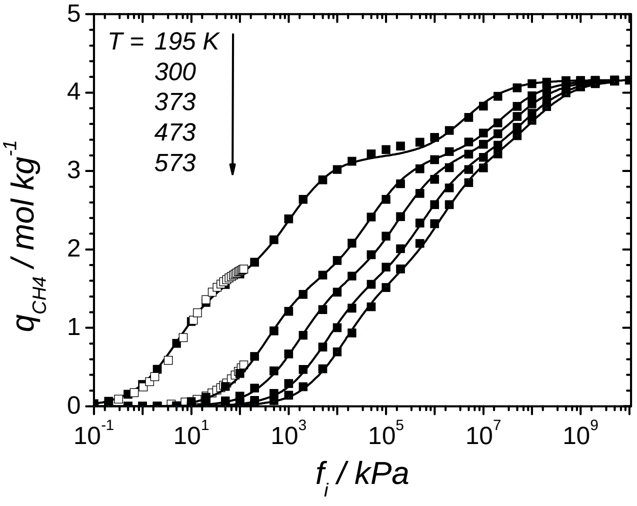

Figure 1. Adsorption isotherms of CH_4 in DDR at 195, 300, 373, 473 and 573 K. Solid symbols, open symbols and lines represent GCMC results, volumetric adsorption measurements [17][Chapter 2] and three-site Langmuir model fits, respectively.

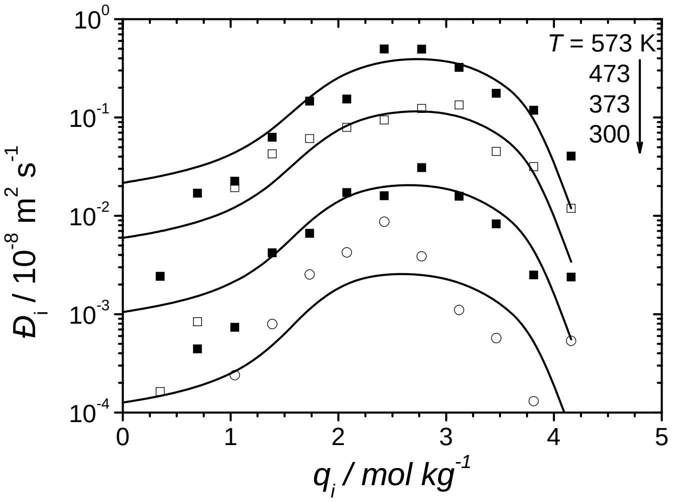

Figure 2. MS Diffusivity of CH_4 in DDR at 300, 373, 473 and 573 K calculated from MD simulations. Lines represent model fit results with the RSM except the data at 300 K, where the line represents a model prediction based on the parameters estimated for 373, 473 and 573 K.

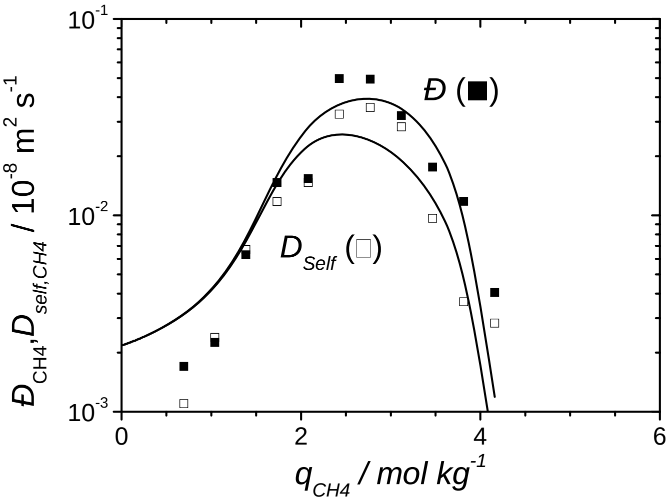

Figure 3. Self and MS diffusivity of CH_4 in DDR at 373 K calculated from MD simulations. The top line is a model fit result of the MS diffusivity data with the RSM. The bottom line is a prediction of the self diffusivity assuming that $Ð_{ii}^{*}=Ð_{i}^{*}$.

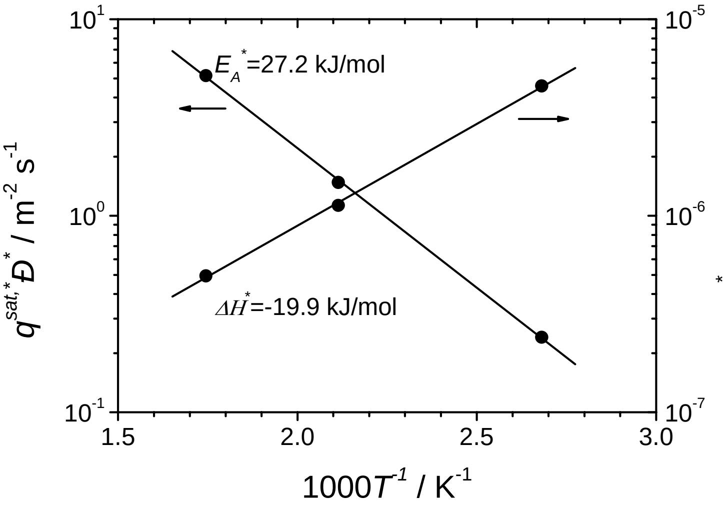

Figure 4. Arrhenius plot of the estimated RS adsorption equilibrium constants and lumped diffusivity parameters of CH_4 in DDR.

Table 1. Three-site Langmuir adsorption constants of the investigated zeolite-host systems. GCMC adsorption data is taken from the indicated references, the adsorption parameters are estimated by the authors.

System	T	Comp.	$q^{sat,A}$	K_0^A	ΔH_{Ads}^A	$q^{sat,B}$	K_0^B	ΔH_{Ads}^B	$q^{sat,C}$	K_0^C	ΔH_{Ads}^C	Ref.
	K		mol kg^{-1}	kPa^{-1}	kJ mol^{-1}	mol kg^{-1}	kPa^{-1}	kJ mol^{-1}	mol kg^{-1}	kPa^{-1}	kJ mol^{-1}	
DDR	[a]	CH_4	1.6	$1.21\cdot10^{-6}$	-20	1.6	$1.83\cdot10^{-8}$	-18	1	$1.69\cdot10^{-9}$	-8.00	TW [b]
DDR	300	O_2	2.4	$3.96\cdot10^{-4}$	-	1.5	$1.99\cdot10^{-5}$	-	1.6	$4.73\cdot10^{-7}$	-	[18]
CHA	300	CH_4	2.9	$1.60\cdot10^{-3}$	-	4.3	$2.24\cdot10^{-5}$	-	1.1	$5.58\cdot10^{-7}$	-	[18]
CHA	300	CO_2	7	$4.64\cdot10^{-3}$	-	1.8	$3.69\cdot10^{-5}$	-	0.8	$3.45\cdot10^{-7}$	-	[18]
CHA	300	Ar	3.3	$2.02\cdot10^{-4}$	-	4	$4.09\cdot10^{-5}$	-	1.7	$1.84\cdot10^{-6}$	-	[18]
CHA	300	Ne	10	$1.81\cdot10^{-5}$	-	9.4	$7.14\cdot10^{-7}$	-	8.8	$9.87\cdot10^{-9}$	-	[18]
FAU	300	CH_4	6.6	$2.78\cdot10^{-4}$	-	3.4	$3.50\cdot10^{-6}$	-	1.2	$3.99\cdot10^{-8}$	-	[18]
FAU	300	CO_2	9.3	$6.53\cdot10^{-4}$	-	1.3	$1.57\cdot10^{-6}$	-	0.9	$2.41\cdot10^{-8}$	-	[18]
FAU	300	Ar	9.1	$8.22\cdot10^{-5}$	-	3.1	$2.35\cdot10^{-6}$	-	3.2	$1.78\cdot10^{-8}$	-	[18]
FAU	300	Ne	16	$9.07\cdot10^{-6}$	-	12	$8.38\cdot10^{-8}$	-	4.6	$2.76\cdot10^{-9}$	-	[18]
MFI	300	CH_4	2.8	$3.25\cdot10^{-3}$	-	0.7	$2.20\cdot10^{-5}$	-	0.5	$1.12\cdot10^{-7}$	-	[19] [c]
MFI	300	CO_2	3.4	$5.64\cdot10^{-3}$	-	1.6	$1.58\cdot10^{-5}$	-	1	$4.27\cdot10^{-7}$	-	[18]
MFI	300	Ar	3.4	$2.49\cdot10^{-4}$	-	2.1	$1.56\cdot10^{-6}$	-	0.8	$1.16\cdot10^{-8}$	-	[18]
MFI	300	Ne	6.3	$1.59\cdot10^{-5}$	-	5.8	$4.27\cdot10^{-7}$	-	5.9	$1.21\cdot10^{-8}$	-	[18]

[a] Based on adsorption isotherm data at 195, 300, 373, 473 and 573 K. [b] TW: Parameters obtained from computer simulations of this work.

[c] Constants taken directly from the indicated reference.

Table 2. Estimated relevant site parameters of various light gases in zeolite DDR, CHA, FAU and MFI.

System	Comp.	T K	K^* kPa^{-1}	K_0^* kPa^{-1}	ΔH_{ads}^* kJ mol^{-1}	$q^{sat,*}\,Đ^*(0)$ 10^{-8} mol kg^{-1} m^2 s^{-1}	$q^{sat,*}\,Đ^*(0)_0$ 10^{-8} mol kg^{-1} m^2 s^{-1}	E_A^* kJ mol^{-1}	$q^{sat,tot}$ mol kg^{-1}	K^{ID} kPa^{-1}	$q^{sat,ID}$ mol kg^{-1}	a -	[Ref]
DDR	CO_2	300	$3.77\cdot10^{-3}$	$3.67\cdot10^{-8}$	-28.6	0.63	25.7	9.37	4.66 [b]	-	-	1	[15]
DDR	N_2	300	$3.67\cdot10^{-5}$	$8.59\cdot10^{-8}$	-15	3.81	13	3.16	5.4 [b]	$5.49\cdot10^{-6}$	1.2	1	[15]
DDR	Ar	300	$2.06\cdot10^{-5}$	-	-	3.16	-	-	5.4 [b]	-	-	1	[2,18]
DDR	Ne	300	$9.87\cdot10^{-6}$	-	-	13.7	-	-	13.6 [b]	-	-	1	[2,18]
DDR	O_2	300	$3.48\cdot10^{-5}$	-	-	5.42	-	-	5.46 [b]	-	-	1	[18]
DDR	CH_4 [a]	300	$2.17\cdot10^{-5}$	$7.54\cdot10^{-9}$	-19.9	0.028	1528	27.2	4.2 [b]	-	-	-	TW [d]
DDR	CH_4	373	$4.57\cdot10^{-6}$			0.24			4.2 [b]	-	-	-	TW
DDR	CH_4	473	$1.18\cdot10^{-6}$			1.52			4.2 [b]	-	-	-	TW
DDR	CH_4	573	$4.88\cdot10^{-7}$			5.08			4.2 [b]	-	-	-	TW
CHA	CH_4	300	$2.07\cdot10^{-5}$	-	-	0.43	-	-	8.32 [b]	-	-	0.8	[18]
CHA	CO_2	300	$1.24\cdot10^{-3}$	-	-	6.21	-	-	9.6 [b]	-	-	0.7	[18]
CHA	Ar	300	$2.00\cdot10^{-5}$	-	-	12.1	-	-	10.0 [c]	-	-	0.8	[18]
CHA	Ne	300	$9.27\cdot10^{-6}$	-	-	35.5	-	-	30 [b]	-	-	0.9	[18]
FAU	CH_4	300	$2.78\cdot10^{-4}$	-	-	4.14	-	-	12.0 [c]	$6.17\cdot10^{-6}$	2.45	0.5	[18]
FAU	CO_2	300	$7.47\cdot10_{4}$	-	-	14.8	-	-	11.5 [b]	-	-	0.5	[18]
FAU	Ar	300	$7.50\cdot10^{-5}$	-	-	22.4	-	-	16.0 [b]	-	-	0.5	[18]
FAU	Ne	300	$5.91\cdot10^{-6}$	-	-	118.5	-	-	33.0 [b]	-	-	0.3	[18]
MFI	CH_4	300	$1.42\cdot10^{-3}$	-	-	9.44	-	-	5.0 [c]	-	-	0.2	[18]
MFI	CH_4	300	$1.39\cdot10^{-3}$	-	-	10.2	-	-	5.0 [c]	$5.18\cdot10^{-5}$	0.82	0.2	[18]
MFI	CO_2	300	$4.18\cdot10^{-3}$	-	-	2.08	-	-	6.0 [b]	$9.50\cdot10^{-7}$	0.91	0.2	[18]
MFI	Ar	300	$1.22\cdot10^{-4}$	-	-	9.56	-	-	6.3 [b]	$1.82\cdot10^{-7}$	1.38	0.3	[18]
MFI	Ne	300	$1.90\cdot10^{-5}$	-	-	15.7	-	-	18.0 [b]	-	-	0.5	[18]

[a] The CH_4 data at 300 K is extrapolated from the constants estimated at 373, 473 and 573 K. [b] q^{sat} is based on the total saturation loading that follows from the adsorption isotherm model parameters listed in Table 1. [c] q^{sat} was fixed during data fitting, but chosen based on adsorption or diffusion data trends. [d] TW: This work.

3.3 Single component diffusivities in DDR, CHA, MFI and FAU

Figure 5 shows the single component MS and self diffusivities of CO_2, N_2, O_2, Ar and Ne in DDR as a function of the loading at 300 K. In Figure 6 the single component MS- and self diffusivities of CO_2, CH_4, Ar and Ne in zeolites CHA, MFI and FAU are presented, also at 300 K. The lines in both figures represent model fits with the RSM of which the estimated parameter values are listed in Table 2. For each zeolite-guest system the adsorption isotherm is described by a three-site Langmuir model. The adsorption isotherm parameters are determined in the current work and are presented in Table 1. The adsorption data, based on GCMC simulations, are taken from literature as indicated in Table 1. A model fit of the MS diffusivities yield a lumped RS diffusivity constant ($q_i^{sat*} Đ_i^*(0)$) and RS adsorption equilibrium constant (K_i^*).

In case of N_2 in DDR, CH_4 in FAU, and CH_4, CO_2 and Ar in MFI the diffusivity data prompted a correction to the free volume relevant for diffusion as described in Section 2.3 of Chapter 5A. For these systems two additional parameters have been determined that describe the site irrelevant for diffusion (ID): K^{ID} and $q^{\mathrm{sat,ID}}$. For the MS diffusivity data of CH_4 in MFI a second fit is presented in Figure 6 where this correction was ignored.

The RS parameters estimated from the MS diffusivity data are used to model the self diffusivities using Equation 21 and 22 of Chapter 5A. The value of parameter a, which represents the ratio of the MS and self exchange diffusivity, is unknown and is optimized to describe the self diffusivity data best. In case of the CH_4 diffusion in CHA only suitable self diffusivity data could be found in literature. Therefore, the RS parameters have been estimated directly from the self diffusivity data, assuming that a equals 0.8. The choice for this specific value of a is made because it is also approximately valid for CO_2, Ne and Ar in CHA.

Even though a variety in loading dependencies is observed, a good RSM description of the MS diffusivity data is obtained in all cases. Only the model fit of the CH_4 self diffusivity data in CHA shows significant deviations: the low loading diffusivity data is under predicted.

It is remarkable that in case of MFI a correction with respect to the free space relevant for diffusion was required for three components (CH_4, CO_2 and Ar) whereas this was only required for one component for the other zeolites. This can very well be due to the more complex pore network of MFI compared to CHA, DDR and FAU. A distinction can be made between diffusion in the straight and zigzag channels. If, for instance, diffusion in MFI occurs predominantly through the straight channels, the space in the zigzag channels might be considered as ‘dead volume’ that is irrelevant for diffusion.

A good relation between the MS- and self diffusivity is obtained through the concept of the self-exchange diffusivity based on RS properties. The proposed relation $Đ_{ii}^* = a_i \cdot Đ_i^*$ leads to good results because the ratio of the RS self-exchange diffusivity and the MS diffusivity are quite independent of the loading. The assumption $a = 1$ appears to be valid for DDR. In case of CHA, MFI and FAU the optimal values of *a* are smaller than one: the ‘friction’ effects between molecules are under predicted when assuming $a = 1$. A possible interpretation is that not only the RS that controls mass transport and additional ‘friction’ occurs at other sites that need to be accounted for. Interestingly, the estimated values of *a* seem to be related to the type of zeolite; DDR ($a \approx 1$), CHA (≈ 0.8), MFI (≈ 0.2) and FAU (≈ 0.5). The only exception in the current dataset is Ne in MFI and FAU. Note that in case of CHA *a* is close to one and very similar to the DDR-value, which could be expected based on their similar topology. The relative low value of *a* in case of MFI (≈ 0.2) could be due to the relative narrow channels that prohibits molecules to pass easily. This could explain why Ne has a somewhat higher value of *a* (≈ 0.5) because it is likely that these small molecules ($d \approx 0.28$ nm) can pass each other much easier in the MFI channels compared to CO_2, Ar and CH_4. DDR and CHA do have very narrow window openings that allow passage of one molecule at a time, but the cages are spacious enough to allow easy passage of all considered molecules. In case of FAU a similar value of *a* as found for CHA and DDR could be expected because also in this large-pore zeolite molecules can pass each other easily in the large cages. But, apparently additional ‘friction’ effects play a role. Possibly mass transport through the relative large cavity imposes additional effects.

It appears that an upper limit of $a = 1$ is found. If mass transport is completely determined by the RS and molecules have an optimal opportunity to pass each other in between the RS (*e.g.* in the cage), the RS self-exchange diffusivity equals the RS MS diffusivity.

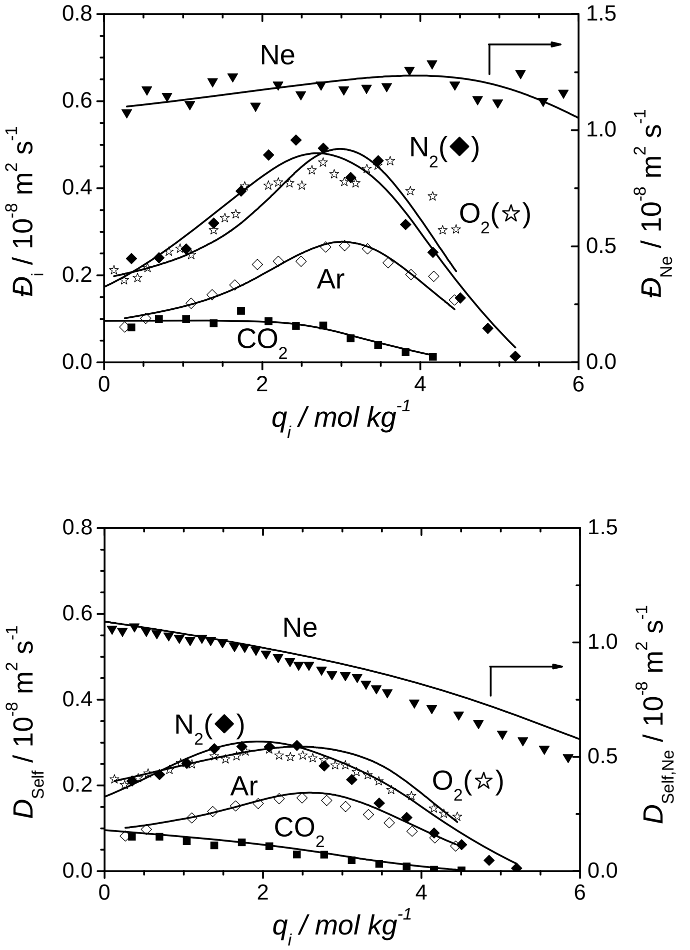

Figure 5. MD diffusion data of CO_2, N_2 [15], O_2, Kr, Ar and Ne [1] in all silica DDR at 300 K. Lines represent modelling results of the RSM: the MS diffusivities are fitted to equation (21), the self diffusivities are predicted assuming $Đ_{ii}^* = Đ_i^*$.

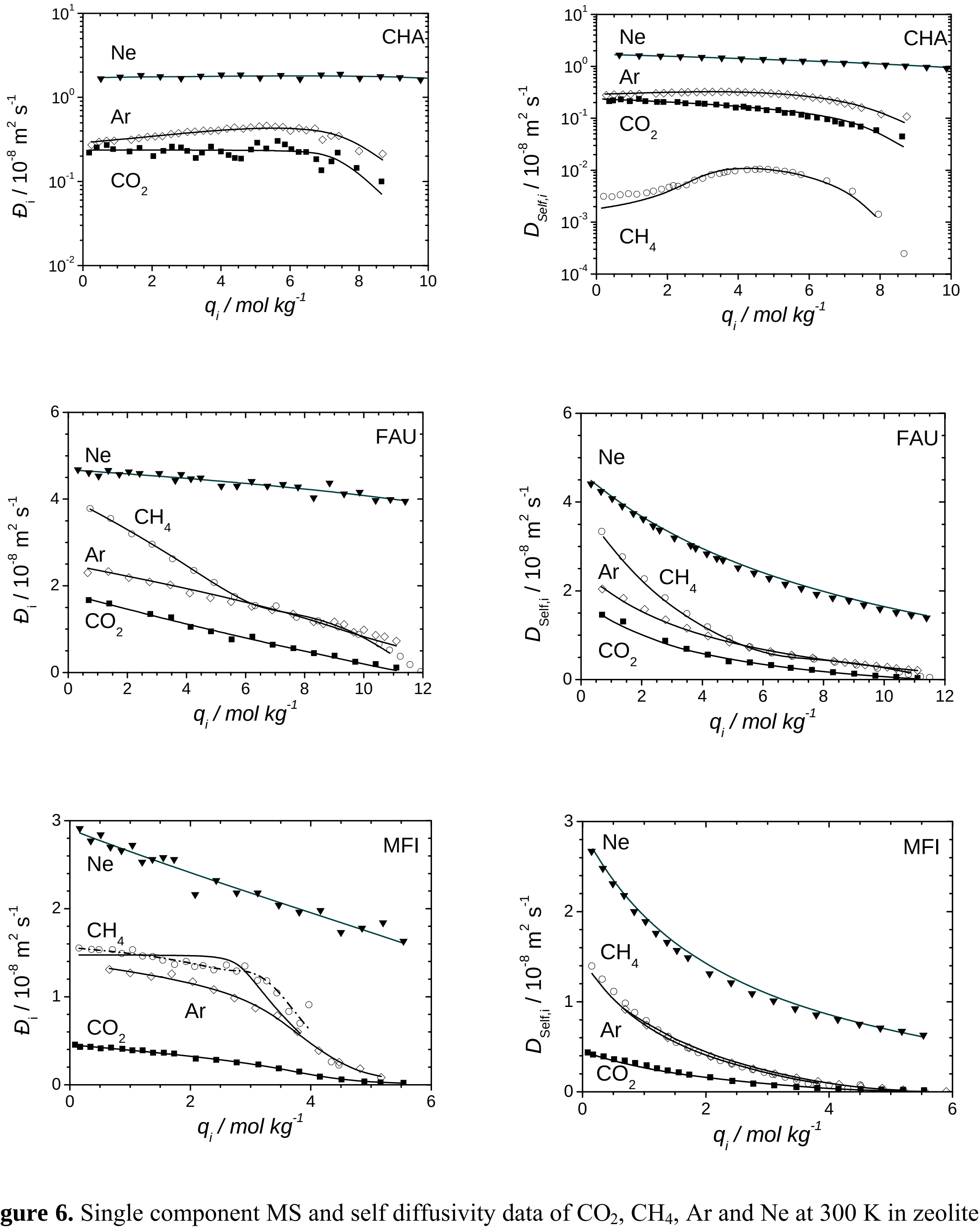

Figure 6. Single component MS and self diffusivity data of CO_2, CH_4, Ar and Ne at 300 K in zeolites CHA, MFI and FAU calculated using MD [1]. The lines represent model fit results as described in the text in more detail. The solid line in case of CH_4 in MFI represents the model fit assuming that the total occupancy is relevant for diffusion, the dashed line when assuming that part of the free space is irrelevant for diffusion.

3.4 Generalization of single component results

A point of interest is the variety of MS diffusivity loading dependencies that is observed, and discussed by Krishna and van Baten in detail [18,20]. In the case of MFI and FAU the diffusivity decreases continuously with increasing loading but for several components in CHA and DDR the diffusivity first increases with increasing loading, passes through a maximum and approaches very low diffusivities near the saturation loading. An important observation is that when the molecule size is close to the zeolite pore size the latter loading dependency is observed [20], which is the case for the considered DDR and CHA systems.

From the diffusivity data the RS adsorption equilibrium constant is derived which provides information on the adsorption properties of the RS. In order to compare the RS adsorption properties to the bulk adsorption properties the ratio of the RS occupancy and the occupancy of the first site (A) of the bulk isotherm is calculated (θ^* / θ^A). This ratio is used to characterize the relative strength of the RS adsorption site. In Figure 7 this ratio is plotted as a function of the ratio of the diameter of a molecule and the size of the zeolite pore or window at a total occupancy of 0.2 for all considered zeolite-guest systems. The RS occupancy is calculated based on the estimated RS adsorption equilibrium constants (Table 2). The molecule size is adopted from Krishna and van Baten [20], the used zeolite pore diameters are given in Section 3.1. Figure 7 reveals that the RS to total loading ratio correlates very well with the molecule diameter to window size ratio. In case of the medium pore zeolite MFI and the large-pore FAU all considered molecules are significantly smaller than the pore diameter and a fairly homogenous distribution of adsorbed molecules is found, *i.e.* the first site of the bulk and RS occupancy are about the same ($\theta^* / \theta^A \sim 1$). For zeolites CHA and DDR the RS (= window site) occupancy becomes much lower than the total occupancy with increasing molecule diameter because in this region the molecule diameter approaches the pore diameter. When the molecule becomes more confined at the RS it has an increasing preference to adsorb at another adsorption location, *i.e.* the RS behaves as an increasingly weaker adsorption site.

So far the discussion about the assumed segregated adsorption is based on the RS adsorption equilibrium constants, which are the outcome of a model fit and no direct measurements. However, Krishna and van Baten have calculated the probability (%) of finding a molecule in a defined window region for several small-pore cage-like zeolites using GCMC simulations [21]. Their results for DDR at 300 K and 2000 kPa are given in Figure 8 as a function of the molecule to pore diameter ratio together with the RS to total occupancy ratio at the same conditions. Both the percentage of molecules in the DDR window and the RS to total occupancy ratio strongly decrease with increasing molecule diameter. Interestingly, the observed reduction of both properties with increasing molecule diameter is of the same order of magnitude; it appears that the level of segregation of adsorption is predicted well by the

RSM based on the diffusivity data. This indicates that the RS adsorption equilibrium constant represents physically meaningful information.

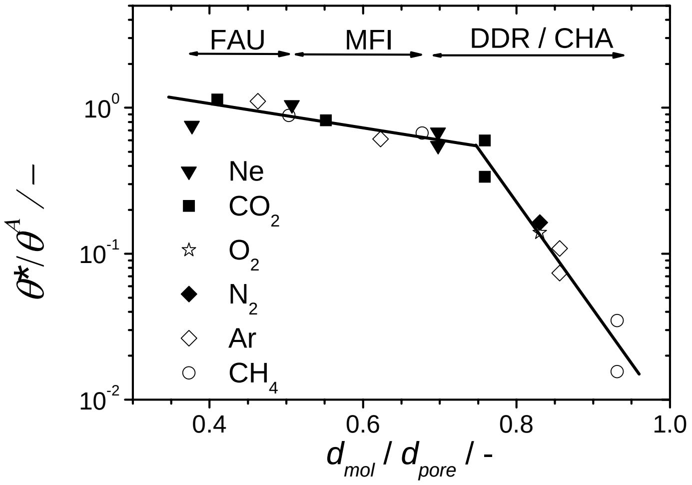

Figure 7. Ratio of the RS and total occupancy of several zeolite-guest systems as a function of the ratio of the molecule diameter and the zeolite pore size, evaluated at a total occupancy of 0.2 at 300 K. Results are based on estimated RS adsorption constants listed in Table 2.

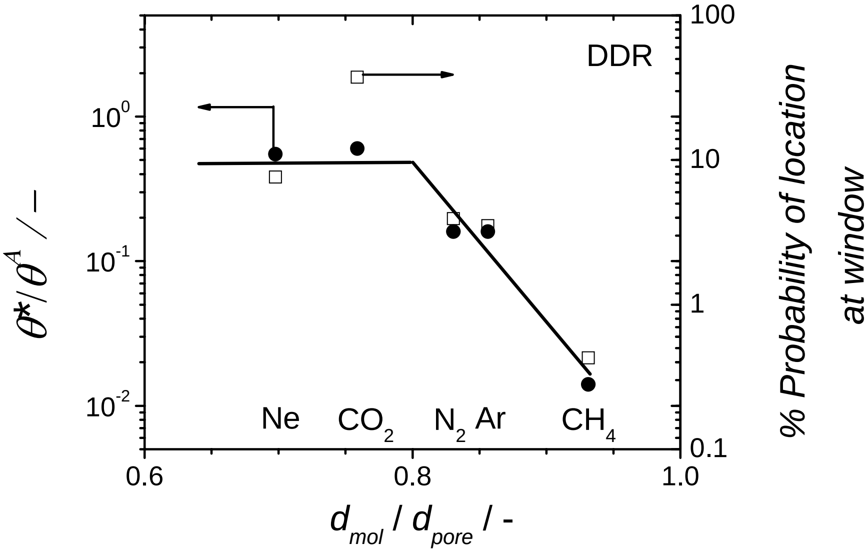

Figure 8. Ratio of the RS and total occupancy of several light gases in DDR as a function of the ratio of the molecule diameter and the zeolite pore size, evaluated at 2000 kPa at 300 K (solid circles), together with the probability of finding a molecule in the DDR window region determined by GCMC simulations (open squares), taken from [21].

3.5 Mixture results

In Figure 9, 10 and 11 the self and MS (Δ_{ii}) diffusivities of several equimolar mixtures (Ar/Ne, CO_2/Ne, CO_2/Ar and CH_4/Ar) in zeolites CHA, FAU and MFI at 300 K are presented as a function of the total loading [1]. Note that the collective diffusivity is analyzed via the modified Onsager coefficient Δ_{ii}. In case of CHA the CH_4/Ar mixture is not considered because the poor CH_4 single component model fit would propagate directly into the mixture results. For MFI no CO_2/Ar data were available. The lines represent modelling results as described in detail in Section 2.2 of Chapter 5A. Some important points regarding the modelling approach are discussed next.

Firstly, the RS saturation loading cannot be determined directly from the diffusivity data. In the binary mixture diffusivity modelling one parameter is unknown: the ratio of the RS saturation loading of the two species in the mixture. It is chosen to optimize this ratio to fit the mixture self- and MS (Δ_{ii}) diffusivities best; the 'optimal' ratios are given in Table 3. The mixture results are therefore no predictions *a priori*.

A complicating factor in the mixture modelling is to account for the free space relevant for diffusion. Several single component results suggested that not all free space is relevant for diffusion. It remains unclear if this irrelevant space for diffusion represents a certain dead volume or a specific positional rearrangement of molecules inside the zeolite. Therefore, extension of this concept to mixtures is not straightforward. In the current work it is chosen to model CH_4 in MFI assuming that all free space is relevant for diffusion; this led to a reasonable model fit of the single component diffusivity data. In the case of CH_4 in FAU and Ar and CO_2 in MFI an adsorption site that represents space irrelevant for diffusion is found at very high loading. Therefore, it is assumed that at the considered mixture loading all molecules inside the zeolite occupy space relevant for diffusion. This assumption is valid at low loadings but may become invalid at high loadings. The saturation loading used to calculate the free space is corrected with respect to the part irrelevant for diffusion as done in the case for the single component system. Mathematically this is expressed by the following relation:

$$1-\theta^{\#}=1-\frac{q_i}{q_{tot,i}^{sat}-q_i^{sat,ID}}-\frac{q_j}{q_{tot,j}^{sat}-q_j^{sat,ID}}, \qquad (1)$$

which is a simplified form of Equation 50 of Chapter 5A to describe the free space relevant for diffusion for a binary mixture.

For all mixtures in CHA and FAU an excellent description of the mixture diffusivity data is obtained. For MFI the modelling results are very good, however some deviations are observed for in particular the CH_4 data. A reason could be the free space irrelevant for diffusion that is not accounted for adequately. The more complex structure of MFI complicates the mixture modelling; nevertheless, still good results are obtained.

The ratio of the RS saturation loadings is chosen to describe the mixture data optimally. This ratio influences the results in two ways. Firstly, it affects the RS exchange diffusivities ($Đ_{ij}^*, Đ_{ji}^*$), *cf.* Equation 26 of Chapter 5A, and secondly it influences the composition at the RS. Particularly the latter aspect influences the results significantly since a difference in saturation loading can lead to (strong) preferential adsorption effects. The optimal RS saturation loading ratios for each zeolite-mixture system are listed in Table 3 together with the bulk saturation loadings based on the total saturation loadings given in Table 2.

In case of the small-pore zeolites DDR and CHA an equal RS saturation loading leads to the best description of the data, for the large-pore zeolite FAU a RS saturation loading equal to the bulk saturation loading seems the most appropriate. For the medium-pore zeolite MFI a ratio in between one and that of the bulk saturation loadings appears optimal. To illustrate the sensitivity for the RS saturation loading ratio a model prediction using another ratio extreme is added for CO_2/Ne mixtures in CHA (Figure 9) and FAU (Figure 10). It becomes clear that using an equal RS saturation loading in the case of FAU and a RS saturation loading ratio equal to the bulk saturation loading ratio for CHA leads to significantly worse model predictions. The interpretation is that in case of the small-pore zeolites the RS (≡ window site) is strongly confined allowing only one molecule to adsorb. The overall (bulk) saturation loading ratio can be very different since this is determined up to a large extent by adsorption in the more spacious cages. In FAU the window region is of such a size that more than one molecule can adsorb leading to RS saturation loading ratios similar as expected based on the bulk properties. MFI has a medium pore size which leads to the situation where it is difficult to predict what the RS saturation loading is, but the RS saturation loading ratio comes down to packing of the molecules at the RS. These effects can be very specific for each zeolite-guest system and hard to predict. However, for the considered light gases two important generalizations can be made: for small-pore zeolites an equal saturation loading and for large-pore zeolites a RS saturation ratio equal to the bulk saturation loading leads to good results. In this way a good *prediction* of mixture diffusivities of light gases in zeolites DDR, CHA and FAU is possible. It is suggested that this approach is valid for light gases in small- and large-pore zeolites in general, or at least provides the extreme cases for mixture diffusion.

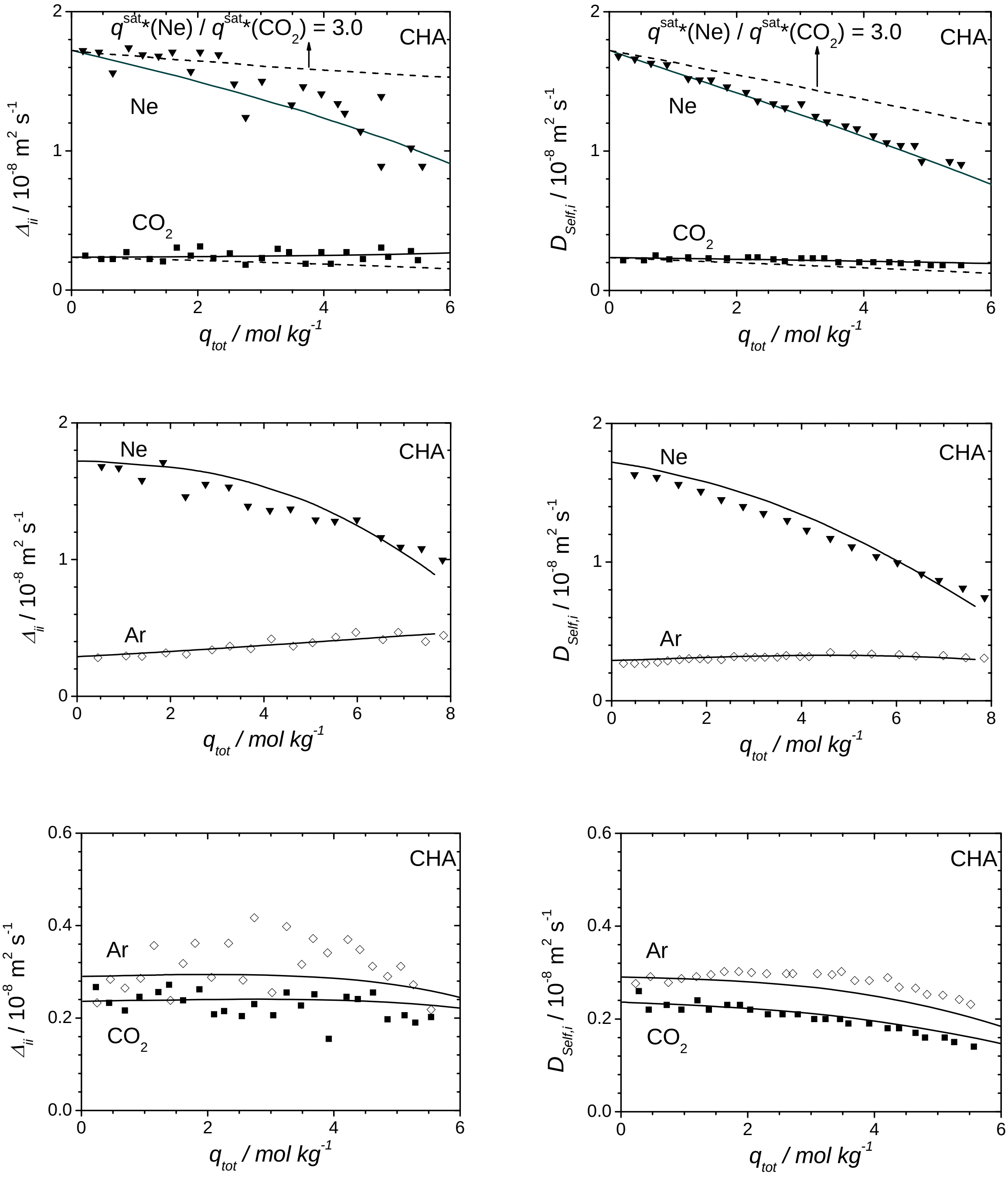

Figure 9. CO_2, Ar and Ne diffusivities (D_{Self} and Δ_{ii}) in a set of mixtures in CHA as a function of the total loading at equal composition at 300 K. The data points, solid lines and dashed lines represent MD simulations results from [1], RSM predictions with optimized RS saturation loading ratios (table 3) and RSM predictions with RS saturation loading ratios equal to the total saturation loading ratio (=3, only CO_2/Ne mixture), respectively.

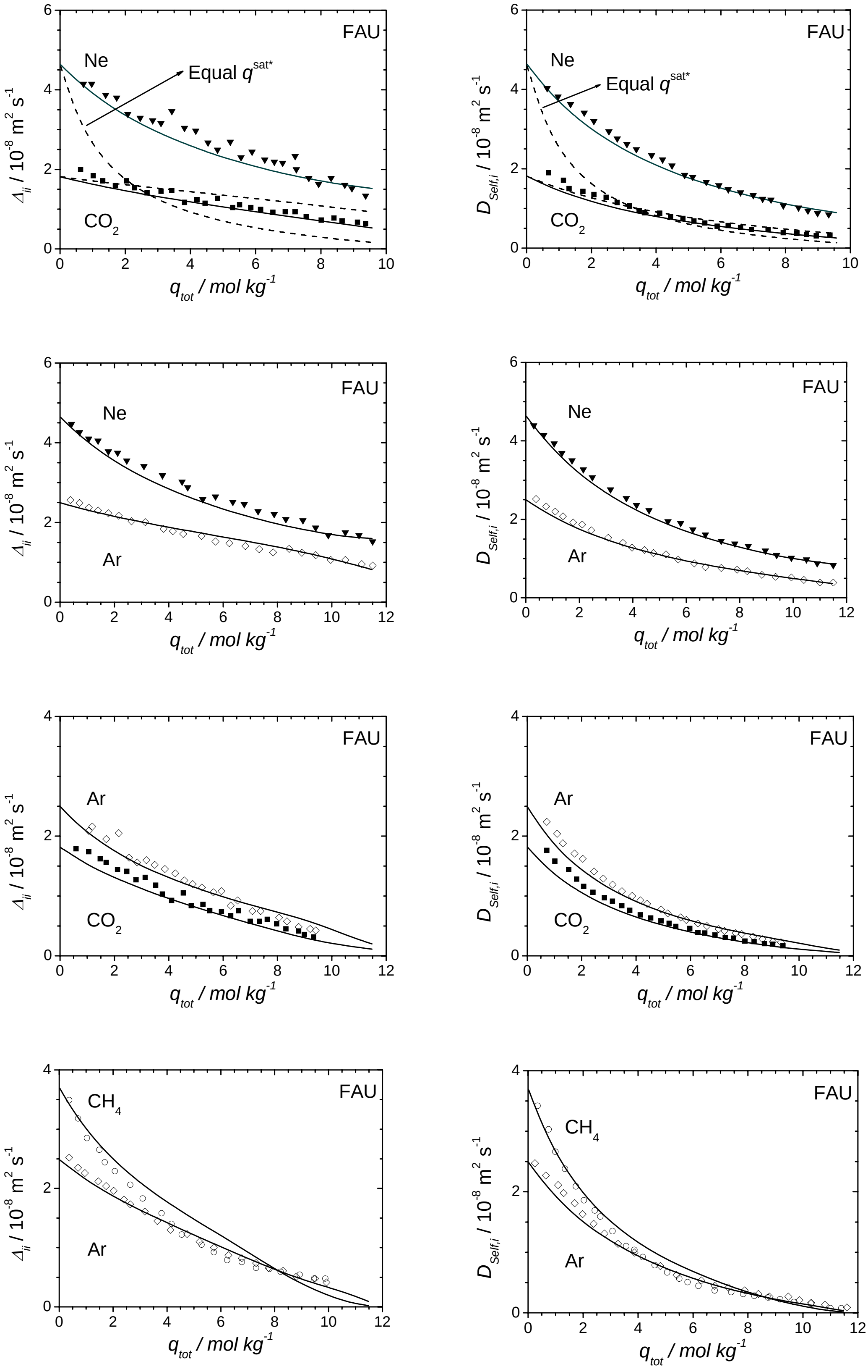

Figure 10. CO_2, CH_4, Ar and Ne diffusivities (D_{Self} and Δ_{ii}) in a set of mixtures in FAU as a function of the total loading at equal composition at 300 K. The data points, solid lines and dashed lines represent MD simulations results from [1], RSM predictions with optimized RS saturation loading ratios (Table 3) and RSM predictions with RS saturation loading ratios equal to one (only CO_2/Ne mixture), respectively.

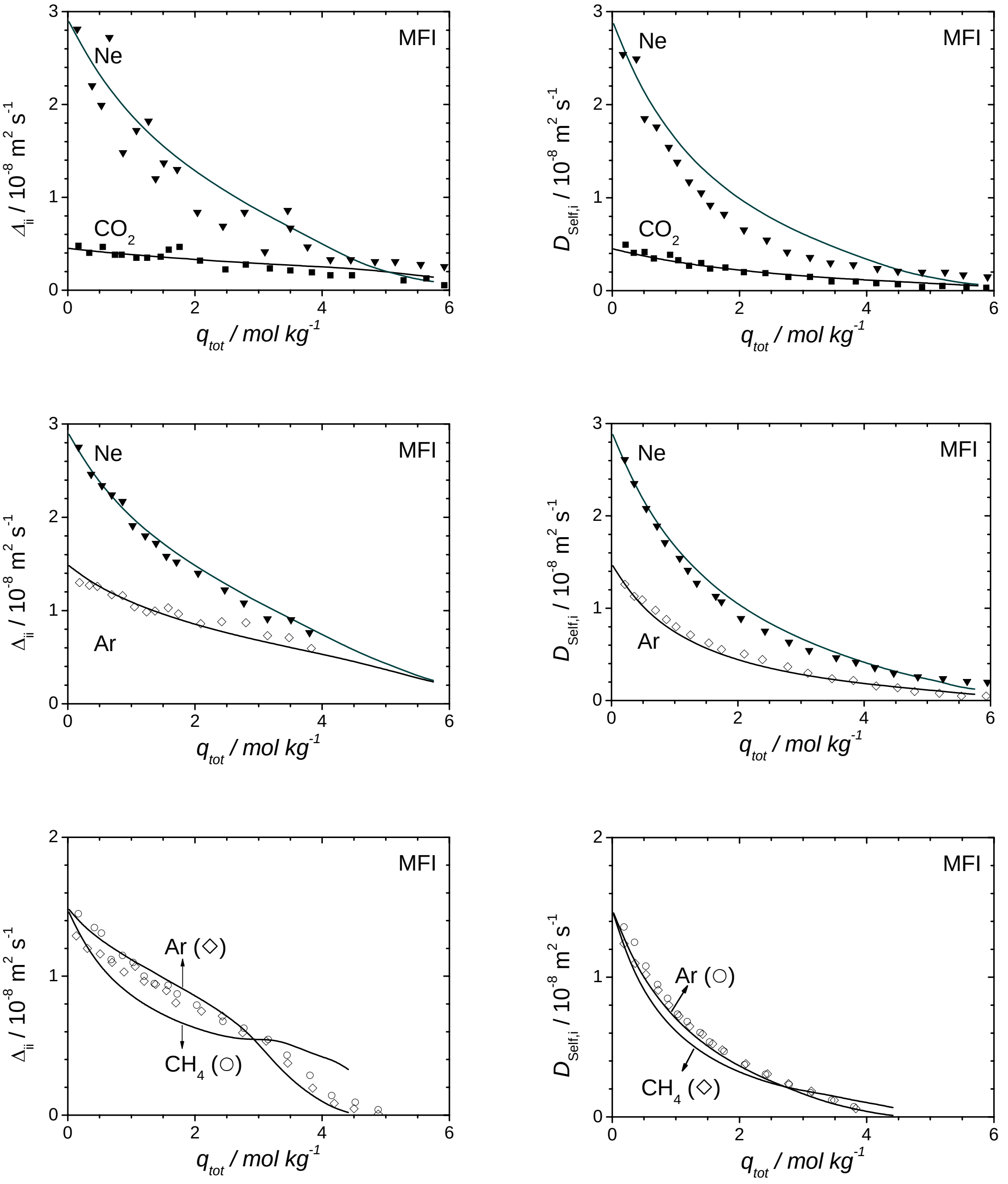

Figure 11. CO$_2$, CH$_4$, Ar and Ne diffusivities (D_{Self} and Δ_{ii}) in a set of mixtures in MFI as a function of the total loading at equal composition at 300 K. The data points and solid lines represent MD simulations results from [1] and RSM predictions with optimized RS saturation loading ratios (Table 3), respectively.

Table 3. RS saturation loading ratios of several gas mixtures in zeolites DDR, CHA, MFI and FAU. Ratios based on the total saturation loading (bulk) together with the ratios that gave the 'optimal' result in the mixture model predictions. The DDR data are taken from [2][Chapter 5C].

Zeolite	Mixture (*i,j*)	q_i^{sat*} / q_j^{sat*}	
		Optimal	Bulk
DDR	Ne/Ar	1.0	2.5
DDR	N_2/CO_2	1.0	1.2
CHA	Ne/CO_2	1.0	3.1
CHA	Ne/Ar	1.0	3.0
CHA	Ar/CO_2	1.0	1.0
MFI	Ne/CO_2	1.5	3.0
MFI	Ne/Ar	1.7	2.9
MFI	Ar/CH_4	1.0	1.3
FAU	Ne/CO_2	3.0	2.9
FAU	Ne/Ar	2.5	2.1
FAU	Ar/CO_2	1.3	1.4
FAU	Ar/CH_4	1.1	1.3

3.6 Application RSM to aluminium containing zeolitic systems

This diffusion study encompasses only all-silica forms of zeolites MFI, DDR, CHA and FAU, which are much more ideal systems than their aluminium containing counterparts. The current approach is highly relevant for practice since DDR [17][Chapter 2] and MFI [22] type zeolites are often used in this form and also zeolite CHA [23] has been synthesised in the all-silica form. However, many applications involve zeolites containing also framework- aluminium and their accompanying charge compensating cations. It is known that the diffusivity in such systems can be very different compared to the all-silica form [24,25], mostly related to the existence of strong and weak adsorption sites [26]. Although the RSM has been applied successfully to all-silica systems, it is an intriguing question up to which extent the RSM can be applied in aluminium-containing systems. Although beyond the scope of the current paper, some aspects are addressed on this topic.

Since the RSM starts from the idea of segregated adsorption such inhomogeneous systems could be an excellent opportunity to apply this model. The RSM could provide the possibility to account for the inhomogeneity of the system. But, the approach as presented in this paper relies on the usage of the IAST to predict mixture loadings and fugacities. An inhomogeneous surface can lead to severe deviations when using the IAST to predict mixture loadings [27]. Since the relevant sites represent a homogeneous part of the inhomogeneous total system, application of the IAST to calculate mixture RS loadings is not expected to be problematic. This in contrast to prediction of the total loadings using the IAST which can be expected to contain deviations. To which extent this imposes insuperable problems depends on the way the diffusion problem is formulated. Simulations studies, like the current work, usually start from a mixture defined by known loadings. In this case the IAST is used to back-calculate the mixture fugacities from known loadings. The calculated fugacities are subsequently used to calculate the RS loadings. In such a calculation scheme the IAST plays a decisive role and errors will probably have a very strong effect on the final result. In practical situations however, usually the mixture *fugacities* are the starting point. In this case the RS loadings and RS exchange diffusivity can be predicted without application of the IAST to total system properties. It is only the free space that is calculated using the IAST in this way. In this case the errors introduced by inappropriate use of the IAST are expected to be minor and at least reasonable results can be expected by applying the RSM.

4 Conclusions

The Relevant Site Model (RSM) has been applied to model single component and mixture diffusivities of several light gases (CO_2, CH_4, Ar and Ne) in zeolites DDR, CHA, MFI and FAU obtained from Molecular Dynamics (MD) simulations. In case of DDR also N_2 and O_2 have been considered. Specific attention has been paid to diffusion of CH_4 of which MS and self diffusivities have been estimated with MD simulations at 300, 373, 473 and 573 K.

Using the RSM a good model description of the loading dependency of the Maxwell Stefan (MS) diffusivity has been obtained for all considered single component zeolite-guest systems. The diffusivity data of CH_4 in FAU and of CO_2, Ar and CH_4 in MFI suggested that not all available free space calculated from the adsorption isotherm is relevant for diffusion. An analysis with the RSM of the CH_4 diffusivity data in DDR led to a temperature independent RS adsorption enthalpy and RS activation energy for diffusion.

The MS diffusivity is related to the self diffusivity via the RS self-exchange diffusivity and RS occupancy with good result for all systems. The RS self-exchange diffusivity ($Đ_{ii}^{*}$) can be related to the RS MS diffusivity ($Đ_{i}^{*}$) via: $Đ_{ii}^{*} = a_i \cdot Đ_{i}^{*}$. The constant a_{i} is one (DDR) or close to one (CHA), and therefore a direct prediction of the 'friction' effects is possible. For zeolite FAU and MFI systems the values of *a* are considerably smaller.

The RS adsorption equilibrium constant estimated from the diffusivity data yields physically meaningful information about the adsorption properties of the RS. A comparison is made of the ratio of the RS and total occupancy and the probability of finding a molecule in the window region of DDR calculated from GCMC simulations [21]. This comparison revealed that the ratio calculated for a series of light gases in DDR correlates very well with the probability of finding a molecule in the window region. Moreover, the level of adsorption segregation, expressed as the ratio of the RS and the total occupancy, correlates well with the molecule to pore (window) diameter ratio. At low ratios (FAU, MFI systems) (almost) no segregated adsorption is found and when the molecule diameter approaches the window diameter (DDR and CHA systems) segregated adsorption is found due to steric effects.

Good predictions of the self- and MS diffusivities of several binary equimolar mixtures (Ar/Ne, CO_2/Ne, CO_2/Ar and CH_4/Ar) in zeolites CHA, FAU and MFI could be made. Key aspects are that the 'friction' effects between molecules and competitive adsorption effects are related to the RS instead of the total occupancy. The RS saturation loadings are unknown and the ratio of the RS saturation loadings in the binary mixture is optimized to obtain the best model predictions. For small-pore zeolites CHA and DDR the RS saturation loadings should be taken equal. This implies that only one molecule can adsorb the strongly confined RS. In case of the large-pore zeolite FAU the optimal RS saturation loading ratio equals the bulk saturation loading. The window region (RS) of FAU allows the adsorption of multiple molecules which results in corresponding adsorption behaviour. For the medium-pore zeolite MFI the optimal RS saturation ratio is in between one and the bulk ratio.

Finally, previous work showed that the RSM has been applied successfully to describe the loading dependency of diffusion of a series light gases and mixtures thereof in zeolite DDR [2,15][Chapter 5B and 5C]. The current work demonstrates that the RSM is not restricted to this particular zeolite, but is successfully extended to light gases in zeolites CHA, MFI and FAU.

References

[1] R. Krishna and J. M. van Baten, *Chemical Engineering Science*, 63, **2008**, 3120, supporting information.

[2] J. van den Bergh, S. Ban, T. J. H. Vlugt, and F. Kapteijn, *Journal of Physical Chemistry C*, 113, **2009**, 21856.

[3] B. Smit, *Molecular Physics*, 85, **1995**, 153.

[4] B. Smit, *Journal of Physical Chemistry*, 99, **1995**, 5597.

[5] T. J. H. Vlugt, R. Krishna, and B. Smit, *Journal of Physical Chemistry B*, 103, **1999**, 1102.

[6] T. J. H. Vlugt and M. Schenk, *Journal of Physical Chemistry B*, 106, **2002**, 12757.

[7] C. Baerlocher, L.B.McCusker, and D.H.Olson, Atlas of Zeolite Framework Types, **2007**, Elsevier, Amsterdam.

[8] D. Dubbeldam, S. Calero, T. J. H. Vlugt, R. Krishna, T. L. M. Maesen, and B. Smit, *Journal of Physical Chemistry B*, 108, **2004**, 12301.

[9] R. Krishna and J. M. van Baten, *Chemical Physics Letters*, 446, **2007**, 344.

[10] D. Frenkel and B.Smit, Understanding Molecular Simulation: from Algorithms to Applications 2nd ed., **2002**, Academic Press, San Diego.

[11] D. Dubbeldam, D. C. Ford, D. E. Ellis, and R. Q. Snurr, *Molecular Simulation*, 35, **2009**, 1084.

[12] R. Krishna and J. M. van Baten, *Journal of Physical Chemistry B*, 109, **2005**, 6386.

[13] D. Dubbeldam and R. Q. Snurr, *Molecular Simulation*, 33, **2007**, 305.

[14] D. Dubbeldam, E. Beerdsen, T. J. H. Vlugt, and B. Smit, *The Journal of Chemical Physics*, 122, **2005**, 224712.

[15] J. van den Bergh, S. Ban, T. J. H. Vlugt, and F. Kapteijn, *Journal of Physical Chemistry C*, 113, **2009**, 17840.

[16] International Zeolite Association, www.iza-structure.org/databases/, Visited **2009**.

[17] J. van den Bergh, W. Zhu, J. Gascon, J. A. Moulijn, and F. Kapteijn, *Journal of Membrane Science*, 316, **2008**, 35.

[18] R. Krishna and J. M. van Baten, *Chemical Engineering Science*, 63, **2008**, 3120.

[19] R. Krishna and J. M. van Baten, *Chemical Engineering Journal*, 133, **2007**, 121.

[20] R. Krishna and J. M. van Baten, *Microporous and Mesoporous Materials*, 109, **2008**, 91.

[21] R. Krishna and J. M. van Baten, *Separation and Purification Technology*, 61, **2008**, 414.

[22] F. Kapteijn, W. J. W. Bakker, J. van de Graaf, G. Zheng, J. Poppe, and J. A. Moulijn, *Catalysis Today*, 25, **1995**, 213.

[23] M. J. Diaz-Cabanas, P. A. Barrett, and M. A. Camblor, *Chemical Communications*, **1998**, 1881.

[24] E. Garcia-Perez, D. Dubbeldam, B. Liu, B. Smit, and S. Calero, *Angewandte Chemie-International Edition*, 46, **2007**, 276.

[25] S. Ban and T. J. H. Vlugt, *Journal of Chemical Theory and Computation*, 5, **2009**, 2858.

[26] M. O. Coppens, A. T. Bell, and A. K. Chakraborty, *Chemical Engineering Science*, 54, **1999**, 3455.

[27] M. Murthi and R. Q. Snurr, *Langmuir*, 20, **2004**, 2489.

5E

The Relevant Site Model: Modelling permeation of CO_2/CH_4, N_2/CH_4 and CO_2/Air mixtures across a DD3R zeolite membrane

Single component (CO_2, CH_4 and N_2) and equimolar binary mixture (CO_2/CH_4, N_2/CH_4 and CO_2/Air) permeation data across a disc-shaped all-silica DDR zeolite membrane have been the subject of a thorough modelling study over a challenging broad temperature (220-373 K) and feed pressure (101-1500 kPa) range.

The mass transport through the zeolite layer is evaluated for two rival, Maxwell Stefan-based, models: the Relevant Site Model (RSM) and the so-called Reed Ehrlich (RE) approach. Both models have been introduced to account for the strong loading dependency of the diffusivity in small-pore cage-like zeolites like DDR. High pressure adsorption isotherms (up to 7000 kPa) measured on DDR crystals are incorporated to describe adsorption on the zeolite.

Both the RSM as the RE approach yield an excellent model fit of the single component permeation data. However, for both models the N_2 and CH_4 data did not allow an accurate estimation of the model fit parameters. Both models can lead to a good prediction of comparable quality of the mixture permeation data based on the single component model fit parameters. The RE approach is very sensitive towards the model input parameters and the estimated mixture loading, which both can be very hard to determine accurately in practice. The RSM does not suffer from both these issues, which is an evident advantage with respect to application of this model.

This chapter is based on the following publication:

J. van den Bergh, Marjo Mittelmeijer-Hazeleger, and F. Kapteijn, *Journal of Physical Chemistry C*, 114, **2010**, 9397.

1 Introduction

The feasibility of using zeolite membranes in chemical industry was demonstrated by the development of a large-scale pervaporation plant based on NaA zeolite membranes to dewater alcohols [1]. Moreover, small-pore zeolite membranes are considered serious candidates for natural gas purification (CH_4/CO_2 separation) [2-5][Chapter 2]. To design a zeolite membrane based process a good model description of multi-component mass transport is required. Preferably a prediction of mixture membrane permeation fluxes is desired based on single component permeation properties [6].

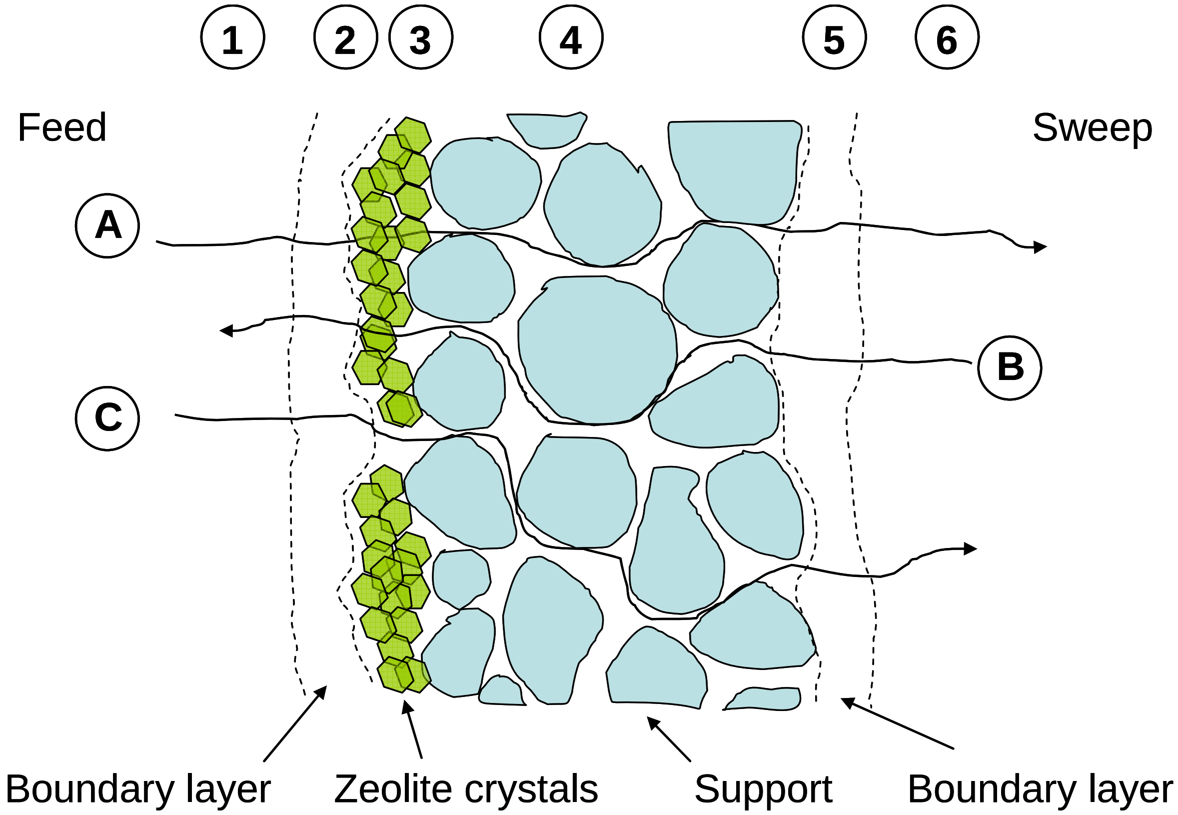

Figure 1. Schematic representation of the permeation of a molecule through a zeolite membrane. A: Starting from the Feed (1) the molecule passes through a boundary layer (2), a layer of intergrown zeolite crystals (3), a macro-porous support layer (4), another boundary layer at the sweep side (5) and ends up in the sweep flow. In the case of B back-permeation of the sweep gas is depicted, which is the inverse trajectory of A. Case C represents permeation through a defect in the zeolite layer.

Zeolite membranes commonly consist of a thin zeolite layer of micrometer thickness on top of a macro-porous support layer as depicted in Figure 1. Several aspects can influence the observed membrane permeation flux. Firstly, a hydrodynamic boundary layer can be present that separates the membrane from the bulk flow. This boundary layer can lead to concentration polarization effects. Recently, it was shown that mixture CO_2/CH_4 fluxes through a tubular SAPO-34 membrane were strongly influenced by such effects at high pressures [7]. Secondly, the macro-porous support layer can introduce a significant additional mass transfer resistance [8-10]. Mass transport through a zeolite crystal is schematically shown in Figure 2. Usually this mechanism is simplified by assuming the intracrystalline diffusion is the rate limiting step and consequently the concentration at the crystal surfaces are considered in equilibrium with the surrounding gas phase. However, surface adsorption can be limiting [11] and molecules can experience surface barriers upon entering and leaving zeolite crystals (*e.g.* [12-14]), as anticipated by Barrer *et al.* [15]. In addition to this, various examples are known that a zeolite crystallite consists of several subunits leading to additional intra-crystalline barriers and anisotropic diffusion [12,16-20]. Anisotropy of diffusion can also be an inherent property of a zeolite topology. In this case a zeolite layer composed of randomly oriented crystals can lead to distinct different mass transport characteristics per individual crystal [21].

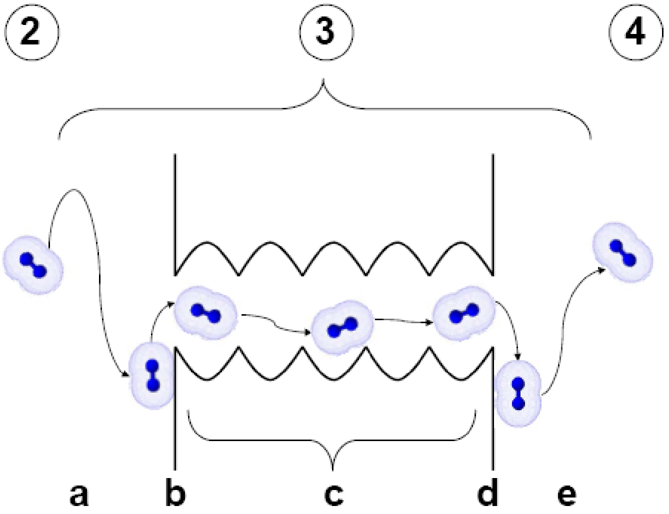

Figure 2. Schematic representation after Barrer [15] of the trajectory of a molecule passing through a zeolite crystal: adsorption at the crystal surface (a), entering of the zeolite pore (b), transport through the zeolite pores (c), escaping from the zeolite pores to the crystal surface (d) and desorption from the surface to the gas phase (e). Numbers are related to Figure 1.

Besides transport through the zeolite layer also parallel flow passing through defects can occur. Under the influence of the thermal expansion mismatch between zeolite crystals and the support layer defects can be created upon temperature increase [22]. Moreover, inter-crystalline defects can close when crystals swell upon adsorption [23]. Counter-diffusion of the sweep gas can influence the feed gas permeation in the boundary layers, the support layer and the zeolite layer by momentum transfer, or in case of the zeolite layer, adsorption.

Intra-crystalline transport description is of utmost importance for accurate model predictions. The generalized Maxwell Stefan approach to mass transport appears to be the most successful approach to describe mixture diffusion through zeolite membranes [6,10,24-28]. However, a recurring problem is the loading dependency of the diffusivity which severely complicates modelling. This loading dependency appears to be very strong in case of small-pore zeolites that consist of cages connected by narrow window openings [29], as is the case for zeolite DDR, which is the subject of this chapter. The major part of this study is devoted to the evaluation of two rival models to account for the observed loading dependency of the diffusivity: the Relevant Site Model [30-32] and the so-called Reed Ehrlich approach [33,34], which are discussed in more detail in Sections 2.2 and 2.1 of Chapter 5A.

The objective of this work is to make a detailed modelling study of a challenging set of experimental data comprising single component (CO_2, N_2 and CH_4) and binary mixture (CO_2/CH_4, N_2/CH_4 and CO_2/Air) permeation across an all-silica DDR zeolite membrane. DDR is a small-pore 8-ring zeolite for which very promising separation performances have been reported with respect to natural gas purification [3,4,35][Chapter 2], alcohol dehydration [36], alkane/alkene separation [37-39] and high temperature H_2 separation [40] [Chapter 3].

High pressure (up to 7000 kPa) single component adsorption isotherms on DD3R crystals are presented, required as input for the single component and mixture membrane permeation modelling. Single component membrane permeation data are used to determine the model fit parameters of the Relevant Site Model and of the Reed Ehrlich approach. Based on these parameters and the adsorption isotherms mixture permeation flux predictions are made and both approaches are compared with each other. Furthermore, a sensitivity analysis on the input Relevant Site Model and Reed Ehrlich parameters is performed.

2 Experimental

2.1 Adsorption experiments

In a previous work adsorption isotherms of N_2, CO_2 and CH_4 on all-silica DD3R crystals were determined by a volumetric method up to 120 kPa [3][Chapter 2]. In the current work adsorption isotherms of these components were measured at 263, 303 and 338 K up to 7000 kPa by a gravimetric method using 2.1 g of crystals. For more details on the equipment the reader is referred to [41] and for more details on the DD3R crystals to [3][Chapter 2].

2.2 Membrane permeation experiments

The disc-shaped DD3R membrane was supplied by NGK Insulators. It consists of a zeolite layer of about 5 μm on top of a macroscopic support which has a reported pore size of 600 nm, a thickness of 1.5 mm and a diameter of 18.5 mm. The membrane was sealed by a custom made silicon O-ring leaving a 12.5 mm free diameter and a membrane area of 1.23×10^{-4} m^2 available for permeation. For SEM pictures of a similar membrane we refer the reader to [36].

Single component membrane permeation fluxes of N_2, CO_2 and CH_4 and binary equimolar N_2/CH_4, CO_2/CH_4 and CO_2/air mixtures were measured between 220 and 373 K. The total feed pressure was varied between 101 and 1500 kPa, the permeate pressure was always 101 kPa. The maximum total feed pressure of the CO_2/air mixture was only 400 kPa. The total feed flow rate was 100 ml min^{-1} (STP) in each experiment. All experiments were performed using 20 ml min^{-1} (STP) He as sweep gas flow. The concentration of the permeate and retentate flow were analysed by a Ledamass Quadrupole Mass Analyzer. A large part of the permeation data has been presented in previous works already [3,35,42][Chapter 2].

3 Results and Discussion

3.1 First considerations

On beforehand it has been verified that concentration polarization effects and He sweep gas counter-permeation do not influence the membrane permeation results. The amount of defect flow is negligible compared to the intra-crystalline permeance for CO_2 and N_2. In case of CH_4 the defect flow contribution has been estimated to be about 10% at the most, which is accounted for in all modelling results. Permeation experiments with the bare support revealed that only in case of CO_2, which has the highest flux, the support resistance is significant. The estimated CO_2 pressure at the support-membrane interface is at most 7 % higher than the permeate pressure. The support effects are accounted for by using the Binary Friction Model [43] for both single component and mixture permeation results. An in-depth discussion of all the aspects considered above is presented in Appendix 5E.I.

3.2 Single component adsorption

Single component adsorption data is required to model zeolite membrane permeation data. Adsorption isotherms of N_2, CO_2 and CH_4 on DD3R crystals have been measured up to 7000 kPa to obtain a good match with the current high pressure permeation data. In Figure 3 these adsorption isotherms of N_2, CO_2 and CH_4 on DD3R crystals are presented at 195, 263, 303 and 338 K. The 195 K isotherms are measured only up to 120 kPa and added to improve the match of the adsorption isotherms with the membrane permeation results. The order in amount adsorbed at any given temperature and pressure is: $CO_2 > CH_4 > N_2$. A good model fit with a dual-site Langmuir isotherm model is obtained over the complete temperature and pressure range for all components (Figure 3):

$$q_i = \frac{q_i^{sat,A} K_i^A p_i}{1 + K_i^A p_i} + \frac{q_i^{sat,B} K_i^B p_i}{1 + K_i^B p_i} \tag{1}$$

The estimated adsorption parameters are listed in Table 1. In case of N_2 the total saturation loading was limited to 5.4 mol kg^{-1}. Note that only in case of CO_2 the level of adsorption of the experimental data is close to saturation. Therefore, only the estimated saturation loading of CO_2 should be considered as an estimate of the real total saturation loading. In case of CH_4 and N_2 the estimated saturation loadings should be considered primarily model fit parameters.

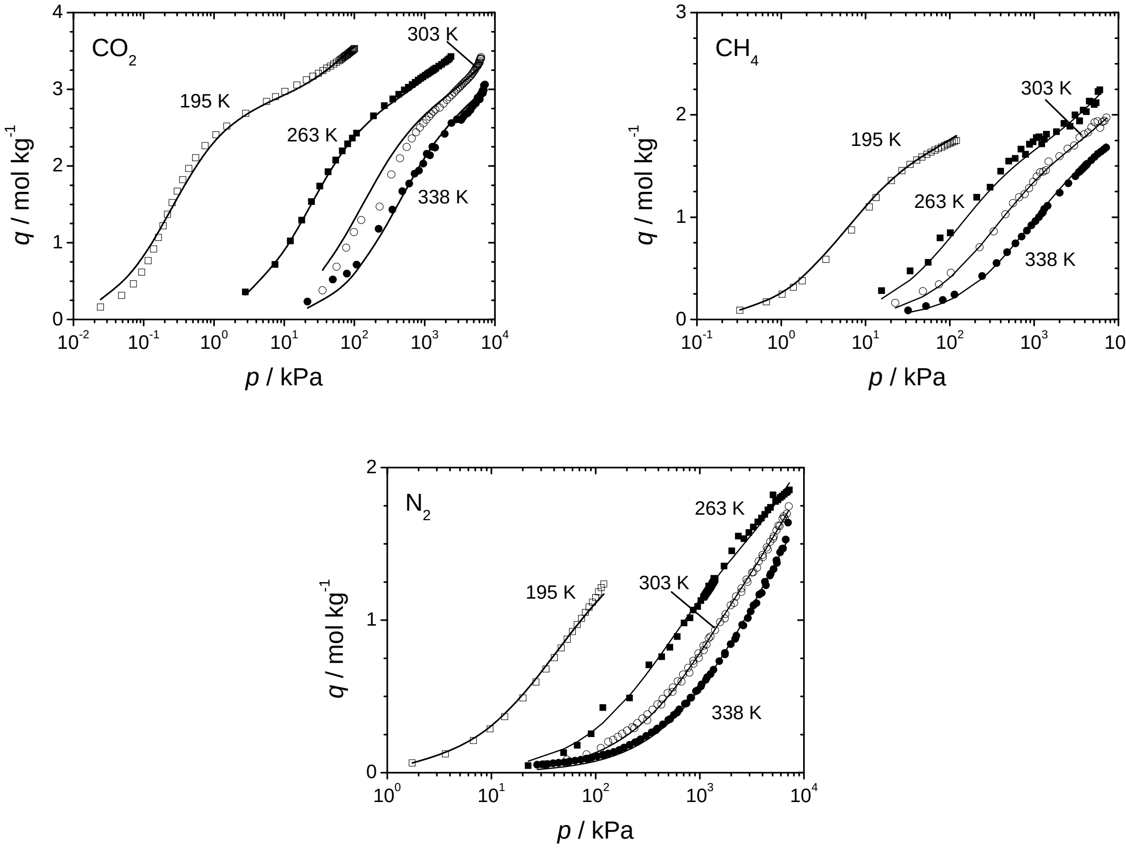

Figure 3. Adsorption isotherms of CO_2, CH_4 and N_2 on DD3R crystals at 195, 263, 303 and 338 K. Lines represent model fit results with a dual site Langmuir isotherm. 195 K data are taken from [3] [Chapter 2].

Table 1. Estimated dual site Langmuir adsorption parameters of CO_2, CH_4 and N_2 in DD3R.

Component	$q^{\text{sat,A}}$	K_0^{A}	$\Delta H_{\text{Ads}}^{\text{A}}$	$q^{\text{sat,B}}$	K_0^{B}	$\Delta H_{\text{Ads}}^{\text{B}}$
	mol kg^{-1}	kPa^{-1}	kJ mol^{-1}	mol kg^{-1}	kPa^{-1}	kJ mol^{-1}
CO_2	2.87	$1.11\cdot10^{-7}$	-28.7	1.41	$1.55\cdot10^{-8}$	-21.7
CH_4	1.71	$1.43\cdot10^{-6}$	-19.0	1.54	$8.08\cdot10^{-8}$	-15.3
N_2^*	1.56	$2.19\cdot10^{-6}$	-15.1	3.84	$5.38\cdot10^{-6}$	-2.61

*The total saturation loading is limited to 5.4 mol kg^{-1} in the data fitting procedure.

3.3 Single component surface diffusivities

Using the Maxwell-Stefan equations with a loading *independent* diffusivity does not allow a good fit of the single component permeation data. In case of a single component systems and the adsorption isotherm is described by a dual-site Langmuir isotherm the solution of the loading independent form of the Maxwell-Stefan equations is:

$$N_i = \frac{\rho}{\delta} Đ_i \cdot \left[q_i^{sat,A} \cdot \ln\left(\frac{1+K_i^A \cdot p_{i,ret}}{1+K_i^A \cdot p_{i,per}} \right) + q_i^{sat,B} \cdot \ln\left(\frac{1+K_i^B \cdot p_{i,ret}}{1+K_i^B \cdot p_{i,per}} \right) \right]. \tag{2}$$

Figure 4 shows the back-calculated (Equation (2)) lumped diffusivity parameter $\rho\delta^{-1}Đ$ as a function of the feed side loading of CH_4, N_2 and CO_2 from membrane permeation data at 303 K. The corresponding feed side pressure ranges from 101 to 1500 kPa. The lumped diffusivity parameter values normalized to that calculated at 101 kPa show for all three components a strong increase of the diffusivity. N_2 shows the weakest dependency, but the feed side loadings are relatively low for this component.

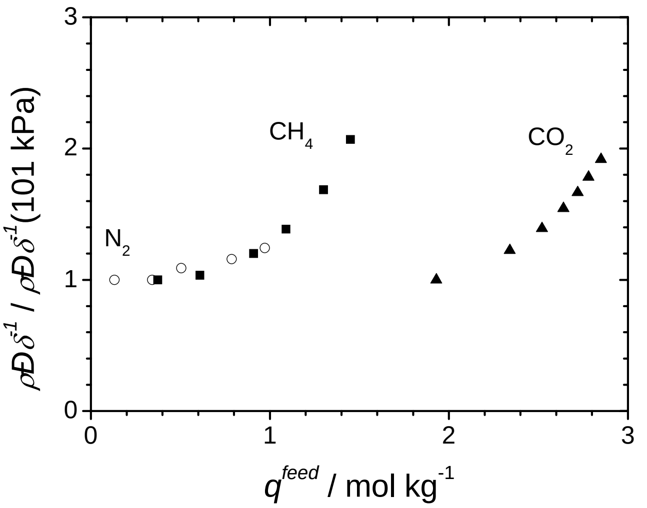

Figure 4. Back-calculated lumped diffusivity parameter of CO_2, CH_4 and N_2 at 303 K as a function of the loading at the feed side of the membrane. Diffusivities are normalized to the value at the lowest feed side loading at a feed pressure of 101 kPa. Support effects and the defect flux of CH_4 are accounted for.

The surface diffusivity is calculated from the lumped diffusivity $\rho\delta^{-1}Đ$ assuming a DD3R framework density of 1714 kg m^{-3} and a membrane thickness of $5 \cdot 10^{-6}$ m. The diffusivities are listed in Table 2 together with literature diffusivity data estimated by Pulsed Field Gradient NMR (PFG-NMR) and Frequency Response (FR) techniques on DDR (ZSM-58) crystals (Si/Al ratio 190). It appears that the membrane diffusivities are about one order of magnitude lower than the PFG-NMR data and in fair agreement with the FR data. Since in the case of PFG-NMR diffusivities are measured at very short length scales, the difference in diffusivities point in the direction of additional diffusion barriers in case of the membrane and the FR measurements, such as surface barriers or intra-crystalline grain boundaries [12,14,21,44].

Table 2. Diffusivities at 300 K estimated from membrane experiments (this work, p_{feed} = 101 kPa), Pulsed Field Gradient Nuclear Magnetic Resonance (PFG-NMR) [45,46] and Frequency Response (FR) [47] experiments at 101 kPa.

Component	$Đ$ (membrane) $m^2\ s^{-1}$	D_{Self} (PFG-NMR) $m^2\ s^{-1}$	D_{Self} (FR) $m^2\ s^{-1}$
CO_2	$1.2 \cdot 10^{-11}$	$1.0 \cdot 10^{-10}$	$4.0 \cdot 10^{-11}$
CH_4	$9.2 \cdot 10^{-14}$	$1.6 \cdot 10^{-12}$	$2.0 \cdot 10^{-13}$
N_2	$7.6 \cdot 10^{-12}$		$3.0 \cdot 10^{-11}$

3.4 Single component permeation modeling

Figure 5 shows the membrane permeation data of CO_2, N_2 and CH_4 as a function of the temperature and feed pressure together with model fit results using the RSM and the Reed Ehrlich approach as described in Section 2.2 and 2.3 of Chapter 5A, respectively. The membrane is modelled assuming that both the feed and sweep side behave as a well-mixed system [6] and that the intracrystalline diffusion is the rate-limiting step. The model fit and fixed parameters of both approaches are listed in Table 3. The total saturation loadings are taken from simulated adsorption isotherms [30,32][Chapter 5B and 5D]. These isotherms match closely with the experimental adsorption isotherms as shown in Appendix 5E.I.

In case of the RSM four parameters can be varied to fit the experimental data: $\rho\delta^{-1}q_i^{sat,*}Đ_{i,0}^{*}(0)$, $E_{A,diff,i}^{*}$, $K_{0,i}^{*}$ and $\Delta H_{Ads,i}^{*}$. For CO_2 all four individual parameters can be estimated properly. From the CH_4 and N_2 data only a lumped diffusivity parameter $\rho\delta^{-1}q_i^{sat,*}Đ_{i,0}^{*}(0)K_{0,i}^{*}$ and an apparent activation energy can be estimated. The main reason is that these permeances are independent of the feed pressure, *i.e.* a very weak adsorption regime is found. These lumped parameters combine information about both adsorption and diffusion which can affect the mixture permeation predictions strongly.

In case of the Reed Ehrlich approach also four parameters are available to describe the experimental data: $\rho\delta^{-1}Đ_{i,0}(0)$, $E_{A,diff}$, $\phi_{i,0}$ and $\delta E_{A,i}$. In case of CO_2 a good estimation of all four independent parameters can be made, however, for CH_4 and N_2 the RE parameters ($\phi_{i,0}$, $\delta E_{A,i}$) are hard to be estimated from the current permeation data due to the low loading of these components at the studied conditions. But the impact of these parameters on the mixture permeation can be very large as will be shown further on.

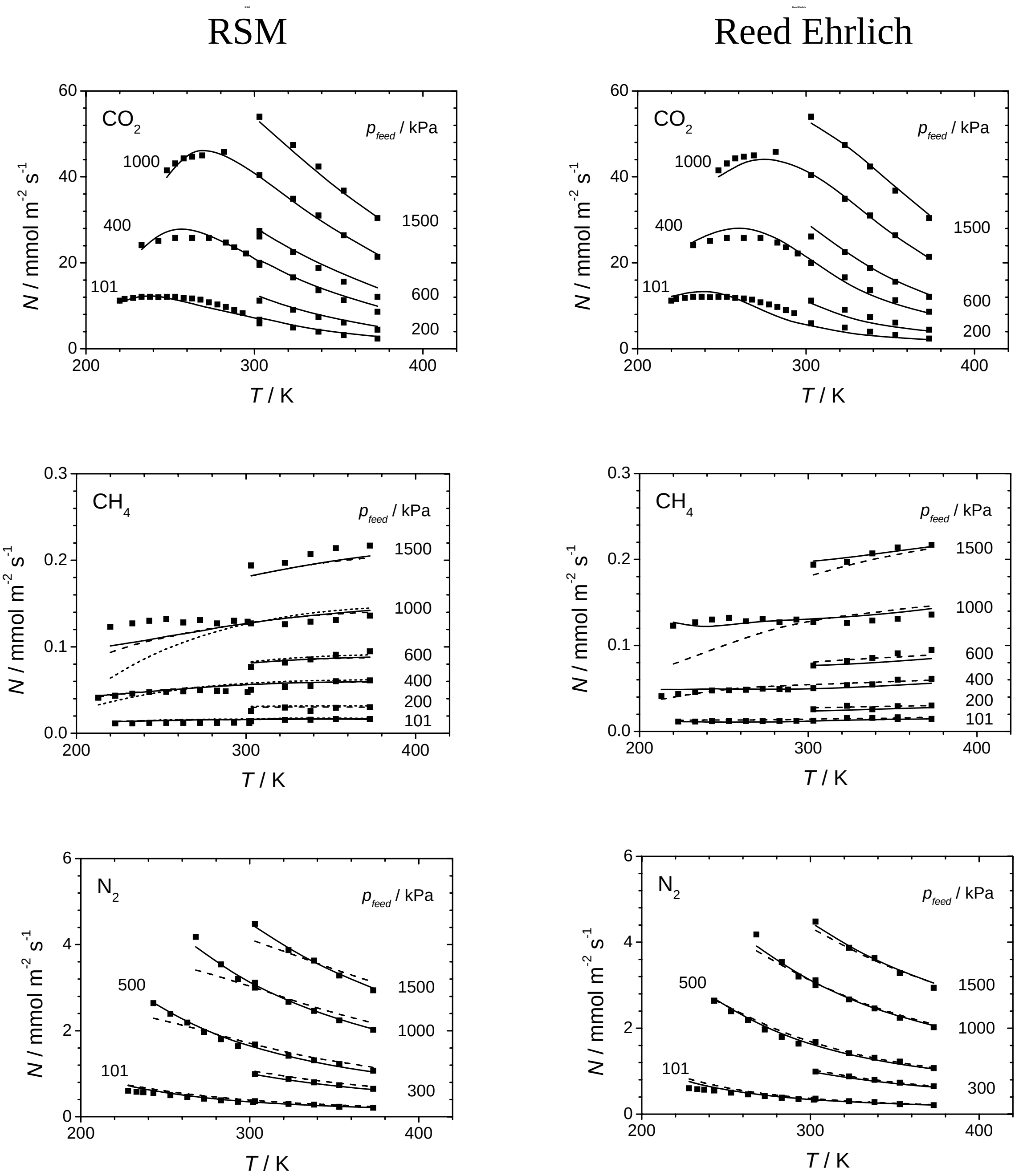

Figure 5. Single component permeation data of CO_2, CH_4 and N_2 across an all-silica DDR membrane as a function of temperature. Symbols represent experimental data, lines represent model fit results by the RSM (left graphs) and the Reed Ehrlich approach (right graphs). Solid, dashed and short-dashed lines correspond to model fit parameters I, II and III in Table 3 respectively.

Table 3. Relevant Site and Reed Ehrlich parameter values obtained from a model fit of the single component membrane permeation data

RSM	$\rho\delta^{-1}q^{sat,*}D_0^{*}(0)$	$E_{A,diff}^{*}$	$\rho\delta^{-1}q^{sat,*}D_0^{*}(0)$ (303 K)	K_0^{*}	ΔH_{Ads}^{*}	K^{*} (303 K)	q_{sat}^{tot}
Component	mol s^{-1} m^{-2}	kJ mol^{-1}	mol s^{-1} m^{-2}	kPa^{-1}	kJ mol^{-1}	kPa^{-1}	mol kg^{-1}
CO_2	194	16.3	0.3	$7.88\cdot10^{-10}$	-32.6	$3.34\cdot10^{-4}$	4.6 [a]
CH_4-I	130	18.5	$8.35\cdot10^{-2}$	$1.0\cdot10^{-9}$ [a]	-19.0 [a]	$1.89\cdot10^{-6}$	4.1 [a]
CH_4-II	12.0	18.3	$8.43\cdot10^{-3}$	$1.0\cdot10^{-8}$ [a]	-19.0 [a]	$1.89\cdot10^{-5}$	4.1 [a]
CH_4-III	1.98	18.4	$1.36\cdot10^{-3}$	$6.5\cdot10^{-8}$ [a]	-19.0 [a]	$1.23\cdot10^{-4}$	4.1 [a]
N_2-I	2.76	8.65	$8.91\cdot10^{-2}$	$1.0\cdot10^{-7}$ [a]	-15.0 [a]	$3.85\cdot10^{-5}$	5.4 [a]
N_2-II	0.31	8.62	$1.01\cdot10^{-2}$	$1.0\cdot10^{-6}$ [a]	-15.0 [a]	$3.85\cdot10^{-4}$	5.4 [a]

Reed Ehrlich	$\rho\delta^{-1}D_0(0)$	$E_{A,diff}$	$\rho\delta^{-1}D_0(0)$ (303 K)	Φ_0	δE_A	Φ (303 K)	q_{sat}^{tot}	z
Component	kg s^{-1} m^{-2}	kJ mol^{-1}	kg s^{-1} m^{-2}	-	kJ mol^{-1}	-	mol kg^{-1}	-
CO_2	1.75	17.4	$1.72\cdot10^{-3}$	1.09	2.31	2.72	4.6 [a]	5 [a]
CH_4-I	0.14	22.0	$2.26\cdot10^{-5}$	1 [a]	4.18	5.25	4.1 [a]	5 [a]
CH_4-II	0.092	20.4	$2.82\cdot10^{-5}$	1 [a]	3.0 [a]	3.29	4.1 [a]	5 [a]
N_2-I	0.062	8.23	$2.35\cdot10^{-3}$	1 [a]	3.0 [a]	3.29	5.4 [a]	5 [a]
N_2-II	0.056	7.80	$2.53\cdot10^{-3}$	1 [a]	2.0 [a]	2.21	5.4 [a]	5 [a]

[a] Fixed parameters in model fit

To investigate the influence of the single component model fit parameters on the mixture predictions a sensitivity analysis is performed by variation of the RS adsorption constant and the RE parameter ϕ_i for N_2 and CH_4. In order to limit the degrees of freedom only the pre-exponential of the RS adsorption equilibrium constant is varied and the RS adsorption enthalpy is fixed at the value of the first site of the adsorption isotherm. The latter assumption is made because the estimated RS adsorption enthalpy of CO_2 (-32.6 kJ mol^{-1}) is quite close to the adsorption enthalpy estimated from the adsorption isotherm (-28.7 kJ mol^{-1}). Also from Molecular Dynamic (MD) simulation results it was found that the RS adsorption enthalpies of N_2, CO_2 and CH_4 were very close to the adsorption enthalpy of the first Langmuir site of the total adsorption isotherms [30,32][Chapter 5B and 5D]. In case of the RE approach a variation of $\delta E_{A,i}$ is made while fixing $\phi_{i,0}$ at the value one.

Two fitting parameters sets are presented for the RE approach, denoted by I and II in Table 3. Set I represent the model fit that describes the experimental data best. Set II is a fit using a $\delta E_{A,i}$ of roughly 1.0 kJ mol^{-1} lower. In case of the RSM the pre-exponential of the RS adsorption equilibrium constant is varied in the region that the experimental and model fit results start to diverge from each other. Just as in case of the RE approach, model fit parameter set I describes the experimental data best. And increasing the RS adsorption constant by one order of magnitude leads to a poorer fit of the experimental data (set II). In case of CH_4 an extra fit result (set III) is presented with an even higher RS adsorption constant because it yields a particularly nice mixture prediction as will become clear later on. This in spite of its poor fit of the permeation results below 300 K at 1000 kPa feed pressure.

Both the RSM and the RE approach provide an accurate description of the permeation data of all three components. In case of CH_4 the RE approach describes the low temperature permeation data at 1000 kPa feed pressure slightly better. Increasing the RS adsorption constant or decreasing $\delta E_{A,i}$ leads to more difficulty of both models to describe the CH_4 flux below 300 K at 1000 kPa feed pressure.

The difference between the different model fit parameter sets for CH_4 is only significant at high loadings (low temperature, high pressure). This illustrates the difficulty to extract with high certainty the model fit parameters for both models. Note that in case of N_2, the weakest adsorbing component, almost no difference is observed between the different fit results in case of the RE approach, in spite of a significant variation in δE_A.

The diffusivity activation energy for CO_2 is about the same for both models. The N_2 and CH_4 RS activation energy are the direct result of the chosen value of the RS adsorption energy, but the values are very similar to the values obtained from the RE approach.

The variation in RS adsorption and diffusivity parameters and RE parameters that allow a good description of the permeation data is large. Results from a MD study of CO_2, CH_4 and N_2 in DDR [29,30,32][Chapter 5B and 5D] are used to decide on the physical meaningfulness of the obtained fit parameters. It is unrealistic to assume that complete quantitative agreement between simulations and experimental data exist, but, qualitative agreement can be expected. From MD simulation results (Table 4) the following order in RS adsorption constants at 303 K would be expected: $CO_2 >> N_2 \geq CH_4$. The order in RS diffusivities at the same temperature is: $N_2 > CO_2 > CH_4$.

Taking parameter set II in case of CH_4 and set I for N_2 leads to an order in RS adsorption constants and diffusivities similar as obtained from the MD results. In case of the estimated RE parameter set I leads to an order in Φ that agrees with the order found using MD: $CH_4 > N_2 > CO_2$.

Table 4. RSM and RE parameter values at 300 K obtained from MD simulations.

Component	K^* (300 K) [32] kPa^{-1}	$q^{sat,*} Đ^*(0)$ (300 K) [32] $mol\ kg^{-1}\ m^2\ s^{-1}$	Φ (300 K) [29] -
CO_2	$3.77 \cdot 10^{-3}$	$6.3 \cdot 10^{-9}$	1.2
N_2	$3.67 \cdot 10^{-5}$	$3.8 \cdot 10^{-8}$	2.0
CH_4	$2.17 \cdot 10^{-5}$	$2.8 \cdot 10^{-10}$	6.0

3.5 Binary mixture prediction

The RSM and RE model equations used to make the mixture predictions are presented in detail in Section 2.2 and 2.1 of Chapter 5A. Note that the assumption of equal RS saturation loadings and a self-exchange diffusivity equal to the Maxwell Stefan diffusivity are made leading to a simplified equation to predict the exchange diffusivity [30-32]. All free space is considered relevant for diffusion.

Figures 6-8 display the permeation results for equimolar feed mixtures of N_2/CH_4, CO_2/CH_4, and CO_2/air together with model predictions by the RSM and the RE approach with the diffusivity and adsorption parameters listed in Table 1 and Table 3. The CO_2/air mixture is approximated by a CO_2/N_2 mixture in the simulations. At this point it is good to realize what mixture effects can be expected for the RSM and RE approach. In case of the RSM there can be: competitive adsorption effects at the RS, reduction of the free space for diffusion $(1-\theta)$ due to the presence of the second component and exchange effects at the RS. In the RE approach the following effects can play a role: competitive adsorption (total loading level), reduction of the free space for diffusion $(1-\theta)$ and a strong dependency of the diffusivity on the loading of the second component ('total loading assumption'). Exchange effects are neglected in the RE approach.

The CH_4 and N_2 permeances in an equimolar mixture (Figure 6) are predicted well by both the RSM and the RE approach. The CH_4 data at low temperature seem to be predicted with higher accuracy by the RE approach. Using parameter set I or II leads to very small differences for both models. This can be understood by realizing that both CH_4 and N_2 are relatively weakly adsorbing, also at the RS. Therefore, no strong competitive adsorption effects are expected and the free space available for diffusion will not be very different in the mixture compared to the single component situation. The N_2 flux prediction at low temperature by the RE approach using parameter set I leads to an overprediction of the N_2 flux. The stronger adsorbing CH_4 induces an increased N_2 diffusivity through the total loading assumption. Using parameter set II leads to a better prediction in this case.

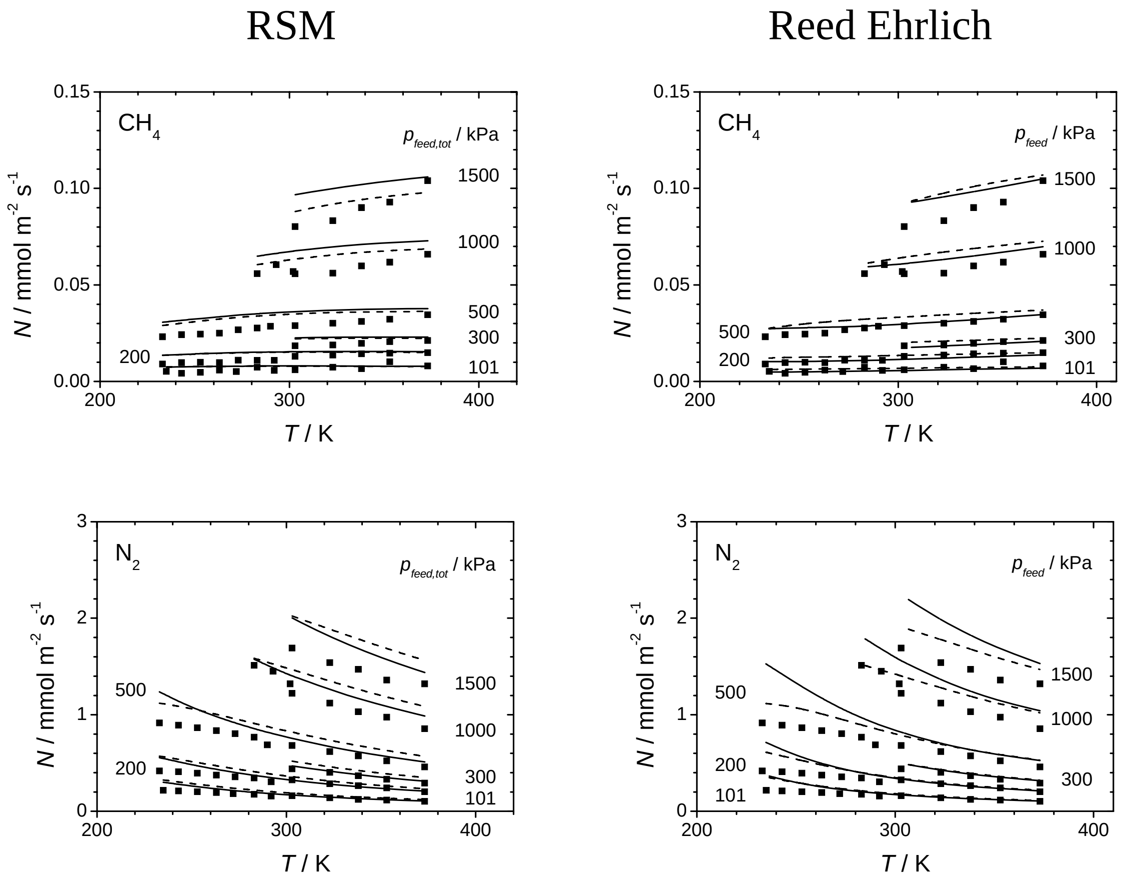

Figure 6. Permeation fluxes of CH_4 and N_2 in an equimolar feed mixture across an all-silica DDR membrane as a function of temperature. Symbols represent experimental data, lines represent model predictions by the RSM (left graphs) and the Reed Ehrlich approach (right graphs). Solid and dashed lines correspond to model predictions using model fit parameters listed in Table 3 denoted by I and II, respectively.

The CH_4 flux in an equimolar mixture with CO_2 is strongly dependent on the used fitting parameters in case of the RE approach (Figure 7). Main reason is that CO_2 adsorbs much stronger than CH_4. The total mixture loading is much higher than the CH_4 loading under single component conditions. The total loading assumption leads to severe overpredictions of the CH_4 flux at high mixture loadings (low temperature, high pressure). However, using parameter set II, with a much weaker CH_4 loading dependency, an accurate prediction of the CH_4 flux can be made. The mismatch using the parameter set I could also be the result of specific blocking effects of CH_4 by CO_2 in the DDR windows that is not accounted for in the RE approach [48]. Furthermore, with increasing pressure the CH_4 flux becomes increasingly underpredicted. A possible explanation for this deviation could be an underprediction of the CH_4 loading by the IAST, which has been shown by Krishna *et al.* [49].

The CO_2 flux is unaffected by the CH_4 model parameters used. In general an accurate prediction is found, but at low temperatures the CO_2 flux is significantly overpredicted. In fact, the CO_2 flux is estimated to be as if no CH_4 is present. The reason for the overprediction is unclear. As shown in Appendix 5E.I, concentration polarization effects cannot be responsible for these deviations. Moreover, it is expected that the CO_2 loading and the total loading are accurately predicted by the IAST [49]. It could be that at high CO_2 loadings exchange effects start to play a role, which are neglected in the RE approach.

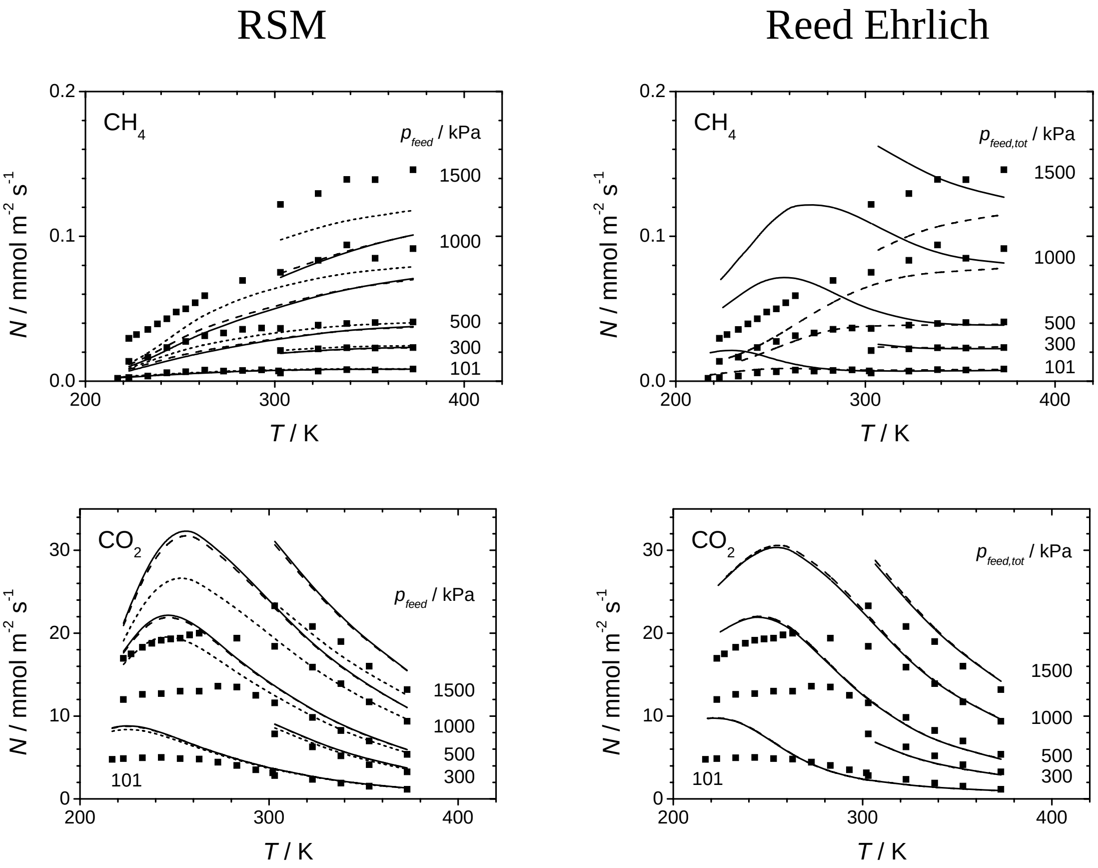

Figure 7. Permeation fluxes of CH_4 and CO_2 in an equimolar feed mixture across an all-silica DDR membrane as a function of temperature. Symbols represent experimental data, lines represent model predictions by the RSM (left graphs) and the Reed Ehrlich approach (right graphs). Solid, dashed and short-dashed lines correspond to model predictions using model fit parameters listed in Table 3 denoted by I, II and III, respectively.

Using the RSM a reasonable prediction of the CH_4 flux is obtained. Similarly as for the RE model an underprediction of the flux with increasing feed pressure is found. The predicted CH_4 fluxes are only modestly dependent on the set of parameters used. Only when moving to parameter set III an improved flux prediction is obtained. At this point exchange effects start to play a role that results in an increased CH_4 flux by the faster permeating CO_2 molecules. The opposite effect is found for the CO_2 flux, which is slowed down. The exchange effects are discussed in more detail later on. Note that although this parameter set leads to the best model prediction, the parameters do not seem realistic since the CH_4 RS adsorption constant is in the order of the CO_2 RS adsorption constant (Section 3.4).

The CO_2 fluxes predicted by the RSM using parameter set I and II are practically the same as found by the RE approach, including the overprediction at low temperatures. Using parameter set III leads to a reduction of this overprediction. In this case all CO_2 fluxes above 300 K are very accurately predicted.

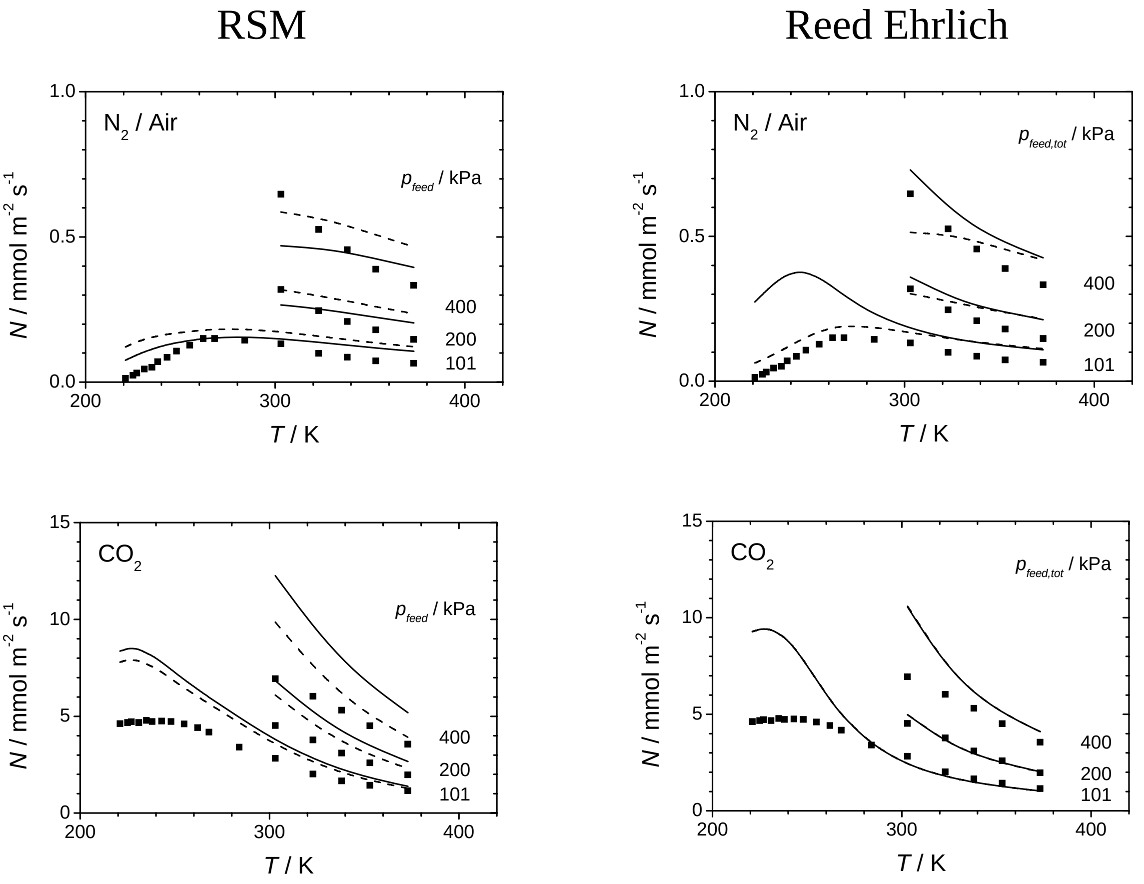

Figure 8. Permeation fluxes of CO_2, N_2 and air across an all-silica DDR membrane as a function of temperature. Symbols represent experimental data of an equimolar CO_2/air feed mixture, lines represent model predictions by the RSM (left graphs) and the Reed Ehrlich approach (right graphs) of an equimolar feed CO_2/N_2 mixture. Solid and dashed lines correspond to model predictions using model fit parameters listed in Table 3 denoted by I and II, respectively.

In case of the CO_2/air mixtures (Figure 8) the RSM yields a reasonable prediction of the CO_2 and air flux. Similar effects as found for the CO_2/CH_4 mixture are observed: the CO_2 flux is overpredicted, particularly at low temperatures and by using parameter set II a reduction of the CO_2 flux and increase of the air flux is found. The competitive adsorption effects at low temperature are captured quite well. Note that the temperature dependency of the predicted air flux above room temperature significantly differs from the experimental flux. The presence of O_2 in the experimental permeation data, not accounted in the model predictions could play a modest role in this. A previous study showed that the O_2 flux increase with decreasing temperature is stronger compared to that of N_2 [3][Chapter 2].

The CO_2 flux prediction by the RE approach is independent of the parameters used to describe the air diffusivity. Similar as in the CO_2/CH_4 data the predicted CO_2 flux follows its single component behaviour resulting in an overprediction, particularly at low temperatures. Using parameter set I leads to an accurate prediction of the air flux above 300 K, but a severe overprediction at low temperatures. Parameter set II yields a much better prediction of the air flux at low temperatures, but compromises the results above 300 K. Similarly as for the CO_2/CH_4 mixture the overprediction at low temperature can be due to unaccounted window blocking effects by CO_2.

3.6 Exchange effects

From the shown modelling results it is not clear up to what extent exchange effects play a role within the RSM. This is further explored taking the CO_2/CH_4 mixture as example. When the RS adsorption equilibrium constant is increased, *i.e.* when moving from parameter set I to III, the lumped diffusivity parameter is decreased consequently (Equation 39, Chapter 5A). These changes have a strong impact on the appearance of exchange effects. Firstly, it is good to realize that exchange effects become more important in general at high occupancy [6]. Moreover, the exchange coefficient ($Đ_{ij}^{*}$) is estimated by a logarithmic interpolation between the pure component diffusivities (Equation 26, Chapter 5A). When the RS adsorption equilibrium constant is increased, the CH_4 single component RS diffusivity is lowered *and* the interpolation shifts more to the CH_4 value leading to a much lower exchange diffusivity. Another aspect is the magnitude of ‘speeding up’ and ‘slowing down’ of each component induced by the momentum transfer between the species. This is strongly dependent on the magnitude of the RS adsorption equilibrium constant. When the CH_4 occupancy is much lower than the CO_2 occupancy and exchange effects are significant a very strong increase of the CH_4 flux can occur while leaving the CO_2 flux almost unaffected at the same time.

Exchange effects only play a significant role when using parameter set III in case of the CO_2/CH_4 and set II in case of the CO_2/air mixture. Therefore, for these situations at 303 K a model prediction neglecting exchange effects ($Đ_{ij}^{*} = \infty$) is compared with the predictions including exchange effects (Figure 9). Inclusion of the exchange effects leads to a significant change of the fluxes. Particularly in case of the CO_2/CH_4 mixture the model predictions are improved by including the exchange effects, similarly as observed for CH_4 in mixtures with ethane or propane in silicalite-1 [6]. It is interesting to see that at the point where exchange effects become important also the symmetry between the ‘slowing down’ of CO_2 and ‘speeding up’ of CH_4 is good.

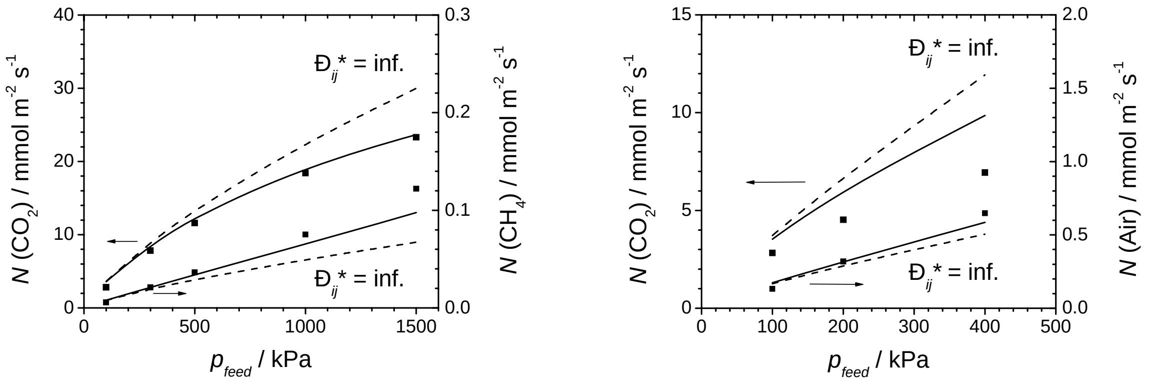

Figure 9. Influence of the exchange effects in the predicted fluxes of the RSM for equimolar CO_2/CH_4 (*left*) and CO_2/air (*right)* feed mixtures as a function of total feed pressure at 303 K. Symbols represent experimental data, solid lines model predictions including exchange effects, and dashed lines predictions neglecting exchange effects (*i.e.* $Đ_{ij}^{*}=\infty$). The CO_2/CH_4 and CO_2/Air predictions are made using parameter set III and II, respectively.

3.7 Evaluation

It appears that with both the RSM and the RE approach good mixture membrane permeation predictions *can* be obtained. The difference between the two models is the parameter sensitivity, which is very strong in case of the RE approach. Specifically the ‘total loading’ assumption can lead to large errors in case of a mixture that constitutes of a strongly and a weakly adsorbing component (CO_2/air and CO_2/CH_4). The RSM does not show this sensitivity. Additionally, in case of the RE approach an accurate prediction of the individual loadings in the zeolite is required, which can be very problematic. With the IAST good results have been obtained, but some difficulties exist. Firstly, a fundamental issue is that segregated adsorption can introduce severe errors in the loadings predicted by the IAST [50]. Segregated adsorption appears to be a phenomenon particularly relevant for small-pore cage-like zeolitic systems like DDR [48,49]. Secondly, to make appropriate use of the IAST single component adsorption isotherms up to sufficient pressures are required. To arrive at a prediction of the IAST the single component isotherms are evaluated at a certain reference pressure. Especially in case of the combination of a strongly and weakly adsorbing component the weaker adsorbing component can be evaluated at reference pressures orders of magnitude higher than its actual partial pressure, and consequently a good adsorption isotherm description in this region is required but usually not available. As shown in Appendix 5E.I this is no problem with the current set of high pressure adsorption isotherms.

It can be argued that the RSM also relies on the total loading as input, however, in contrast to the individual loadings, estimation of the total loading by the IAST does not seem problematic [49].

Finally, in all modelling results it is assumed that intra-crystalline diffusion through the membrane layer is the rate-limiting step. However, the reported diffusivities could be an indication that also surface or intercrystalline barriers play a role [21]. If they do, the estimated diffusivities and loading (and pressure) profile in the membrane can differ much from the model situation.

4 Conclusions

Model predictions of the fluxes of equimolar (gas phase) CO_2/CH_4, N_2/CH_4 and CO_2/air mixtures across an all-silica disc-shaped DDR zeolite membrane have been made and compared to experimental data. A challenging set of experimental conditions is considered: the temperature ranged from 220 to 373 K and the total feed pressure ranged from 101 to 1500 kPa. In case of the CO_2/air mixture the total feed pressure was limited to 400 kPa.

High pressure (up to 7000 kPa) adsorption data of CO_2, N_2 and CH_4 in DDR could be described accurately by a dual-site Langmuir isotherm and were used as input for all modelling results.

The Maxwell-Stefan diffusivities of CO_2, N_2 and CH_4 increase strongly as a function of their loading in the zeolite. The estimated MS diffusivities are about one order of magnitude lower than literature self-diffusivities obtained by PFG-NMR, an indication of the presence of surface or internal barriers in the membrane.

Two rival models were evaluated to account for the observed loading dependency of diffusion: the Relevant Site Model (RSM) and the so-called Reed Ehrlich (RE) approach. Both models lead to an accurate fit of the single component permeation data, but for N_2 and CH_4 certain parameters were strongly correlated. Nevertheless, good mixture predictions could be made by both models based on the estimated single component parameter values.

The quality of the best predictions of the RSM and the RE approach is comparable. The RE approach, however, is very sensitive to the used input parameter values, which are very hard to determine accurately from the single component data. Additionally, an accurate prediction of the mixture loading is required for the RE approach, which can be very challenging. The RSM does not suffer from both these issues, which are evident advantages with respect to application of this model.

Acknowledgement

NGK Insulators is gratefully acknowledged for supplying the DDR membrane.

Appendix I

1 Introduction

In this appendix more detailed results are presented to support the main chapter. Particular emphasis is on a detailed study on the influence and modelling of the support effects, defect characterization and the influence of concentration polarization effects. Moreover several aspects related to single component and mixture adsorption modelling are evaluated.

2 Experimental: Support permeation experiments

In this study an asymmetric disc-shaped zeolite membrane has been used that consists of a thin zeolite layer on top of a macro-porous α-alumina support. To determine the influence of the support on the composite membrane permeation properties, permeation measurements with a bare support have been carried out. The support is supplied by NGK insulators and has a reported pore size of 600 nm, a thickness of 1.5 mm and a diameter of 18.5 mm. The support was sealed by a custom made silicon O-ring leaving a 12.5 mm free diameter and a membrane area of 1.23×10^{-4} m^2 available for permeation. The permeance of H_2, CO_2, N_2, He and CH_4 were determined in pressure drop operation (no sweep gas). The temperature was varied between 303 and 373 K. The feed pressure was varied between 110 and 150 kPa, the permeate pressure was always at atmospheric pressure. The feed flow rate was set to 100 ml min^{-1} (STP), the permeate flow was measured by a bubble flow meter.

3 Results

3.1 Support effects

To isolate the influence of the membrane support on the flux through the composite membrane permeation experiments through a bare support have been performed. The main objective of these measurements is to obtain an accurate description of the mass transport through the support. For the description of mass transport in the macro-porous support the so-called Binary Friction Model (BFM) is applied [43]. A single component flux (*N*) through the macro-porous support can be represented as:

$$N_i = -\frac{1}{RT}\frac{\varepsilon}{\tau}\left(D_{Kn,i} + \frac{B_0\,\overline{p}}{\eta}\right)\frac{\Delta p_i}{\delta_{supp}}, \tag{3}$$

where η is the viscosity, δ_{supp} the support thickness, D_{Kn} the Knudsen diffusivity B_0 the permeability, R the gas constant, T the temperature and p the pressure. The Knudsen diffusivity and permeability (for cylindrical pores) are defined as:

$$D_{Kn,i}^{eff} = \frac{d_0}{3}\sqrt{\frac{8RT}{\pi M_i}}, \qquad B_0 = \frac{d_0^2}{32}. \tag{4}$$

ε, τ, d_0 and M_i represent the porosity, tortuosity, pore size and molar mass, respectively. Equation (3) can be cast into the form $y = ax + b$ to estimate the ratio of the support porosity and tortuosity:

$$-\frac{N_i}{\Delta p_i}\frac{RT}{v_m} = \frac{\varepsilon}{\tau}\frac{d_0}{3\delta_{supp}} + \frac{\varepsilon}{\tau}\frac{d_0{}^2}{32\delta_{supp}}\frac{\overline{p}}{\eta v_{m,i}}, \qquad v_{m,i} = \sqrt{\frac{8RT}{\pi M_i}}. \tag{5}$$

A plot of $-NRT\Delta p^{-1}v_m{}^{-1}$ versus $\overline{p}\eta^{-1}v_m{}^{-1}$ is presented in Figure 10. This plot is based on permeation experiments of He, H$_2$, CO$_2$, N$_2$ and CH$_4$ through the bare support in a temperature range of 303 to 373 K. A good correlation between the model and experiments is obtained. Given the pore size (600 nm) and thickness (1.5 mm) of the support the $\varepsilon\tau^{-1}$-factor can be estimated independently from the tangent and the intercept with the *y*-axis of the curve. Both lead to a $\varepsilon\tau^{-1}$ value of 0.11.

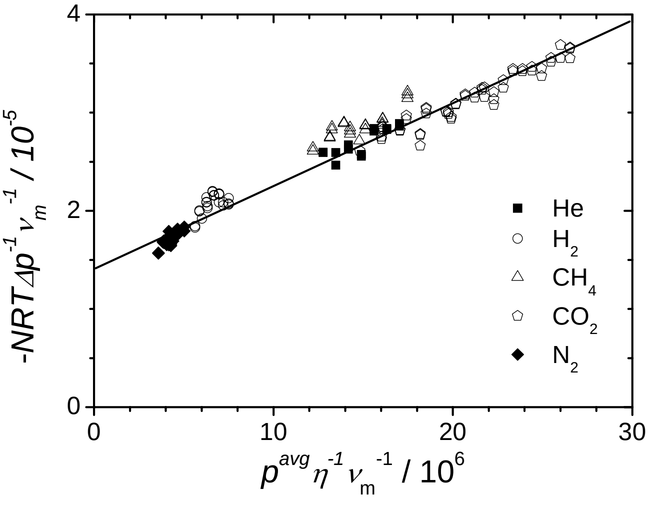

Figure 10. Correlation of permeation measurements of He, H$_2$, CH$_4$, CO$_2$ and N$_2$ through an α-alumina support to the support pore size (d_0), tortuosity (τ) and porosity (ε). The properties listed on the x- and y-axis are based on a rearrangement of a mathematical description of a mass transport mechanism that involves Knudsen diffusion and viscous flow as presented in the text (Equation (3)).

Mixture mass transport through the macro-porous support in the membrane permeation results is modelled by the Binary Friction Model (BFM) [43]. The base equation for mixtures to start from accounts for friction between the molecules and the wall by viscous forces and Knudsen type friction, and momentum exchange between the different species:

$$\frac{\tau}{\varepsilon}\nabla p_i = RT\cdot\sum_{j=1}^{n}\phi_{ij}\left(\frac{x_iN_j - x_jN_i}{Đ_{ij}}\right) - f_{im}RT\cdot N_i\,, \tag{6}$$

where the wall friction factor (f_{im}) can be represented as:

$$f_{im} = \left(D_{Kn,i} + \frac{B_0}{\kappa_i}\right)^{-1}. \tag{7}$$

Note that $\left(\varepsilon/\tau\right)^{-1}$ is added to the left hand side of Eq. (6) to account for the effectiveness of the diffusivities and permeability. The definitions of the Knudsen diffusivity (D_{Kn}) and permeability (B_0) have been presented in Equation (4). κ_i is based on the pure component viscosities (η_i^o), total pressure, molar fractions (x_j) and the interaction parameter ξ_{ij}:

$$\kappa_i = \frac{1}{p_{tot}}\frac{\eta_i^o}{\sum_{j=1}^{n}x_j\xi_{ij}}\,. \tag{8}$$

ξ_{ij} can be estimated as proposed by Wilke [51]:

$$\xi_{ij} = \frac{\left[1+\left(\eta_i^0/\eta_j^0\right)^{1/2}\left(M_i/M_j\right)^{1/4}\right]^2}{\left\{8\left[1+M_i/M_j\right]\right\}^{1/2}}\,. \tag{9}$$

The exchange diffusivity ($Đ_{ij}$) is estimated using the method of Füller *et al.* [52]:

$$Đ_{ij} = \frac{10^{-7}T^{1.75}\left(\frac{1}{M_i}+\frac{1}{M_j}\right)^{1/2}}{p_{tot}\left(\left[\sum v\right]_i^{1/3}+\left[\sum v\right]_j^{1/3}\right)^2} \tag{10}$$

The summation of the atomic diffusion volumes (v) leads to the molar diffusion volume. The correction factor for diffusion in the transition region (ϕ_{ij}) is assumed to be a function of the ratio of an averaged mean free path (λ_{ij}) and the pore radius (r^0):

$$\lambda_{ij} = \frac{kT}{\sqrt{2}\pi\sigma_{ij}^2 p_{tot}}, \tag{11}$$

where σ_{ij} is an averaged collision diameter of components *i* and *j*. The collision diameters of CO_2, N_2 and CH_4 are 0.394, 0.38 and 0.376 nm, respectively. At the highest *T* (373 K) and the lowest *p* (101.3 kPa) the mean free path is the longest. At these conditions the Knudsen numbers (d_0 / λ_i) are 5.6, 6.7 and 7.5 for CO_2, N_2 and CH_4, respectively. Therefore it is assumed that $\phi_{ij} = 1$.

The support plays relatively a minor role in the permeation results. The relative transport resistance contribution of the support is illustrated by the percentage of the partial pressure drop over the support of the total pressure drop over the composite membrane. This percentage is the highest in case of CO_2 and ranges from 7% at low temperature up to 1% at 373 K due to the different transport mechanisms in the zeolite and support layer. The negative apparent activation energy for diffusion in the zeolite layer increases the transport resistance in the zeolite layer with temperature compared to the support layer where a combination of viscous flow, Knudsen diffusion and gaseous diffusion occurs. For N_2 and CH_4 the pressure drop over the support compared to the pressure drop over the total membrane is always below 0.4 and 0.01 %, respectively.

3.2 Defect flow

To assess the quality of the membrane, isobutane permeation experiments have been performed. Isobutane is too large to fit into the DDR pores and can only pass through the membrane defects. Figure 11 shows the isobutane permeance at 303 and 373 K as a function of the feed pressure. A very low permeance ($\sim 5 \cdot 10^{-12}$ mol m^{-2} s^{-1} Pa^{-1}) is found which demonstrates the excellent quality of the membrane. The permeance is not significantly dependent on the feed pressure. This excludes a significant contribution of viscous flow. Assuming that the permeation mechanism is purely Knudsen flow leads to an acceptable description of the permeance represented by the lines in Figure 11.

The molar mass dependency of the Knudsen diffusion (*cf.* Equation (4)) leads to an expected defect flow of about 0.7, 1.1 and $1.9 \cdot 10^{-11}$ mol m^{-2} s^{-1} Pa^{-1} at 303 K for CO_2, N_2 and CH_4, respectively. In case of CH_4 the defect flux is accounted for in the single component and mixture modelling.

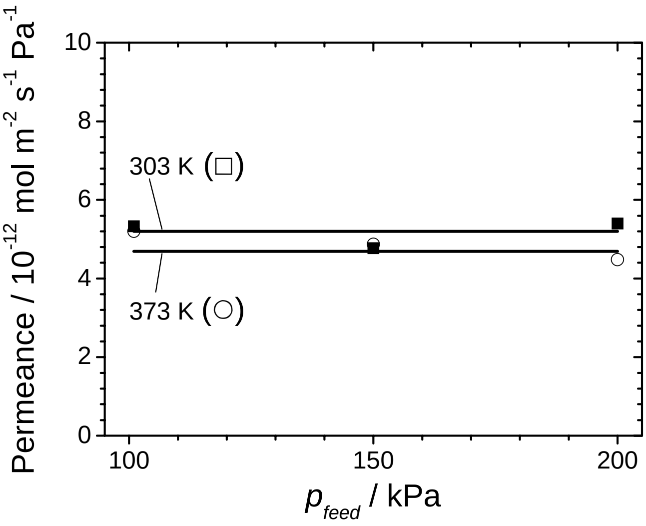

Figure 11. Isobutane permeance through the DD3R membrane at 303 and 373 K as a function of the feed pressure. He is used as sweep gas; permeance pressure 101 kPa. Lines represent modelling results assuming purely Knudsen flow through defects.

3.3 Concentration polarization

Concentration polarization effects can have a large influence on the permeation results, particularly when the flux through the membrane and the selectivity are high. These conditions are most likely met in case of the CO_2/CH_4 mixture permeation data through the DD3R membrane. Since the CO_2/CH_4 selectivity is very high (≥ 100) the CO_2 partial pressure at the surface of the membrane could be much lower than its concentration in the bulk if concentration polarization effects play a role. For CH_4 the opposite would be true. Increasing the total feed flow rate can reduce the boundary layer thickness and consequently the mass transport resistance in this layer which can lead to an increased CO_2 and a decreased CH_4 flux at increased feed flow rate.

To investigate these effects the total feed flow rate of an equimolar CO_2/CH_4 mixture is increased from 100 to 500 ml min^{-1} (STP). This has been done for two situations: 1) 10 bar total feed pressure and 303 K and 2) 2 bar total feed pressure and 233 K. The first case represents a situation with a high CO_2 flux and high selectivity, the second case represents a situation with a very high selectivity and a somewhat lower CO_2 flux. It is good to realize at this point that in the membrane module both the feed and the sweep gases are fed perpendicular onto the centre of the disc-shaped membrane. In both cases the effect of the increase of the feed flow rate are very low. The CO_2 permeance increases with only 3 % in case 1 and remained constant in case 2. CH_4 is a poor indicator due to its very low concentrations at the permeate side. But no changes larger than 10 % have been observed. It can be concluded that concentration polarization effects play no significant role in the current study.

3.4 He sweep gas effects

All membrane permeation experiments have been carried out with He as sweep gas. The back-permeance of He could have an influence on the feed gas membrane permeance [53]. The feed gas permeance could be reduced due to correlation (‘friction’) effects of the He molecules with the feed gas molecules in the zeolite crystal layer or in the macro-porous support. Earlier permeation study through the same DD3R membrane pointed out that intra-crystalline correlation effects appear to be almost absent in most cases [3][Chapter 2]. This appears to be a typical property of small-pore cage-like zeolites [29], which can be understood by realizing that transport seems to be controlled by relatively weak adsorbing window sites [30][Chapter 5B]. Correlations between different species only become apparent at a significant occupancy. Therefore, intra-crystalline correlation effects of the very weakly adsorbing He are neglected in the modelling work.

The effect of the He back-permeance on the feed gas fluxes through the support is investigated by a modelling study. Mass transport is modelled by the BFM [43] described above. The permeate compositions have been determined experimentally and the BFM is used to calculate the partial pressures at the interface of the support and the zeolite top layer. The porosity and tortuosity of the support have been determined in Section 3.1. Figure 12 shows the estimated partial pressure at the support-membrane interface as a function of the He back-permeance. Data are presented for the single component permeation of CO_2 and CH_4 at 303 K and 1000 kPa feed pressure. The curves in Figure 12 are representative for all studied conditions in this work. The influence of the He flux becomes significant when its flux is higher than 10^{-2} mol m^{-2} s^{-1}. The effect on the normalized partial pressure is the same for a component with a high flux (CO_2, $N = 4.0\times10^{-2}$ mol m^{-2} s^{-1}) as for a component with a very low flux (CH_4, $N = 1.2\times10^{-4}$ mol m^{-2} s^{-1}). The effect of the He at high back-permeances on the feed gas partial pressure at the zeolite layer-support interface is not via the exchange diffusivity $Đ_{ij}$. To facilitate the high He back-permeance a sub-atmospheric total pressure is found at the interface. The total pressure gradient over the support that is now created needs to be compensated by an increased opposing partial pressure gradient of the feed gases. Hence, the feed gas partial pressure at the interface increases.

The He back-permeance was not determined in all experiments. However, the highest back-permeance measured is about 10^{-3} mol m^{-2} s^{-1}. This value was measured using 101 kPa Ne as feed gas and 101 kPa He as sweep gas at 303 K [3][Chapter 2]. Therefore, a stagnant He layer ($N_{He} = 0$) is assumed in all simulations.

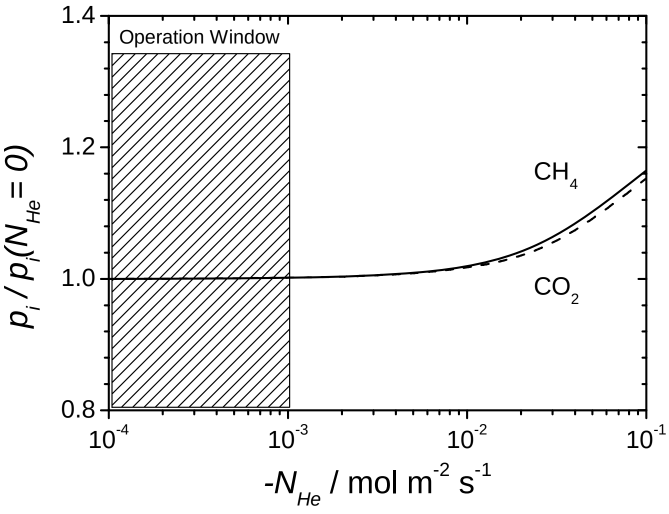

Figure 12. Influence of the He back-permeance on the estimated partial pressure at the support-membrane interface. The partial pressure is normalized to the situation with no back-permeance of He. Data are based on the extreme case (high fluxes) for the single component membrane permeation data of CO_2 and CH_4 at 303 K and 1000 kPa feed pressure. Helium is used as sweep gas at 101 kPa.

3.5 Binary mixture adsorption

To model mixture permeance the individual and total loading in the mixture needs to be estimated. A well-known method to calculate mixture loadings is the Ideal Adsorbed Solution Theory (IAST) [54]. In this approach mixture loadings are estimated based on single component adsorption isotherms. However, when adsorption becomes segregated the IAST may fail [50]. Since a better approach is lacking, the IAST is used in our study. Recently, single component adsorption isotherms have been computed by Grand Canonical Monte Carlo (GCMC) methods of CO_2, CH_4 and N_2 up to saturation loading together with equal partial fugacity mixture isotherms of CO_2/CH_4, CH_4/N_2 and CO_2/N_2 in DDR at 303 K [31,48][Chapter 5C]. From these studies it followed that the weaker adsorbing component is underpredicted by the IAST. At 1000 kPa total pressure the predicted loading of CH_4 mixed with CO_2, N_2 mixed with CH_4 and N_2 mixed with CO_2 are about 60, 80 and 85 % of the GCMC value, respectively. The stronger adsorbing component is only slightly overpredicted and the total loading is accurately predicted in these cases.

Besides this fundamental shortcoming of the IAST for heterogeneous adsorption systems errors can also be introduced when the single component isotherms are evaluated outside of the experimental range for which they have been measured. Figure 13 shows the pressure at which the single component isotherms are evaluated in case of CO_2/CH_4 and CO_2/N_2 mixtures at a total feed pressure of 1000 kPa. CO_2 is much stronger adsorbing than CH_4 and N_2. The CO_2 isotherm is evaluated close to its corresponding pressure in the mixture: 500 kPa. CH_4 and N_2 are evaluated at much higher pressures, especially at low temperatures. At 300 K the

CH_4 isotherm is evaluated at 7000 kPa and N_2 at ~20,000 kPa. This means that in case of N_2 already at this point the experimental pressure range is exceeded and for CH_4 the same occurs below 300 K. Note that at a total feed pressure of 100 kPa the same picture as shown in Figure 13 is obtained, but then all pressures are roughly one order of magnitude lower.

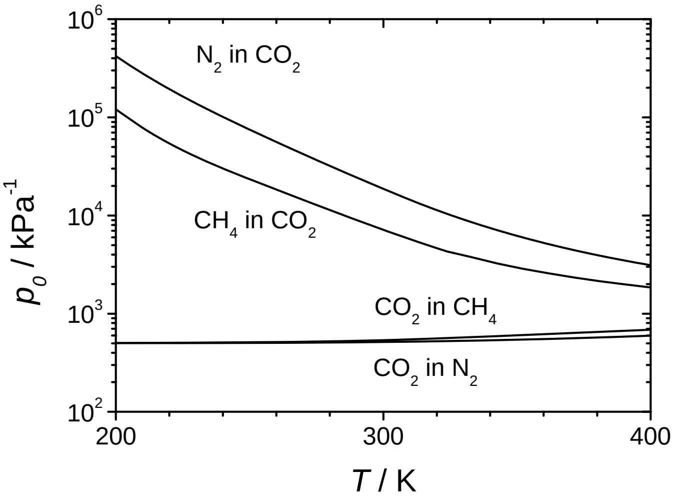

Figure 13. Pressures at which the single component isotherms are evaluated when predicting binary mixture loadings for CO_2/CH_4 and CO_2/N_2 mixtures using the IAST. Data are calculated at a total feed pressure of 1000 kPa, mixtures are equimolar in the gas phase. Used dual-site Langmuir parameters are listed in Table 1.

To estimate how well the currently estimated dual-site Langmuir parameters predict the loading outside the experimental range a comparison is made with isotherms calculated from GCMC simulations up to saturation [30,32][Chapter 5B and 5D]. The results of N_2, CO_2 and CH_4 adsorption at 300 K (GCMC) and 303 K (experimental) are shown in Figure 14. A very good agreement between the experimental and GCMC results is found. In case of CO_2 the experimentally determined adsorption parameters provide a good prediction up to saturation loading. Analysis of the CO_2 profile shows two steps in the isotherm. The experimental data reach up to the beginning of the second step, thereby providing enough information to model up to saturation. In case of CH_4, three steps can be distinguished. The experimental data reach up to the beginning of the second step and consequently the first two steps are described accurately. Note that in a previous work CH_4 adsorption data were presented up to 120 kPa [3][Chapter 2]. In this case only information on the first step of the isotherm was available and also a much lower saturation loading was obtained from fitting this data. It was the most difficult to extract reliable adsorption constants from the N_2 data. Clearly the assumed total saturation loading in the fitting procedure leads to an overprediction of the N_2 loading outside of the experimental range.

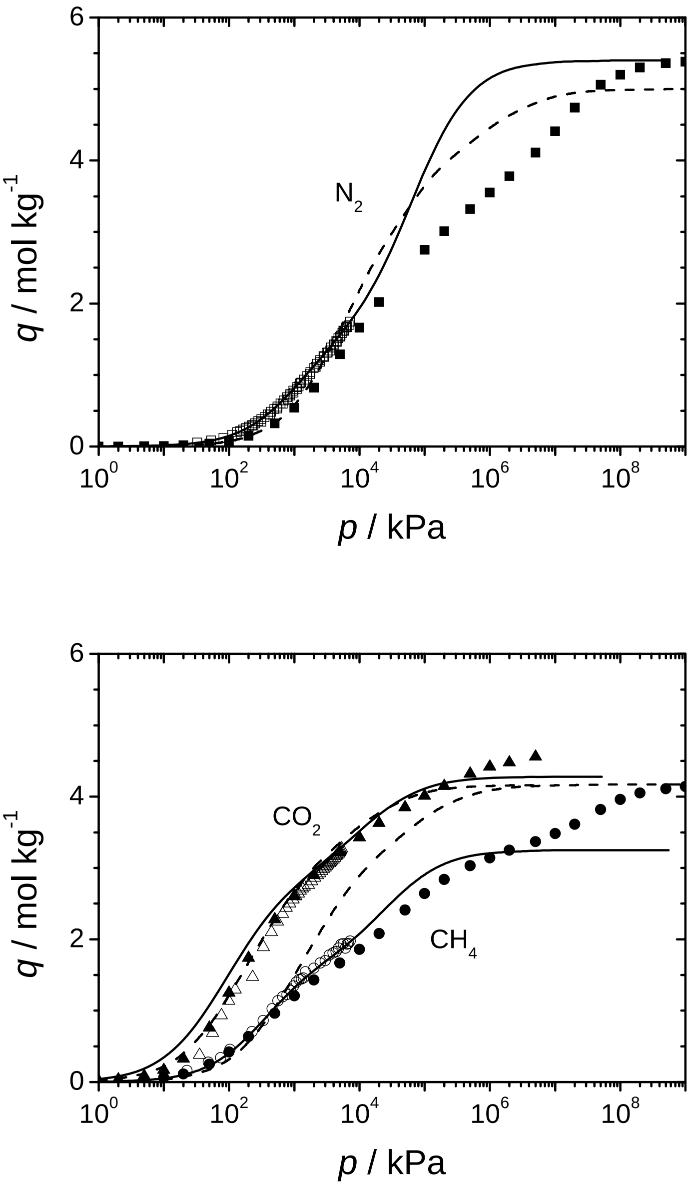

Figure 14. Comparison of experimental adsorption data (open symbols) of CO_2, N_2 and CH_4 in DD3R crystals at 303 K with isotherms obtained from GCMC simulations at 300 K (closed symbols) [30,32][Chapter 5B and 5D]. Solid lines represent model fit results of the experimental data. Dashed lines are modelling results of the statistical model isotherm [55]; the model fit is based on data up to 1000 kPa, above 1000 kPa the lines represent model predictions.

Li *et al.* [33] used the Statistical Model Isotherm (SMI) proposed by Ruthven [55] to obtain an isotherm up to the theoretical saturation loading based on relative low pressure data. The advantage of this approach would be an improved extrapolation of the isotherm at high pressure. Li *et al.* claimed that this isotherm is particularly suited for small-pore cage-like zeolites like CHA and DDR [33]. The loading in this case can be described as follows:

$$q_i = \frac{q_i^{sat}}{\Omega_i} \frac{K_i p_i + \sum_{m=2}^{\Omega_i} \frac{(K_i p_i)^m}{(m-1)!} \left[\frac{1 - \frac{m}{\Omega_i + 1}}{1 - \frac{1}{\Omega_i + 1}} \right]^m}{1 + K_i p_i + \sum_{m=2}^{\Omega_i} \frac{(K_i p_i)^m}{(m)!} \left[\frac{1 - \frac{m}{\Omega_i + 1}}{1 - \frac{1}{\Omega_i + 1}} \right]^m}, \tag{12}$$

where Ω represents the maximum number of molecules per cavity. The use of this isotherm is now evaluated by fitting the SMI to the GCMC data of CO_2, N_2 and CH_4 up to 1000 kPa; the higher pressure data are predicted based on this model fit. The maximum number of molecules per cage are assumed to be 5, 5 and 6 for CO_2, CH_4 and N_2, respectively. The SMI prediction is good in case of CO_2, but very poor for CH_4 and N_2 (Figure 14). Clearly one should be very cautious to rely on model extrapolations of this type of isotherm.

Single component isotherms of CO_2, N_2, CH_4 have been calculated from GCMC simulations between 195 to 573 K. These data have been fitted by a three-site Langmuir isotherm of which the constants are listed in Refs [30,32][Chapter 5B and 5D]. Given the good agreement of the experimental and GCMC isotherms it is assessed if using the GCMC isotherms as input for the IAST calculations has advantages over using the experimental isotherms.

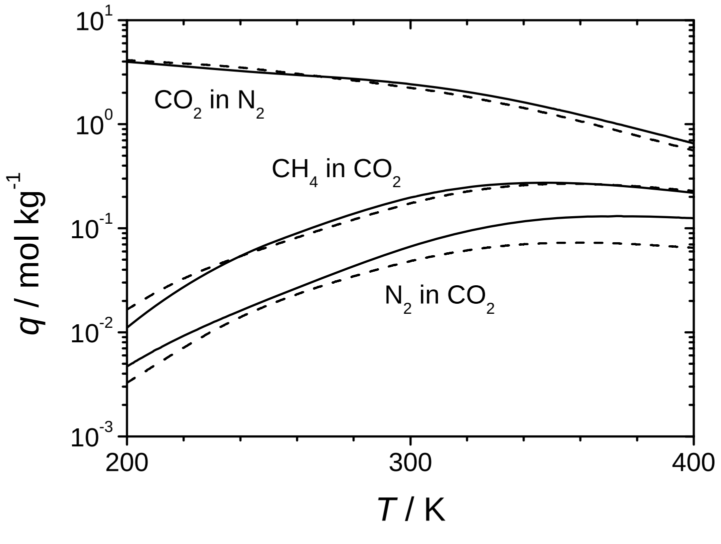

Figure 15. Mixture loadings predicted by the IAST of CO_2/CH_4 and N_2/CO_2 mixtures with equal partial pressure at a total pressure of 1000 kPa. Solid lines are predictions using the experimental adsorption data and dashed lines GCMC data fits, respectively.

Figure 15 shows the loading prediction of a mixture of CO_2/CH_4 and CO_2/N_2 at equal partial pressure of 500 kPa. The CO_2 loading is only presented in a mixture with N_2 because it is nearly identical to its loading in a mixture with CH_4. Only the N_2 loading is quite sensitive to the input isotherm parameters: it is higher when the experimental isotherms are used. This is due to the overprediction of the N_2 loading by these model fit parameters at pressures outside of the experimental range, as shown in Figure 13. Note that Figure 15 also reveals strong competitive adsorption effects of CO_2 over N_2 and CH_4 pushing their loadings downward, specifically at low temperatures.

References

[1] Y. Morigami, M. Kondo, J. Abe, H. Kita, and K. Okamoto, *Separation and Purification Technology*, 25, **2001**, 251.

[2] J. Caro and M. Noack, *Microporous and Mesoporous Materials*, 115, **2008**, 215.

[3] J. van den Bergh, W. Zhu, J. Gascon, J. A. Moulijn, and F. Kapteijn, *Journal of Membrane Science*, 316, **2008**, 35.

[4] T. Tomita, K. Nakayama, and H. Sakai, *Microporous and Mesoporous Materials*, 68, **2004**, 71.

[5] S. G. Li, J. G. Martinek, J. L. Falconer, R. D. Noble, and T. Q. Gardner, *Industrial & Engineering Chemistry Research*, 44, **2005**, 3220.

[6] J. M. van de Graaf, F. Kapteijn, and J. A. Moulijn, *AIChE Journal*, 45, **1999**, 497.

[7] A. M. Avila, H. H. Funke, Y. Zhang, J. L. Falconer, and R. D. Noble, *Journal of Membrane Science*, 335, **2009**, 32.

[8] J. M. van de Graaf, E. van der Bijl, A. Stol, F. Kapteijn, and J. A. Moulijn, *Industrial & Engineering Chemistry Research*, 37, **1998**, 4071.

[9] F. T. de Bruijn, L. Sun, Z. Olujic, P. J. Jansens, and F. Kapteijn, *Journal of Membrane Science*, 223, **2003**, 141.

[10] F. Kapteijn, W. Zhu, J. A. Moulijn, and T. Q. Gardner, Zeolite Membranes: Modeling and Application, in: Structured Catalysts and Reactors, Cybulski, A. and Moulijn, J. A. (Eds), Ch. 20, **2005**, Taylor & Francis Group, Boca Raton, FL, 701.

[11] S. L. Reitmeier, O. C. Gobin, A. Jentys, and J. A. Lercher, *Angewandte Chemie-International Edition*, 48, **2009**, 533.

[12] E. Lehmann, C. Chmelik, H. Scheidt, S. Vasenkov, B. Staudte, J. Karger, F. Kremer, G. Zadrozna, and J. Kornatowski, *Journal of the American Chemical Society*, 124, **2002**, 8690.

[13] J. Kärger, P. Kortunov, S. Vasenkov, L. Heinke, D. R. Shah, R. A. Rakoczy, Y. Traa, and J. Weitkamp, *Angewandte Chemie-International Edition*, 45, **2006**, 7846.

[14] L. Zhang, C. Chmelik, A. N. C. van Laak, J. Kärger, P. E. de Jongh, and K. P. de Jong, *Chemical Communications*, **2009**, 6424.

[15] R. M. Barrer, *Journal of the Chemical Society-Faraday Transactions*, 86, **1990**, 1123.

[16] M. H. F. Kox, E. Stavitski, J. C. Groen, J. Perez-Ramirez, F. Kapteijn, and B. M. Weckhuysen, *Chemistry-A European Journal*, 14, **2008**, 1718.

[17] E. Stavitski, M. R. Drury, D. A. M. de Winter, M. H. F. Kox, and B. M. Weckhuysen, *Angewandte Chemie-International Edition*, 47, **2008**, 5637.

[18] L. Karwacki, M. H. F. Kox, D. A. M. de Winter, M. R. Drury, J. D. Meeldijk, E. Stavitski, W. Schmidt, M. Mertens, P. Cubillas, N. John, A. Chan, N. Kahn, S. R. Bare, M. Anderson, J. Kornatowski, and B. M. Weckhuysen, *Nature Materials*, 8, **2009**, 959.

[19] L. Karwacki, E. Stavitski, M. H. F. Kox, J. Kornatowski, and B. M. Weckhuysen, *Angewandte Chemie-International Edition*, 46, **2007**, 7228.

[20] O. Geier, S. Vasenkov, E. Lehmann, J. Kärger, U. Schemmert, R. A. Rakoczy, and J. Weitkamp, *Journal of Physical Chemistry B*, 105, **2001**, 10217.

[21] J. van den Bergh, J. Gascon, and F. Kapteijn, Diffusion in Zeolites, in: Zeolites and Catalysis: Synthesis, Reactions and Applications, Cejka, Jiri, Corma, A., and Zones, S. I. (Eds), Ch. 13, **2010**, Wiley, New York, 361.

[22] S. Miachon, P. Ciavarella, L. van Dyk, I. Kumakiri, K. Fiaty, Y. Schuurman, and J. A. Dalmon, *Journal of Membrane Science*, 298, **2007**, 71.

[23] J. B. Lee, H. H. Funke, R. D. Noble, and J. L. Falconer, *Journal of Membrane Science,* 321, **2008**, 309.

[24] R. Krishna and J. A. Wesselingh, *Chemical Engineering Science*, 52, **1997**, 861.

[25] R. Krishna and L. J. P. van den Broeke, *Chemical Engineering Journal and the Biochemical Engineering Journal*, 57, **1995**, 155.

[26] F. Kapteijn, J. A. Moulijn, and R. Krishna, *Chemical Engineering Science*, 55, **2000**, 2923.

[27] W. D. Zhu, P. Hrabanek, L. Gora, F. Kapteijn, and J. A. Moulijn, *Industrial & Engineering Chemistry Research*, 45, **2006**, 767.

[28] G. R. Gavalas, *Industrial & Engineering Chemistry Research*, 47, **2008**, 5797.

[29] R. Krishna and J. M. van Baten, *Microporous and Mesoporous Materials*, 109, **2008**, 91.

[30] J. van den Bergh, S. Ban, T. J. H. Vlugt, and F. Kapteijn, *Journal of Physical Chemistry C*, 113, **2009**, 17840.

[31] J. van den Bergh, S. Ban, T. J. H. Vlugt, and F. Kapteijn, *Journal of Physical Chemistry C*, 113, **2009**, 21856.

[32] J. van den Bergh, S. Ban, T. J. H. Vlugt, and F. Kapteijn, *Separation and Purification Technology*, 73, **2010**, 151.

[33] S. Li, J. L. Falconer, R. D. Noble, and R. Krishna, *Industrial & Engineering Chemistry Research*, 46, **2006**, 3904.

[34] R. Krishna, D. Paschek, and R. Baur, *Microporous and Mesoporous Materials,* 76, **2004**, 233.

[35] J. van den Bergh, W. Zhu, F. Kapteijn, J. A. Moulijn, K. Yajima, K. Nakayama, T. Tomita, and S. Yoshida, *Research on Chemical Intermediates*, 34, **2008**, 467.

[36] J. Kuhn, K. Yajima, T. Tomita, J. Gross, and F. Kapteijn, *Journal of Membrane Science*, 321, **2008**, 344.

[37] W. Zhu, F. Kapteijn, J. A. Moulijn, M. C. den Exter, and J. C. Jansen, *Langmuir*, 16, **2000**, 3322.

[38] W. Zhu, F. Kapteijn, J. A. Moulijn, and J. C. Jansen, *Physical Chemistry Chemical Physics*, 2, **2000**, 1773.

[39] J. Gascon, W. Blom, A. van Miltenburg, A. Ferreira, R. Berger, and F. Kapteijn, *Microporous and Mesoporous Materials*, 115, **2008**, 585.

[40] J. van den Bergh, A. Tihaya, and F. Kapteijn, *Microporous and Mesoporous Materials*, 132, **2010**, 137.

[41] M. C. Mittelmeijer-Hazeleger, A. F. P. Ferreira, and A. Bliek, *Langmuir*, 18, **2002**, 9613.

[42] J. van den Bergh, W. Zhu, J. C. Groen, F. Kapteijn, J. A. Moulijn, K. Yajima, K. Nakayama, T. Tomita, and S. Yoshida, *Studies in Surface Science and Catalysis*, 170 A, **2007**, 1021.

[43] P. J. A. M. Kerkhof, *The Chemical Engineering Journal and the Biochemical Engineering Journal*, 64, **1996**, 319.

[44] J. Karger, P. Kortunov, S. Vasenkov, L. Heinke, D. R. Shah, R. A. Rakoczy, Y. Traa, and J. Weitkamp, *Angewandte Chemie-International Edition*, 45, **2006**, 7846.

[45] N. Hedin, G. J. DeMartin, W. J. Roth, K. G. Strohmaier, and S. C. Reyes, *Microporous and Mesoporous Materials*, 109, **2008**, 327.

[46] S. E. Jee and D. S. Sholl, *Journal of the American Chemical Society*, 131, **2009**, 7896.

[47] N. Corcoran and R. Chance, Poster 151 at: Diffusion Fundamentals I, Leipzig, 2005.,

[48] R. Krishna and J. M. van Baten, *Chemical Physics Letters*, 446, **2007**, 344.

[49] R. Krishna and J. M. van Baten, *Separation and Purification Technology*, 61, **2008**, 414.

[50] M. Murthi and R. Q. Snurr, *Langmuir*, 20, **2004**, 2489.

[51] C. R. Wilke, *Journal of Chemical Physics*, 18, **1950**, 517.

[52] W. N. Fueller, P. D. Schettler, and J. C. Giddings, *Industrial & Engineering Chemistry Research*, 58, **1966**, 19.

[53] J. M. van de Graaf, Permeation and separation properties of supported silicalite-1 membranes, **1998**, PhD Thesis, Delft University of Technology, Delft.

[54] A. L. Myers and J. M. Prausnitz, *AIChE Journal*, 11, **1965**, 121.

[55] D. M. Ruthven, *Nature Physical Science*, 232, **1971**, 70.

5F

Reconciling the Relevant Site Model and dynamically corrected Transition State Theory

The Relevant Site Model (RSM)[Chapter 5A)] closely resembles the well-known concept of dynamically corrected Transition State Theory (dcTST) which is often used in molecular simulations to study the dynamics of rare events. In the present chapter, we investigate this parallel in detail. It turns out that the essential elements in the RSM, the ratio of the RS and total loading an the probability of jumping to the next cage, are directly related to those in dcTST, *i.e.* the probability that a molecule is on top of the free energy barrier and the transmission coefficient κ. Therefore, the RSM provides a direct link between properties at the molecular scale and the macroscopic Maxwell-Stefan diffusivity. The formalism may be used to predict the Maxwell-Stefan diffusivity from dcTST simulations and the adsorption isotherm.

This chapter is based on the following publication:

T. J. H. Vlugt, J. van den Bergh, D. Dubbeldam, and F. Kapteijn, *Chemical Physics Letters*, **2010**, doi:10.1016/j.cplett.2010.06.047.

1 Introduction

Understanding transport diffusion in zeolites is of crucial importance in the chemical industry, for example for the design of catalysts or zeolite membranes [1,2]. Unfortunately, the Maxwell-Stefan (MS) approach to mass transport is seriously hindered by the observation that in zeolites the corrected transport diffusivity often strongly depends on the loading [2]. Therefore, there is a considerable interest in predictive models describing the dependency of the transport diffusivity on the concentration. Recently, we introduced the Relevant Site Model [3-5][Chapter 5A-D] to describe the concentration dependency of the transport diffusivity (often called Maxwell-Stefan diffusivity or corrected diffusivity) of small guest molecules adsorbed in zeolites. The model is formulated around the central idea of segregated adsorption in cage-like zeolites, *i.e.* molecules are located either in the cage or at its window site. Only molecules located at the window site between the two cages will make a contribution to mass transport. The RSM can correctly describe the concentration dependency of the transport diffusivity of small molecules like N_2, CO_2, CH_4 and mixtures thereof in DDR, CHA, MFI, and FAU-type zeolites [3-5][Chapter 5A-D] and adequately describes the permeation and separation of gas mixtures through a DDR membrane [5,6][Chapter 5E]. The idea that only a fraction of the molecules (*i.e.* those molecules that are present at the so-called relevant site) make a contribution to mass transfer strongly resembles the idea of dynamically corrected Transition State Theory (dcTST) [7-9]. This technique is often used in molecular simulations to compute the hopping rate of molecules between two basins of attraction that are separated by a large free energy barrier, for which conventional Molecular Dynamics (MD) simulations provide insufficient statistics. The self-diffusivity directly follows from the hopping rate and the characteristic distance between the two basins of attraction. Essentially, this calculation is split into two parts: the calculation of the probability that a molecule is on top of the free energy barrier and the calculation of the flux for molecules that are initiated on top of the free energy barrier. In the present work, we will show that the RSM model can correctly describe the two individual parts of the dcTST calculation. Therefore, the RSM provides a direct link between properties at the molecular scale and the macroscopic Maxwell-Stefan diffusion coefficient.

2 Results

In the RSM, the concentration dependency of the MS diffusivity $Đ$ is given by [3][Chapter 5A]:

$$Đ = Đ^{*}(0)(1-\theta)\frac{q^{*}}{q}, \qquad (1)$$

in which $Đ^{*}(0)$ is a constant, q is the loading of guest molecules in the zeolite, q^{*} is the loading of molecules at the so-called relevant site, and θ is the occupancy of the zeolite ($\theta = q/q^{sat}$, q^{sat} being the saturation loading of the zeolite). Throughout the chapter, properties evaluated at the relevant site are denoted with a superscript *. The loading at the relevant site is modelled using a Langmuir type isotherm:

$$q^{*} = \frac{q^{sat*}K^{*}f}{1+K^{*}f}, \qquad (2)$$

in which K^{*} and q^{sat*} are the Langmuir constants of the relevant site and f is the fugacity that results in the total loading q of guest molecules in the zeolite. Equations (1) and (2) combined with the adsorption isotherm *q(f)* are sufficient to describe the loading dependency of the MS diffusivity. Following our earlier work, the self-diffusivity of guest molecules in small-pore cage-type zeolites is well approximated by [3-5][Chapter 5B-D]:

$$D_{self} = \frac{Đ}{1+\theta^{*}}, \qquad (3)$$

with $\theta^{*} = q^{*}/q^{sat,*}$, leading to the following final expression for the self-diffusivity :

$$D_{self} = Đ^{*}(0)\cdot\frac{q^{*}}{q}\cdot\frac{1-\theta}{1+\theta^{*}}, \qquad (4)$$

In Figure 1 we show a fit of Equation (4) to the self-diffusivity of methane in all-silica LTA-type zeolite at 600K, obtained from MD simulations. This zeolite contains cages that are interconnected by small windows. Adsorption sites are present both in the cages and in the windows [10]. Clearly, both D_{Self} and $Đ$ are strongly dependent on the loading. The MD data is taken from [4,11]. For details on the computation of D_{Self} using MD, as well as the required adsorption isotherm *q(f)* we refer the reader to Appendix 5F.I. Indeed, the RSM can correctly predict the concentration dependence of D_{Self}, capturing correctly the maximum of D_{Self} around q = 10 molecules/cage (mol./cage). In the fitting procedure, we used a constant value of q^{sat} of 18 mol./cage which follows from the adsorption isotherm. An even better fit of D_{Self} is obtained by also fitting the value of q^{sat}; for q^{sat} = 16 mol./cage the RSM perfectly captures the MD data. Setting q^{sat} = 16 mol./cage may be justified by the fact that at this loading, the adsorption isotherm shows a clear inflection (Appendix 5F.I). However, we feel that this is not a crucial issue here. Figure 1 also shows the MS diffusivity computed from the self diffusivity and Equation (3), showing an excellent agreement with the MS diffusivity obtained from MD simulations. This confirms that Equation (3) is indeed a good approximation to relate the self and MS diffusivity in this type of zeolite-host system.

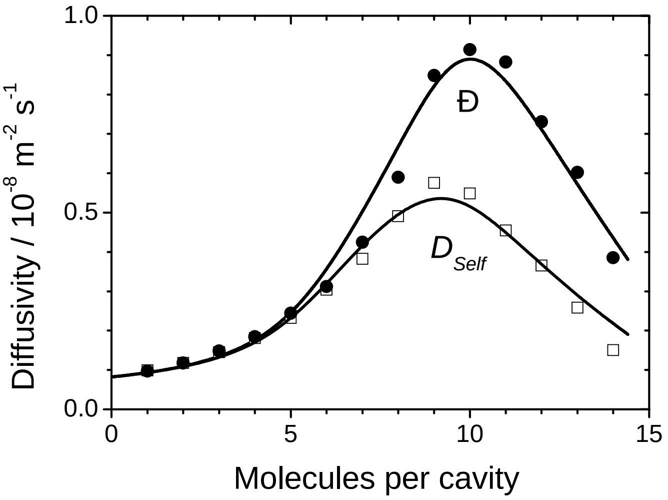

Figure 1. Computed self-diffusivity D_{Self} from MD simulations (methane in all-silica LTA at 600 K) fitted to Equation (4) using the computed adsorption isotherm *q(f)* (see Appendix 5F.I). The best fit is obtained for $q^{sat*}\text{Đ}^{*}(0)$ = 27.5 10^{-8} [m^2s^{-1} molecule per cage] and K^{*} = 6.34 10^{-10} Pa^{-1}. We used a fixed saturation loading (q^{sat}) of 18 molecules per cage. An even better fit of the data is obtained by also fitting the value of q^{sat} (Figure 5). Also shown is the computed Maxwell-Stefan diffusivity Đ from molecular simulations compared with the result from Equation (3), using the values for $q^{sat*}\text{Đ}^{*}(0)$ and K^{*} reported above.

It is instructive to compare the obtained results with dcTST. Following Beerdsen *et al.* [12], we consider the transfer of one single guest molecule from basin of attraction A to basin of attraction B, in the presence of the zeolite and all other guest molecules [7,12]. The hopping rate predicted by TST equals:

$$k_{A\to B}^{TST} = \sqrt{\frac{k_B T}{2\pi M}}\,\frac{\exp\left(-\beta F\left(x^{\#}\right)\right)}{\int\limits_{cageA}\exp\left(-\beta F\left(x^{\#}\right)\right)dx}, \tag{5}$$

in which k_B is the Boltzmann constant, T is the absolute temperature, β =1/(k_BT), and $F(x)$ is the free energy of a single guest molecule at position x in the presence of the other guest molecules and the zeolite (this term is usually computed from umbrella sampling simulations [7]. It is important to note that $F(x)$ will strongly depend on the concentration of guest molecules adsorbed in the zeolite. The top of the free energy barrier is denoted by $x^{\#}$. The reaction coordinate x is chosen as the line connecting the centres of two neighbouring cages. The mapping of the (multidimensional) free energy onto the one-dimensional reaction coordinate x results in a maximum of $F(x)$ near $x^{\#}$ [11]. The actual hopping rate $k_{A\rightarrow B}$ equals [7,12]:

$$k_{A\rightarrow B} = \kappa \cdot k_{A\rightarrow B}^{TST}, \tag{6}$$

in which κ is the transmission coefficient which accounts for recrossings of trajectories starting from $x^{\#}$. Its value depends on both the concentration of guest molecules as well as on the precise choice of $x^{\#}$ [11]. Provided that the free energy barrier is sufficiently large, Equation (6) is an exact expression for the hopping rate and one can show that it does not depend on the precise choice of $x^{\#}$. The concentration dependent self-diffusivity follows directly from the concentration dependent hopping rate:

$$D_{Self} = \lambda^2 k_{A\rightarrow B}, \tag{7}$$

in which λ is the distance between the basins of attraction. It is important to note that dcTST provides access to the self-diffusivity and *not* the Maxwell-Stefan diffusivity. The probability that a molecule is located at position x is directly related to its free energy by $P(x) = C\exp[-\beta F(x)]$ in which C is a constant [11]. Assuming that the relevant site is located near the top of the free energy barrier [13,14], we propose that the fraction of molecules at the top of the barrier is given by:

$$\frac{q^*}{q} \sim w\left(x^{\#}\right), \tag{8}$$

in which we defined $w(x^{\#})$ as:

$$\frac{\exp\left(-\beta F\left(x^{\#}\right)\right)}{\int\limits_{cageA} \exp\left(-\beta F\left(x^{\#}\right)\right)dx} \tag{9}$$

Figure 2 shows that for loadings lower than 14 molecules per cage this linear relation holds very well. Inserting Equations (5-8) into Equation (4) shows that the concentration dependency of the transmission coefficient κ is given by:

$$\kappa \sim \kappa_0 \frac{1-\theta}{1+\theta^*}, \tag{10}$$

in which κ_0 is the transmission coefficient at zero loading. This relation predicts that when the zeolite is fully occupied (θ = 1) both the self and Maxwell Stefan diffusivity will become zero. Consider the situation that a small guest molecule is adsorbed in the zeolite at a very low concentration. In this situation, for an optimal choice of $x^{\#}$ the transmission coefficient will be very close to 1 by definition, leading to:

$$\kappa = \frac{1-\theta}{1+\theta^*}. \tag{11}$$

In Figure 3 we compare the prediction of Equation (11) to the value of κ obtained directly from molecular simulations. In the simulations, $x^{\#}$ was positioned exactly in the middle between the two cages, indeed resulting $\kappa \approx 1$ for a small molecule like methane at low loading. Clearly, Equations (8) and (11) capture the correct trends, showing a maximum difference with the data obtained from molecular simulations of around 15 %.

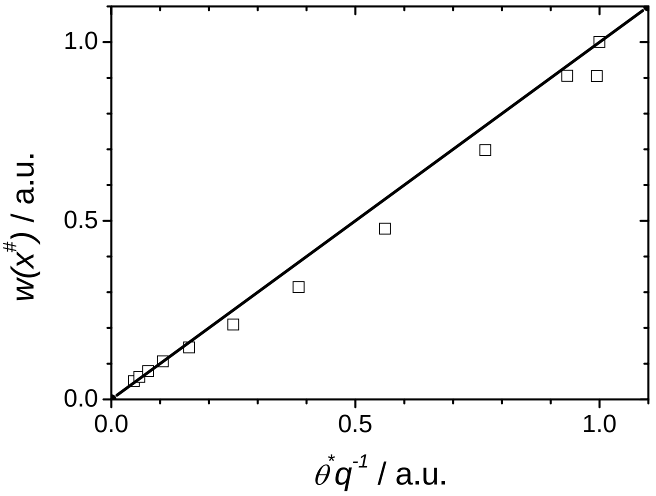

Figure 2. Test of Equation (8) using the values for $q^{sat*}\text{Đ}^*(0)$ and K^* from Figure 1. The methane loading varies from 1 mol./cage to 14 mol./cage. Both axes are scaled in such a way that at the data point at q = 13 corresponds to (1,1). The data for $w^{\#}$ were taken from the simulations of Ref. [11].

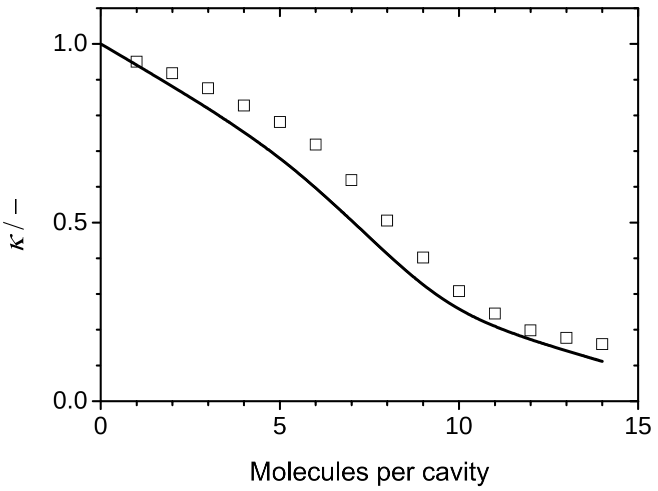

Figure 3. Computed transmission coefficient κ from dcTST simulations (symbols, taken from Ref. [11]), compared with the prediction of Equation (11) (line). For both $q^{sat^*} Đ^*(0)$ and K^*, the same values as in Figure 2 are used.

3 Concluding remarks

In summary, we showed that the RSM can correctly describe the concentration dependent self- and Maxwell-Stefan diffusivity of methane in the all-silica LTA-type zeolite at 600 K. The two key terms present in the RSM, the ratio of the RS and total loading an the probability of jumping to the next cage, closely resemble the probability that a guest molecule is on top of the barrier and the transmission coefficient κ, which are the key ingredients of the dcTST approach. Therefore, the RSM could be considered as a macroscopic model describing the microscopic information of hopping process of adsorbed guest molecules between interconnected cages, and it may be used to predict the value of the transmission coefficient. For molecules larger than methane, $\kappa \neq 1$ for low loadings [11]. It is an open question whether in this case $\kappa \sim (1-\theta)/(1+\theta^*)$ or whether modifications of the RSM are needed. Using Equation (3), the approach presented here can also be used to predict the MS diffusivity from dcTST simulations. This is in particular useful for systems in which the dynamics is so slow that conventional MD simulations can not be used to compute this.

Appendix I

Zeolite structure and force field

The LTA zeolite framework consists of large spherical α-cages (8 per unit cell) of approximately 11 Å, that are interconnected via windows with a diameter of approximately 4.1 Å. Its unit cell has a cubic space group $Fm\bar{3}c$ with $a = b = c = 24.555$ Å, and $\alpha = \beta = \gamma = 90$ ° [15]. In all simulations, LTA-type zeolite was modelled as a rigid structure [16], with atomic positions taken from the Atlas of Zeolite Framework Types [17]. Non-framework cations are not present as we only consider an all-silica zeolites here. The guest-host and guest-guest interactions were modelled using Lennard-Jones potentials that were truncated and shifted at 12 Å. The guest-host interactions are dominated by the dispersive interactions between the guest molecules and the oxygen atoms of the zeolite [16]. Methane is considered as a chargeless united atom. The used force field accurately reproduces the thermodynamic properties of alkanes in various all-silica zeolite framework types [18,19]. For more information about the force field, we refer the reader to Refs. [18,19].

Computing adsorption isotherms

Monte Carlo simulations in the grand-canonical (μVT) ensemble [7] were used to compute the adsorption isotherm of methane in all-silica LTA. In these simulations, a fixed chemical potential (or fugacity f) of methane was imposed, resulting in a certain average number of adsorbed guest molecules in the zeolite host. In these simulations, it is important to block the inaccessible parts of the pore structure [20]. The use of a rigid zeolite is justified here, as it is well-known that framework flexibility is not important for computing adsorption properties of alkanes in all-silica zeolites [21]. For more information about the simulation technique, the reader is referred to Refs. [7,18,22].

Computing self- and Maxwell-Stefan diffusivities

Self- and Maxwell-Stefan diffusivities were previously computed using Equilibrium Molecular Dynamics simulations [7,23,24] in the NVT ensemble, see Ref. [11]. The temperature is controlled using a Nosé-Hoover Chain thermostat [25]. The self- and Maxwell-Stefan diffusivities follow directly from the mean-squared displacements of the methane molecules, see for example Refs. [26,27]. It was reported earlier for this system that diffusivities obtained with flexible and with rigid frameworks are practically the same [28]. The self-diffusivity was also computed using dynamically corrected Transition State Theory [7], leading to exactly the same value of the computed self-diffusivity at all loadings reported in this chapter [11]. This technique computes the hopping rate of methane molecules between the α-cages by considering the probability that a molecule is on top of the barrier between the cages, as well as the flux of methane molecules at the top of the barrier. These contributions are computed using umbrella sampling simulations [7] and Molecular Dynamics simulations respectively. More details on the dynamically corrected Transition State Theory are given in Ref. [11,12].

Adsorption isotherm of methane in all-silica LTA at 600 K

In Figure 4, the computed adsorption isotherm of methane in all-silica LTA at 600 K is presented. The isotherm can be described well using a multi-site Langmuir isotherm:

$$q(f) = \sum_{i}^{n} \frac{q_i^{sat} K_i f}{1 + K_i f}, \tag{12}$$

in which q_i^{sat} is the saturation loading of site *i* and K_i is its adsorption constant. The fugacity is denoted by *f*. The data in Figure 4 is well described using *n* = 5, the estimated parameters are presented in Table 1.

Table 1. Estimated five-site Langmuir isotherm parameters describing the CH4 adsorption data in LTA at 600 K. The maximum loading is fixed at 18 mol./cage.

i	1	2	3	4	5
q_i^{sat} / mol. cage^{-1}	5.38	4.17	4.42	0.838	3.19
K_i / Pa^{-1}	$3.80\cdot10^{-8}$	$1.87\cdot10^{-9}$	$6.55\cdot10^{-11}$	$1.50\cdot10^{-12}$	$1.71\cdot10^{-15}$

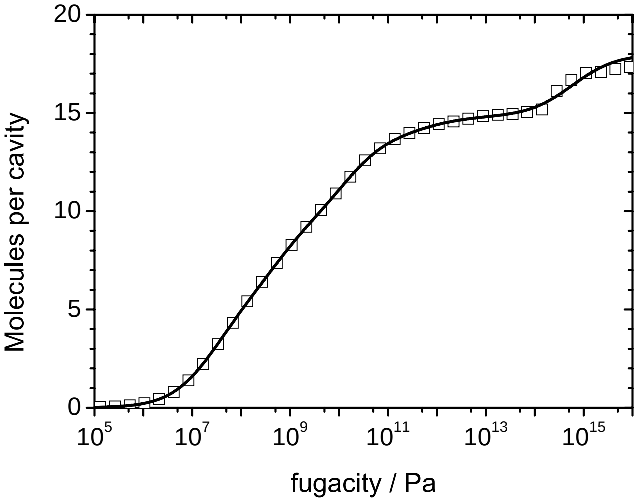

Figure 4. Computed adsorption isotherm of methane in all-silica LTA-type zeolite at 600 K. The line shows a fit to a five-site Langmuir isotherm (Equation (12)).

Influence of q^{sat} on the fitted self diffusivity

In Figure 5, the sensitivity of the computed self diffusivity as a function of the total loading q for various values of q^{sat}. Clearly, the data from MD simulations is best described using q^{sat} = 16 mol./cage, but the differences are small.

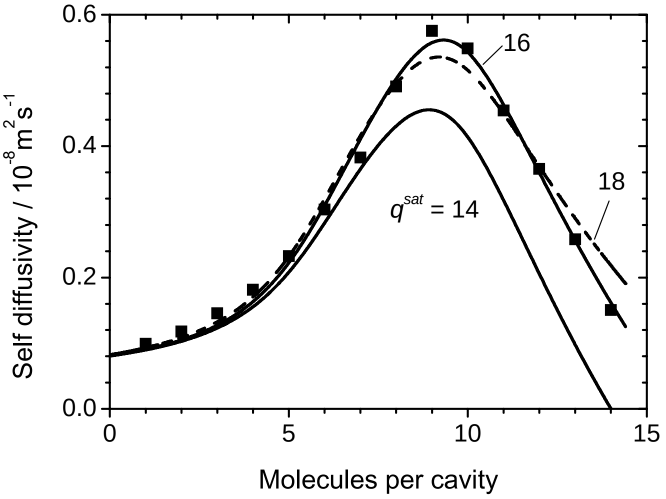

Figure 5. Computed self-diffusivity of methane in all-silica LTA-type zeolite at 600 K (squares), fitted to Equation (4) for various values of q^{sat}.

References

[1] R. Krishna and J. A. Wesselingh, *Chemical Engineering Science*, 52, **1997**, 861.

[2] R. Krishna and J. M. van Baten, *Chemical Engineering Science*, 64, **2009**, 3159.

[3] J. van den Bergh, S. Ban, T. J. H. Vlugt, and F. Kapteijn, *Journal of Physical Chemistry C*, 113, **2009**, 17840.

[4] J. van den Bergh, S. Ban, T. J. H. Vlugt, and F. Kapteijn, *Journal of Physical Chemistry C*, 113, **2009**, 21856.

[5] J. van den Bergh, S. Ban, T. J. H. Vlugt, and F. Kapteijn, *Separation and Purification Technology*, 73, **2010**, 151.

[6] J. van den Bergh, M. C. Mittelmeijer-Hazeleger, and F. Kapteijn, *Journal of Physical Chemistry C*, 114, **2010**, 9397.

[7] D. Frenkel and B.Smit, Understanding Molecular Simulation: from Algorithms to Applications 2nd ed., **2002**, Academic Press, San Diego.

[8] C. H. Bennett, Exact Defect Calculations in Model Substances, in: Diffusion in solids: recent developments, Nowick, A. S. and Burton, J. J. (Eds), Ch. 2, **1975**, Academic Press, New York,

[9] D. Chandler, *Journal of Chemical Physics*, 68, **1978**, 2959.

[10] S. Fritzsche, R. Haberlandt, G. Hofmann, J. Kärger, K. Heinzinger, and M. Wolfsberg, *Chemical Physics Letters*, 265, **1997**, 253.

[11] D. Dubbeldam, E. Beerdsen, T. J. H. Vlugt, and B. Smit, *The Journal of Chemical Physics*, 122, **2005**, 224712.

[12] E. Beerdsen, B. Smit, and D. Dubbeldam, *Physical Review Letters*, 93, **2004**,

[13] A. Schuring, S. M. Auerbach, S. Fritzsche, and R. Haberlandt, *Journal of Chemical Physics*, 116, **2002**, 10890.

[14] E. Beerdsen, D. Dubbeldam, and B. Smit, *Journal of Physical Chemistry B*, 110, **2006**, 22754.

[15] J. J. Pluth and J. V. Smith, *Journal of the American Chemical Society*, 102, **1980**, 4704.

[16] A. G. Bezus, A. V. Kiselev, A. A. Lopatkin, and P. Q. Du, *Journal of the Chemical Society-Faraday Transactions II*, 74, **1978**, 367.

[17] C. Baerlocher, L.B.McCusker, and D.H.Olson, Atlas of Zeolite Framework Types, **2007**, Elsevier, Amsterdam.

[18] D. Dubbeldam, S. Calero, T. J. H. Vlugt, R. Krishna, T. L. M. Maesen, and B. Smit, *Journal of Physical Chemistry B*, 108, **2004**, 12301.

[19] D. Dubbeldam, S. Calero, T. J. H. Vlugt, R. Krishna, T. L. M. Maesen, E. Beerdsen, and B. Smit, *Physical Review Letters*, 93, **2004**,

[20] R. Krishna and J. M. van Baten, *Langmuir*, 26, **2010**, 2975.

[21] T. J. H. Vlugt and M. Schenk, *Journal of Physical Chemistry B*, 106, **2002**, 12757.

[22] T. J. H. Vlugt, R. Krishna, and B. Smit, *Journal of Physical Chemistry B*, 103, **1999**, 1102.

[23] M. P. Allen and D.J.Tildesley, Computer simulation of liquids, **1987**, Clarendon Press, Oxford.

[24] D. C. Rapaport, The art of molecular dynamics simulation, **2004**, Cambridge University Press, Cambridge.

[25] G. J. Martyna, M. E. Tuckerman, D. J. Tobias, and M. L. Klein, *Molecular Physics*, 87, **1996**, 1117.

[26] D. Dubbeldam and R. Q. Snurr, *Molecular Simulation*, 33, **2007**, 305.

[27] R. Krishna, *Journal of Physical Chemistry C*, 113, **2009**, 19756.

[28] S. Fritzsche, M. Wolfsberg, R. Haberlandt, P. Demontis, G. B. Suffritti, and A. Tilocca, *Chemical Physics Letters*, 296, **1998**, 253.

6

Summary and evaluation: DD3R membranes in separation and catalytic processes

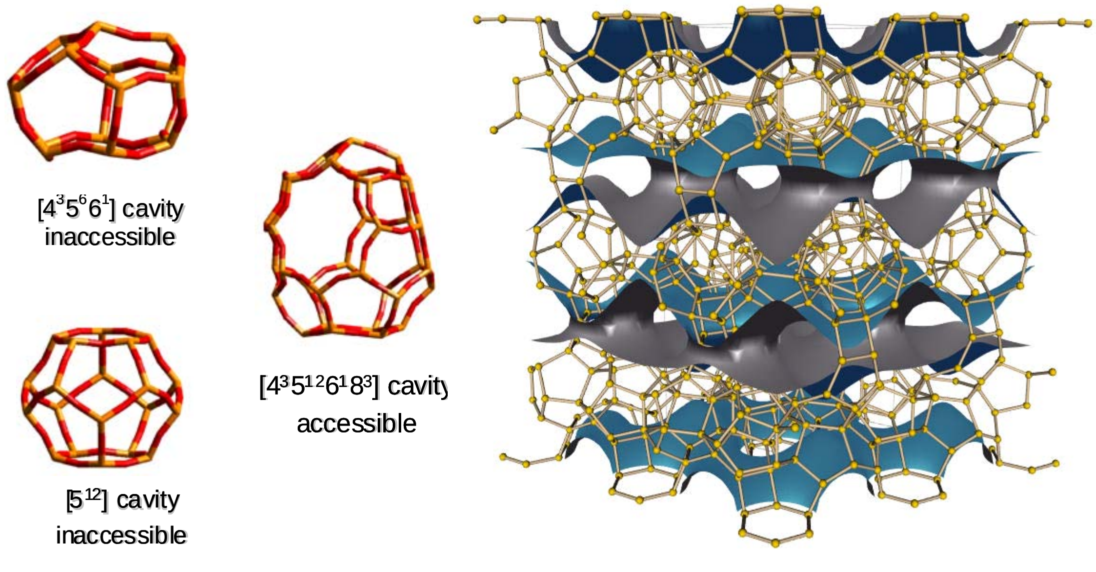

Summary

Around 2004 the annual energy consumption of the Dutch (petro-)chemical industry was estimated to be 460 PJ of which 200 PJ could be allocated to separation processes [1]. In 2009, 15% of the global energy consumption was required for separation and purification processes to produce commodities. Moreover, it is expected that in 2040 the global commodity demand is three times higher than in 2009 leading to an enormous energy demand increase in the coming decades related to separation processes [2]. These two examples clearly illustrate the need for the development of new innovative energy-efficient separation technologies. Membrane technology is considered a serious candidate to replace traditionally used thermally-driven separation processes, because of the large energy reduction that can be achieved [2-4]. An application particularly relevant for this thesis, is natural gas purification, which is by far the largest industrial gas separation application [5].

The focus of this thesis has been on a DD3R zeolite membrane. Zeolites are crystalline aluminosilicates with pores of sub-nanometer dimensions. Specific advantages of zeolite membranes are their high thermal and chemical stability and their molecular sieving ability. Two key aspects differentiate DD3R from other zeolites that make this zeolite particularly interesting to study: its small pore size and the possibility to synthesize it in an all-silica form. The 8-ring window has approximate dimensions of 0.36 × 0.44 nm which makes this material very interesting for separation of light gases which is not possible with larger-pore zeolites, like zeolite MFI. Other 8-ring zeolites are available, however very few have been synthesized successfully in all-silica form. Since it appears to be extremely challenging to make high quality membranes for gas separation from aluminum containing zeolites [6], the all-silica nature of DD3R is a clear advantage.

Anticipating the special properties of the DD3R topology in gas separation, the goal of the project has been to study the *application of DD3R zeolite membranes in separation and catalysis*. Special attention is paid to the understanding and modeling of the mass transport across such a membrane. The thesis objective has been approached by performance testing of a disc- and tubular-shaped DD3R membrane supplied by NGK-insulators in several gas separations and in one reactive separation: the dehydrogenation of isobutane in a DD3R zeolite membrane reactor. The permeation properties of a series of light gases and mixtures thereof have been analyzed as a function of temperature and pressure and compared to mass transport mechanisms available in literature. Because currently available mass transport models did not lead to satisfactory results a new approach to describe diffusion in zeolites has been proposed (the Relevant Site Model). Diffusivity data calculated from MD simulations have been used to develop and verify this new model.

Permeation and separation characteristics (Chapter 2 & 3)

Adsorption experiments of a series of light gases on DD3R crystals revealed the following order in amount adsorbed at 303 K and 120 kPa: $CO_2 = N_2O >> Kr \approx CH_4 > CO > N_2 \approx O_2 \approx Ar > H_2$. In case of Ne no significant adsorption could be detected. These isotherms could be modelled well by a single or dual-site Langmuir isotherm.

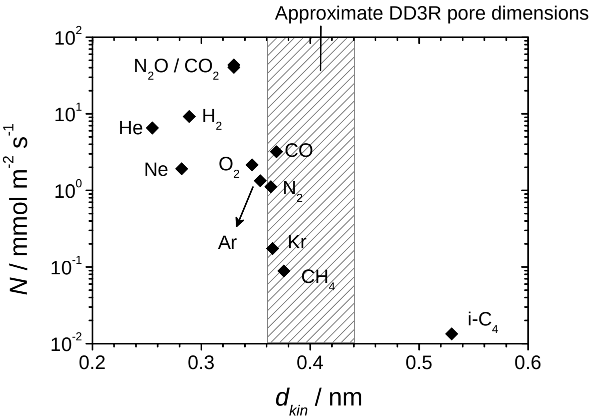

Figure 1. Single component fluxes through a DD3R membrane as a function of the kinetic diameter of the molecule at 303 K. Isobutane, CO and H_2 have been measured on the tubular membrane, all other components on a disc. The disc-data are multiplied with a factor 6 (Chapter 3).

The permeation and separation characteristics of light gases through DD3R membranes can be explained by taking into account: (1) steric effects introduced by the window opening of DD3R leading to molecular sieving and activated transport (Figure 1), (2) competitive adsorption effects, as observed for mixtures involving strongly adsorbing gases, and (3) momentum exchange between diffusing molecules in the zeolite. Momentum transfer appears only relevant in mixtures below 373 K that involve strong adsorbing component (CO_2 or N_2O). Competitive adsorption is also found only in case of mixtures that involve strong adsorbing components. Suppression of the flux of the weakly adsorbing component can be very strong and becomes manifest at low temperatures (< 303 K).

The single component permeance behaviour as a function of the temperature can be explained well by a surface diffusion mechanism [7] (Figure 2). In this case both diffusion and adsorption in the zeolite determine the observed permeance. Isobutane is too large to enter the DD3R pores and passes only through membrane defects. An important observation is that also the permeance of the weaker adsorbing components (H_2, He, N_2, CO) show monotonically decreasing permeances with increasing temperature and can be described by the surface diffusion mechanism. This result challenges the well-established idea that with increasing temperature a mass transport mechanism shift from adsorbed to non-adsorbed phase (activated gaseous

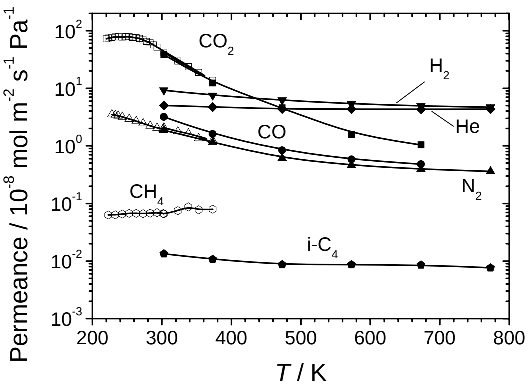

Figure 2. Permeance of CO_2, H_2, He, CO, N_2, CH_4 and isobutane through the DD3R membrane as a function of the temperature (Figure 5, Chapter 3).

diffusion) occurs in zeolite membranes. Both the disc and tube-shaped membrane showed a very similar permeation behaviour. The only difference between the two is that the permeance of the tubular membrane is a factor six higher, which is attributed to the smaller thickness of the membrane.

Although the observed mass transport mechanism is of the surface diffusion type, the components behave as much weaker adsorbing gases as could be expected from the adsorption isotherms. This is explained by the fact that mass transport is controlled by the weakly adsorbing window adsorption sites in DD3R (Chapter 5).

Binary permeation experiments revealed that particularly for natural gas separation (CO_2/CH_4) excellent results are obtained: very high separation factors (> 500 @ 303 K) (Figure 3) and high CO_2 fluxes, confirming the results of Tomita *et al.* [8]. The selectivity decreases with increasing total feed pressure, but up to 1500 kPa total feed pressure the selectivity remains above 100 up to 373 K. The N_2/CH_4 separation factor is quite good, but the low N_2 flux is clearly limiting successful application.

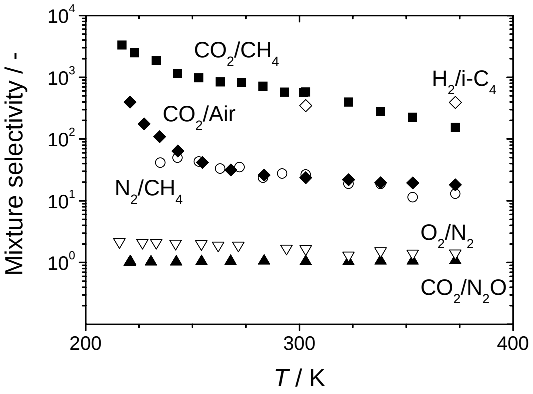

Figure 3. Selectivities of the investigated equimolar mixtures at 101 kPa total feed pressure as a function of the temperature.

Since the separation is predominantly due to molecular sieving, the O_2/N_2-separation factor is relatively low (≤ 2). Interestingly, CO_2 and N_2O behave (almost) identical in DD3R and cannot be separated (selectivity ~ 1). The ideal H_2/CO and CO_2/CO selectivities range from 3 to 12 and 10 to 2 between 303 and 673 K, respectively. These mixture selectivities were always below 5 and much lower than the ideal selectivities because of non-differential operation of the tubular membrane. The H_2/isobutane mixture selectivity at 101 kPa total feed pressure is ~ 400 in an equimolar binary mixture over a broad temperature range (303 – 773 K). The high separation factor is due to exclusion of isobutane from the DD3R pores.

Isobutane dehydrogenation (Chapter 4)

Alkane dehydrogenation reactions are industrially very relevant, but they are also class of reactions where the conversion can be (severely) equilibrium-limited at practical high temperature conditions necessary to perform the reaction. Low conversions lead to a large flow of alkane/alkene mixtures that needs to be separated and recycled. Particularly the separation of alkanes/alkenes is very energy intensive [9]. An approach to increase the single-pass conversion is by using a membrane reactor (MR). By *in situ* removal of the product H_2 an apparent equilibrium shift can be accomplished.

Because of the excellent H_2/isobutane selectivity and a reasonable H_2 permeance (~ $4.5 \cdot 10^{-8}$ mol m^{-2} s^{-1} Pa @ 773 K) the dehydrogenation of isobutane has been studied in a DD3R zeolite membrane reactor (MR) at 712 and 762 K. Experiments in a conventional packed bed reactor (PBR) served as benchmark, Cr_2O_3 on Al_2O_3 is used as catalyst.

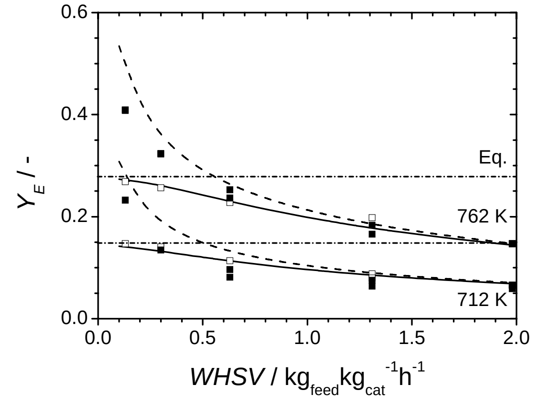

Figure 4. Isobutene yield in a packed bed (open symbols) and DD3R membrane reactor (closed symbols) at 762 and 712 K as s function of the *WHSV*. Solid, dashed and dash-dot lines represent PBR model fit results, MR model predictions and the equilibrium conversion, respectively.

At low residence times isobutene yields above the equilibrium yield based on feed conditions could be obtained. At 762 K and 0.13 $kg_{feed}kg_{cat}^{-1}h^{-1}$, the isobutene yield in the membrane reactor (MR) is 0.41, where the equilibrium yield is ~ 0.28. The increased yield is attributed to removal of H_2 from the reaction zone by the membrane. The removal of H_2 mildly promotes coke formation, suppresses hydrogenolysis reactions and slightly reduces the catalyst activity. During several months of high temperature operation the membrane quality did not change notably. The membrane permeation parameters and reaction rate constants have been estimated independently from membrane permeation and PBR experiments, respectively. From these parameters the behaviour of the MR can be simulated well. Two important dimensionless parameters determine the MR performance primarily, the Damköhler (Da) and membrane Péclet number (Pe_δ). For a significant improvement of the MR performance as compared to a PBR $Da \geq 10$ and $Pe_\delta \leq 0.1$. $DaPe_\delta$ should be ≈ 1 to optimally utilize both catalyst and membrane activity. In the current MR design both the hydrogen removal capacity and catalyst activity stand in the way of successful application. Using a more active catalyst *and* a more favourable area to volume ratio could greatly improve the MR performance. Operation at a higher feed pressure could be a possible solution. Since membranes with higher fluxes are already available, it is the limited catalyst activity and stability under relative low temperature and H_2 lean conditions that is an important limiting factor regarding application of MRs in dehydrogenation reactions.

Mass transport modelling: The Relevant Site Model (Chapter 5)

Together with excellent separation results a remarkable strong loading dependency of diffusion of light gases in DD3R is found. It is well known that the diffusivity in zeolites is dependent on the loading, but simulation and experimental data point out that especially for small-pore 8-ring zeolites very strong loading dependencies of the diffusivity are quite common [10-12]. This strong loading dependency complicates macroscopic modelling of permeation behaviour of such zeolite membranes, which is required for module design.

The best model currently available, based on the so-called Reed Ehrlich approach, turned out only modestly successful to model CH_4/CO_2 and CH_4/N_2 mixture permeation across an all-silica DD3R membrane [13].

Therefore, a new model has been introduced in this thesis to capture the loading dependency of the diffusivity in zeolites in the formulation of a macroscopic transport model. The model is formulated around the idea of segregated adsorption in cage-like zeolites, *i.e.* that molecules are located either in the cage or in the window (Figure 5). Furthermore, it is assumed that only the molecules located at the window site are able to make a successful jump to another cage. This so-called Relevant Site Model (RSM) is based on the Maxwell-Stefan framework for mass transport but includes one extra parameter that describes the adsorption properties of the 'relevant site'. Key feature of the RSM as applied to mixtures is that competitive adsorption effects and 'speeding up and slowing down' (momentum exchange) effects between guest molecules are related to the RS loading instead of the overall loading, which can be very different. In addition to the RSM the concept of free space relevant for diffusion has been introduced. Because the diffusivity often approaches very small values when the loading in the zeolite approaches its saturation loading a 'confinement' factor is introduced to indicate the available free space. Now it is argued that due to, for example, side pockets or positional rearrangements not all free space is relevant for diffusion. A method has been put forward to account for these effects in modelling work.

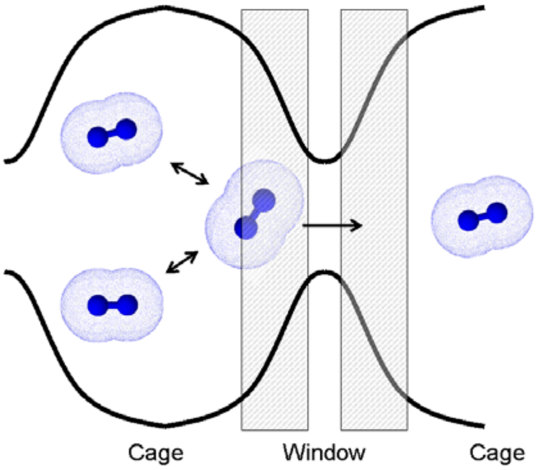

Figure 5. Schematic representation of a molecule located at a window site, in equilibrium with molecules present in the cage.

Application to zeolite DDR (Chapter 5B & C)

Firstly, the RSM has been applied to a set of single component diffusivity data of CO_2 and N_2 in DDR computed using molecular dynamic (MD) simulations. The RSM describes the Maxwell Stefan diffusivity data very well up to saturation. The observed strong diffusivity loading dependency is explained by the relative low window site occupancy that is typically much lower than the total occupancy at lower loadings. The RSM is successfully applied to non-isothermal diffusivity data of CO_2 and N_2 in DDR. Relating intermolecular correlation effects (momentum exchange) to the RS occupancy instead of the total occupancy leads to a quantitative prediction of the observed correlation effects and, consequently, the self diffusivity. Analysis of the N_2 data suggests positional rearrangements in the DDR cages in a certain loading range. These effects have been incorporated in the model successfully using the concept of free space relevant for diffusion.

Then, the RSM has been subjected to an extensive set of diffusivity data of N_2/CO_2 and Ne/Ar mixtures in zeolite DDR, directly computed using molecular dynamics. A large part of the considered data has been taken from literature [14]. It has been shown that the RSM provides excellent mixture diffusivity predictions from single component diffusivity data. The results are comparable to the 'Reed-Ehrlich' approach as put forward by Krishna and co-workers. A clear improvement by the RSM is found in the case of the N_2 diffusivity in N_2/CO_2 mixtures (Figure 6), attributed to the specific window blocking effect by CO_2 which is inherently incorporated in the RSM by relating adsorption to the relevant (=window) site.

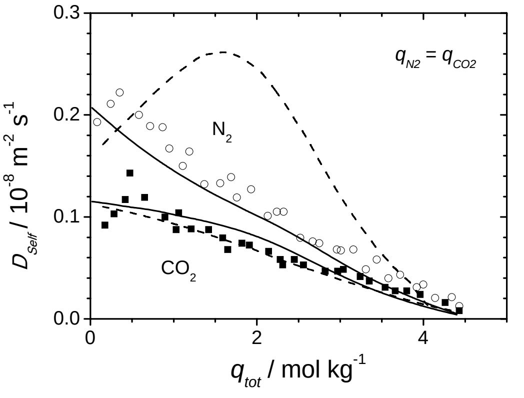

Figure 6. CO_2 and N_2 self diffusivities (D_{Self}) in DDR as a function of total loading at equal composition. The data points, solid lines and dashed lines represent MD simulations results from [14], RSM predictions and model predictions of the 'Reed Ehrlich' approach, respectively.

Extension to other zeolites (Chapter 5D)

After the successful application of the RSM to describe the loading dependency of diffusion in zeolite DDR it has also been successfully applied to a variety of light gases (CH_4, CO_2, Ar and Ne) and binary mixtures thereof in other zeolite topologies, DDR, CHA, MFI and FAU, utilizing the extensive diffusivity dataset published by Krishna and van Baten for this variety of zeolite-guest systems (*e.g.* [14])[Chapter 5D]. From the RS approach a measure for the level of adsorption segregation is derived: the ratio of the RS and total occupancy. The predicted level of adsorption segregation correlates well with the level of confinement of a molecule at the RS: the ratio of molecule diameter to zeolite pore diameter. Moreover, the predicted degree of adsorption segregation of the studied light gases in DDR is in good agreement with molecular simulations results, indicating the physical meaningfulness of the estimated RS adsorption parameters. The binary mixture diffusivity modelling points out that in case of the small-pore zeolites (DDR and CHA) the data is described best with equal RS saturation loadings for both components. For the large pore zeolite FAU the ratio of the RS saturation loadings equals that of the bulk saturation loadings. The geometry of the RS strongly influences the RS saturation loading: in case of the small-pore zeolites the RS (=

window site) is restricted to only one molecule but when the RS becomes larger more then one molecule can be found at the RS.

Application to DD3R membrane permeation data (Chapter 5E)

Having demonstrated the usefulness of the RSM using simulated diffusivities, the model has been applied to membrane permeation data. Single component (CO_2, CH_4 and N_2) and equimolar binary mixture (CO_2/CH_4, N_2/CH_4 and CO_2/Air) permeation data across a disc-shaped all-silica DDR zeolite membrane have been the subject of a thorough modelling study over a challenging broad temperature (220-373 K) and feed pressure (101-1500 kPa) range. Also here a comparison with the Reed Ehrlich approach is made.

Both the RSM as the RE approach yield an excellent model fit of the single component permeation data. However, for both models the N_2 and CH_4 single component permeation data did not allow an accurate estimation of the model fit parameters. Both models can lead to a good prediction of comparable quality of the mixture permeation data based on the single component model fit parameters (Figure 7). The RE approach is very sensitive towards the model input parameters and the estimated mixture loading, which both can be very hard to determine accurately in practice. The RSM does not suffer from both these issues, which is an evident advantage with respect to application of this model.

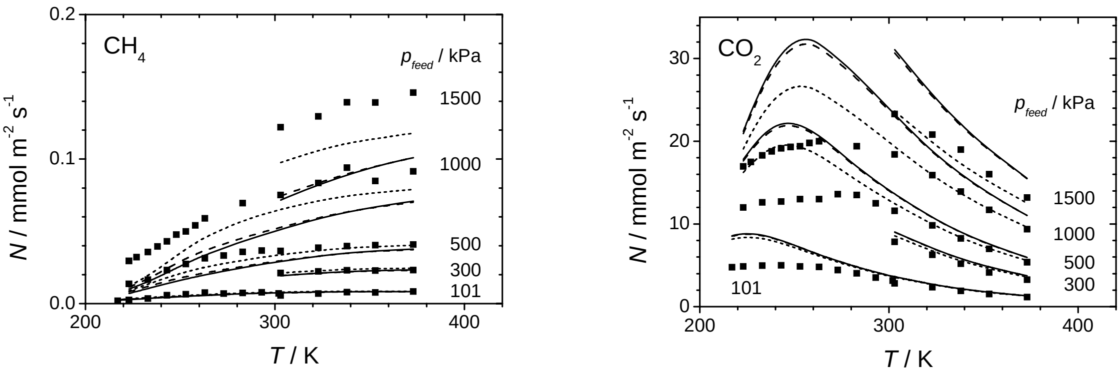

Figure 7. Permeation fluxes of CH_4 and CO_2 in an equimolar feed mixture across an all-silica DDR membrane as a function of temperature. Symbols represent experimental data, lines represent model predictions by the RSM. Solid, dashed and short-dashed lines are the results of a sensitivity analysis on the single component input parameters.

Reconciliation with dynamically corrected Transition State Theory (Chapter 5F)

The RSM closely resembles the well-known concept of dynamically corrected Transition State Theory (dcTST) which is often used in molecular simulations to study the dynamics of rare events. Therefore we investigated this connection in detail. It turns out that the ratio of the RS and total occupancy and a factor containing the exchange effects and free space available for diffusion in the RSM are directly related to those in dcTST, *i.e.* the probability that a molecule is on top of the free energy barrier and the transmission coefficient κ. Therefore, the RSM provides a direct link between properties at the molecular scale and the macroscopic Maxwell-Stefan diffusivity.

Concluding remarks & future outlook

What is the added value of this thesis in a broader perspective? To start with, a large part of this thesis is devoted to the introduction of a new model to describe mass transport in zeolites: the relevant site model (RSM). This model adequately captures mass transport phenomena in small-pore cage-like zeolites like DD3R. Moreover, this model appears useful to describe mass transport in other types of zeolites as well. The RSM offers handles to incorporate effects on the micro-scale into an engineering model (Maxwell Stefan approach to mass transfer). This is a definite step forward regarding mass transport modelling for design.

A powerful tool in the development of this model has been Molecular Dynamic (MD) simulations. Where experimental membrane permeation data can be influenced by several phenomena, like crystal grain boundaries or surface barriers, in MD simulations the intrinsic diffusion phenomena can be studied separately. Although always a reality check needs to be made with respect to experimental data, these methods have developed in the last decades in such a way that impressive results can be obtained, particularly for all-silica zeolites. Zeolites, and other crystalline materials like metal organic frameworks, are excellently suited for this kind of approach due to their ordered structure.

It has been demonstrated that the studied DD3R membranes are of excellent quality for gas separation applications. Moreover, stable operation is demonstrated, also at high temperatures. (Reactive) Separations where small molecules, like CO_2, H_2 or H_2O [15], can be removed based on molecular sieving can be an attractive application. However, in case of H_2, the flux seems currently still too low to compete with other available membranes (*e.g.* Pd). Clearly natural gas purification and biogas treatment seems the target application with DD3R membranes. Note that this should involve CO_2/CH_4 separations. Although the N_2/CH_4 separation factor is high, the current N_2 flux can be considered too low for successful use for this bulk application. Also CO_2 removal of flue gas can be interesting given the reasonable CO_2/air separation factor, but the CO_2 flux decrease with increasing temperature also reveals clear limitations for applications at elevated temperatures. Although this small-pore zeolite membrane retains its molecular sieving properties at high temperatures, the fluxes at these conditions are relatively low. The high CO_2 flux at lower temperatures is due to the strong adsorption in the zeolite. At high temperatures these adsorption effects disappear and the size of the molecule appears the decisive factor in the obtained magnitude of the flux. It seems that the small molecules H_2 and He provide an upper limit of the flux at high temperatures. If then the H_2 flux is too low for applications, it can be doubtful if the current generation of this type of small-pore zeolite membrane will be suitable for *any* high temperature application. It is then the classical flux-selectivity trade-off [16] that makes small-pore zeolite membranes unsuitable for these type of applications, at least when applied at the macro-level. Note that the very small H_2O molecule with its relative high boiling point could be a positive exception. But, finally it is good to emphasize that the excellent separation performance in CO_2/CH_4 separations can be considered a breakthrough in the development of zeolite membranes for gas separation applications. This application could be a driver for a more widespread application of zeolite membranes. This development inclines us to be optimistic that, after the first application of a zeolite membrane in alcohol dehydration, also the first gas separation applications appear to be within reach.

References

[1] H. van Suijdam; C. A. M. van der Klein; P. W. Kwant; Tj. R. Gorter; J. Maat; J. H. W. de Wit; B. Ph. ter Meulen; J. de Wit; D. den Ouden; L. A. M. van der Wielen; H. E. A. van der Akker; P. Scholten; van Damme; E. E. Wolff, and H. M. Wijngaard, Innovation Roadmap Scheidingstechnologie, **2004**.

[2] W. J. Koros, Closing Technology Gaps to Enable Energy-Efficient Membrane-Based Separations, Presentation at EuroMembrane 2009, Montpellier, **2009**.

[3] W. J. Koros, *AIChE Journal*, 50, **2004**, 2326.

[4] R. D. Noble and R. Agrawal, *Industrial & Engineering Chemistry Research*, 44, **2005**, 2887.

[5] R. W. Baker and K. Lokhandwala, *Industrial & Engineering Chemistry Research*, 47, **2008**, 2109.

[6] J. Caro, D. Albrecht, and M. Noack, *Separation and Purification Technology*, 66, **2009**, 143.

[7] F. Kapteijn, J. M. van de Graaf, and J. A. Moulijn, *AIChE Journal*, 46, **2000**, 1096.

[8] T. Tomita, K. Nakayama, and H. Sakai, *Microporous and Mesoporous Materials*, 68, **2004**, 71.

[9] J. A. Moulijn, M.Makkee, and A.van Diepen, Chemical process technology, **2001**, Wiley, New York.

[10] R. Krishna and J. M. van Baten, *Microporous and Mesoporous Materials*, 109, **2008**, 91.

[11] E. Beerdsen, D. Dubbeldam, and B. Smit, *Journal of Physical Chemistry B*, 110, **2006**, 22754.

[12] A. I. Skoulidas and D. S. Sholl, *Journal of Physical Chemistry A*, 107, **2003**, 10132.

[13] J. van den Bergh, W. Zhu, J. C. Groen, F. Kapteijn, J. A. Moulijn, K. Yajima, K. Nakayama, T. Tomita, and S. Yoshida, *Studies in Surface Science and Catalysis*, 170 A, **2007**, 1021.

[14] R. Krishna and J. M. van Baten, *Chemical Engineering Science*, 63, **2008**, 3120, supporting information.

[15] J. Kuhn, K. Yajima, T. Tomita, J. Gross, and F. Kapteijn, *Journal of Membrane Science*, 321, **2008**, 344.

[16] L. M. Robeson, *Journal of Membrane Science*, 320, **2008**, 390.

Samenvatting

De geschatte jaarlijkse energieconsumptie van de Nederlands (petro-)chemische industrie rond 2004 was 460 PJ, waarvan 200 PJ kan worden toegeschreven aan scheidingsprocessen [1]. In 2009 was 15 % van de wereldenergieconsumptie benodigd voor scheiding- en zuiveringsprocessen om basisproducten te produceren. Bovendien is de verwachting dat in 2040 de wereldwijde vraag naar basisproducten drie keer hoger is als in 2009, wat leidt tot een enorme energievraagtoename gerelateerd aan scheidingsprocessen in de komende decennia [2]. Deze twee voorbeelden illustreren helder de noodzakelijkheid om nieuwe, energie-efficiënte scheidingstechnologieën to ontwikkelen. Membraantechnologie wordt als serieuze kandidaat gezien om de traditioneel gebruikte thermisch-gedreven scheidingsprocessen te vervangen vanwege de grote energiereductie die kan worden gerealiseerd [2-4]. Een toepassing die erg relevant is voor dit proefschrift is aardgaszuivering, welke met afstand de grootste industriële toepassing op het gebied van gasscheiding is [5].

Het centrale thema van dit proefschrift zijn DD3R zeolietmembranen. Zeolieten zijn kristallijne aluminosilicaten met poriën van subnanometer-dimensies. Speciale voordelen van zeolietmembranen zijn hun hoge thermische en chemische stabiliteit en hun moleculaire zeefeigenschappen. Twee belangrijke aspecten onderscheidt DD3R van andere zeolieten wat het bestuderen van deze zeoliet bijzonder interessant maakt: de kleine poriegrootte en de mogelijkheid het als puur silica te synthetiseren. De elliptische 8-ring porie heeft een afmeting van ongeveer 0.36 × 0.44 nm wat dit materiaal erg interessant maakt voor de scheiding van lichte gassen, wat niet mogelijk is met zeolieten met grotere poriën zoals MFI. Andere 8-ring zeolieten zijn bekend, maar zeer weinig van deze structuren zijn succesvol gesynthetiseerd in een puur-silica-vorm. Omdat het zeer moeilijk blijkt te zijn om membranen van hoge kwaliteit voor gasscheidingen te maken op basis van zeolieten die aluminium bevatten [6] is de puur-silica-vorm van DD3R een duidelijk voordeel.

Gezien de speciale eigenschappen van DD3R op het gebied van gasscheiding is het volgende project gedefinieerd: *toepassing van DD3R zeolietmembranen in scheidings- en katalytische processen*. Bijzondere aandacht is besteed aan het begrijpen en modelleren van massatransport door dit type membraan. De doelstellingen zijn getracht te behalen middels het testen van een schijf- en buisvormig membraan, beschikbaar gesteld door NGK Insulators, in verschillende gasscheidingen en toepassing in één reactieve scheiding: dehydrogenering van isobutaan in een DD3R zeolietmembraanreactor. Het permeatiegedrag van een serie lichte gassen en mengsels van deze gassen zijn geanalyseerd as een functie van de temperatuur en druk en vergeleken met massatransportmechanismen beschreven in de literatuur. Omdat de resultaten van de beschikbare massatransportmodellen niet voldeden is er in dit proefschrift een nieuw model voorgesteld om diffusie in zeolieten modelmatig te beschrijven: het ‘Relevant Site Model’ (RSM). Diffusiviteitdata berekend middels Moleculaire Dynamica (MD) simulaties zijn gebruikt om dit model te ontwikkelen en te verifiëren.

Permeatie- en scheidingskarakteristieken (Hoofdstuk 2 & 3)

Adsorptie-experimenten van een serie lichte gassen op DD3R kristallen leverde de volgende volgorde op in geadsorbeerde hoeveelheid bij 303 K en 120 kPa: CO_2 (koolstofdioxide) = N_2O (lachgas) >> Kr (krypton) ≈ CH_4 (methaan) > CO (koolstofmonoxide) > N_2 (stikstof) ≈ O_2 (zuurstof) ≈ Ar (argon) > H_2 (waterstof). In het geval van Ne (neon) kon geen significante adsorptie worden gedetecteerd. De isothermen konden goed worden beschreven middels een één- of twee-site Langmuir isotherm.

De permeatie- en scheidingskarakteristieken van lichte gassen door DD3R membranen kan verklaard worden door: (1) de DD3R poriegrootte wat leidt tot moleculaire zeefeffecten en geactiveerd transport, (2) competitieve adsorptie-effecten, zoals waargenomen voor mengsels die sterk adsorberende gassen bevatten, en (3) impulsoverdracht tussen moleculen in de zeoliet. Impulsoverdracht lijkt alleen relevant in mengsels beneden 373 K die sterk adsorberende componenten (CO_2, N_2O) bevatten. Ook competitieve adsorptie-effecten zijn alleen gevonden in het geval van mengsels die sterk adsorberende componenten bevatten. Onderdrukking van de flux van de zwakker adsorberende component kan zeer sterk zijn en wordt vooral zichtbaar bij lage temperaturen (< 303 K). Het permeatiegedrag van een pure component kan goed uitgelegd worden middels een oppervlaktediffusiemechanisme [7]. In dit geval wordt de membraanpermeatie bepaald door zowel adsorptie als diffusie in de zeoliet. Isobutaan is te groot om de DD3R poriën in the gaan en permeëert alleen door een zeer klein aantal defecten in het membraan. Een belangrijke observatie is dat de fluxen van de zwakker adsorberende componenten (H_2, He, N_2, CO) een continu dalende trend laten zien met toenemende temperatuur en goed kunnen worden beschreven met het oppervlaktediffusie-mechanisme. Dit resultaat stelt het breed geaccepteerde idee ter discussie dat met toenemende temperatuur een verschuiving van het transportmechanisme plaatsvindt in zeolietmembranen van een geadsorbeerde fase (oppervlaktediffusie) naar een niet-geadsorbeerde fase massatransport (geactiveerde gasfase diffusie).

Zowel het schijf- als het buisvormige membraan lieten een zelfde permeatiegedrag zien. Het enige verschil tussen de twee is dat de permeatie in het geval van het buisvormige membraan een factor zes hoger is. Dit verschil is toegeschreven aan het feit dat het buisvormige membraan dunner is. Hoewel het waargenomen massatransportmechanisme het best beschreven wordt door oppervlaktediffusie, gedragen de gassen zich als zwakker adsorberende gassen als kon worden verwacht op basis van de adsorptie-isothermen. Dit kan worden verklaard doordat massatransport wordt bepaald door zwak adsorberende adsorptiesites in DD3R (Hoofdstuk 5).

Permeatie-experimenten met binaire mengsels lieten vooral voor aardgaszuivering (CO_2 / CH_4 scheiding) uitstekende resultaten zien: zeer hoge scheidingsfactoren (> 500 @ 303 K) en hoge CO_2 fluxen, wat de eerdere resultaten van Tomita *e.a.* [8] bevestigt. De selectiviteit daalt met toenemende totale voedingsdruk, maar tot 1500 kPa voedingsdruk blijft de selectiviteit hoger dan 100 tot bij 373 K. De N_2/CH_4 scheidingsfactor is goed, maar de relatief lage N_2 flux staat een succesvolle toepassing in de weg. Omdat de scheiding voornamelijk wordt veroorzaakt door een moleculair zeefmechanisme is de scheiding van O_2 van N_2, die vrijwel even groot zijn, lastig en is de scheidingsfactor betrekkelijk laag (≤ 2). Het is fascinerend dat CO_2 en N_2O zich (nagenoeg) identiek gedragen in DD3R en niet kunnen worden gescheiden (selectiviteit ~ 1). De 'ideale' H_2/CO en CO_2/CO selectiviteiten variëren van 3 tot 12 en van 10 tot 2 tussen respectievelijk 303 en 673 K. De selectiviteiten in een mengsel waren altijd lager dan 5, en dus veel lager dan de ideale selectiviteiten, door niet-differentiële operatie van het buisvormige membraan. De H_2/isobutaan mengselselectiviteit is ~ 400 in een equimolair binair mengsel over een breed temperatuursbereik (303 – 773 K). Deze hoge selectiviteit is wordt veroorzaakt doordat isobutaan to groot is om de DD3R poriën binnen te gaan.

Isobutaandehydrogenering (Hoofdstuk 4)

Dehydrogenering van alkanen zijn industrieel zeer relevante reacties, maar het is ook een klasse van reacties waar de conversie (sterk) evenwichtsgelimiteerd kan zijn bij praktische hoge temperaturen, die noodzakelijk zijn om de reactie uit te voeren. Lage conversies leidt tot een grote hoeveelheid alkaan/alkeen-mengsel dat moet worden gescheiden en gerecycled. Vooral de scheiding van alkaan/alkeen-mengsels is erg energie-intensief [9]. Een aanpak om de conversie te verhogen is de toepassing van een membraanreactor (MR). Door *in situ* het geproduceerde waterstofgas te verwijderen kan een verschuiving van de evenwichtsconversie worden bewerkstelligd. Door de uitstekende H_2/isobutaan selectiviteit en een redelijke H_2 membraanpermeance (~ $4.5 \cdot 10^{-8}$ mol m^{-2} s^{-1} Pa^{-1} @ 773 K) is de dehydrogeneringsreactie van isobutaan bestudeerd in een DD3R zeolietmembraanreactor bij 712 en 762 K. Experimenten in een conventioneel gepakt-bed-reactor (PBR) zijn gebruikt als referentie, Cr_2O_3-Al_2O_3 is gebruikt als katalysator.

Bij hoge verblijftijden is de isobuteenopbrengst (yield) hoger dan de evenwichtsopbrengst. Bij 762 K en 0.13 $kg_{voeding}kg_{kat}^{-1}u^{-1}$ is de isobuteenopbrengst in de MR 0.41, terwijl de evenwichtsopbrengst *ca.* 0.28 is. De hogere opbrengst is toegeschreven aan de verwijdering van H_2 van de reactiezone door het membraan. De verwijdering van H_2 bevordert enigszins de vorming van coke, onderdrukt hydrogenolysereacties en lijkt de katalytische activiteit iets te verminderen. Tijdens verschillende maanden van membraanoperatie bij hoge temperatuur veranderde de membraankwaliteit niet merkbaar. De massatransportparameters van het membraan en de reactiesnelheidconstanten zijn onafhankelijk bepaald van respectievelijk membraanpermeatie en PBR experimenten. Middels deze parameters kon het gedrag van de MR goed worden gesimuleerd.

De prestatie van de MR wordt voornamelijk bepaald door twee belangrijke dimensieloze getallen: het Damköhler (*Da*) en een Pécletgetal betrokken op het membraan (Pe_δ). Om een significante verbetering van de MR ten opzichte van de PBR te bereiken moet $Da \geq 10$ en

$Pe_\delta \leq 0.1$. Als $DaPe_\delta \sim 1$ wordt zowel het membraan als de katalysator optimaal benut. In de huidige MR is zowel de katalytische activiteit als de membraanpermeatie van H_2 te laag voor succesvolle toepassing van dit type MR. Het gebruik van een actievere katalysator en een gunstigere verhouding van het membraanoppervlak ten opzichte van het reactorvolume zou de prestatie van de MR al een stuk kunnen verhogen. Ook het werken bij hogere voedingsdrukken zou een mogelijke oplossing kunnen zijn. Omdat er al membranen met hogere waterstoffluxen bestaan is het vooral de beperkte katalysatoractiviteit bij lage temperatuur en waterstofarme omstandigheden dat succesvolle toepassing van membraanreactoren in dehydrogeneringreacties in de weg staat.

Modellering massatransport: Het Relevant Site Model (Hoofdstuk 5)

Samen met uitstekende resultaten voor verschillende relevante scheidingsprocessen laat zeoliet DD3R een sterke afhankelijk van de diffusiviteit als functie van de belading zien. Het is algemeen bekend dat de diffusiviteit van zeolieten beladingsafhankelijk is, maar simulaties en experimentele gegevens laten zien dat vooral in het geval van kleine-porie 8-ring zeolieten deze beladingsafhankelijkheid vaak voorkomt [10-12]. Deze sterke beladingsafhankelijkheid van de diffusiviteit bemoeilijkt het modelleren van dit type zeolietmembranen noodzakelijk voor het maken van een procesontwerp. Het beste model wat op dit moment beschikbaar is, gebaseerd op een model oorspronkelijk voorgesteld door Reed and Ehrlich [13], bleek beperkt succesvol om permeatiedata van CH_4/CO_2- en CH_4/N_2-mengsels door een DD3R membraan te beschrijven [14].

Daarom is er in dit proefschrift een nieuw model geïntroduceerd om deze beladingsafhankelijkheid van de diffusiviteit in een macroscopische formulering te incorporeren (Hoofdstuk 5A). Het model is geformuleerd rond het idee dat adsorptie in kooi-achtige zeolieten sterk gesegregeerd kan zijn: d.w.z. moleculen worden gevonden ofwel in de kooi ofwel in het venster van de kooi. Daarnaast wordt aangenomen dat alleen de moleculen die in het venster van de kooi zitten een succesvolle sprong naar de volgende kooi kunnen maken. Dit zogenaamde Relevant Site Model (RSM) is gebaseerd op de Maxwell-Stefan vergelijkingen voor massatransport, maar bevat een extra parameter die de adsorptie-eigenschappen van de ‘relevante site’ beschrijft. Een belangrijke eigenschap van het RSM wanneer toegepast op mengsels is dat competitieve adsorptie effecten en het ‘versnellen’ en ‘afremmen’ van gastmoleculen onderling worden gerelateerd aan de belading van de relevante site in plaats van de totale zeolietbelading, welke zeer verschillende kunnen zijn. Naast het RSM is ook het concept van vrije ruimte voor diffusie geïntroduceerd. Omdat de diffusiviteit vaak zeer lage waarden bereikt wanneer de belading de verzadigingsbelading benadert wordt vaak een factor aan de diffusiviteit toegevoegd die de beschikbare vrije ruimte aangeeft. In het huidige werk wordt het beargumenteerd dat, bijvoorbeeld door de aanwezigheid van zijholtes of door herpositionering van moleculen, niet alle vrije ruimte relevant is voor diffusie. Een methode is voorgesteld om deze effecten in modelleerwerk mee te nemen.

Toepassing op zeoliet DDR (Hoofdstuk 5B & 5C)

Allereerst is het RSM toegepast op een set diffusiedata van puur CO_2 en N_2 in DDR, berekend middels moleculaire dynamica (MD) simulaties (Hoofdstuk 5B). Het RSM beschrijft de Maxwell-Stefan-diffusiviteitdata erg goed tot op de verzadigingsbelading. De waargenomen sterke beladingsafhankelijkheid van de diffusiviteit is verklaard op basis van de relatief lage bezettingsgraad van het kooivenster (= de relevante site), welke kenmerkend lager is dan de totale bezettingsgraad bij lage beladingen. Het RSM is ook succesvol toegepast op niet-isotherme diffusiviteitsdata van CO_2 en N_2 in DDR. Door inter-moleculaire correlatie-effecten (impulsoverdracht) te relateren aan de bezetting van de relevante site in plaats van de totale bezetting was het mogelijk een kwantitatieve voorspelling van deze correlatie-effecten en de zelfdiffusiviteit te maken. Een analyse van de N_2 data suggereert positionele herschikkingen in de DDR-kooien in een bepaald beladingsbereik. Deze effecten zijn geïncorporeerd in het model middels het concept van de vrije ruimte relevant voor diffusie.

Vervolgens is het RSM onderworpen aan een extensieve set diffusiviteitdata van N_2/CO_2- en Ne/Ar-mengsels in zeoliet DDR. Ook deze dataset is gegenereerd middels MD simulaties (Hoofdstuk 5C) waarvan een groot gedeelte data uit de literatuur betreft [15]. Het is aangetoond de het RSM uitstekende voorspellingen van diffusiviteiten in een mengsel oplevert op basis van diffusiedata van de pure componenten. Deze resultaten zijn vergelijkbaar met de ‘Reed-Ehrlich’-aanpak als voorgesteld door Krishna en van Baten. Maar er is een duidelijk betere voorspelling door het RSM in het geval van de N_2 diffusiviteit in N_2/CO_2 mengsels, wat toegeschreven wordt aan specifieke obstructie-effecten van CO_2 in de kooivensters ten aanzien van N_2. Dit effect is inherent aanwezig in het RSM doordat competitieve adsorpie-effecten gerelateerd zijn aan de relevante (= venster) adsorptiesite voor diffusie.

Toepassing op andere zeolieten (Hoofdstuk 5D)

Na de succesvolle toepassing van het RSM in de beschrijving van de beladingsafhankelijkheid van de diffusiviteit in zeoliet DDR is het ook succesvol toegepast op een variëteit van lichte gassen (CH_4, CO_2, Ar en Ne) en binaire mengsels hiervan in andere zeoliettopologieën (DDR, CHA, MFI and FAU). Voor deze analyse is wederom een deel van de uitgebreide dataset van diffusiviteiten gepubliceerd door Krishna en van Baten gebruikt (b.v. [15]). Van de RS aanpak is een indicator voor het niveau van de gesegregeerdheid van adsorptie gedefinieerd: de verhouding van de bezettingsgraad op de relevante adsorptiesite en de totale bezettingsgraad in de zeoliet. Het voorspelde niveau van de gesegregeerdheid van adsorptie correleert goed met de mate van ingeslotenheid op de relevante site: de verhouding van de diameter van het molecuul en van de zeolietporie. Bovendien is de voorspelde gesegregeerdheid van adsorptie van de bestudeerde lichte gassen in DDR in goede overeenstemming met resultaten van moleculaire simulaties, wat aangeeft dat de bepaalde adsorptieparameters van de relevante site fysisch realistisch zijn. Het modelleren van de diffusiviteiten van binaire mengsels in de verschillende zeolieten liet zien dat in het geval van kleine-porie zeolieten (DDR en CHA) de data het best beschreven kan worden met de aanname dat de verzadigingsbelading van beide componenten op de relevante site gelijk is. In het geval van het grote-porie zeoliet FAU levert een verhouding van de verzadigingsbeladingen van de relevante site gelijk aan de verhouding van de totale verzadigingsbeladingen het beste resultaat op. De geometrie van de relevante site beïnvloedt de verzadigingsbelading van de relevante site dus zeer sterk: in het geval van de kleine-porie zeolieten is de relevante site beperkt tot maar één molecuul; wanneer de ruimte op de relevante site toeneemt kan er meer dan een molecuul tegelijk aanwezig zijn.

Toepassing op DD3R membraanpermeatiedata (Hoofdstuk 5E)

Het model is ook gebruikt om experimentele membraanpermeatiedata te beschrijven. Permeatiedata door een schijfvormig DD3R membraan van pure gassen (CO_2, CH_4 en N_2) en binaire, equimolaire mengsels (CO_2/CH_4, N_2/CH_4, CO_2/lucht) zijn het onderwerp geweest van een grondige modelleerstudie. De permeatiedata is gemeten in een breed temperatuur- (220 - 373 K) en drukbereik (101 – 1500 kPa). Ook in deze studie is het RSM met de Reed-Ehrlich-aanpak vergeleken.

Zowel het RSM als de Reed-Ehrlich-aanpak levert een uitstekende model fit van de permeatiedata van de pure componenten op. Voor beide modellen kon geen nauwkeurige bepaling worden gedaan van de diffusieparameters van N_2 en CH_4 op basis van de permeatiedata van de pure gassen. Beide modellen kunnen, op basis van de bepaalde diffusieparameters van de pure gassen, een goede voorspelling van de permeatie van de mengsels opleveren van vergelijkbare kwaliteit. De Reed-Ehrlich-aanpak is erg gevoelig wat betreft de bepaalde diffusieparameters en de geschatte belading van de componenten in de zeoliet, welke beide moeilijk te bepalen kunnen zijn in de praktijk. Het RSM heeft dit probleem niet, wat een duidelijk voordeel is wat betreft de toepassing van dit model ten opzichte van de Reed-Ehrlich-aanpak.

Parallellen met de dynamisch gecorrigeerde Transition State Theory (Hoofdstuk 5F)

Het RSM heeft een sterke gelijkenis met het welbekende concept van de dynamisch gecorrigeerde Transition State Theory (overgangsstaat) theorie (dcTST). Deze theorie wordt veelvuldig gebruikt in moleculaire simulaties om de dynamica van zeldzame gebeurtenissen te bestuderen. Het blijkt dat de verhouding van de bezettingsgraad van de relevante site en de totale bezettingsgraad, en een factor die de correlatie effecten en beschikbare ruimte voor diffusie bevatten in het RSM zich één op één verhouden met bepaalde parameters in dcTST: de kans dat een molecuul gevonden wordt op de top van de energiebarrière, en de transmissiecoefficient κ. Om deze reden verschaft het RSM een directe link tussen eigenschappen op moleculair niveau en de macroscopische Maxwell-Stefan diffusiviteit.

Concluderende opmerkingen & toekomstperspectief

Wat is nu de toegevoegde waarde van dit proefschrift in een bredere context? Om te beginnen is een groot gedeelte van dit proefschrift gewijd aan de introductie van een nieuw model om massatransport in zeolieten te beschrijven: het relevant site model (RSM). Dit model beschrijft de massatransportverschijnselen in kleine-porie kooi-achtige zeolieten, zoals DDR, goed. Verder lijkt dit model geschikt om ook in andere typen zeolieten toegepast te worden. Het RSM maakt het mogelijk om effecten op moleculair niveau te incorporeren in een macroscopische aanpak geschikt voor procesontwerp.

Moleculaire Dynamica (MD) simulaties zijn een krachtig hulpmiddel in de ontwikkeling van dit model geweest. Waar experimentele membraanpermeatiedata sterk beïnvloed kunnen zijn door bijvoorbeeld korrelgrenzen in kristallen of oppervlaktebarrières, kan in MD simulaties de intrinsieke diffusieverschijnselen in zeolieten onafhankelijk worden bestudeerd. Natuurlijk zal er altijd een ‘reality check’ gemaakt moeten worden ten opzichte van experimentele gegevens, maar het moet gezegd worden dat het vakgebied van de computersimulaties zich dusdanig heeft ontwikkeld in de afgelopen decennia dat indrukwekkende resultaten kunnen worden behaald, in het bijzonder voor zeolieten die volledig uit silica bestaan. Zeolieten, en andere kristallijne materialen zoals metaal-organische-structuren (MOFs), zijn door hun geordende structuur uitstekende materialen om middels zulke methoden te onderzoeken.

Verder is het aangetoond dat de bestudeerde DD3R membranen van uistekende kwaliteit zijn voor toepassing op het gebied van gasscheidingen. Hiernaast is een langdurig stabiel bedrijf gedemonstreerd, ook bij hoge temperaturen. (Reactieve) scheidingen waarbij kleine moleculen, zoals CO_2, H_2 of H_2O, kunnen worden verwijderd gebaseerd op een moleculair zeefmechanisme kunnen interessante toepassingen zijn. Hoewel in het geval van H_2 de flux op dit moment te laag lijkt om te concurreren met andere typen membranen, zoals palladium. Het is duidelijk dat aardgas- en biogaszuivering de meest veelbelovende toepassing lijkt voor DD3R membranen, vooral waar dit CO_2/CH_4 scheiding betreft. Hoewel voor N_2/CH_4 goede scheidingsfactoren zijn gemeten is de huidige N_2 flux te laag voor een succesvolle toepassing in dit bulkproces. Ook verwijdering van CO_2 van rookgas kan interessant zijn gezien de redelijke CO_2/lucht scheidingsfactor, maar de afname van de CO_2-flux met toenemende temperatuur legt ook beperkingen met betrekking tot hoge temperatuurtoepassingen bloot. Hoewel DD3R zijn moleculaire zeefeigenschappen bij hoge temperatuur behoudt, zijn de fluxen bij deze condities relatief laag. De hoge flux van CO_2 bij lagere temperaturen komt voornamelijk door de sterke adsorptie in de zeoliet. Bij hoge temperaturen verdwijnen deze sterke adsorptie-effecten en lijkt de grootte van het molecuul de doorslaggevende factor in de hoogte van de geobserveerde flux. Het lijkt erop dat de kleine moleculen, H_2 en He, in dit opzicht een bovengrens aangeven voor de flux bij hoge temperatuur. Als in dit geval de H_2-flux al te laag lijkt om een toepassing te vinden is het op zijn minst twijfelachtig of de huidige generatie van dit type kleine-porie, zeolietmembraan geschikt zal zijn voor welke toepassing bij hoge temperaturen dan ook. Het is in dit geval de klassieke flux-selectiviteit koppeling [16] dat zeolietmembranen ongeschikt maakt voor dit soort toepassingen. Let wel dat het zeer kleine H_2O molecuul met zijn relatief hoge kookpunt een positieve uitzondering op de voorgaande discussie kan zijn.

Uiteindelijk is het goed te benadrukken dat vooral de uitstekende resultaten op het gebied van CO_2/CH_4-scheiding gezien kunnen worden als een doorbraak in de ontwikkeling van zeolietmembranen voor toepassingen op het gebied van gasscheidingen. Deze toepassing zou een belangrijke drijvende kracht kunnen worden voor een bredere toepassing van zeolietmembranen in de chemische industrie. Deze ontwikkeling neigt ons optimistisch te zijn dat na de eerste toepassing van zeolietmembranen in de ontwatering van alcoholen ook de eerste toepassing op het gebied van gasscheiding binnen handbereik is.

Referenties

[1] H. van Suijdam; C. A. M. van der Klein; P. W. Kwant; Tj. R. Gorter; J. Maat; J. H. W. de Wit; B. Ph. ter Meulen; J. de Wit; D. den Ouden; L. A. M. van der Wielen; H. E. A. van der Akker; P. Scholten; van Damme; E. E. Wolff, and H. M. Wijngaard, Innovation Roadmap Scheidingstechnologie, **2004**.

[2] W. J. Koros, Closing Technology Gaps to Enable Energy-Efficient Membrane-Based Separations, Presentation at EuroMembrane 2009, Montpellier, **2009**.

[3] W. J. Koros, *AIChE Journal*, 50, **2004**, 2326.

[4] R. D. Noble and R. Agrawal, *Industrial & Engineering Chemistry Research*, 44, **2005**, 2887.

[5] R. W. Baker and K. Lokhandwala, *Industrial & Engineering Chemistry Research*, 47, **2008**, 2109.

[6] J. Caro, D. Albrecht, and M. Noack, *Separation and Purification Technology*, 66, **2009**, 143.

[7] F. Kapteijn, J. M. van de Graaf, and J. A. Moulijn, *AIChE Journal*, 46, **2000**, 1096.

[8] T. Tomita, K. Nakayama, and H. Sakai, *Microporous and Mesoporous Materials*, 68, **2004**, 71.

[9] J. A. Moulijn, M.Makkee, and A.van Diepen, Chemical process technology, **2001**, Wiley, New York.

[10] R. Krishna and J. M. van Baten, *Microporous and Mesoporous Materials*, 109, **2008**, 91.

[11] E. Beerdsen, D. Dubbeldam, and B. Smit, *Journal of Physical Chemistry B*, 110, **2006**, 22754.

[12] A. I. Skoulidas and D. S. Sholl, *Journal of Physical Chemistry A*, 107, **2003**, 10132.

[13] D. A. Reed and G. Ehrlich, *Surface Science*, 102, **1981**, 588.

[14] J. van den Bergh, W. Zhu, J. C. Groen, F. Kapteijn, J. A. Moulijn, K. Yajima, K. Nakayama, T. Tomita, and S. Yoshida, *Studies in Surface Science and Catalysis*, 170 A, **2007**, 1021.

[15] R. Krishna and J. M. van Baten, *Chemical Engineering Science*, 63, **2008**, 3120, supporting information.

[16] L. M. Robeson, *Journal of Membrane Science*, 320, **2008**, 390.

List of publications

Journals

[1] J. van den Bergh, C. Gücüyener, J. Gascon, and F. Kapteijn, Isobutane dehydrogenation in a DD3R zeolite membrane reactor, *Chemical Engineering Journal*, **2010**, Submitted manuscript.

[2] T. J. H. Vlugt, J. van den Bergh, D. Dubbeldam, and F. Kapteijn, Reconciliation of the relevant site model and dynamically corrected transition state theory, *Chemical Physics Letters*, **2010**, doi:10.1016/j.cplett.2010.06.047.

[3] J. van den Bergh, S. Ban, T. J. H. Vlugt, and F. Kapteijn, Diffusion in zeolites: extension of the relevant site model to light gases and mixtures thereof in zeolites DDR, CHA, MFI and FAU, *Separation and Purification Technology*, 73, **2010**, 151.

[4] J. van den Bergh, A. Tihaya, and F. Kapteijn, High temperature permeation and separation characteristics of an all-silica DDR zeolite membrane, *Microporous and Mesoporous Materials*, 132, **2010**, 137.

[5] J. van den Bergh, M. C. Mittelmeijer-Hazeleger, and F. Kapteijn, Modelling permeation of CO_2/CH_4, N_2/CH_4 and CO_2/air mixtures across a DD3R zeolite membrane, *Journal of Physical Chemistry C*, 114, **2010**, 9397.

[6] J. van den Bergh, S. Ban, T. J. H. Vlugt, and F. Kapteijn, Modelling the loading dependency in zeolites: the relevant site model, *Journal of Physical Chemistry C*, 113, **2009**, 17840.

[7] J. van den Bergh, S. Ban, T. J. H. Vlugt, and F. Kapteijn, Modeling the loading dependency of diffusion in zeolites: the relevant site model extended to mixtures in DDR-type zeolite, *Journal of Physical Chemistry C*, 113, **2009**, 21856.

[8] J. van den Bergh, W. Zhu, J. Gascon, J. A. Moulijn, and F. Kapteijn, Separation and permeation characteristics of a DD3R zeolite membrane, *Journal of Membrane Science*, 316, **2008**, 35.

[9] J. van den Bergh, W. Zhu, F. Kapteijn, J. A. Moulijn, K. Yajima, K. Nakayama, T. Tomita, and S. Yoshida, Separation of CO2 and CH4 by a DDR membrane, *Research on Chemical Intermediates*, 34, **2008**, 467.

[10] J. van den Bergh, W. Zhu, J. C. Groen, F. Kapteijn, J. A. Moulijn, K. Yajima, K. Nakayama, T. Tomita, and S. Yoshida, Natural gas purification with a DDR zeolite membrane; permeation modelling with Maxwell-Stefan equations, *Studies in Surface Science and Catalysis*, 170 A, **2007**, 1021.

Contributions in books

[1] J. van den Bergh, J. Gascon, and F. Kapteijn, Diffusion in zeolites, in: Zeolites and catalysis: synthesis, reactions and applications, Cejka, Jiri, Corma, A., and Zones, S. I. (Eds), Ch. 13, **2010**, Wiley, New York, 361.

[2] J. van den Bergh, N. Nishiyama, and F. Kapteijn, Zeolite membranes in catalysis; what is new and how bright is the future?, in: Novel concepts in catalysis and chemical reactors, Cybulski, A., Moulijn, J. A., and Stankiewicz, A. (Eds), Ch. 10, **2010**, Wiley, New York, 211.

Oral presentations

Johan van den Bergh, Shuai Ban, Thijs Vlugt and Freek Kapteijn, *A new approach to model diffusion in zeolites: The relevant site model,* 5th International zeolite membrane meeting, **2010**, Loutraki, Greece.

Johan van den Bergh, Shuai Ban, Thijs Vlught and Freek Kapteijn; *Modelling the loading dependency of diffusion in zeolites: The relevant site model,* Workshop International Research and Training Group: Diffusion in porous materials, **2009**, Eindhoven, The Netherlands, invited lecture.

Johan van den Bergh, Anna Tihaya, Isabelle Aerts, and Freek Kapteijn, *Isobutane dehydrogenation in a DD3R zeolite membrane reactor*, Netherlands Process Technology Symposium 9, **2009**, Veldhoven, The Netherlands.

Johan van den Bergh, Shuai Ban, Thijs Vlught and Freek Kapteijn; *Modelling the loading dependency of diffusion in zeolites: The relevant site model.* 10th International Conference on Inorganic Membranes, **2008**, Tokyo, Japan, Keynote.

Johan van den Bergh, Freek Kapteijn and Jacob A. Moulijn, *Permeation and separation of permanent gases through a DDR (zeolite) membrane,* Netherlands Process Technology Symposium 7, **2007**, Veldhoven, The Netherlands.

Johan van den Bergh, Weidong Zhu, Freek Kapteijn and Jacob A. Moulijn, *Natural gas upgrading by a DDR membrane; permeation modelling with Maxwell-Stefan equations,* 4th International zeolite membrane meeting, **2007**, Zaragoza, Spain.

Dankwoord / Acknowledgements

Als er een ding duidelijk is na vier jaar werken aan dit proefschrift is het wel dat hulp van anderen, op welke wijze dan ook, onmisbaar is geweest om tot dit eindresultaat te komen. Daarom wil ik allereerst Freek heel erg bedanken voor alle begeleiding en zeer constructieve input tijdens mijn promotietraject. Eigenlijk moet ik je vooral bedanken dat jij me allereerst toch wel hebt overgehaald om hieraan te beginnen als vervolg van mijn afstudeerwerk. Ik heb veel van je geleerd en ik ben vooral blij met de vrijheid die je me gegeven hebt. Hoewel je agenda toch wat voller raakte toen je groepshoofd werd had je altijd op korte termijn wel een gaatje voor me om even wat zaken door te spreken en je responsietijd op e-mails en conceptartikelen was altijd uitstekend.

Rob, het is erg leuk om jouw kamergenoot te zijn geweest de afgelopen vier jaar, en nog steeds ben tot op heden. Ook was het uitermate handig om zoveel Athena-expertise zo dicht bij de hand te hebben. Elly en Els bedankt voor alle zaken die jullie voor mij geregeld hebben. En sorry voor alle keren dat ik Freek's agenda weer in de war heb gestuurd als ik 's ochtends 'even' nog wat zaken met Freek kwam kortsluiten…Bart, Harrie, Kevin en Willy mijn dank is groot voor de technische ondersteuning. Jullie stonden altijd klaar om op zeer korte termijn gestrande experimenten weer op gang te helpen. Jullie bijdrage aan de smering en continuïteit van de CE-activiteiten kan niet overschat worden. Sander, bedankt voor de adsorptiemetingen en voor de uitleg over de apparatuur, zodat ik na je vertrek zelfstandig verder kon gaan. Furthermore, I would like to thank all CE members of the present and the past during my stay for the very nice atmosphere in the group. There has always been a rich variety in nationalities and cultures with people coming and going. There was always time for a relaxed talk at the coffee machine, nice group outings and visits to interesting and 'gezellige' conferences. I will not forget this very nice period!

Het was ook goed samenwerken binnen de groep om het onderzoek rond te krijgen. Jorge, het was altijd goed om ideeën uit te wisselen over zeolieten en MOFs. Vooral je input in het dehydrogeneringswerk was erg bruikbaar en heeft ook een mooi artikel opgeleverd. Canan, many thanks to you as well for your tremendous effort in the dehydrogenation work. Your enthusiasm was great and you really helped me to finish my thesis on time. Nicla, Anna en Isabelle, ik heb jullie mogen begeleiden tijdens jullie MSc of BSc afstudeerwerk en wil jullie bedanken voor de leuke en gezellige tijd. Nicla, thanks for your work with the high temperature permeation experiments, too bad we did not arrive at the planned catalytic experiments. Anna, je hebt een enorme hoeveelheid werk verzet! Nauwkeurig gemeten membraanpermeaties, direct bruikbaar in publicaties. Erg belangrijk ook was je werk aan de membraanreactor. Veel problemen, maar jouw ervaringen vormden wel de basis om het werk later met nieuwe inzichten succesvol af te ronden. Isabelle, misschien was de oorspronkelijke opzet van hoe ik het model zag niet optimaal, maar we hebben veel geleerd onderweg welke oplosmethoden wel en niet goed werken. Leuk om te zien dat je je nu stort op het maken van animaties voor CE. Shuai and Thijs, I really enjoyed our cooperation on the RSM papers. Shuai, for you it was a busy time to do this work together with finishing your own thesis. But I think you agree with me that it was worth it in the end! Thijs, bedankt voor de leuke discussies en je uitermate nuttige commentaar op de artikelen. Leuk dat je in mijn commissie plaatsneemt. Marjo, bedankt voor de hogedrukmetingen. Je moest even geduld hebben maar uiteindelijk heeft het een leuk artikel opgeleverd.

Next to research I have been involved in teaching assistance in the courses CaRE and PT2 for several times. The contacts with students have been great. I have always been part of a team, and I would like to thank Daniel, Malte, Dirk, Christian, Bandar, Yasu, Pedro, Amer, Michiel, Jorge and Freek for the good times. Although checking homework could be a discouraging task, I also remember having a lot of fun also because of the ‘creative’ answers of the students.

Het is heel belangrijk om naast het werk ook uit andere hoeken afleiding en support te krijgen. Ontspanning nummer 1 voor mij is volleybal. Even lekker met sport bezig zijn en het hoofd leegmaken. Heren 1 van SNA bedankt voor alle fun en gezelligheid op de trainingen en bij de wedstrijden.

Verder wil ik ook mijn (schoon)familie bedanken. Hoewel zo’n promotieonderzoek nu niet direct tot ieders verbeelding spreekt, zijn jullie altijd geïnteresseerd geweest in wat ik doe en wat mijn voortgang was. Ik ben er trots op dat we zo’n hechte familie mogen zijn, het doet me altijd goed jullie te zien. Daarnaast dank ik God, van wie ik geloof dat Hij mij het talent en de kracht gegeven heeft dit werk tot een goed einde te brengen. En dan tot slot, lieve Lenny, dank aan jou in het bijzonder voor alle hulp en geduld met mij tijdens dit project. Dat je me de ruimte gaf om deze klus te klaren. In de afgelopen periode zijn we getrouwd, in Dordrecht gaan wonen en ik zie enorm uit naar december als we ons kind verwachten!

Johan

About the author

Johan van den Bergh was born on the first of April, 1982 in Dordrecht, the Netherlands. He obtained his HAVO diploma in 1999, after which he started his studies in chemical engineering at the Hogeschool Brabant in Breda. In 2003 he obtained his BEng degree en continued his studies in chemical engineering at Delft university of Technology. In 2006 he finished his Masters thesis and graduated cum laude under the supervision of Prof. dr. Freek Kapteijn and Dr. ir. Weidong Zhu within the Catalysis Engineering group, part of ChemE within the faculty of Applied Sciences at Delft University of Technology. This thesis entitled 'Permeation of permanent gases through DD3R membranes' was awarded the first prize of the two-yearly Dutch Gas Industry prize in 2008. In 2006 Johan started his PhD thesis entitled' DD3R zeolite membranes in separation and catalytic processes; Modelling and application' under supervision of Prof. dr. Freek Kapteijn. The aim of this project has been to investigate the possibilities of application of this type of membrane in the chemical industry. A large part of the work has been devoted to development of mass transport models required for process design. This research has led to a dozen of scientific publications and several oral presentations in (international) conferences.